Controls on zircon dissolution and crystallization during metamorphism

Tara R. McElhinney
BSc (Hons) University of Glasgow

Submitted in fulfilment of the requirements for the Degree of MSc by Research

School of Science and Engineering
College of Geographical and Earth Sciences
University of Glasgow

October 2019

Abstract

The response of zircon to prograde metamorphic reactions has been investigated in late Proterozoic metapelites from the Scottish Highlands. Samples from rocks undergoing greenschist and amphibolite facies metamorphism record changes in the zircon populations associated with specific stages in the reaction history. Appin Phyllites from Onich record changing zircon distribution and morphology across three distinct events, an early regional event is recorded in the matrix, a later contact event produces a population of zircon within biotite porphyroblasts, and finally partial retrogression of biotite produces chlorite. Leven Schists from Glen Roy record a progressive sequence of metamorphism from garnet zone to staurolite zone to sillimanite zone. Dissolution-reprecipitation occurs at each stage of the reaction history in the Leven Schists and produces modified garnet which can be recognised based on the resulting change to the texture and chemistry of product garnet. Within the Leven Schists, two distinct stages of modification can be recognised; the formation of cloudy garnet during staurolite growth and the formation of secondary clear garnet during sillimanite growth. During staurolite formation, dissolution-reprecipitation partially replaces garnet with large, irregular quartz inclusions and small <1 μm rounded fluid inclusions. Additionally, the original concentric growth zoning is modified producing localised low pyrope zones of cloudy garnet and releasing Ca into the rock. The products of dissolution-reprecipitation are more reactive than clear garnet owing to the high defect density within cloudy garnet. The release of Ca from dissolution-reprecipitation also moves the sillimanite isograd to lower P-T space. As a result, the higher the proportion of cloudy garnet formed during staurolite formation, the more likely the rocks will react to form sillimanite. Sillimanite formation results in the formation of reequilibrated secondary clear garnet, where fluid inclusions are eradicated and a low Ca, high Mg product garnet forms. Garnet therefore records three identifiable stages in its temporal evolution; (1) clear, unmodified garnet, (2) cloudy garnet formed via dissolution-reprecipitation during staurolite formation, and (3) secondary clear garnet, reequilibrated during sillimanite formation. Analysis of zircon within the matrix and biotite porphyroblasts in the Appin Phyllites, and within garnet in the Leven Schists enable an understanding of how zircon populations change through metamorphism.

Within both the Appin Phyllites and Leven Schists zircon is present in two distinct populations; (a) inherited detrital zircon, and (b) authigenic microzircon. Microzircon are fine <1 μm^2, euhedral zircon that display no internal structure or zonation. Microzircon appear to be reactive in the presence of fluids and thus have the ability to trace fluid-mediated metamorphic processes. By analysing zircon populations in garnet in the Leven Schists, the stages in temporal evolution of garnet can be utilised to understand temporal changes to the morphology and distribution of zircon. Within clear garnet, zircon are heterogeneously distributed, the primary influence on the abundance of zircon is the mineralogy of the matrix. Micaceous matrix, and the garnet that overgrows it, contains more microzircon than quartz-rich matrix. Following dissolution-reprecipitation, detrital zircon and particularly microzircon decrease in abundance. Additionally, microzircon become finer and are more frequently hosted within fluid and mineral inclusions, suggesting these populations formed during dissolution-reprecipitation. Within sillimanite-zone schists the secondary clear garnet contains the lowest number of microzircon. The Appin Phyllites record a much higher abundance of microzircon in later formed contact porphyroblast phases than within the earlier formed regional matrix. Both the Leven Schists and Appin Phyllites record an absence of microzircon within chlorite-retrogressed domains suggesting that effective microzircon dissolution occurs during chloritization but there is no new zircon crystallization.

This is the first comprehensive study of prograde zircon evolution, recording consistent changes to the distribution and morphology of zircon from lower greenschist Appin Phyllites to mid-amphibolite facies Leven Schists. These changes present the opportunity to trace metamorphic processes in complex polymetamorphic rocks where dating presently proves near impossible.

Table of contents

List of figures

List of tables

Acknowledgements

I received a great deal of support throughout the research and writing of this thesis. I'd first like to thank my supervisor, Dr Tim Dempster whose expertise was invaluable in formulating this research topic, and whose thoughtful discussions and feedback assisted in guiding me throughout this study.

I would like to thank Peter Chung for his analytical expertise and Robert MacDonald for his help with sample preparation. I thank the whole Earth Science department for providing me with the skills and knowledge necessary to complete this research. Thanks to my colleagues within the office who provided motivation and support through the research and writing of this thesis.

In addition, I would like to thank my parents who have guided me through the last year with support and encouragement. A final thank you to my friends, who were always available when I needed a distraction or sympathetic ear.

Declaration

I declare that the information presented in this thesis is the result of my own work, except where acknowledged to others, carried out at the School of Geographical and Earth Sciences, University of Glasgow. This research was supervised by Dr. Tim Dempster. Any published work by other authors has been given full acknowledgement in the text.

Tara McElhinney

Chapter 1 Zircon in metamorphism

1.1 Introduction

Zircon is a common accessory mineral present in a wide range of sedimentary, metamorphic and igneous rocks (Finch & Hanchar, 2003). It is an important detrital mineral, durable enough to withstand a number of physical and chemical processes including weathering, erosion and transport (Finch & Hanchar, 2003; Deer et al., 2013a). As such zircon grains are commonly composite, formed over a series of events which can be identified through zoning (Williams, 2001). Grains commonly consist of a detrital core, thought to be of magmatic origin, and relict magmatic or metamorphic zones (Rubatto, 2017). Zircon is a zirconium orthosilicate ($ZrSiO_4$) with a tetragonal structure consisting of alternating edge-sharing SiO_4 tetrahedra and ZrO_8 dodecahedra, chains of alternating polyhedra are joined laterally by the edge sharing dodecahedra (Nasdala et al., 2001; Botis et al., 2013; Deer et al., 2013a). Owing to its structure zircon has the ability to incorporate a wide range of trace elements such as U, Th, Hf and HREE (heavy rare earth elements) (Kohn & Kelly, 2018). Non-stochiometry in zircon can result from either the incorporation of impurities in interstitial sites, and/or the replacement of constituent components Zr or Si with alternative cations (Finch & Hanchar, 2003). The large radius of the crystallographic site of Zr^{4+} (0.84A) means trace elements readily substitute for Zr in the lattice, while Si^{4+} has a smaller ionic radius producing a smaller site (0.26A), less compatible for substitution (Finch & Hanchar, 2003; Kohn & Kelly, 2018). Substitutions can be homovalent or heterovalent, interstitial sites are invoked in the latter to accommodate impurities capable of balancing charges (Speer, 1982; Finch & Hanchar, 2003).

1.1.1 Zircon uses

Zircon is used in a wide range of geochemical investigations owing to its near ubiquity, affinity for trace elements and perceived durability in crustal conditions (Froude et al., 1967; Mojzsis et al., 2001; Wilde et al., 2001; Cawood et al., 2003; Utsomomya et al., 2004; Nemchin et al., 2006; Thomas, 2011). U/Th-Pb zircon geochronology is one of the most commonly used absolute dating tools due to the abundance of U/Th in zircon, the ease of measuring and interpreting concentrations of both parent and daughter isotopes within zoned grains, and the

near ideal behaviour of the system within zircon; with a high closure temperature and low diffusivity of parent and daughter isotopes (Fraser et al., 1997; Nasdala et al., 2001). Zircon excludes Pb^{2+} during crystallization so any Pb present is radiogenic removing an uncertainty surrounding the quantity of daughter material initially present (Nasdala et al., 2001). The development of ion microprobes enabled the dating of zircon over distances of just a few μm making the concentrically zoned grains an asset, with the ability to date multiple zircon-forming events (Williams, 2001).

Early Earth studies commonly involve zircon analysis on the grounds that it is the only readily identifiable mineral from the Hadean Earth (Trail et al., 2007; Harrison, 2009; Valley et al., 2015; Bindeman et al., 2018). Zircon can be used in sedimentary provenance studies (Košler, et al., 2002; Andersen, 2004; Thomas, 2011), as well as investigations of the timing and duration of igneous events (Brown & fletcher, 1999; Kamo et al., 2003; Väisänen & Kirkland, 2008; Cramer et al., 2015; Bucholz et al., 2017; Siégel et al., 2018) and metamorphic events (Cawood et al., 1999; Santosh et al., 2007; Wang et al., 2007; Rojas-Agramonte et al., 2011; Cui et al., 2013). The main limitations to U/Th-Pb geochronology involve the interpretation of growth zoning and the limited understanding of zircon behaviour during metamorphism (Rubatto, 2002). The interpretation of isotopic ages requires the assumption of a closed system with no leaching of constituents, resulting in the alteration of Pb contents and the production of ambiguous ages (Davis et al., 1968). Zircon has a closure temperature >900°C for the U/Th-Pb system, only under extreme thermal conditions can the system be reset by diffusion (Lee et al., 1997). Contrary to this zircon shows evidence of reactivity across a range of metamorphic conditions (Nasdala et al., 2001; Kohn et al., 2015). Zircon has also been proposed as a host for the immobilization of radioactive nuclides from nuclear waste due to its perceived durability (Ewing & Lutze, 1997; Ewing, 1999; Volkkov, 1999; Trocellar & Delmas, 2001). The reactivity of zircon therefore has many implications for a wide variety of fields (Ellsworth et al., 1994) and thus understanding its behaviour is a priority.

1.2 The reactivity of zircon

The traditional view of zircon as a physically and chemically unreactive mineral, highly resistant to metamorphism and erosion (Poldevaart, 1955; Gastil et al., 1967), is quickly becoming antiquated as an increasing number of studies across a range of metamorphic conditions report evidence of zircon reacting through dissolution, recrystallization and crystallization from a fluid (Hoskin & Black, 2000; Rubatto et al., 2001; Williams, 2001; Dempster et al., 2004; Rasmussen, 2005; Rubatto & Hermann, 2007; Dempster et al., 2008a; Hay & Dempster, 2009a; Vonlanthen et al., 2012; Dempster & Chung, 2013; Wang et al., 2014). Temperature was originally viewed as a first order control over the reactivity of zircon with the assumption that it would only react at extreme conditions (Hoskin & Schaltegger, 2003). The perceived immobility of high field strength elements (HFSE) during metamorphism perpetuated the idea of unreactive zircon but a growing body of work shows Zr can be effectively mobilised by hydrothermal fluids (Nasdala et al., 2001; Geisler et al., 2007; Zhao et al., 2016). Pioneering this work was the discovery of pore-filling authigenic titanite within sandstone with high Zr concentrations requiring the transportation of Zr under diagenetic conditions (Rubatto, 2002). There are four main processes that form zircon during metamorphism, (a) crystallization from a melt during high grade metamorphism (Schaltegger et al., 1999; Hermann & Rubatto, 2003; Whitehouse & Platt, 2003) (b) solid-state reactions (Fraser et al., 1997; Degeling et al., 2001), (c) coupled dissolution-reprecipitation (Schwartz et al., 2010; Peterman et al., 2016), and (d) precipitation from a Zr-saturated fluid (Fraser et al., 1997; Bingen et al., 2001; Möller et al., 2003). Dissolution produces textural evidence in the form of irregular, embayed margins on grains and more rarely internal alteration textures (Hay & Dempster, 2009a; Peterman et al., 2016). New crystallization of metamorphic zircon occurs predominantly as outgrowths around existing detrital grains and discrete microzircon (Dempster et al., 2004; Dempster et al., 2008a).

Outgrowths of zircon were first discovered around detrital grains within sandstones (Bond, 1936; Smithson, 1937; Butterfield, 1948), although the source for the Zr and mechanism of formation remained unexplored until more recently (Sláma et al., 2007). Microzircon were first reported by Dempster et al (2004) within greenschist facies slate as a population of discrete, anhedral, very fine zircon crystals. It is well established that zircon containing no oscillatory zoning

is metamorphic (Möller et al., 2003) and microzircon have no apparent internal structure or zoning (Dempster et al., 2004). They have since been reported in a series of low-medium grade metasediments (Dempster et al., 2008a; Dempster et al., 2008b; Hay & Dempster, 2009a; Dempster & Chung, 2013; Wang et al., 2014) but the literature surrounding microzircon is limited. Microzircon demonstrate clear evidence of metamorphic formation, decreasing in both size and abundance throughout the reaction history, coupled with their absence in sedimentary rocks (Dempster et al., 2008a). The presence of the small zircon population within a range of silicates suggests their formation is not due to exsolution from a Zr-rich host (Dempster et al., 2008a).

1.2.1 Zircon behaviour during high grade metamorphism

The behaviour of zircon within high grade anatectic-subanatectic rocks is generally well studied (Hanchar & Miller, 1993; Fraser et al., 1997; Bingen et al., 2001; Whitehouse & Platt, 2003; Thomaschek et al., 2003; Wan et al., 2011; Kröner et al., 2014). Outgrowths on detrital zircon typically increase in abundance and thickness with metamorphic grade (Rubatto, 2002), this more distinct morphological change may explain the prevalence of high-grade studies. Outgrowths measured at amphibolite facies are typically a few μm wide and occur on just ~10% of grains and within anaectic metapelites they are 10s μm wide on ~80% grains (Rubatto, 2002). The increased amounts of zircon growth at higher temperature are attributed to the increased solubility of Zr in a melt phase, a facet of its incompatibility in most crystal structures (Nehring et al., 2010). The melt also provides a vehicle for Zr to be transported to a proximal site where conditions promote growth (Bea et al., 2006; Kelsey et al., 2008; Hallett & Spear, 2015). In order for new metamorphic zircon to form, dissolution of existing populations must occur (Fraser et al., 1997). The increased dissolution produces complex internal structures and irregular margins (Bingen et al., 2001). Alongside dissolution, grains are also subject to mechanical disturbance, in high grade mylonitic rocks fracturing and size reduction of zircon results from strain (Wayne & Sinha, 1988). There has been one report of <1 μm crystals of zircon, morphologically similar to microzircon, forming within garnet in kyanite-zone restitic metapelites (Peterman et al., 2016). This is the only report of microzircon above medium grade. The lack of microzircon documented at higher grade could

potentially be based around; (a) impediment/retardation of microzircon growth, (b) preservational bias, or (c) analytical biases, where mineral separates are readily used in geochronological studies and would exclude microzircon populations (Dempster et al., 2008a; Hay & Dempster, 2009a). At extremely high pressures and temperatures zircon undergoes a transformation to reidite (Finch & Hanchar, 2003) increasing in density by ~11% (Akaogi et al., 2018). The conversion is rare occurring predominantly in impact craters under ultra-high pressure conditions equivalent to loading at depths of ~330 km (Akaogi et al., 2018).

1.2.2 Zircon behaviour during low-medium grade metamorphism

Analyses of zircon populations in low grade metamorphic rocks were initially limited to authigenic outgrowths predominantly in clastic sedimentary rocks (Bond, 1936; Butterfield, 1948; Saxena, 1966; Baruah et al., 1995). Only in the last few decades following the increased use of scanning electron microscopy and advancement in analytical techniques have finer metasedimentary populations been explored (Dempster et al., 2004; Rasmussen, 2005; Hay & Dempster, 2009a; Hay et al., 2010). There is evidence of significant zircon dissolution and growth at temperatures as low as ~250^{o}C, within prehnite-pumpellyite facies metasediments (Rasmussen, 2005). During burial of sandstones heated to <100^{o}C minor outgrowths form and local alteration of zircon occurs (Hay & Dempster, 2009b), illustrating that zircon is reactive at extremely low temperatures. The delicate nature of these low grade outgrowths means they are unlikely to survive sedimentary processes posing preservational bias problems (Hay & Dempster, 2009b). Detrital zircon margins are typically embayed and non-planar (Hay & Dempster, 2009a), these grains contain thin outgrowths (Rasmussen, 2005; Kohn & Kelly, 2018), and where present microzircon may dominate the zircon population at low grade (Dempster et al., 2004). All published studies of microzircon have been between upper greenschist to lower amphibolite facies regionally metamorphosed rocks leaving higher grade and contact metamorphosed rocks unexplored. Interbedded pelitic and psammitic schists, apparently similar to those within which microzircon are reported, yield no evidence of microzircon (Rasmussen, 2005; Hay et al., 2010) raising questions regarding the controls on its formation and/or biases in the observations. The main gap in understanding progressive zircon reactivity is within medium grade rocks with studies typically focussing on low and high grade

conditions. A study by Dempster et al (2008a) of lower amphibolite facies schists shows a large population of microzircon compared to similar upper greenschist samples (Dempster et al., 2004), despite this link amphibolite facies literature remains limited.

Zircon reactivity over a wide range of conditions poses uncertainty regarding which stages in a metamorphic history promote dissolution and (re)crystallization. It's believed certain P-T conditions are more conducive to the growth of zircon and others to dissolution (Kohn & Kelly, 2018). A range of studies show zircon formation during prograde metamorphism (Liati & Gebauer, 1999; Beckman & Möller, 2018), retrograde metamorphism (Fraser et al., 1997; Roberts & Finger, 1997; Kohn et al., 2015) and at peak metamorphism (Liati & Gebauer, 1999; Hoskin & Black, 2000; Rubatto et al., 2001; Rubatto, 2002).

1.3 Factors influencing zircon reactivity

The 'ideal' zircon grain is stable under crustal and upper mantle conditions (Geisler et al., 2007), however grains with high defect densities or unusual chemical compositions are prone to dissolution (Kohn & Kelly, 2018), acting as a possible source of Zr for new zircon growth (Rubatto, 2002). The disparity between zircon reactivity in apparently similar rocks or between autonomous zircon within a single rock (Nasdala et al., 2001) raises questions about the controls over zircon reactivity at both the whole-rock and grain scale.

1.3.1 Temperature

Temperature was traditionally the primary factor considered to impact zircon reactivity, where only rarely at conditions below upper-amphibolite to granulite facies could dissolution and crystallization occur (Hoskin & Schaltegger, 2003). Complications with understanding temperature arise from the nature, number and timing of thermal pulses, all of which will impact zircon reactivity (Williams, 2001). A range of analyses carried out on low temperature 'inert' zircon deemed unreactive yield ambiguous results (Geisler et al., 2001; Degeling, 2002). Zircon shows relatively low thermal expansion with only slight lengthening of the ZrO_8 dodecahedra during heating meaning Zr release at higher temperatures is unlikely to be solely attributable to lattice relaxation (Finch & Hanchar 2003). At higher

temperatures, the increased kinetic energy of Zr allows its transportation more effectively (Weber et al., 1994; Nasdala et al., 2001). Additionally, where temperatures are higher, reactions are catalysed as diffusion rates increase and ionic mobility is enhanced promoting Zr transportation, in this sense temperature can assist in promoting thermodynamic equilibrium (Finch & Hanchar, 2003). There are many other factors, commonly overlooked, which require consideration alongside temperature.

1.3.2 Radiation damage

The durability of many accessory phases enriched in HFSE (high field strength elements) is compromised by alpha decay, as such amorphization can increase the reactivity of zircon by altering its physical and chemical properties (Holland & Gottfried, 1955; Nasdala et al., 2001; Balan et al., 2003; Anderson et al., 2008). The properties that make zircon useful for geochronometry have a detrimental impact on its durability (Hay et al., 2010). While alpha radiation and spontaneous fission are responsible for only minor damage, ballistic collisions resulting from the recoil of alpha daughter nuclei directly amorphizes micrometric sections of the lattice (Weber et al., 1994; Nasdala et al., 1996; Balan et al., 2003; Geisler et al., 2007). The decay produces amorphous areas where chemical transport is promoted relative to adjacent crystalline areas (Weber et al., 1994; Geisler et al., 2007). Zircon grains contain variable concentrations of radioactive parent elements influencing the likelihood of a grain to become metamict, zircon typically contains between 5-4000 ppm U and 2-2000 ppm Th (Ellsworth et al., 1994). Zircon is chemically heterogeneous (Köppel & Grünenfelder, 1971; Nasdala et al., 1996), since radiation damage is a function of the U/Th concentration and time, the non-uniform distribution of U/Th produces a structurally variable grain (Chakoumakos et al., 1987; Smith et al., 1991; Hay & Dempster, 2009a). The quasi-amorphous areas formed from ballistic collisions become metamict when overlap of the damaged lattice occurs eliminating islands of crystalline zircon (Balan et al., 2003). Consequently, zircon has two end members which behave antithetically during metamorphism; unreactive, crystalline zircon and its reactive, metamict counterpart (Nasdala et al., 2001).

The enhanced reactivity of metamict grains is attributed to increased diffusion rates within the damaged lattice increasing its susceptibility to leaching and differential

recrystallization (Ewing et al., 1982; Ellsworth et al., 1994; Meldrum et al., 1998; Farnan et al., 2003; Hay & Dempster, 2009a). Dissolution is the response of a mineral to achieve a lower energy state, within metamict zircon the larger number of defects increases the interfacial energy and thus its susceptibility to dissolution (Ruiz-Agudo et al., 2014). As well as the direct weakening from metamictization, swelling of amorphous areas by up to 18% generates a series of radial fractures enabling fluid infiltration to the interior of detrital grains, and creating further potential reaction fronts (Balan et al., 2003; Hay & Dempster, 2009a). Metamict zircon are also more prone to contain a hydrous component in their structure, lowering the stability of grains further (Botis et al., 2013).

Radiation damage is stored in zircon provided it is not annealed, annealing can occur simply through the reformation of disrupted bonds by reordering of neighbouring atoms or through the recrystallization of damaged areas (Weber et al., 1994; Nasdala et al., 2001). Metamict zircon may begin to recover at protracted periods above 225-250^{o}C in the presence of a fluid (Nasdala et al., 2001; Kohn & Kelly, 2018). For full structural recovery, annealing occurs in stages and requires temperatures in excess of 900-1000^{o}C (Nasdala et al., 2004; Deer et al., 2013a; Rubatto, 2017). At high temperatures annealing is promoted producing a smaller population of reactive metamict grains while at lower temperature the proportion of metamict grains is larger promoting dissolution and yielding Zr, and thus more potential zircon (Dempster et al., 2008a).

1.3.3 Fluid composition and availability

The formation of microzircon and zircon outgrowths on non-metamict grains requires the transportation of Zr beyond the grain scale (Rasmussen, 2005). Dissolution-reprecipitation can proceed with minimal fluid and limited Zr solubility, however it is limited to within a single detrital grain (Rubatto, 2017). The transportation of Zr to a distal site requires a corrosive fluid (Rasmussen, 2005). Halogens released during dehydration reactions allow the mobilisation and transportation of HFSE as F complexes (Rubin et al., 1993; Rasmussen, 2005). Zr solubility also increases with pressure as the alkalinity and Si-content of fluids rises (Ayers et al., 2012; Rubatto, 2017), it follows that the presence of a corrosive fluid is particularly important at lower grade.

Reaction rates are highly dependent on the presence of a hydrothermal fluid (Putnis & Austrheim, 2010). With a fluid present transport of elements can occur via advection and diffusion through an interconnected pathway and as such activation energies for a reaction in the presence of a fluid are typically 10 orders of magnitude lower than solid-state transformations (Putnis & Austrheim, 2010; Putnis, 2015). Solid state replacement processes also rely on the presence of defects, such as intrinsic vacancies within a crystal structure, which increase with increasing temperature (Putnis, 2002; Altree-Williams et al., 2015). At lower temperature vacancies are predominantly extrinsic meaning dissolution-reprecipitation is promoted over kinetically difficult solid-state transformations (Altree-Williams, 2015). Dissolution-reprecipitation requires the dissolution of a mineral by an aqueous fluid producing an interfacial film at the reaction front which is supersaturated with respect to the product phase, resulting in subsequent reprecipitation (Ruiz-Agudo et al., 2014). The availability of fluids is locally controlled by the presence of pathways that enable infiltration, porosity can be intrinsic or deformation-induced (Putnis & Putnis, 2007; Putnis & Austrheim, 2010; Putnis, 2015). Deformation is arguably as important as the presence of a fluid in a rock with a low intrinsic porosity such as fine-grained pelitic metasediments (Dempster et al., 2008a; Rubatto, 2017).

1.3.4 Nucleation

While microzircon have been reported in a range of low grade metasedimentary rocks (Dempster et al., 2004; Dempster & Chung, 2013) they have not been reported in apparently similar studies where other evidence of zircon reactivity is preserved (Rasmussen, 2005; Hay et al., 2010). Consequently, an understanding of what promotes the formation of outgrowths in place of microzircon neoblasts is essential. Difficulty nucleating has been suggested as one possible explanation for the formation of microzircon (Dempster et al., 2008a). New zircon should preferentially grow on existing detrital grains (Kohn, 2016), where new atoms are added to vacant sites at the surface forming outgrowths (Higgins, 2006). Nucleation is promoted by higher temperatures and the presence of a structure, i.e. remnants of detrital grains, where one or both are unfavourable zircon may exist as a separate authigenic population (Dempster et al., 2008a).

1.3.5 Bulk rock composition

The stability of zircon is also a function of the bulk-rock chemistry. Zircon within a Zr-poor rock will react at a lower temperature than its Zr-rich counterpart as the stability of zircon is a function of the bulk Zr content of a rock (Kelsey & Powell, 2011). The balance of Zr within a rock requires consideration, namely the Zr-bearing minerals that can be dissolved more efficiently than zircon as internally-sourced Zr can be garnered from other phases (Fraser et al., 1997). Metamorphic zircon formation tends to be more common in pelites, rather than mica-poor, clastic metasediments (Dempster et al., 2004; Rasmussen, 2005; Dempster et al., 2008a). Various explanations have been provided to explain the disparity e.g. the different bulk chemistry of the rocks (Rasmussen, 2005). Pelites typically contain F concentrations between 780-940ppm, producing potentially more corrosive fluids than psammite where F contents range from 180-449ppm (Koritnig, 1969; Gao et al., 1998; Rasmussen, 2005). While the differences in the structural state of zircon between the two rock types has been invoked elsewhere; the pelite, and the original mudstone, contains a larger proportion of smaller radiation-damaged detrital grains potentially yielding more available Zr (Dempster & Chung, 2013).

1.3.6 Conclusion

Recent literature has focussed on the impact of metamorphism on zircon as many now agree it is not the unreactive mineral it was once perceived to be (Nasdala et al., 2001; Dempster et al., 2004; Kelly & Harley, 2005). Microtextural analysis is applied to understand the change to zircon morphology during events and the application of this to geochronology as a new multistep approach to dating (Vavra et al., 1999; Rubatto, 2002; Breeding et al., 2004; Kelly & Harley, 2005). While the increased identification of zircon reactivity promotes a new narrative in which zircon is a dynamic phase, the role of a variety reactivity-promoting factors remains ambiguous. Understanding zircon behaviour during metamorphism presents the possibility of utilising zircon as a tracer of metamorphic events as well as improving zircon geochronology.

Chapter 2 Zr-bearing phases

2.1 Zr repositories

Zr is a relatively abundant trace element within crustal rocks, with whole rock Zr abundance ranging from 100-500ppm, and more rarely up to 1000ppm in metapelitic rocks (Kelsey & Powell, 2011). Zr is inherited from sedimentary protoliths meaning the mass balance should remain consistent throughout the metamorphic history (Degeling et al., 2001; Kohn et al., 2015), except in an open system where hydrothermal fluids may act as an external source of Zr (Fraser et al., 1997). As the primary constituent of zircon, an awareness of whole-rock Zr contents and the minerals which incorporate a significant amount of Zr aids in understanding zircon formation through time (Degeling et al. 2001). Minerals containing >10 ppm Zr are potential parents to new metamorphic zircon (Degeling, 2002; Bea et al., 2006). It was originally believed that Zr was only accommodated by zircon in most rocks (Watson & Harrison, 1983) but improved analytical techniques and the advent of mass spectrometry produce a clearer picture of Zr behaviour. There are in total 99 known primary Zr minerals but only 3 of these are widely abundant; baddeleyite which is most common in olivine-normative rocks, zircoclinonolite-zirkelite, typically restricted to nepheline-normative rocks and zircon (Bea et al., 2006). Zr in zircon has a theoretical stochiometric value of 49.76% but due to a range of cation substitutions zircon will rarely, if ever, reach this value (Bea et al., 2006). For example, zircon always contains Hf up to ~1 wt% (Deer et al., 2013a). The substitution occurs as Hf^{4+} and Zr^{4+} are geochemically almost identical (Claiborne et al., 2006). Aside from these primary minerals Zr commonly occurs in minerals for which it is not an essential constituent (Hoskin & Schaltegger, 2003).

Zircon equilibrium in metamorphic rocks is highly temperature dependant (Kohn & Kelly, 2018). Up to 99% of Zr is hosted in zircon at low grade (Kohn & Kelly, 2018) however with increasing temperature additional mineral phases grow and incorporate Zr, as a result the mode of zircon must decrease (Degeling, 2002; Kohn et al., 2015). During prograde metamorphism zircon is dissolved (Fraser et al., 1997; Bingen et al., 2001; Degeling et al, 2001; Degeling, 2003) and the evidence is preserved as dissolution/alteration textures in detrital grains. During exhumation and uplift, as the temperature drops mineral phases that were once

stable undergo resorption releasing Zr and promoting the precipitation of metamorphic zircon (Fraser et al., 1997; Bingen et al., 2001). The mass balancing of Zr for microzircon has never been attempted and similarly their growth has never been pinned to a specific point on the P-T path although textures indicate their growth during prograde metamorphism (Dempster et al., 2008a).

2.1.1 Zr in accessory phases

Accessory minerals by definition comprise <5% of the volume of a rock (Tropper, 2014) however they may have a large influence on the mobility of trace elements such as Zr (Anderson et al., 2008). Accessory minerals, mainly zircon (ZrO_2), rutile (TiO_2) and ilmenite ($FeTiO_2$), contain >80-90% of the whole-rock Zr budget (Green, 1994; Bea & Montero, 1999; Kohn & Kelly, 2018). Zr can replace Ti easily as they have similar ionic radii and are homovalent, as such Zr is common in ilmenite and rutile (Pearce, 1990; Kelsey & Powell, 2011). Ilmenite is typically more common in metamorphic rocks (Kelsey & Powell, 2011) but rutile can incorporate larger amounts of Zr (Degeling, 2002). Two populations of ilmenite and rutile are common in metamorphic rocks, (a) authigenic aligned populations, and (b) detrital grains trapped as inclusions (Ague & Eckert, 2012). Bingen et al (2001) present textural evidence of ilmenite acting as a source of Zr for new zircon growth through coronas and growth structures. Ilmenite within high grade metabasic rocks have the highest reported concentration of Zr at 3850 ppm (Bingen et al., 2001) while lower abundances are reported in more felsic rocks and anorthosites <114 ppm (Charlier et al., 2007). There is limited data available for Zr contents in metasedimentary ilmenite however the suggestion of decreasing Zr with decreasing silica content within igneous studies (Bea et al., 2006) may indicate low concentrations within authigenic ilmenite in pelites and psammites. While detrital ilmenite Zr contents are inherited, silica-rich fluids within metasediments may impact its stability. The most studied accessory phase is rutile due to the use of Zr-in-rutile geothermometry (Zack et al., 2004; Jiao et al., 2010; Meyer et al., 2011; Kooijman et al., 2012). The modal abundance of rutile within metamorphic rocks is temperature-dependant, within pelites rutile concentrations increase from 30 ppm at 430°C up to 8400 ppm at 1100°C, containing 100s-1000s ppm Zr (Degeling, 2002; Zack et al., 2004; Kohn & Kelly, 2018). During cooling, baddeleyite exsolution can occur in rutile within metabasites, releasing ZrO_2 into a less stable phase which can react with quartz to form zircon (quartz +

baddeleyite → zircon) (Zack et al., 2004; Beckman & Möller, 2018). A similar reaction can occur in ilmenite where baddeleyite exsolution produces zircon rims around detrital ilmenite grains (Bingen, et al., 2001; Morisset & Scoates, 2008). At greenschist facies rutile can react to form titanite, provided Ca is available (Cave et al., 2015). Rutile contains on average 1360 ppm Zr while titanite contains just 302 ppm Zr (Cave et al., 2015). The rutile to titanite transformation releases 504 ppm Zr from rutile that is not incorporated into the product titanite (Cave et al., 2015). Any additional Zr released from rutile cannot be incorporated into titanite and so will be released liberating up to 63% of the Zr in rutile. Rutile and ilmenite therefore have the potential to act as a source and sink of Zr at different stages on the P-T path. This is similar to the behaviour of zircon and potentially many other Zr-bearing accessory minerals.

Aside from Ti-bearing minerals, Zr can substitute into less compatible mineral lattices (Bea et al., 2006). The breakdown of these non-Ti-bearing minerals also increases the chance of zircon formation as the Zr is less likely to form another Ti-bearing phase (Degeling, 2002). Allanite often contains high Zr contents up to 400 ppm (Bea et al., 2006) however, the contents are variable based on its ability to incorporate a wide range of divalent, trivalent and tetravalent major elements, trace elements and REE with a range of ionic radii (Gieré, 1986; Ercit, 2002). The formation of xenotime is commonly associated with the growth of zircon and the two often co-exist and exhibit isotypic behaviour, as such xenotime contains highly variable Zr contents up to ca. 20 wt% (Casillas et al., 1995; Bea & Montero, 2006). Accessory minerals such as monazite, apatite and other Fe oxides typically have extremely low Zr contents, having a negligible impact on the overall Zr budget (Kelsey & Powell, 2011).

2.1.2 Zr in major mineral phases

Zr behaviour in major minerals is less well constrained than within accessory phases (Kooijman et al., 2012). Several silicates and oxides have been found to contain small yet significant concentrations of Zr (Bea et al., 2006). An understanding of the Zr contents within these rock-forming minerals is vital, despite their lower Zr concentrations the high modal abundance of major phases mean they have the capacity to contain a larger proportion of the whole-rock Zr budget than accessory minerals (Villaseca et al., 2007). Garnet, amphibole and

pyroxene can represent significant repositories of Zr (Fraser et al., 1997; Kohn et al., 2015), Zr uptake by these phases should be much lower in pelites than metabasites which have larger proportions of these minerals (Kohn et al., 2015).

Garnet is generally thought to contain <100 ppm Zr (Degeling, 2002; Kelsey & Powell, 2011) but has a Zr-rich end member kimzeyite ($Ca_3Zr_2Al_2SiO_{12}$) with reported Zr contents up to 29.9 wt% (Milton et al., 1961) and 18.4 wt% (Jamtveit et al., 1997). Kimzeyite is rare and garnet most commonly occurs as almandine where Zr substitutes in place of other cations in the lattice (Kelsey & Powell, 2011). Substitution in almandine involves the replacement of Fe^{3+} or Al^{3+} with Zr^{4+} on the octahedral site and the coupled substitution of Si^{4+} with Al^{3+} on the tetrahedral site (Fraser et al., 1997; Degeling et al., 2001; Deer et al., 2013b). As temperatures increase the amount of Zr in garnet typically increases up to 150 ppm in granulite facies rocks (Ague & Eckert, 2012). Garnet porphyroblasts in the Rogaland aureole contain just 1 ppm Zr at 700°C increasing to 139 ppm at 900°C (Degeling, 2002). The increase is attributed to thermal expansion of the lattice promoting the substitution of larger Zr (0.72 A) in place of Fe (0.65 A) (Degeling, 2002). Based on this mechanism of substitution, more Fe-rich garnets will be able to incorporate higher amounts of Zr (Degeling, 2002). Relatively high Zr concentrations have been reported within pyrope (Mason & Allen, 1973) as well as grossular (Westrenen et al., 2001). Zr values for spessartine in metamorphic rocks remain uninvestigated. However, owing to Mn having the smallest ionic radius spessartine would theoretically contain less Zr than almandine, pyrope and grossular where larger sites for substitution are available. Bea et al. (2006) note extremely low Zr concentrations within garnets in low grade pelites in comparison to those within meta-igneous rocks suggesting Zr contents are, at least in part, dependant on the whole-rock chemistry.

Substitution of major element phases in staurolite is well explored with the replacement of tetravalent cations (Si^{4+}) with trivalent cations (Al^{3+}) or divalent cations (Mg^{2+}, Fe^{2+}) (Deer et al., 2013c). Trace element data is limited, however one study of staurolite within amphibolite facies pelites reports up to 193 ppm Zr, higher than the Zr contents of garnet in the same rock (Corrie & Kohn, 2008). Staurolite typically does not have a wide range of chemical compositions but the presence of trivalent and divalent Fe cations in the lattice (Hawthorne et al.,

1993) means a substitution similar to that in garnet could be invoked. Amphibole, particularly hornblende, and pyroxene are both subject to contrasting reports on their Zr contents, HFSE abundances tend to be controlled by their major element composition (Marks et al., 2004). Both pyroxene and amphibole contain optimal sites around 0.70 A which could accommodate 0.72 A Zr (Marks et al., 2004). Clinopyroxene contains the highest concentrations of Zr in Mg-rich rocks, up to 158 ppm (Bea et al., 2006). Orthopyroxene more rarely contains elevated Zr up to 24 ppm in felsic granulites (Degeling, 2002; Bea et al., 2006). Amphibole can accommodate elevated Zr concentrations within alkaline and calc-alkaline igneous rocks (Marks et al., 2004). While within metabasites increasing Fe and Na have been linked to high Zr values in amphibole (Marks et al., 2004). Silicate melts are a potentially significant source and sink of Zr, with the ability to achieve contents in excess of 1000ppm (Kelsey & Powell, 2011). However, melts are unlikely to reach this concentration without zircon precipitation and typically become saturated at a few hundred ppm even at elevated temperatures (Watson & Harrison, 1983; Boehnke et al., 2013).

Biotite contains among the lowest Zr contents of the silicates despite having a Ti-rich high temperature end-member, phlogopite (Degeling, 2002). The anomalously low concentration in biotite is ascribed to its reduced stability at higher temperatures where thermal expansion is most effective (Degeling, 2002). However, based on the almost identical ionic radii of Zr and Ti (Kelsey & Powell, 2011) theoretically the thermal expansion required to enable Zr replacement in phlogopite should be negligible. Muscovite consistently contains low Zr contents below detection (Bea et al., 2006; Kelsey & Powell, 2011). There is limited trace element data available for chlorite, none of which report Zr concentrations. Chlorite is a phyllosilicate, structurally similar to biotite and muscovite (Deer et al., 2009) which contain little to no Zr. On this basis and due to its simple chemistry, chlorite may not have the ability to accommodate significant quantities of Zr. Feldspar, both alkali and plagioclase, in igneous and metamorphic rocks contain Zr contents commonly below detection probably linked to their restricted chemical composition and thus the absence of adequate sites in the lattice for substitution (Bea et al., 2006; Kohn et al., 2015).

Releasing Zr from these sinks occurs through dissolution of the Zr-bearing phase (Fraser et al., 1997; Bingen et al., 2000; Whitehouse & Platt, 2003). Zircon will only form if the Zr released from the breakdown of the phases is not incorporated into the product, for example if garnet breakdown yields orthopyroxene the Zr may be accommodated in the latter preventing new zircon growth (Degeling et al., 2001). The impact that breakdown of an individual phase has on the zircon population depends on the abundance of Zr-bearing phases. If garnet contains a small amount of Zr, its breakdown would be unlikely to result in the growth of significant quantities of zircon. However, in the absence of a melt or Ti-oxides garnet may contain a large proportion of the effective Zr budget (Kelsey & Powell, 2011). Therefore, an understanding of the impact a single mineral phase can have on the available Zr budget is dependant on the whole rock Zr budget (Kelsey & Powell, 2011).

Zr values for all major silicate minerals, but especially garnet, should be viewed with caution, based on the presence of unrecognised zircon inclusions. Microzircon inclusions are particularly abundant within garnet, present in numbers up to $8x10^6$ within a 5 mm porphyroblast (Dempster et al., 2008). This would produce values up to 100 ppm higher for Zr within the garnet (Dempster et al., 2008a). Microzircon remain largely unrecognised, if the inclusions are not mapped prior to Laser ablation inductively coupled plasma mass spectrometry (LA-ICP-MS) or ion microprobe analyses, the method predominantly used in the studies listed, the probability of directly measuring one or more of these zircon is high given typical analytical volumes, producing anomalous Zr values.

2.2 Porphyroblasts as potential monitors of prograde changes in the zircon population

Zr is a potentially important trace element in garnet, in order to understand zircon dissolution and recrystallization the response of garnet to metamorphism is also important. Garnet is additionally important because it has the ability to record the prograde history of the rock and hence can be used to understand the prograde history of zircon. The following section will discuss the prograde evolution of garnet within Barrovian Schists in order to understand garnet as a canvas to interpret changes to zircon populations.

2.2.1 Prograde garnet evolution

Garnet is a common mineral in metamorphic rocks and more rarely occurs in igneous and sedimentary rocks (Deer et al., 2013b). It is stable over a wide range of pressures, temperatures and bulk compositions (P-T-X) (Chakraborty & Ganguly, 1991). The general composition of garnet is $X_3Y_2(SiO_4)_3$ where X represents a site for divalent cations (e.g. Mg^{2+}, Fe^{2+}, Mn^{2+}) and Y for trivalent cations (e.g. Al^{3+}, Fe^{3+}) (Robinson et al., 1971; Deer et al., 2013b). Garnet consists of a series of end-member compositions (Grew et al., 2013), the four most common in metasediments are almandine $Fe_3Al_2(SiO_4)_3$, pyrope $Mg_3Al_2(SiO_4)_s$, spessartine $Mn_3Al_2(SiO_4)_3$, and grossular $Ca_3Al_2(SiO_4)_3$ (Deer et al., 2013b). The presence of a divalent, trivalent and tetravalent site in its lattice means garnet can accommodate a variety of cations with a range of different ionic radii and charges (Li et al., 2018). Structurally garnet has been compared to zircon (Robinson et al., 1971; Finch & Hanchar, 2003), consisting of alternating ZO_4 tetrahedra and YO_6 octahedra sharing corners to produce a 3d network within which X/divalent ions are surrounded by oxygen cubes (Deer et al., 2013b). Garnet is the most studied mineral in metamorphic petrology owing to a range of properties that make it a useful monitor of metamorphic processes (Degeling, 2001). Garnet is characterised by sluggish volume diffusion, even at sub-solidus temperatures it shows relatively low diffusivity of trace and major elements (Martin et al., 2011). Because of the slow diffusion of divalent cations garnet has the ability to preserve chemical zoning (Carson, 2006). Garnet zoning could be used as a geothermobarometer to track changes in P-T-X conditions during metamorphic events (Jiang & Lasaga, 1990; Spear et al., 1991; Raimondo et al., 2017). Additionally, it has a high resistivity to elastic deformation allowing its use as a geobarometer where pressure can be directly measured from the analysis of mineral inclusions (Baxter et al., 2017). The resistance ensures that during decompression the lattice doesn't expand enabling the preservation of a significant proportion of the lithostatic pressure from formation (Baxter et al., 2017).

The Barrovian metamorphic sequence, first defined in the northeast of Scotland by Barrow (1983; 1912), records a systematic change in mineralogy through progressive regional metamorphism of clastic sediments based on the first appearance of index minerals (Ague, 1997). Barrow's findings were subsequently

applied to a series of moderate pressure, high temperature orogenic settings which showed the same mineralogical patterns (Gangopadhyay & Sen, 1972; Raymond, 1995; Carosi et al., 1998; Will et al., 2004). The well-studied sequences provide a natural laboratory in which to assess the nature of mineralogy within convergent settings (Viete et al., 2011), with garnet especially well studied e.g. Atherton, 1968, Dempster, 1985, Viete et al., 2011.

2.2.1.1 Garnet growth

Garnet forms from the breakdown of chlorite in Barrovian sequences at upper greenschist facies (Harte & Hudson, 1979). Porphyroblast growth requires the dissolution of source minerals, transportation of the chemical constituents to a nucleation site and the rearrangement of these constituents to form the product garnet which is sufficiently sized to be thermodynamically stable (Lanari & Engi, 2017). Once nucleation of proto-porphyroblast garnet occurs growth is centred around the existing grain over the formation of new nuclei, which requires more energy (Lanari & Engi, 2017). The rate limiting factors during garnet growth are commonly nucleation and intergranular diffusion (Carlson, 2011). As garnet grows it records changing equilibrium conditions producing concentric chemical zoning (Loomis, 1983). Chemical zoning is the result of differential availability and partitioning of elements between garnet and the matrix in response to changing P-T-X conditions (Atherton & Edmunds, 1966; Loomis, 1983; Martin et al., 2011). Concentric zoning of garnet was discovered in the advent of the electron microprobe in the 1950s-1960s (Ramberg, 1952; Kretz, 1959; Hollister, 1966; Atherton & Edmunds, 1966; Harte & Henley, 1966). Garnet typically exhibits zoning from core to rim (Harte & Henley, 1966; Atherton & Edmunds, 1966; Hollister, 1966; Atherton, 1968; Dempster, 1985; Chakraborty & Ganguly, 1991; Gatewood et al., 2015; Dempster et al., 2017a) as well as diffusive zoning around inclusions (Tracy, 1982; Hames & Menard, 1993), along fractures and cracks (Hames & Menard, 1993; Whitney, 1996), and in contact with the matrix (Tracy et al., 1976; Baxter et al., 2017; Dempster et al., 2017b). Concentric zoning of divalent major element cations (Ca^{2+}, Mn^{2+}, Mg^{2+} & Fe^{2+}) in garnets is well studied and typically predictable, showing systematic changes to zoning profiles with metamorphic grade (Atherton, 1968; Yardley, 1977; Dempster, 1985; Chakraborty & Ganguly, 1991). Up to staurolite zone divalent cations show ‘normal zoning’, with a bell-shaped Mn profile decreasing from core to rim and complementary

bowl-shaped Fe & Mg profiles (Dempster, 1985; Chakraborty & Ganguly, 1991; Ikeda, 1993). High core Mn values are attributed to the early partitioning of Mn into garnet owing to Rayleigh fractionation depleting Mn from the matrix (De Béthune et al., 1975; Banno & Chii, 1978; Ganguly, 1991). Garnet traps the available Mn in its structure producing progressively lower concentrations in the later formed rims (Viete et al., 2011). As the Mn content decreases in garnet it is substituted by Fe and Mg producing diametric profiles (Chakraborty & Ganguly, 1991).

At the greenschist-upper greenschist facies transition, when garnet forms, the Ca^{2+} available is buffered by plagioclase (Franceschelli et al., 1982; Maruyama et al., 1982). With increasing metamorphic grade, the anorthite content of plagioclase increases until the peristerite solvus where oligoclase appears, co-existing with albite initially but increasing in abundance at higher temperatures (Brown, 1962; Crawford, 1966). At the peristerite solvus the almandine isograd is crossed and garnet incorporates Ca which was originally solely accommodated by the anorthite component in plagioclase (Crawford, 1966). As oligoclase increases in abundance the amount of Ca incorporated into the garnet decreases producing a Ca-rich core and generally Ca-poor rims (Brown, 1962; Franceschelli et al., 1982). Ca^{2+} zoning in garnet is much less predictable than the other major cations, ranging from unzoned to complex zoning within a single sample (Ganguly & Chakraborty, 1991). Unlike Mn, Ca is a constituent component in many other mineral phases, the appearance and disappearance of these Ca-bearing phases will alter the distribution coefficient of Ca in garnet resulting in an irregular profile (De Béthune et al., 1975). It's also been suggested Ca equilibrium is achieved at a smaller scale than the other cations owing to its extremely low diffusion rate in garnet preserving irregularities in grossular profiles (Chernoff & Carlson, 1997). At slightly higher grade, within sillimanite zone rocks, garnet remains consistent in zoning with Fe and Mg increasing from core to rim and Mn & Ca generally decreasing. Additionally, at sillimanite-zone a reverse zoned rim appears with flattening of the Mn profile and reversal of Fe profiles (Edmunds & Atherton, 1971; Yardley, 1977; De Béthune et al., 1975; Dempster, 1985; Ikeda, 1993). The prevalence of reverse-zoned rims adjacent to biotite and eccentric nature of the zoning independent of the porphyroblast shape suggests it is not a growth feature (De Béthune et al, 1975; Dempster, 1985). Cation exchange with

matrix phases during retrogression poses one possible explanation, either between garnet and biotite (Dempster, 1985) or between garnet and chlorite (Banno & Chii, 1978). Elsewhere high Mn rims are interpreted as a feature of garnet resorption (Grant & Wiblen, 1971; De Béthune et al., 1975; Banno & Chii, 1978) whereby garnet dissolution releases some Mn which is not compatible with any growing phases and so begins to diffuse back into the remaining garnet, inwards from the reaction front at the margin producing a gradual sloping profile (De Béthune et al., 1975).

2.2.1.2 Diffusion in garnet

Garnet is a refractory mineral (Hollister, 1966). The sluggish intergranular and intragranular diffusivity of ions within garnet preserves chemical zoning, impeding reequilibration (Baxter et al., 2017). As with most silicate minerals diffusion rates in garnet increase exponentially with temperature (Yardley, 1977) resulting in the modification of growth zoning by kinetic relaxation over time (Carlson, 2006; Caddick et al., 2010; Baxter et al., 2017). Multicomponent diffusion occurs within garnet where multiple major elements undergo diffusion concomitantly, when one divalent cation diffuses out of a domain it is replaced by another maintaining stochiometry (Ague & Carlson, 2013). Contradictory reports of the temperature at which garnet zoning relaxes have raised questions about what stage diffusion becomes effective enough to produce a chemically homogeneous grain (Jiang & Lasaga, 1990). It was previously believed that at upper sillimanite grade zoning would be eliminated from garnet cores leaving only a reverse-zoned rim (Dempster, 1985), but the discovery of intact-zoned garnets alongside those with flat compositional profiles proves the difficulty in predicting a specific point on the P-T path where chemical homogenisation occurs (Yardley, 1977; Dempster, 1985; Florence & Spear, 1991; Calson & Schwarze, 2008; Caddick et al., 2010). There appear to be many factors that influence the elimination of zoning, one being garnet grain size. In order to eliminate zoning the diffusion of all cations must be effective at the grain scale, so the larger the grain is the higher the temperature or longer the duration of diffusion required to remove zoning (Dempster, 1985). Elements each have different diffusion rates within garnet, Mn has been reported to achieve small-scale equilibrium at upper greenschist facies while Ca may require in excess of middle amphibolite facies conditions meaning

intergranular diffusion of Ca is slower (Carlson, 2002; Spear, 2014; Dempster 2017b).

Garnet is zoned in trace elements such as Cr, Y and Zr (Griffin et al., 1989; Hickmott & Shimizu, 1990; Degeling et al., 2001; Turkina & Sukhorukov, 2017). Zr^{4+} zoning in garnet is reported solely in the rim, increasing by more than a factor of 10 at the margins, while the interiors of grains are consistently low (Schwandt et al., 1996; Degeling, 2002; Koreshkova et al., 2017). The Zr-rich rims have been linked to changing Zr equilibrium during garnet growth (Schwandt et al., 1996) however they could be; (a) a facet of Zr diffusion back into garnet during partial resorption, similar to Mn (Degeling, 2002), (b) a measure of the preference of Zr for Fe-rich garnet concentrated at the rim, or (c) a measure of microzircon populations which could dominate marginal garnet. Zr zoning is most pronounced in garnet-zone porphyroblasts while at staurolite-zone the change at the rim is less pronounced and by sillimanite zone the Zr zoning is reportedly irregular (Schwandt et al., 1996). Aside from Zr-rich rims the distribution is reasonably uniform, not concentrated around fractures or inclusions (Degeling et al., 2001).

Alteration of garnet zoning can occur by direct cation exchange and substitutions, larger scale intracrystalline diffusion (Caddick et al., 2010) and dissolution-reprecipitation (Martin et al., 2011; Dempster et al., 2017a). Trace element zoning in garnet can be preserved to higher temperatures, commonly granulite facies, long after major element zoning has been erased (Hickmott et al., 1987; Baxter et al., 2017). However, there are concerns raised about which trace elements actually achieve rock-scale chemical equilibrium during growth, particularly Zr (Chernoff & Carlson, 1997; Chernoff & Carlson, 1999).

2.2.1.3 Garnet modification

Garnet commonly interacts with fluids and melts to form secondary phases e.g. the formation of chlorite during retrogression (Lanari & Engi, 2017). At high temperatures garnet becomes less stable and undergoes dissolution to form staurolite (Harte & Hudson, 1979; Dempster et al., 2017a) and sillimanite (Dempster et al., 2017a; Dempster et al., 2018) predominantly via dissolution-reprecipitation (Dempster et al., 2017a). Dissolution-reprecipitation is the response of garnet to certain fluid-mediated metamorphic reactions (Martin et

al., 2011; Ruiz-Agudo et al., 2014; Ague & Axler, 2016; Konrad-Schmolke, 2018). It involves the simultaneous dissolution of a precursor crystal and subsequent reprecipitation of new material (Putnis, 2007). This will create a re-equilibrated composition resulting in the immobilization of some elements and the release of others (Martin et al., 2011; Ruiz-Agudo et al., 2014). The process may change the composition of garnet and partially replace it with quartz forming cloudy garnet (Martin et al. 2011; Dempster et al., 2017a). Cloudy garnet is recognisable based on the high abundance of quartz inclusions which are commonly irregularly shaped, as well as the presence of abundant microscopic fluid inclusions <5 μm which typically display crystallographic alignment (Martin et al., 2011; Dempster et al., 2017a). The altered garnet contains up to 28 vol.% inclusions while clear garnet contains just ~10 vol.% (Dempster et al., 2017a). Dissolution-reprecipitation is increasingly invoked as the mechanism of re-equilibration of solids in the presence of a fluid (Putnis & Putnis, 2007; Ruiz-Agudo et al., 2014) and is especially important in garnet because it can be recognised texturally (Dempster et al., 2017a). During uplift and exhumation as temperature and pressure decreases garnet may become unstable and undergo resorption. This late dissolution releases trace and major elements that were once a part of the lattice to potentially form new minerals in equilibrium with the fluid (Fraser et al., 1997).

2.3 Disequilibrium in the Barrovian sequence

The progressive sequence of garnet previously discussed in 2.2 is consistent with chemical equilibrium, however assemblages often do not reflect equilibrium (Pattison & Spear, 2017). Equilibrium dictates that the composition of minerals crystallizing in metamorphic rocks is a function of the pressure, temperature and bulk composition of the rock and interstitial fluids at any one-time during formation (Wilbur & Ague, 2006). The concept of continuous equilibrium throughout a metamorphic event at the rock-scale is questionable (Pattison & Spear, 2017). Disequilibrium results in the preservation of the history of events, particularly within garnet. Much of the evidence of disequilibrium during growth is difficult to identify, explaining its novelty as a concept (Kelly et al., 2013). Disequilibrium in completed reactions produces chemically zoned grains, such as garnet (Wilbur & Ague, 2006; Pattison & Tinkham, 2009; Kelly et al., 2013) while disequilibrium during growth is primarily recognisable by the presence of one or

more reactants or reaction textures indicating a reaction did not go to completion (Carlson, 2002; Kelly et al., 2013).

For a mineral-forming reaction to proceed, overstepping of a chemical or mechanical energy threshold must occur enabling nucleation (Gaidies et al., 2011; Spear et al., 2014; Lanari & Engi, 2017). While overstepping of the garnet isograd reaction is widely reported the amount of overstepping required to nucleate the phase is still uncertain (Spear et al., 2014; Wolfe & Spear, 2017). Nucleation is difficult to infer as any evidence is eliminated when a porphyroblast overgrows its primary nucleation site (Kelly et al., 2013). Zoned garnets are assumed to be in equilibrium with the whole-rock composition throughout their growth implying there is no negligible delay in reactions at the interface, and intergranular diffusion is sufficiently fast to distribute material homogeneously at the reaction front (Caddick et al., 2010). However, metamorphic crystallization likely requires some degree of transient nonequilibrium (Carlson, 2002; Ague & Carlson, 2013).

The absence of a fluid phase is a common limiting factor in mid-crustal rocks producing a disequilibrium assemblage because of the kinetic impediment and missing reactant (Ferry & Dipple, 1992; Lasaga & Rye, 1993; Dempster et al., 2017a). Fluid availability influences reaction rates, assisting in the dissolution and transport of material (Putnis, 2015). Intergranular diffusion rates of some elements may be quick enough to keep pace with growing garnet, those with slower diffusion rates create partial disequilibrium (Ague & Carlson, 2013). Equilibrium during crystallization is required to at least the hand specimen scale to allow the application of garnet zoning to geothermobarometry (Chernoff & Carlson, 1997; Caddick et al., 2010; Spear et al., 2014; Pattison & Spear, 2017).

Disequilibrium may be a function of local variations in cloudy and clear garnet (Dempster et al., 2018). The presence of cloudy garnet increases reactivity and may trigger prograde reactions while clear domains remain metastable (Dempster et al., 2018). As grade increases equilibration becomes more effective producing a homogeneous garnet by removing the concentric zoning but also through eliminating inclusions associated with cloudiness (Dempster et al., 2017a). Garnet preserves porphyroblast textures which often allow the analysis of kinetic impediments to both crystallization and equilibration (Ague & Carlson, 2013). The preservation of these chemical relics is indicative that thermodynamic equilibrium

was not reached during the evolution of the rock (Lanari & Engi, 2017). The partial equilibration of garnet results in the preservation of a variety of textural and chemical states that can be linked to stages in its evolution. Garnet can therefore be used to put together a history of events in these schists and understand the response of zircon to different reactions.

2.4 Aims of the study

This study aims to track zircon growth and dissolution across changing P-T-X throughout greenschist to upper amphibolite facies Barrovian metamorphosed schists and produce the first record of zircon behaviour throughout progressive metamorphism. Porphyroblast phases will be used predominantly, biotite in the lower grade schists and garnet in the higher. Garnet is particularly useful, it is one of the most studied mineral in metamorphic petrology (Hollister, 1966; Yardley, 1977; Dempster et al., 1985; Hames & Menard, 1993; Carlson, 2006; Baxter et al., 2017; Dempster et al., 2017) producing a comprehensive record of garnet behaviour. As such garnet has an important link to the less understood zircon. Zircon remains enigmatic, it has the ability to (re)crystallize over a wide range of conditions (Rubatto, 2002) but much remains to be learned about the factors that promote or inhibit reactivity (Vorhies et al., 2013).

Zircon population studies within similar Barrovian polymetamorphic rocks have been carried out, however the studies tend to be within mineral separates focussing on U/Th-Pb systematics (Vorhies et al., 2013). The use of mineral separates biases abundance studies of the zircon, delicate outgrowths and microzircon are removed in the separation process so only robust members of the original detrital population remain (Dempster et al., 2004; Hay & Dempster, 2009a). This study makes use of polished sections to maintain petrographic context. Zircon growth and dissolution will be characterised through analysing microzircon populations, detrital populations, outgrowth abundance and morphology, and dissolution textures.

2.4.1 Geological setting and sampling

This study analyses metasedimentary rocks from the Dalradian Supergroup, the Dalradian rocks are subdivided into the Appin Group, Argyll Group and Southern Highlands Group (Phillips & Key, 1992). The Appin Group rocks are sampled from Glen Roy (Grid Ref: NN 29861 85688), they are garnet-, staurolite-, and sillimanite-zone Leven Schists. The schists contain alternating layers of fine-grained micaceous and quartzofeldspathic matrix with 1-4 mm garnet porphyroblasts (Dempster et al., 2017a). Lower grade biotite-zone Appin Phyllites from the Appin Group will also be analysed. They are sampled from Onich (Grid Ref: NN61330 03200) and are composed of a similar alternating pelitic and quartz-rich matrix with 1-4 mm biotite porphyroblasts.

The Dalradian sequence is primarily composed of Late Proterozoic-early Palaeozoic clastic metasedimentary rocks, with local carbonates and basic volcanics (Stephenson et al., 2013). The sedimentary rocks were metamorphosed during ocean closure in the Grampian Orogeny in the late Neoproterozoic and early Cambrian (Strachan et al., 2002; Rooney et al., 2011; Vorhies et al., 2013; Breeding et al., 2014). The Grampian Orogeny produced a terrane with metamorphic grade generally increasing progressively northward (Tanner et al., 2013). The extent of early Precambrian metamorphism in the Dalradian block is unknown and remains controversial (Dempster et al., 2002; Hutton & Alsop, 2004; Dempster & Jess, 2015).

Lambert et al (1982) produce dates specifically for the Leven Schists of 655 +/- 25 ma using Rb-Sr isotopic studies however, what this age represents is uncertain as the rocks have been entirely recrystallized and the polymetamorphic nature of the terranes cast doubt on the ability of the Rb-Sr system to produce a robust age of sedimentation or metamorphism (Phillips & Key, 1992; Tanner & Bluck, 1999). The Appin Group has been dated at 656 +/- 9 ma using Re-Os geochronology (Rooney et al., 2011), producing much more robust sedimentation ages than Rb-Sr. The date has been produced from Ballachulish slates directly overlying the Leven Schists, so they were likely deposited close to this time. Peak metamorphism at Glen Roy has been estimated between 500-600^{o}C and 5-8 kbar (Richardson & Powell, 1976; Wells, 1979; Powell & Evans, 1983; Phillips & Key, 1992). The prograde regional metamorphism accompanied deformation with the

thermal peak coinciding with the second stage of folding and creation of S2 fabrics (Phillips & Key, 1992).

The Appin Group schists at Onich are also polymetamorphosed, first undergoing a regional event in the Grampian Orogeny, similarly to Glen Roy, before a second low grade contact event following the emplacement of the Ballachulish granite during the Caledonian Orogeny in the Devonian (Roberts & Treagus, 1977; Pattison & Harte, 2001). There is limited literature regarding the dates and peak metamorphic conditions of the Appin Phyllites, particularly at Onich. The Ballachulish Igneous Complex has been dated using U-Pb in zircon at 423 +/- 0.3 ma (Fraser et al., 2004) indicating the most recent contact event occurred around this time.

While the Appin Phyllite rocks record two key stage, the contact biotite metamorphic growth over early regionally metamorphosed biotite-zone schists, the Leven Schists record a more progressive sequence of prograde reactions involving transformations from garnet zone into staurolite-zone and finally into sillimanite-zone assemblages. The analysis of the matrix in the Appin Phyllites should enable an understanding of zircon behaviour during early low grade regional metamorphism, while biotite porphyroblasts should record changes to zircon morphology during biotite growth. The disequilibrium recorded in garnet within the Leven Schists will allow an understanding of how zircon changes in morphology and abundance through the garnet-staurolite-sillimanite transformations.

2.4.2 Index mineral-forming reactions in the Leven Schists

Index minerals can form as a result of several different reactions, primarily based on the different bulk chemistry and original mineralogy of a rock (Prakash et al., 2018). Different reactions commonly occur at different P-T conditions e.g. kyanite forms at middle amphibolite facies due to staurolite breakdown (Lal & Singh, 1978) and at lower greenschist facies due to pyrophyllite breakdown (Prakash et al., 2018). The recognition of a single isograd requires a precise understanding of the conditions surrounding mineral formation. Most minerals can form over a wide range of temperature and pressure depending on a number of other factors (Prakash et al., 2018). The Leven Schists were specifically chosen because they

have been extensively studied (Anderson, 1956; Haselock & Winchester, 1981; Lambert et al., 1982; Treagus et al., 2013), specifically at Glen Roy (Dempster et al., 2017a; Dempster et al., 2018) as such their metamorphic history has been well-constrained.

The main mineral forming reactions have been explored in recent years with analysis of the petrographic and textural relationships to produce a thorough reaction history of the schists not solely based on the use of graphical techniques.

Staurolite production in the Leven Schists was originally attributed to:

Garnet + muscovite + chlorite → staurolite + biotite + quartz

(Phillips & Key, 1992)

based on the use of KFMASH system. Staurolite occurs in close proximity to garnet, typically within micaceous fabrics indicative of garnet and muscovite consumption during staurolite formation, additionally garnet with adjacent staurolite shows evidence of marginal dissolution (Phillips & Key, 1992). However, there is a lack of evidence that primary chlorite existed in the schists producing uncertainty surrounding its role in staurolite production (Dempster et al., 2017a). Instead a chlorite-free alternative seems likely:

Fe-rich garnet + muscovite + water → staurolite + biotite + quartz

(Dempster et al., 2017a)

In place of chlorite a small amount of water is invoked to balance the hydrous component of staurolite (Dempster et al., 2017a). The common absence of chlorite in a range of amphibolite facies biotite-garnet rocks suggests this reaction has the potential to be invoked regularly in Barrovian pelites to explain staurolite production (Dempster et al., 2017a). Reactions involved in sillimanite production typically involve the consumption of staurolite according to KFMASH:

(a) Staurolite + muscovite + quartz → biotite + sillimanite + H_2O

(McLellan, 1985)

(b) Staurolite + chlorite → sillimanite + biotite + H_2O

(Guidotti, 1974)

(c) Staurolite + quartz → garnet + sillimanite + H_2O

(McLellan, 1985)

Each reaction produces a different textural pattern between products, (a) forms sillimanite with intergrowths of biotite, (b) similar in texture to (a) but involves chlorite dissolution in place of muscovite, and (c) produces sillimanite within late garnet. Most rocks containing sillimanite show evidence of staurolite dissolution (Pattison & Spear, 2017) however, based on the absence of any textural evidence of significant staurolite consumption within the Glen Roy schists (Figure. 2.1a) a staurolite-free reaction is invoked:

Garnet + muscovite → sillimanite + biotite + quartz

(Dempster et al., 2018)

Garnet shows evidence of more extensive dissolution (Figure. 2.1b) than its staurolite-zone counterpart and staurolite porphyroblasts show an affinity for micaceous matrix over adjacent quartzofeldspathic layers (Dempster et al., 2018). The reaction history of the Leven Schists enables a better understanding of the chronology of zircon growth based on the textural relationship with the host phase(s). The complication in defining index-mineral forming reactions within these rocks is likely to be a far-reaching issue in Barrovian metamorphosed rocks

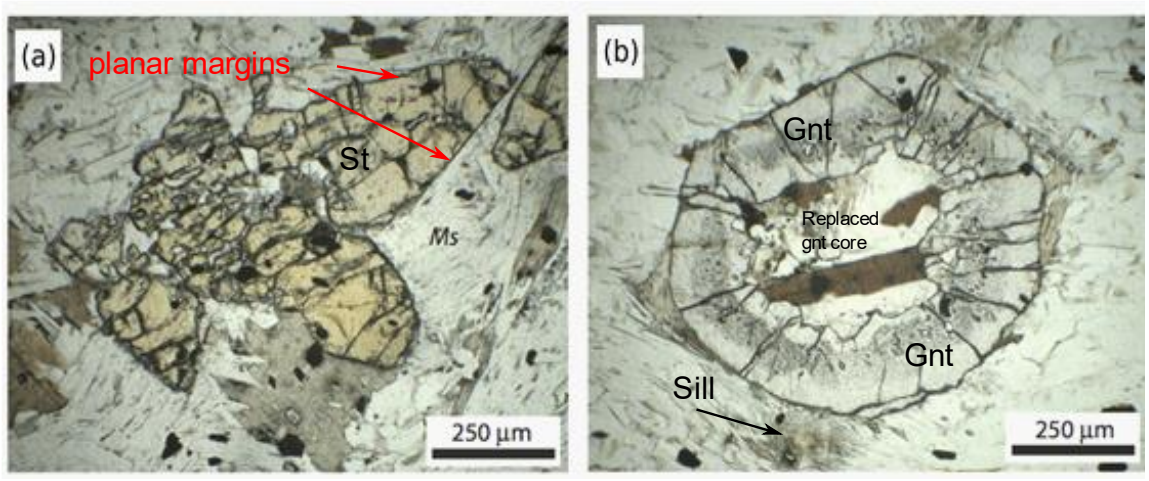

FIGURE 2.1: PPL image of reaction textures in sillimanite-zone Glen Roy schists, images taken from Dempster et al., 2019, (a) staurolite with planar margins preferentially growing in micaceous matrix, and (b) atoll garnet with adjacent sillimanite that has undergone extensive dissolution in the core

where understanding the conditions and reactions involved in the formation of index minerals may be complex.

2.4.3 Wider significance

As a useful mineral for geothermometry and geobarometry (Martin et al., 2011) the coexistence of garnet with zircon ultimately opens the possibility of linking U/Th-Pb zircon ages to metamorphic conditions, allowing the application of absolute ages to stages on the P-T-t path (Rubatto, 2002). Garnet records changing P-T-X conditions during growth (Whitney et al., 1996; Hallett & Spear, 2015) so the analysis of zircon populations within these well-constrained garnets can assist in furthering the understanding of zircon behaviour during metamorphism and enabling the production of more robust U-Th/Pb geochronology within zircon. The reactivity of zircon appears to be linked to fluid fluxes (Rasmussen, 2005), therefore zircon populations also present the possibility of being used as a tracer of fluid flow during metamorphism (Dempster & Chung, 2013) and potentially assisting in understanding dissolution-reprecipitation. Zr diffusion within garnet has a much higher closure temperature than major elements, where divalent cation zoning is typically eliminated at upper amphibolite facies, Zr may persist to granulite facies. This makes Zr in garnet a potentially very useful geochemical tracer and thermometer up to high temperatures and pressures if Zr behaviour can be better understood.

Chapter 3 Methodology

This study analyses garnet-, staurolite-, and sillimanite-zone Leven Schists from Glen Roy and biotite-zone Appin Phyllites from Onich. The biotite-zone Appin Phyllites were originally analysed as part of my undergraduate research project for submission as part of my BSc. Most of the data for these schists was therefore collected prior to the start of this study and the collection of the Glen Roy data, however it was entirely reinterpreted in the context of this study. As a result, most of the analysis and data collection occurred in the same way, where collection or analysis of data was different it will be discussed below.

3.1 Sample preparation

Samples for this study were sliced and prepared as 0.5 μm thick polished sections. Mineral separate analyses are traditionally used in zircon studies (Froude et al., 1983; Mojzsis et al., 2001; Cawood et al., 2003; Thomas, 2011). Polished sections were used in place of mineral separates to preserve petrographic context and prevent biasing of zircon populations based on size and stability (Hay & Dempster, 2009). During zircon separation, information on host mineral and textural relationships that could link to the temporal change in zircon are removed. Additionally, microzircon and delicate detrital fringes may not survive the separation processes thus biasing the preserved zircon based on their size and durability.

3.2 Analysis

Analyses involved the use of transmitted light microscopy (TLM) and scanning electron microscopy (SEM). The location of the analyses are listed throughout the results and discussion. They are identified by sample number followed by porphyroblast number e.g. garnet GR02-1 is in sample GR02 and is labelled porphyroblast 1.

3.2.1 Transmitted light microscopy

Initial petrographic analysis was carried out using TLM to infer textural relationships between porphyroblast and matrix phases. TLM was predominantly

used as a precursor to SEM analyses, highlighting areas of interest within garnet or the matrix as well as mineralogical and textural analyses quickly and easily.

TLM was additionally useful in place of SEM for analyses which weren't focussed on the surface of the section e.g. the analysis of fluid inclusions. Where TLM captures the full 0.5 µm section thickness the SEM only interacts with the surface layer, imaging only the upper surface. Petrographic microscopes have the potential to capture information on more planes than SEM within a polished section. Thus imaging alignment in multiple planes and enabling a better understanding of fluid inclusion abundance and alignment within a domain.

3.2.2 Scanning electron microscopy

The SEM uses focussed beams of electrons from an electron gun that interact with the surface of a polished section. The resulting release of secondary electrons (SE) from the sample allows mapping of the topography of a specimen, a closer surface will produce a more rapid return rate for SE than a lower relief area. Additionally, backscattered electrons (BSE) are produced when an electrons path is deviated by the force of the nuclei, instead of interacting they are scattered. BSE images contain information on the chemistry of the specimen, with high mean atomic number minerals appearing bright and low mean atomic number features, dark. For example quartz will appear darker than biotite because quartz has a lower mean atomic number than biotite. For quantitative chemical data X-Ray detectors map the emissions from the specimen, with different elements producing different x-rays depending on the structure of an atom (Goldstein et al., 2017). The samples were coated in a thin carbon film ca. 15 nm thick for SEM analysis using a vacuum coater. This coating prevents charging improving the accuracy of elemental data and the quality of imaging.

The SEM has the benefit of higher resolution imaging at a significantly higher magnification compared to TLM, the X-ray detector also allows composition to be inferred in detail. The SEM was used for (a) garnet analysis, and (b) mapping zircon populations.

3.2.2.1 Garnet analysis

Garnet classification requires a two-step approach incorporating both chemical and textural analyses. Energy-dispersive x-ray (EDX) analysis was utilised in the Carl Zeiss Sigma SEM to analyse the chemistry of garnet grains, and in turn attempt to infer the history. Porphyroblasts were mapped as well as line scans using Oxford software in the aim of identifying changes in the major divalent cation chemistry of the garnet (Ca, Mg, Mn & Fe).

Running averages were used to smooth curves for garnet chemical transects. The spot size of the beam is 2.5 μm so based on the spacing size of each transect the running average was conducted an appropriate number of times. E.g. for a 5 μm spaced transect running averages was carried out twice to eliminate noise as much as possible and produce a smooth profile. Where inclusions or infilled fractures were captured these were removed from the chemical transects to ensure the profiles were illustrating changes to garnet chemistry.

Analyses were carried out using BSE imaging to capture the textural characteristics of garnet such as mineral inclusions, fluid inclusions and fractures. Fluid inclusion density was measured using BSE images on ImageJ software. The thresholds were set to measure the % abundance of the dark, and thus low mean atomic number, fluid inclusions. Using this method care must be taken to separate fluid inclusions from fractures and larger, more irregularly-shaped quartz inclusions, both are silicate- rich and appear within the same colour thresholds.

3.2.2.2 Zircon mapping

The FEI Quanta 200F environmental SEM was used in order to capture BSE images for mapping zircon populations in garnet porphyroblasts and transects in the matrix. Operated at 20 kV and moderate beam currents when zoomed to 1500x the resolution was sufficient to capture the finest microzircon 10s nm wide. Increasing contrast and decreasing brightness to enable the identification of high mean atomic number features, from here the spot ID feature was used to analyse zircon and differentiate from other bright, high mean atomic number features such as monazite.

BSE images were then captured as a series of frames at brightness and contrasts where high mean atomic number features were easily identifiable, e.g. where ilmenite appears slightly darker than zircon. Mapping of entire porphyroblasts or transects of the matrix were carried out in this way producing a series of images ca. 100 μm wide. The frames were then montaged using Inkscape, from here a map of the analysed area is produced which enables the interpretation of inclusion populations with the petrographic context of the textural characteristics of the surrounding garnet or composition of the surrounding matrix. Quantitative data can be extracted from these maps directly. Zircon sizes can be measured using the ruler tool in Inkscape allowing any changes to the size of micro- or detrital populations to be quantified.

Automated EDX feature mapping could not be applied to most of the schists s the extremely small size of some of the zircon meant they weren't captured. As a result, the mapping was biased against the smaller proportion of microzircon, typically those <0.2 μm^2. Within the biotite-zone Onich schist EDX mapping was used on one of the samples as the microzircon within these lower grade schists are coarser than the higher grade Leven Schists.

Where an average value is given, e.g. for average zircon size within a given domain, the standard deviation is to 1σ where n=-1. The values are accurate to the 68% confidence level.

Chapter 4 Petrology of the schists

4.1 Biotite-zone

Biotite-Zone Appin phyllites were sampled from Onich, Scotland (NN61330 03200). The schists are polymetamorphosed, they first underwent a regional event during the Camrbian-Ordovician, forming an aligned schistose matrix, followed by a low-grade contact event during the emplacement of the Ballachulish granite and associated diorites during the Caledonian Orogeny, forming biotite porphyroblasts (Roberts & Treagus, 1977; Buntebarth, 1991; Pattison & Harte, 2001). Sample Ball 2.8 which is a quartz-rich pelite and Ball 2.9 which is comprised of quartz-rich pelite and pelite separated by a heavy mineral band (Table 4.1).

TABLE 4.1: Modal abundance of constituent minerals in biotite-zone schists from Onich subdivided by the three main compositions; pelite (Ball 2.8), quartz-rich pelite (Ball 2.8 & Ball 2.9) and heavy mineral band (Ball 2.8)

	PELITE	QTZ-RICH PELITE	HEAVY MINERAL BAND
BIOTITE (PORPHYROBLASTS	3	10	24
BIOTITE (MATRIX)	4	5	5
CHLORITE (RETROGRADE)	14	11	17
MUSCOVITE	73	31	22
QUARTZ	6	34	32
PLAGIOCLASE	8	16	13
ALLANITE	2.6	2.1	0.8

The schists are layered, layers are generally > 10mm thick, except for the heavy mineral band which is ca. 1mm. Pelitic layers are dominated by fine-grained <0.125 mm muscovite (Table. 4.1) (Figure 4.1a). Quartz-rich pelite layers contain equal proportions of quartz and muscovite and are slightly coarser grained ca. 0.25 mm (Figure. 4.1c). The heavy mineral band contains the lowest proportion of muscovite, comprised primarily of coarser quartz (0.5 mm) and abundant biotite porphyroblasts (Figure. 4.1b). the heavy mineral band separates quartz-

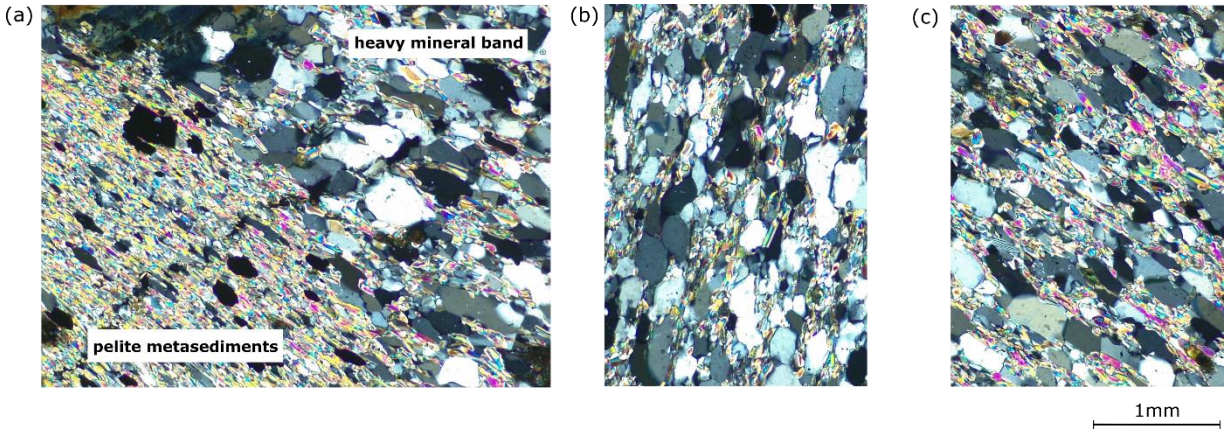

FIGURE 4.1: XPL (cross-polarised) TLM images of the compositional classifications of the biotite-zone schists in Ball 2.9, (a) fine micaceous pelite (left) meeting the heavy mineral band (right), (b) quartz-rich, coarse heavy mineral band, and (c) interbedded pelite and quartz-rich pelite

rich and mica-rich layers likely representing original bedding. The matrix records a slaty S2 cleavage rthat dips slightly steeper than S1 undeformed bedding (Roberts & Treagus, 1977), followed by the formation of biotite porphyroblasts during the contact event (Pattison & Harte, 2001).

Biotite exists as two distinct populations, ca. 0.25 mm matrix biotite, and 1-3 mm porphyroblasts. Biotite porphyroblasts show partial retrogression to chlorite forming bands (Figure. 4.2b-c) and much of the matrix biotite has been completely replaced by chlorite (Figure. 4.2d). Chloritization is most extensive in the heavy mineral band (Table. 4.1) where all biotite shows evidence of at least partial alteration. Matrix biotite is aligned to s3 and biotite porphyroblasts also show some evidence of alignment in the same orientation (Figure. 4.3). Biotite is occasionally linked to quartz-rich pressure shadows (Figure. 4.2a). The quartz is >0.5 mm and the shadows are best developed adjacent to larger biotite porphyroblasts. Smaller ca. 1 mm biotite porphyroblasts generally aren't associated with these coarse quartz margins (Figure. 4.2c).

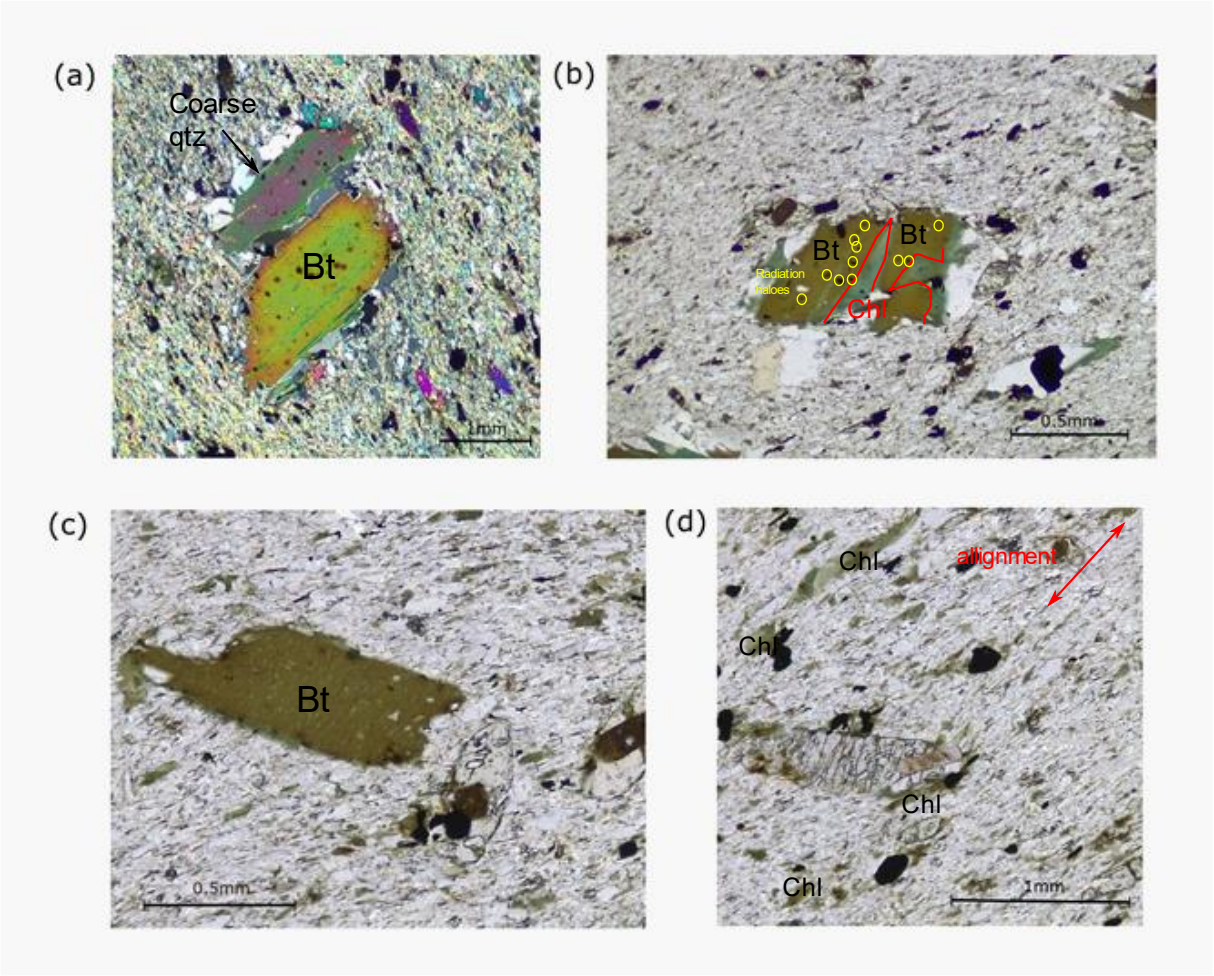

FIGURE 4.2: TLM images of biotite morphology in Ball 2.8, (a) XPL image of biotite porphyroblasts with coarse quartz pressure shadows, (b) PPL image of partially chlorite retrogressed biotite with irregular margins, biotite contains radiation haloes from allanite and zircon inclusions, (c) PPL image of predominantly unaltered biotite porphyroblast, and (d) PPL image of aligned matrix biotite entirely retrogressed to chlorite

Allanite is the main accessory phase, particularly abundant in pelitic layers. The <0.1-0.3 mm allanite is consistently rimmed by >0.1 mm of epidote (Figure. 4.4a & c). Detrital ilmenite is also present, representing ca. 2% of the rocks (Figure. 4.4b). It is spatially linked to biotite generally included within or at the margins of porphyroblasts (Figure. 4.4d). Apatite is present in small proportions (<0.1%), it is predominantly included within biotite and forms elongate prismatic grains <0.5 mm long.

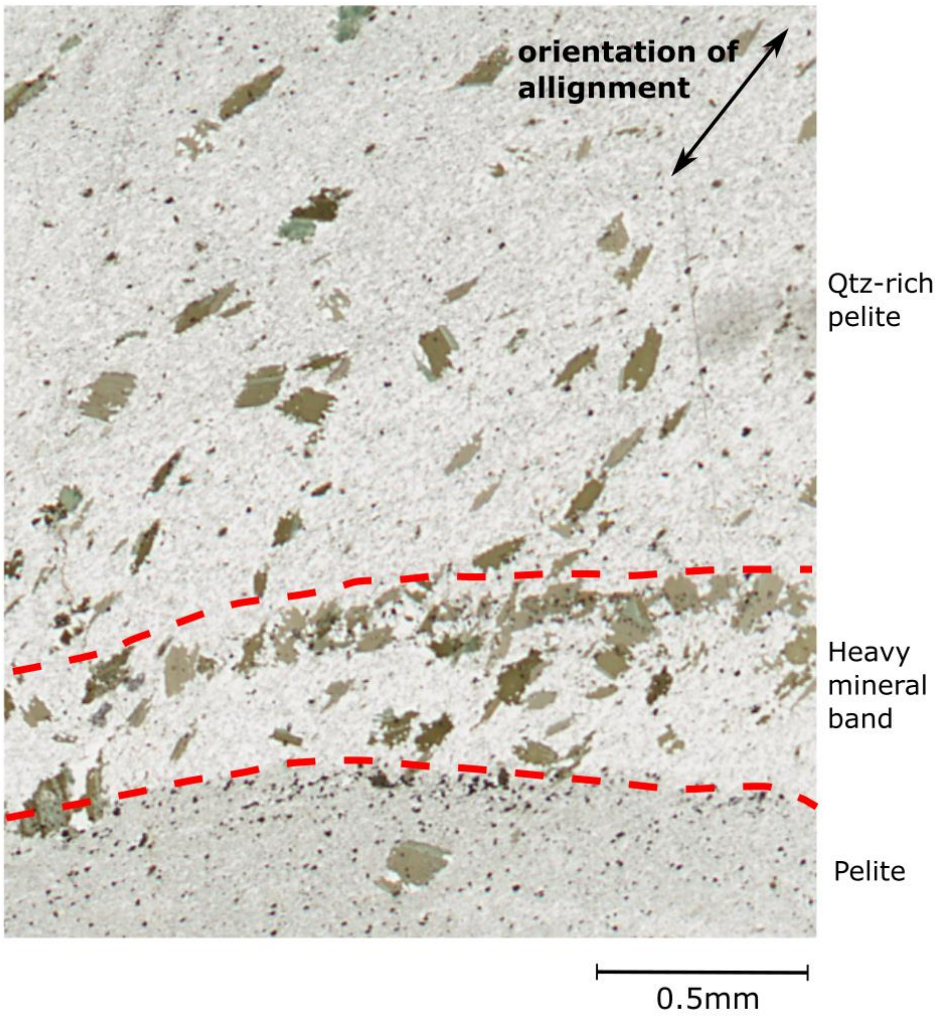

FIGURE 4.3: Scan of section 2-9 showing the distribution and alignment of biotite across the three main compositional bands

The biotite schists contain vestiges from three metamorphic stages (Roberts & Treagus, 1977; Pattison and Harte, 2001). The aligned, fine-grained muscovite-rich matrix formed during an early regional event, large biotite porphyroblasts formed during later contact metamorphism and finally chlorite from the retrogression of biotite following late fluid infiltration. The alignment of biotite porphyroblasts (Figure. 4.3) is indicative of some deformation during the contact event of potentially a later regional event that succeeded biotite growth.

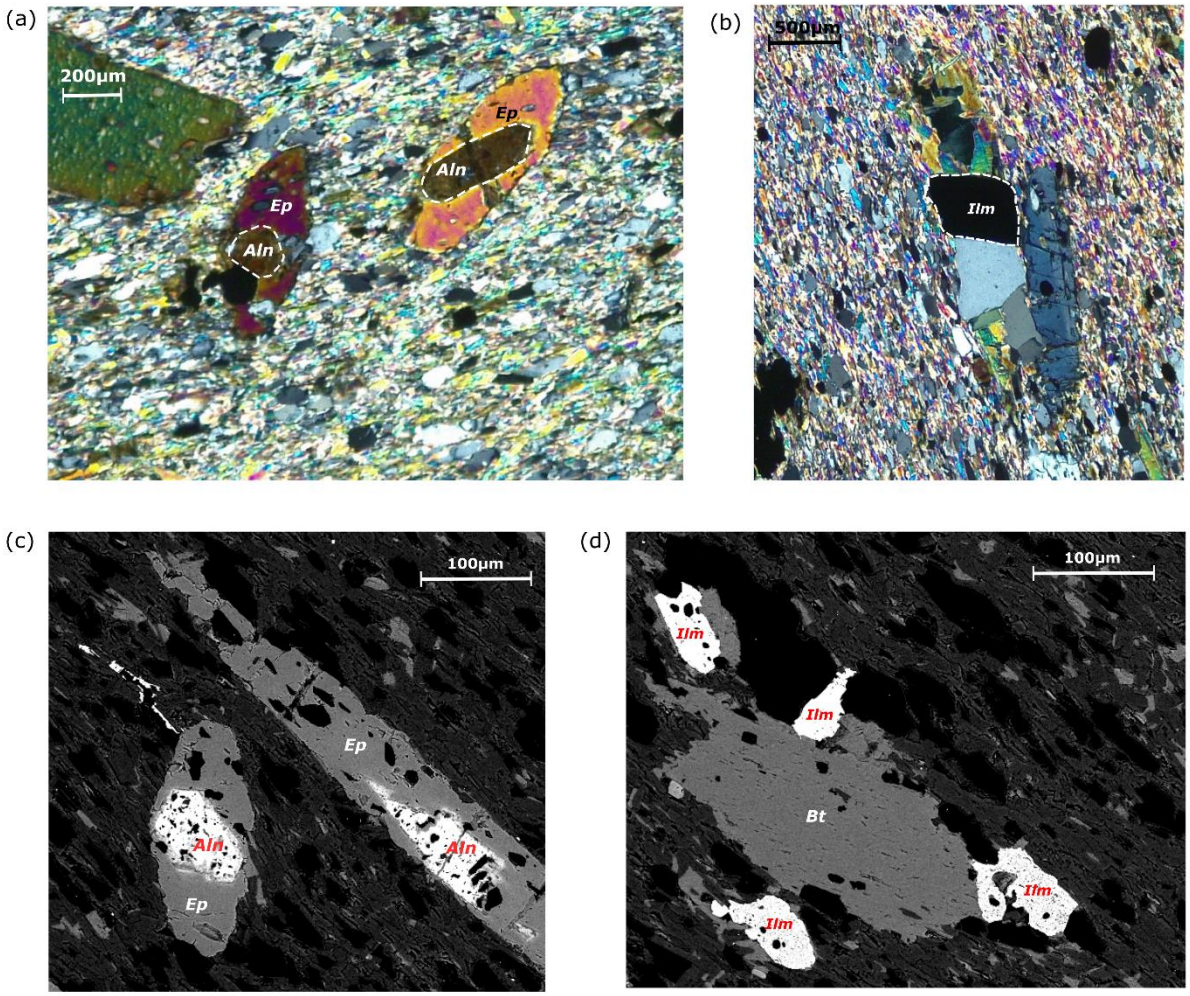

FIGURE 4.4: Accessory phases in Ball 2.8 and 2.9; (a) XPL photomicrograph of allanite rimmed with epidote, (b) XPL image of a detrital ilmenite grain contained within a biotite and quartz rich pressure shadow (c) BSE (backscattered electron) image of allanite within epidote, and (d) BSE image of ilmenite grains illustrating the close spatial link between ilmenite and biotite

4.2 Staurolite-zone

Staurolite-zone Leven schists were sampled from Glen Roy, Scotland (NN29861 85688). The Leven Schists are polymetamorphosed, undergoing a complex tectono-thermal evolution during the Grampian Orogeny in the Late Neoproterozoic and Early Cambrian (Phillips & Key, 1992; Strachan et al., 2002; Vorhies et al., 2013). The extent of earlier Precambrian metamorphism is unknown (Dempster et al., 2002; Hutton & Alsop, 2004). Three polished sections were used based on their varying proportions of staurolite; GR01, GR02 and GR05. GR01 contains 3.7% staurolite while GR02 and GR05 contain none. Similarly, they have varying proportions of modified cloudy garnet which has undergone dissolution-

reprecipitation. In GR01 the garnet is predominantly modified, GR05 contains a small amount of cloudy garnet and GR02 contains garnet that is entirely clear. The modal mineralogy of the schists is described in Table 4.2. There is little difference between the matrix of the samples while the proportion of porphyroblast phases and cloudy garnet varies.

TABLE 4.2: Modal abundance of the main constituent minerals within staurolite-zone Leven schists GR01, GR02 and GR05. Values from this study were combined with Dempster et al., 2017a and averaged

	GR01	GR02	GR05
GARNET (CLR)	3.9	8.5	6.8
GARNET (CLDY)	5.4	0	0.2
MUSCOVITE	33.7	23.5	38.1
BIOTITE	10.3	18	14.7
QUARTZ	27	30.1	28
PLAGIOCLASE	10.9	10.80	9.6
STAUROLITE	3.7	0	0
RETORGRADE CHLORITE	2.9	0	0.5
MONAZITE	0.7	0.3	0.3
OPAQUES	0.8	1.7	0.5
CLOUDY GARNET (%)	58.5	0	2.9

The matrix is composed of micaceous and quartzofeldspathic layers, the thickness of which varies from thin interbedded <0.2 mm layers (Figure. 4.5b) up to ca. 2.5-3 mm thick (Figure. 4.5a). Micaceous layers display a strong S2 fabric cross-cut by open folds formed during a third deformational phase (Phillips et al., 1994; Dempster et al., 2017). S1 formed early in the metamorphic history during the development of muscovite + biotite + chlorite, while S2 formed following an increase in metamorphic grade during the 2nd stage of deformation accompanying the formation of biotite + muscovite + garnet +/- staurolite (Phillips & Key, 1992). Micaceous domains are very fine-grained <0.1 mm^2, they are dominated by muscovite with some biotite. Biotite shows retrogression to chlorite. There are two populations of biotite, 0.5 mm matrix phase and a population of 2-5 mm biotite porphyroblasts. The finer matrix population typically shows more extensive retrogression (Figure. 4.6a) while biotite porphyroblasts show <30% chloritization.

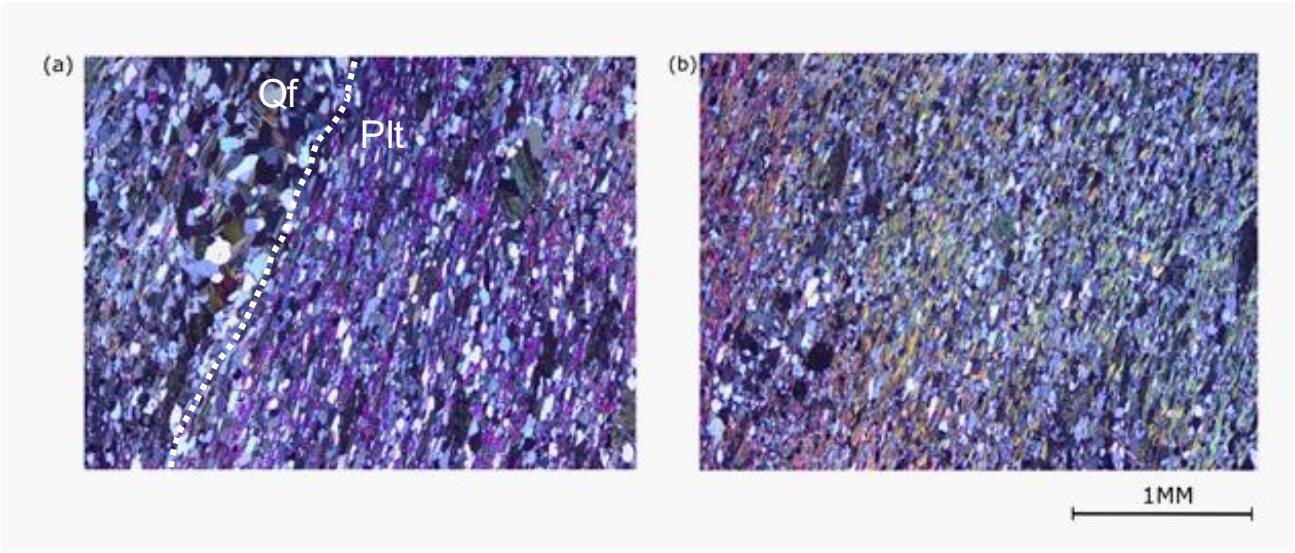

FIGURE 4.5: XPL images of matrix composition and fabric in GR01, (a) thick quartzofeldspathic (right) and micaceous (left) layers, and (b) finely interbedded quartzofeldspathic and micaceous layering

Bands of chlorite are typically planar and are parallel to biotite cleavage, which is perpendicular to the fabric in some of the larger biotite porphyroblasts (Figure. 4.6b). Porphyroblasts comprise 72% of the biotite population and typically display irregular margins while finer biotite margins are more planar.

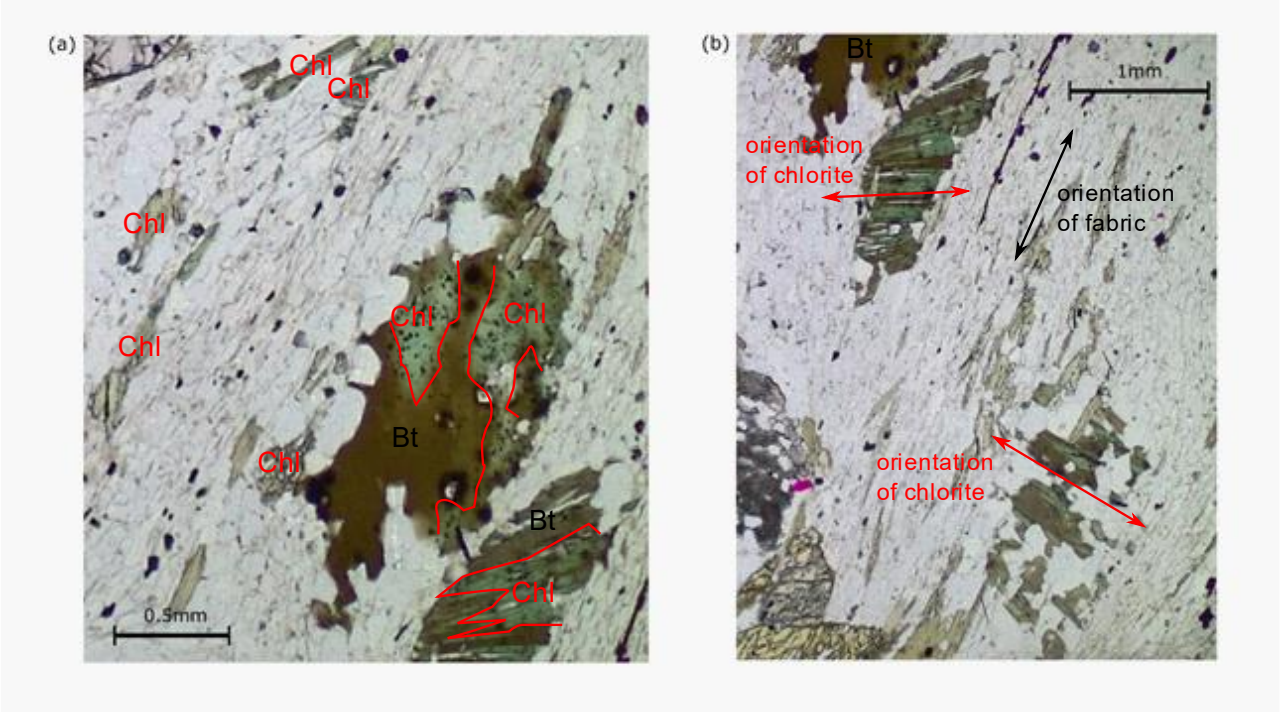

FIGURE 4.6: PPL image of biotite morphology within GR01, (a) completely chloritized matrix biotite and partially altered larger porphyroblasts (b) chloritization typically formed bands roughly perpendicular to matrix fabrics

Quartzofeldspathic layers are dominated by quartz ca. 70% and plagioclase ca. 20%, grain size ca. 0.25 mm is slightly coarser than within adjacent micaceous layers. Quartz is especially coarse ca. >0.5 mm forming pressure shadows on biotite and garnet porphyroblasts. Plagioclase shows some limited sericitization (Dempster et al., 2018), evidence of alteration is rare and where present sericite occupies <3% of the grain.

Garnet and staurolite also form porphyroblasts. Garnet is the most abundant phase comprising 47% of porphyroblasts, they are typically 2-4 mm and more rarely up to 6 mm. Garnet is euhedral-subhedral and displays one or more irregular margins with abundant quartz inclusions producing an embayed structure, particularly in

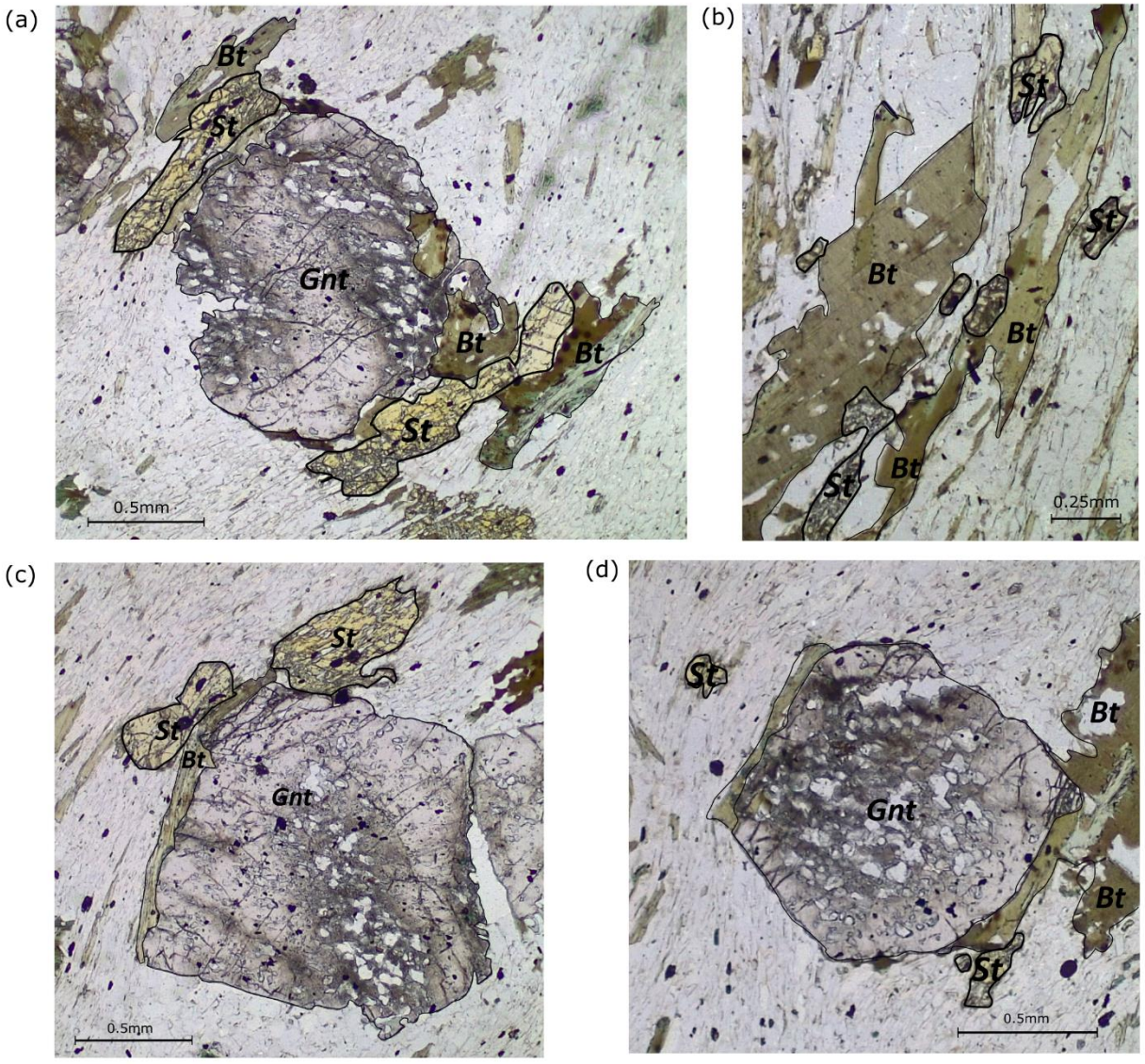

FIGURE 4.7: PPL images of staurolite growth in GR01, (a) staurolite growth in biotite at the margins of garnet, (b) small staurolite form in biotite porphyroblasts away from garnet, (c) staurolite grows on planar, clear margin of garnet away from dissolution, and (d) small garnet porphyroblasts typically yield smaller staurolite grains

staurolite-bearing GR01. Garnet shows evidence of partial retrogression with chlorite focussed along marginal fractures. Staurolite is typically <2 mm and formed at the margins of biotite and/or garnet (Figure. 4.7). The size of the adjacent porphyroblast phases seems to influence the size of the staurolite formed. Where adjacent to large >3mm garnet porphyroblasts the staurolite is larger (Figure. 4.7a) than alongside a <2mm porphyroblast (Figure. 4.7d). Garnet porphyroblasts with adjacent staurolite generally contain larger proportions of cloudiness. Staurolite typically forms adjacent to unmodified margins of garnet that shows no evidence of dissolution (Figure. 4.7c). Staurolite occasionally forms in contact with garnet margins but more commonly within biotite at the rim (Figure. 4.7a & c). Across the samples as the proportion of staurolite increases, so too does the proportion of cloudy garnet and chlorite. Biotite adjacent to staurolite contains more extensive retrogression with chlorite forming bands parallel to the fabric (Figure. 4.7a). Staurolite predominantly occurs in mica-dominated layers (Dempster et al., 2017).

4.3 Sillimanite-zone

Sillimanite-zone Leven Schists were sampled from the northern side of upper Glen Roy (NN2671 9239). The sillimanite-zone schists have shared a similar history to the staurolite-zone; likely undergoing Precambrian metamorphism followed by a complex tectonothermal history during the Grampian Orogeny (Phillips & Key, 1992). One sillimanite-poor sample was analysed (UGR1) containing 0.1% sillimanite and one sillimanite-rich sample (UGR0) containing 1.6%. The modal mineralogy of the sillimanite-zone schists is described in Table 3. Aside from the proportion of index mineral phases and cloudy garnet there is little difference between the two samples.

The matrix mineralogy of the Upper Glen Roy samples is similar to the lower grade staurolite-zone rocks, but the structure of the layers differs. The fabric is generally more strongly folded and the compositional layering less obvious (Figure 4.8). The micaceous layers are typically <0.1 mm thick and the quartzofeldspathic layers slightly coarser than the staurolite-zone samples and reach up to 0.5 mm thick. The schistose matrix is dominated by micaceous layers with interbedded, thin 1-3 mm quartzofeldspathic layers. Biotite is present as a matrix <0.5 mm and a 1-3 mm porphyroblast phase. Retrogression is limited with most biotite

TABLE 4.3: Modal abundance of the main constituent minerals in sillimanite-zone samples UGR0 and UGR1. Values from this study were combined with those of Dempster et al., 2018 and averaged

	UGR0	UGR1
GARNET (CLR)	1.4	1.8
GARNET (CLDY)	7	3
MUSCOVITE	37.9	39.1
BIOTITE	11.49	13.79
QUARTZ	22.2	27.2
PLAGIOCLASE	11.6	11.9
STAUROLITE	2.1	TRACE
SILLIMANITE	1.6	0.1
CHLORITE	0.5	0.5
MONAZITE	1.2	0.9
OPAQUES	0.7	0.7
RUTILE	0.2	TRACE
CLOUDY GARNET (%)	84	64

porphyroblasts containing no chlorite and no matrix chlorite. The most extensive retrogression occurs in biotite in the core of atoll garnet structures where the biotite is often <30% replaced by chlorite.

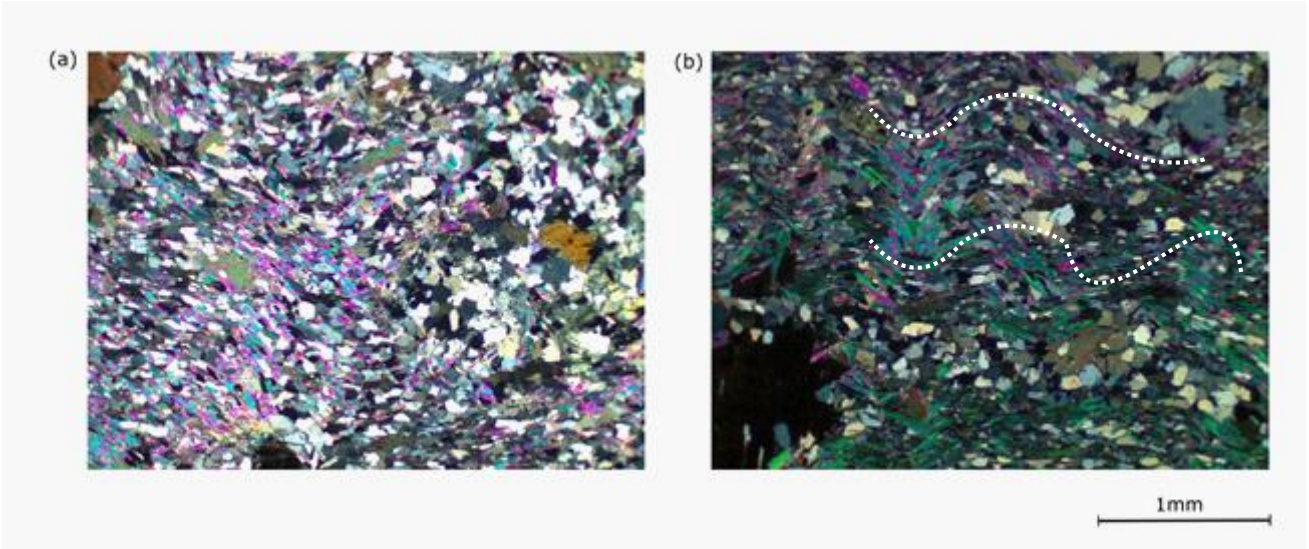

FIGURE 4.8: XPL images of matrix composition and layering in UGR0 sillimanite schist, (a) interbedded quartzofeldspathic and micaceous bands with indistinct layering typical of the schists, and (b) mica-rich bands reveal a strongly folded fabric

Garnet porphyroblasts are subhedral to euhedral and typically 2-4 mm^2. Garnet contains a higher proportion of cloudiness than within the staurolite-zone samples (Tables. 4.2). Despite the increased proportion of cloudiness within garnet most porphyroblasts still show at least one planar margin while the remaining are embayed and irregular. The abundance of sillimanite is proportional to the amount of staurolite and cloudy garnet. UGR1 is comprised of more intact, clear garnet and therefore less staurolite and sillimanite while UGR0 contains more cloudy garnet and as a result contains more staurolite and sillimanite. Staurolite typically occurs proximally to biotite and garnet porphyroblasts and is subhedral to anhedral and generally <3 mm (Figure. 4.9a) while smaller more euhedral ca. 1 mm porphyroblasts occur in the matrix primarily within micaceous layers (Figure. 4.9b).

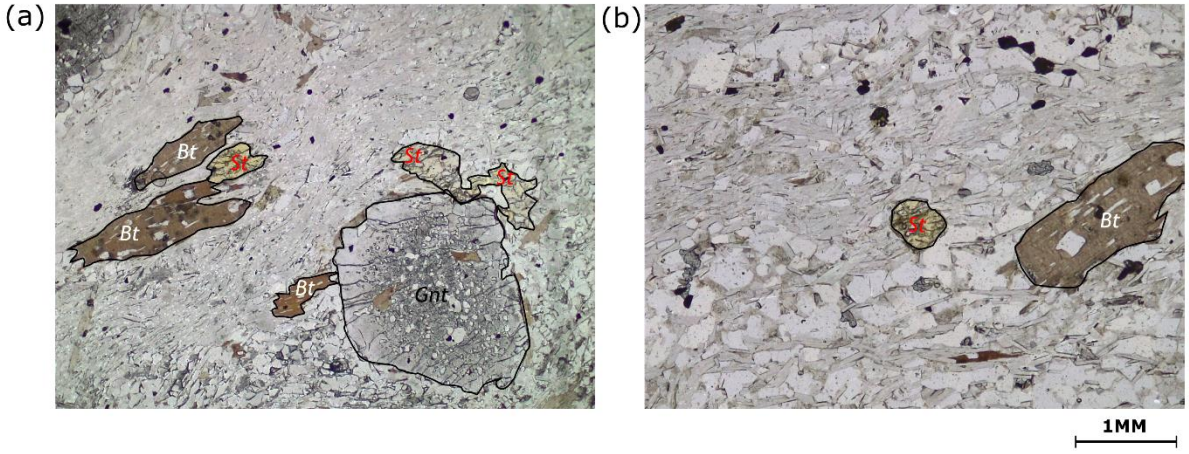

FIGURE 4.9: PPL images of the location of staurolite within sillimanite-zone schist UGR1 (a) subhedral staurolite associated with garnet and biotite porphyroblasts (b) equant staurolite within the micaceous matrix over 1MM from nearest porphyroblast phase

Sillimanite occurs at the margins of most garnet within both UGR0 and UGR1 (Figure. 4.10a) however more rarely sillimanite forms mats within the matrix (Figure. 4.10f). Within UGR0 sillimanite tends to form fibrolite mats along embayments between 0.25-1.5 mm^2 while in UGR1 single needles <0.1 mm^2 are more common at garnet margins (Dempster et al., 2018) (Figure 4.10a-c). Marginal sillimanite illustrates an affinity for micaceous fabrics preferentially forming away from quartzofeldspathic layers and quartz-rich pressure shadows. Sillimanite is also commonly included in garnet as fibrolite mat inclusions 0.2-0.5 mm^2 (Figure. 4.10d-f), sillimanite inclusions are limited to cloudy domains and more common in UGR0 than UGR1. Sillimanite more rarely occurs as fracture fill within garnet margins that have undergone extensive dissolution (Figure. 4.10e).

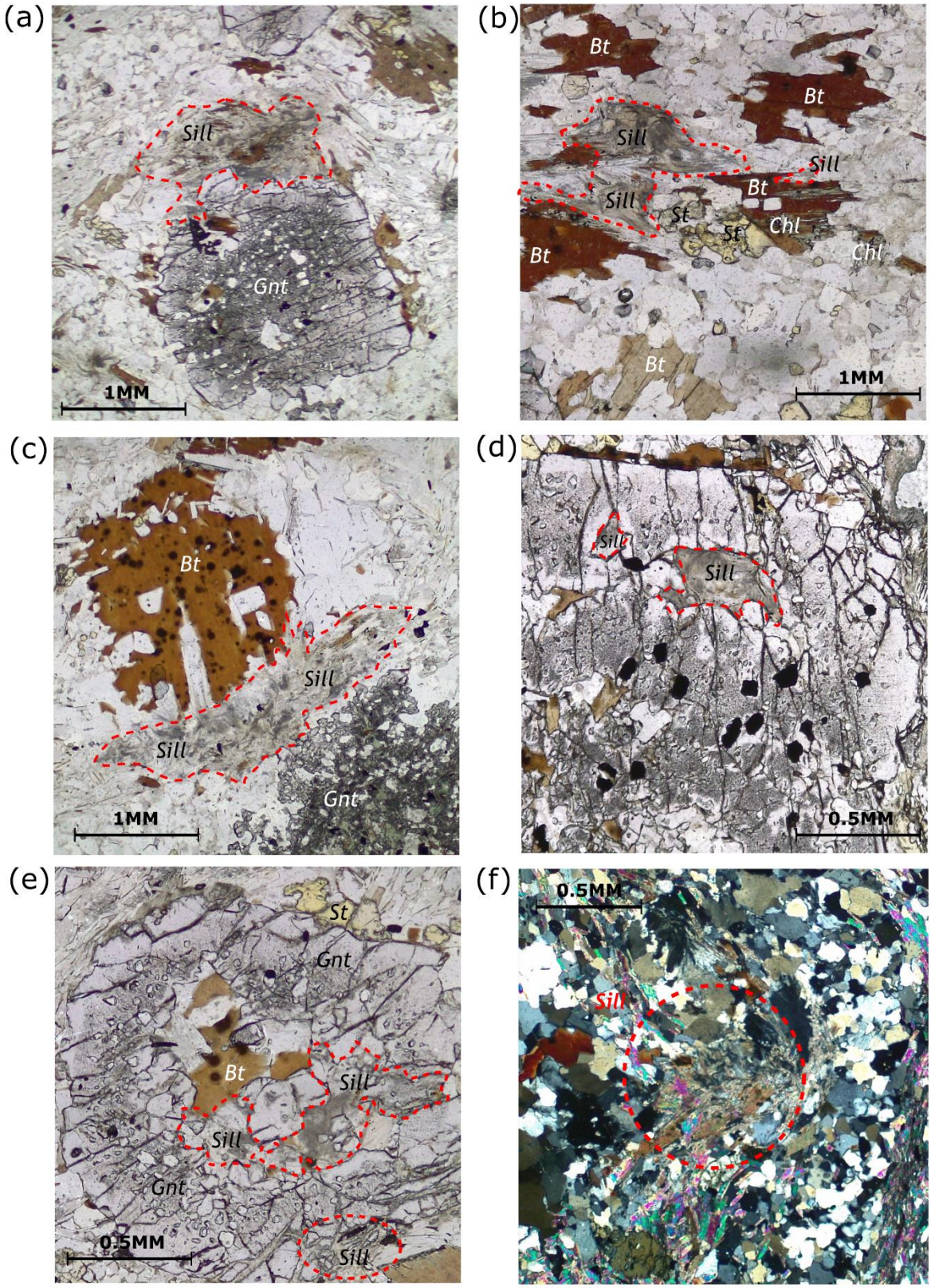

FIGURE 4.10: Photomicrograph images of sillimanite-rich UGR0, all images are in PPL except (f) which is XPL (a) extensive sillimanite algal mat surrounding garnet porphyroblast (b) sillimanite (Sill) mat in the matrix surrounding staurolite and biotite which shows partial retrogression to chlorite (c) sillimanite mat adjacent to biotite and extensively dissolved garnet (d) sillimanite inclusion in garnet with clear rim (e) atoll garnet with sillimanite inclusions and fracture fill at margins (f) sillimanite mat in the matrix forming distally from garnet

Garnet characteristics

5.1 Introduction

The petrology of the schists is described in chapter 4 while this chapter will focus on garnet in more detail due to its ability to record modification, and within it changes to zircon populations. Dissolution-reprecipitation occurs when a fluid comes into contact with a mineral with which it is undersaturated (Altree-Williams et al., 2015). It involves the dissolution of a less stable parent phase and the reprecipitation of a more stable solid daughter phase from the fluid (Putnis, 2002; Putnis, 2009; Ruiz-Agudo et al., 2014; Konrad-Schmolke et al., 2018). The processes may be spatially and temporally coupled, with both dissolution and reprecipitation occurring within an interfacial fluid film at the reaction interface (Martin et al., 2011; Ruiz-Agudo et al., 2014; Kondratiuk et al., 2015; Ague & Axler, 2016; Ruiz-Agudo et al., 2016). Within garnet, CDR (coupled dissolution-reprecipitation) has the potential to be fingerprinted (Martin et al., 2011; Dempster et al., 2017; Dempster et al., 2019).

The samples were previously collected, prepared and analysed as part of separate studies on dissolution-reprecipitation within garnet, both the staurolite-zone schists (Dempster et al., 2017) and sillimanite-zone schists (Dempster et al., 2019). Within these studies cloudy garnet was characterised, and textural and chemical changes were linked to specific reactions during staurolite and sillimanite formation. This classification of the garnet is crucial in understanding the evolution of zircon populations, as garnet preserves vestiges of different stages of the metamorphic history. Primary analyses of the texture and chemistry of garnet in which zircon will be mapped are required in order to link zircon dissolution and growth to the evolution of the schists. These analyses utilise the work of Dempster et al. (2017; 2019) to classify garnet, using the mineral and fluid inclusion density and chemical changes associated with a series of fluid-mediated reactions. Many of the observations within Glen Roy garnets in the forthcoming chapter are in agreement with the work of Dempster et al (2017; 2019) and build on them with the aim to better understand dissolution-reprecipitation processes within garnet.

5.2 Staurolite-zone garnet

5.2.1 Previous work

Garnet within staurolite-bearing schists from Glen Roy is texturally complex. One aspect of this complexity is post-growth modification in the presence of a fluid through dissolution-reprecipitation. Based on the degree of modification garnet can be subdivided into three domains; clear, cloudy and ambiguous (Dempster et al., 2017). Clear garnet represents the unmodified parent phase, cloudy garnet has undergone dissolution-reprecipitation and thus is representative of the reequilibrated product phase, and ambiguous garnet is a texturally intermediate state. Dempster et al (2017) constrained the textural characteristics of clear and cloudy garnet within the staurolite-zone schists at Glen Roy. Cloudy garnet was characterized primarily by the formation of small, aligned fluid-filled inclusions and an increase in mineral inclusion abundance following dissolution-reprecipitation, particularly large, irregularly shaped quartz inclusions (Dempster et al., 2017). The small, low relief inclusions are treated as fluid inclusions, due to their small size there are no bubbles or fluid features, but the cavities resemble fluid inclusions in other garnet dissolution-reprecipitation studies (Martin et al., 2011; Dempster et al., 2017; Dempster et al., 2019). While clear garnet appears light in colour when viewed in PPL (plain polarised light), this modified garnet appears dark due to the high density of inclusions. Additionally, disruption to concentric growth zoning in cloudy garnet was detailed within Mn, Mg and Fe (Dempster et al., 2017). Mg and Fe are consistently higher in cloudy garnet than adjacent clear, while modified Mn contents vary spatially within a single porphyroblast. Mn is lower compared to adjacent clear garnet in the core and vice versa in the rim (Dempster et al., 2017). Analyses of the staurolite schists in this study utilises the textural and chemical indicators defined above as a basis for classification, while attempting to quantify the changes to texture and chemistry in these rocks through the analysis of a larger sample size.

5.2.2 Clear garnet

Garnet within the Glen Roy schists can be defined as clear if it is not subject to coupled dissolution-reprecipitation (Dempster et al., 2017). As a result, clear

garnet has undergone limited post-growth modification and is representative of garnet morphology during growth within these schists. Clear garnet is most abundant within staurolite-absent/garnet-zone schists. As staurolite increases in abundance, the proportion of clear garnet decreases (Table. 5.1). The abundance of garnet appears to have no influence on the proportion of cloudiness. GR02 contains the most garnet and is the only sample to display no cloudy garnet.

TABLE 5.1: The modal abundance of staurolite and garnet and the proportion of clear, cloudy and ambiguous garnet within the staurolite-zone schists

		Sample		
		GR01	**GR02**	**GR05**
Modal abundance	**Staurolite**	4.1	0	0
	Garnet	8.8	8.9	7.5
% garnet	**% Clear garnet**	36	100	94
	% Cloudy garnet	59	0	5
	% Ambiguous garnet	5	0	1

5.2.2.1 Results: texture of clear garnet

Garnet within GR02 typically displays planar margins (Figure. 5.1). The porphyroblasts have a few transgranular fractures (Figure. 5.1a) and very limited

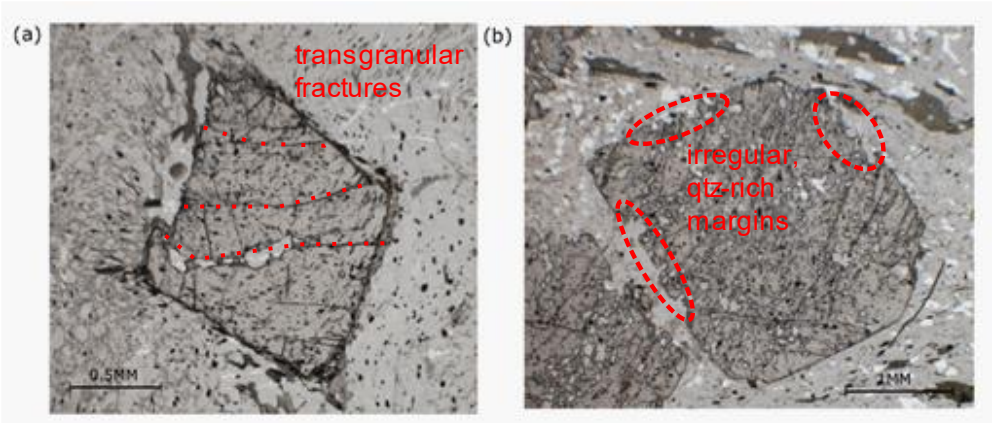

FIGURE 5.1: PPL images of clear garnet porphyroblast morphology within GR02, (a) euhedral garnet with a few transgranular fractures and limited evidence of dissolution, and (b) euhedral-subhedral garnet, irregular margins impinge on quartz-rich matrix

smaller-scale fractures (<0.25 mm long), producing limited interconnectivity. Clear garnet contains few fluid inclusions, making up less than 0.5%. Some porphyroblasts contain fluid inclusions locally surrounding fractures and mineral inclusions (Figure. 5.2a-b) and at porphyroblast rims (Figure. 5.2c). These fluid inclusion-bearing porphyroblasts make up <5% of the garnet population and are all <1.5 mm. Garnet hosts a variety of mineral inclusions, predominantly quartz, ilmenite, zircon and allanite. Mineral inclusion abundances within garnet can vary from 6% to 27% within a single porphyroblast. The mineral inclusions form trails aligned to the fabric of the matrix which are commonly curved, particularly towards the rim (Figure. 5.3a). Inclusions are not homogeneously distributed

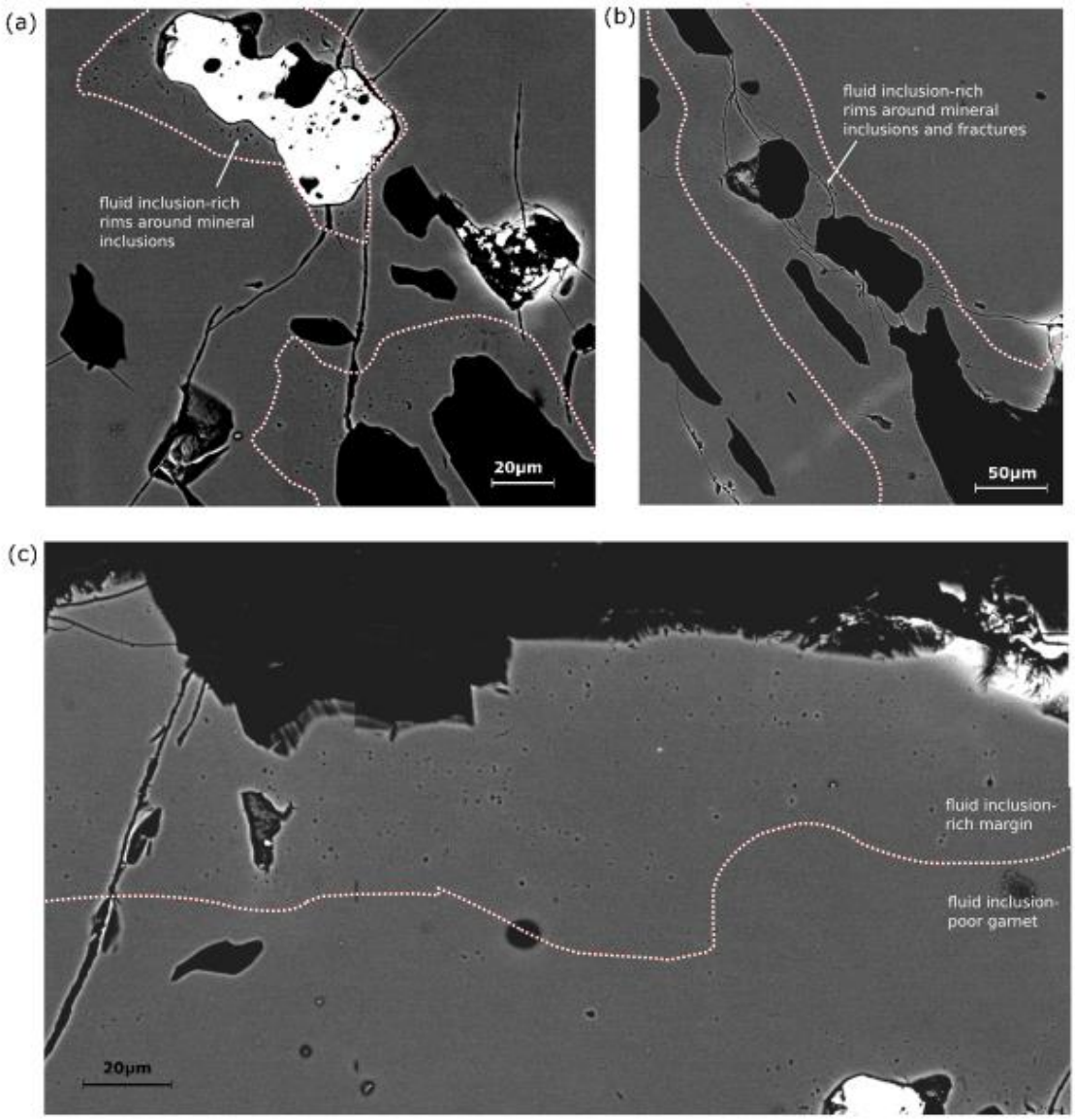

FIGURE 5.2: BSE images of fluid inclusion morphology in clear garnet GR02-8, (a) fluid inclusions surrounding ilmenite and quartz inclusions and associated microcracks, (b) fluid inclusions surrounding fractures, and (c) fluid inclusions at garnet rim

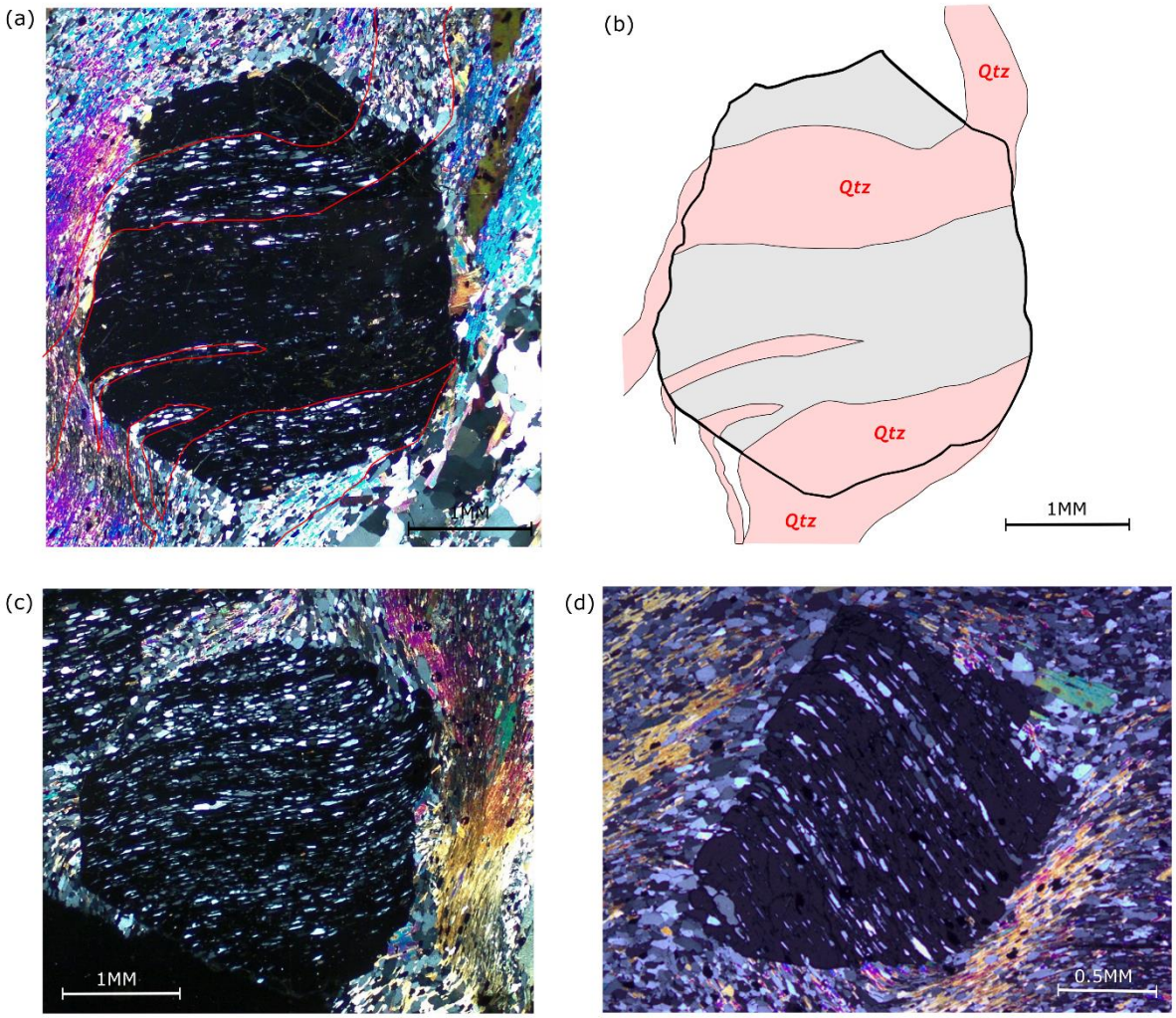

FIGURE 5.3: Mineral inclusion trails within GR02, (a) XPL photomicrograph of garnet with curving inclusion trails and the surrounding matrix, and (b) schematic illustrating the location of quartz inclusion-rich layers in the garnet and adjacent matrix in red, the remaining garnet is inclusion-poor and dominated by ilmenite inclusions, (c) XPL image of garnet with less obvious compositional layering in adjacent matrix, inclusions show a steady increase in size from the core to the rim, (d) XPL image illustrating changes in quartz inclusion size, varying in layers, with inclusion trails of coarse quartz and adjacent trails of finer quartz

within garnet. The inclusion trails are compositionally layered forming silicate-dominated bands and metal oxide-dominated domains. Mineral inclusions within the garnet occasionally show lateral continuity with matrix fabrics (Figure. 5.3b). Quartzofeldspathic matrix bands can commonly be traced into quartz inclusion-rich areas within garnet. However, they are more often subject to slight deflection (Figure. 5.3c) where the matrix appears to curve surrounding garnet changing the orientation of the fabric. The quartz inclusions are commonly coarser and more well-rounded than matrix quartz (Figure. 5.3a & 5.3d). Concentric changes to mineral inclusion morphology within garnet are variable, from core to rim

inclusions occasionally get larger, from ca. <0.1 mm in the core to ca. 0.15-0.3 mm in marginal garnet (Figure. 5.4c). However, inclusions commonly also remain consistent in size within a garnet (Figure. 5.4a) or changes in size may be localised to specific layers of inclusion trails (Figure. 5.4d).

Quartz is the most abundant inclusion type, comprising on average 6.8% of the volume of garnet within GR02. Quartz inclusions are typically <50 µm and more rarely reach up to 100 µm, most have a regular shape and are commonly elongate and aligned. Clear garnet within GR02 contains 1.7% ilmenite, 1.5% zircon and <1% allanite. Ilmenite occurs as two distinct morphologies; (a) large, irregularly-shaped aligned grains up to 50 µm with evidence of internal alteration (Figure. 5.4a-b), and (b) fine <3 µm euhedral grains (Figure. 5.4c-e). Detrital ilmenite has regular margins with the enclosing garnet, characteristic of recrystallization (Figure. 5.4b). Allanite, an epidote-group mineral with a wide range of compositions (Gieré & Sorensen, 2004), is irregularly shaped, most inclusions are >30 µm and display internal alteration textures (Figure. 5.5) producing a low REE

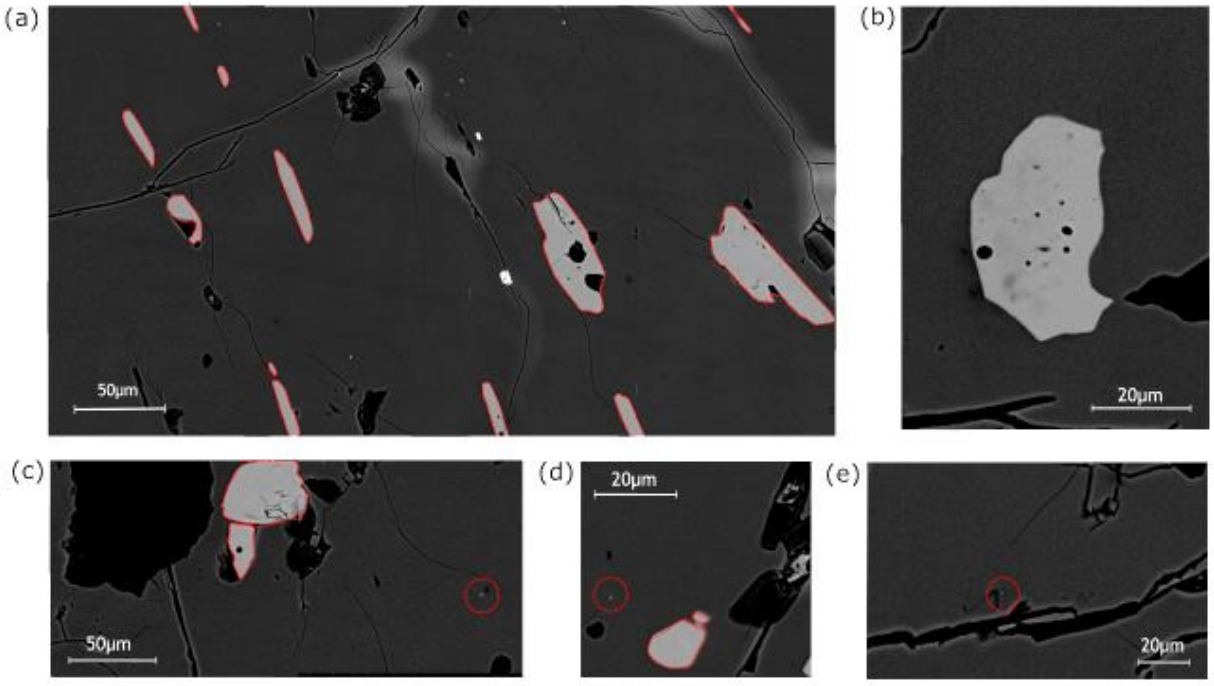

FIGURE 5.4: BSE images of ilmenite within GR01-4, (a) aligned ilmenite inclusions, (b) ilmenite morphology, regular contact with garnet and internal alteration and replacement by quartz, (c-d) metamorphic ilmenite (circled in red) typically occur proximally to detrital ilmenite, (e) authigenic fine-grained ilmenite adjacent to a quartz-filled fracture

allanite that appears darker (Figure 5.5). Zircon inclusion distribution and morphology will be discussed in detail in chapter 6.

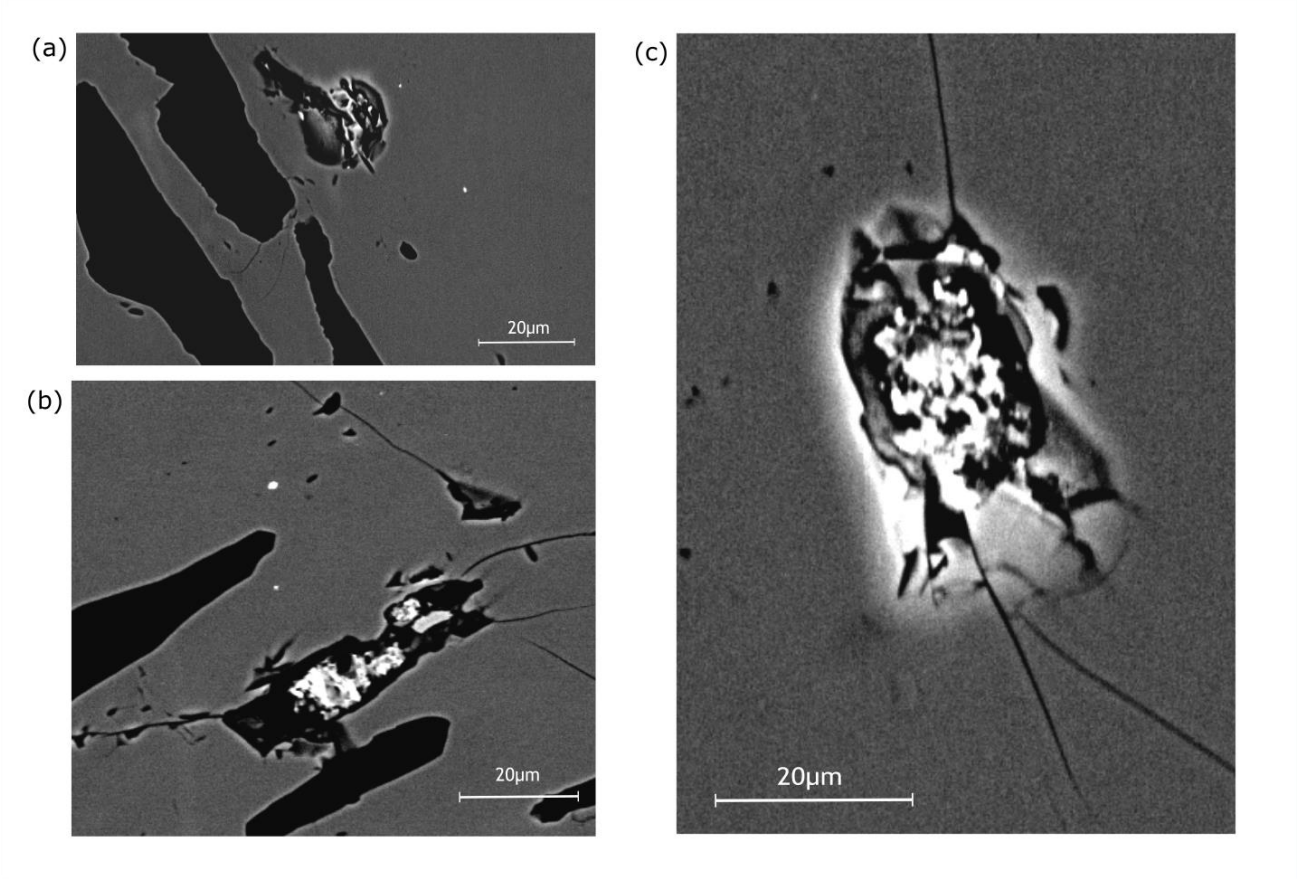

FIGURE 5.5: BSE images of allanite within clear garnet; (a) large allanite and quartz inclusion, (b) large allanite inclusion with surrounding microcracks in garnet, (c) allanite showing evidence of internal alteration producing a patchy BSE image with variability in the brightness

5.2.2.2 Results: chemistry of clear garnet

Clear garnet shows concentric divalent cation zoning from core to rim (Figure. 5.6). Mn produces a bell-shaped curve decreasing from 17 mol.% sps at the core to <1 mol.% sps at the margins. Fe and Mg display complimentary bowl-shaped profiles, Fe increases from 60 mol.% alm at the core to 80 mol.% alm at the rim, while Mg is lower but also increases from 9 mol.% in the core to <1 mol.% at the rim. Ca shows a less concentric profile with more small-scale fluctuations but generally mimics Mn, decreasing from 21 mol.% grs in the core to 13 mol.% grs at the rims.

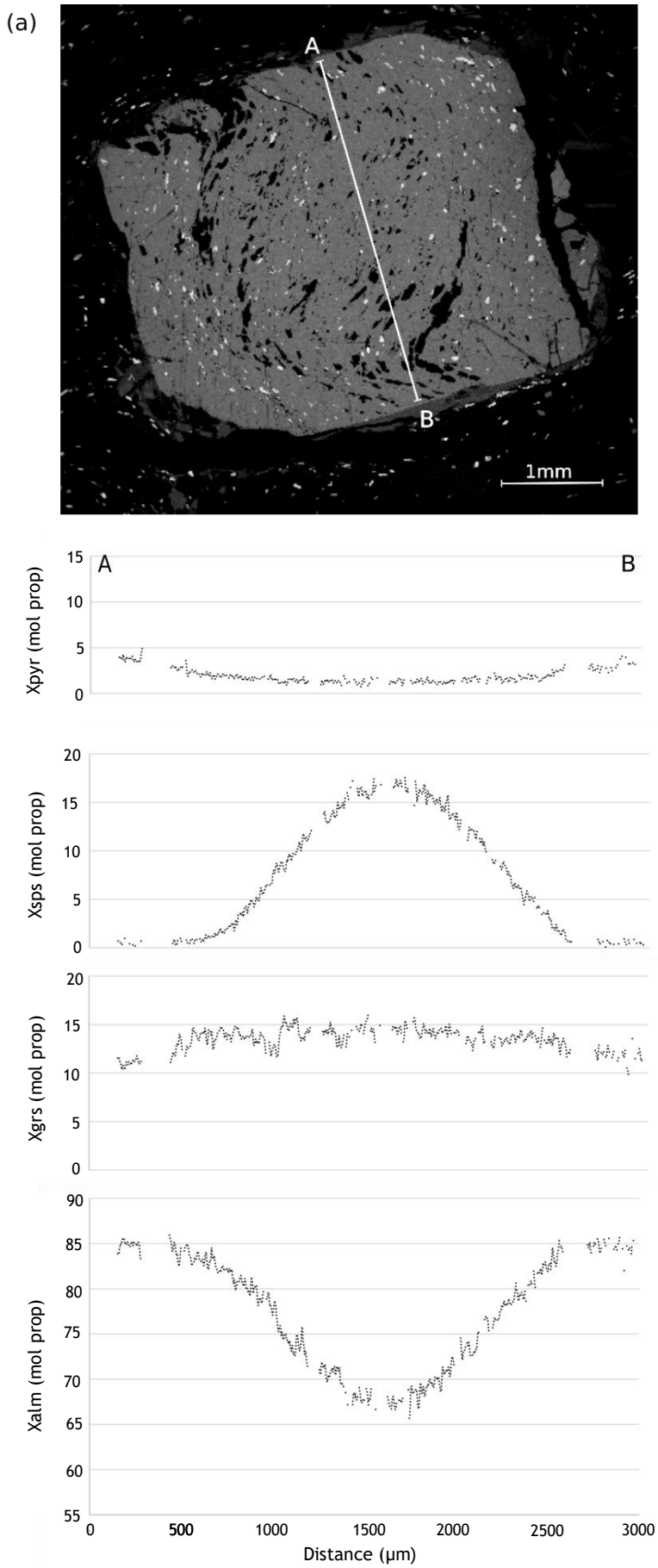

FIGURE 5.6: Zoning of major elements in clear garnet GR05-7, (a) BSE image of the porphyroblast showing the location of transect A-B, (b) pyrope profile with the molecular proportion of Mg across transect A-B (c) spessartine profile with the mol prop of Mn, (d) grossular profiles with the mol prop of Ca, and (e) almandine profile with the mol prop of Fe

5.2.2.3 Interpretation of clear garnet

Clear garnet is chemically heterogeneous (Lanari & Engi, 2017). The chemistry of clear garnet is consistent with growth zoning (Figure. 5.6) (Atherton, 1968; Dempster, 1985; Chakraborty, 1991; Gatewood et al., 2015), indicative it has undergone limited modification following porphyroblast growth and thus volume diffusion within garnet remains negligible at staurolite grade (Woodsworth, 1977; Carlson, 2006; Caddick et al., 2010; Ague & Carlson, 2013). Because garnet has been subject to limited modification it can serve as an archive of changing P-T-X conditions during growth (Spear et al., 1984; Jiang & Lasaga, 1990; Spear et al., 1991; Lanari & Engi, 2017; Raimondo et al., 2017) provided large-scale chemical equilibrium was achieved for the elements analysed (Chernoff & Carlson, 1997; Ague & Carlson, 2013; Spear et al., 2014)

Inclusions within garnet form when dissolution and/or diffusion is not effective enough to allow the removal of minerals adjacent to the porphyroblasts growing face (Passchier & Trouw, 2005). Garnet therefore captures matrix phases, particularly those which are difficult to dissolve, as inclusions (Passchier & Trouw, 2005; Baxter et al., 2017). Ilmenite within garnet displays evidence of internal alteration (Figure. 5.4b), typical of detrital grains. Allanite is likely sourced from the breakdown of detrital monazite early in the metamorphic history, likely at the breakdown of detrital monazite early in the metamorphic history, likely at conditions close to the chloritoid-biotite isograd (Overstreet, 1967; Williams, 2001; Gregory et al., 2007). The irregular morphology of allanite and its coexistence with matrix quartz is further indication monazite breakdown occurred prior to garnet growth. Allanite displays evidence of internal modification, likely a feature of metamictization. Metamictization results in the release of REE (rare earth elements) from radiation damaged zones (Gregory et al., 2007; Gieré & Sorensen, 2004) forming a low REE allanite locally that appears darker in BSE imaging (Figure. 5.5). Inclusion trail banding captures sedimentary layering from the matrix phase that the garnet overgrew. Compositional layering in the matrix produces quartz inclusion-rich bands of garnet where porphyroblasts overgrow quartzofeldspathic layers, and ilmenite-rich bands consistent with micaceous domains in the matrix.

Inclusion trails have a curved morphology indicating garnet growth was syntectonic (Zwart, 1960; Bell & Johnson, 1989; Ashley et al., 2016) capturing an early stage of deformation in the the core of garnet and tracking progressive changes to the orientation of the fabric and/or garnet through the preserved inclusion trails (Passchier & Trouw, 2005). Inclusion banding can be traced into the adjacent matrix in some porphyroblasts however, in most recrystallization of the matrix and the deflection of fabrics caused by continuing deformation after garnet growth produces a less distinct pattern. Fluid inclusions form surrounding fractures and mineral inclusions suggesting they are representative of garnet growth in fluid-rich areas (Crawford & Hollister, 1986).

Concentric changes to inclusion size within garnet may be a facet of; matrix grain size, changing garnet growth rates and changes to fluid composition, all of which can promote or inhibit dissolution and diffusion (Carlson, 1991; Carlson et al., 1995; Daniel & Spear, 1998; Dempster et al., 2017). The concentric increase in mineral inclusion size present in some garnets is further indication garnet growth may be syntectonic. As temperatures increase the matrix becomes coarser and as a result the later formed rims contain coarser inclusions than the earlier formed core (Passchier & Trouw, 2005). Generally, quartz inclusions are larger and more rounded than matrix quartz. Alternatively, the matrix grain size can reduce through time mechanically (Vernon, 2018). Following the formation of garnet, deformation has the ability to decrease the matrix grain size producing a population of coarse inclusions within garnet and a finer matrix. Dissolution may influence inclusion morphology resulting in the preservation of a population of rounded inclusions, despite a more angular matrix (Passchier & Trouw, 2005).

5.2.3 Cloudy garnet

When clear garnet described in 5.2.2 undergoes coupled dissolution-reprecipitation its texture and chemistry is modified producing cloudy garnet. While clear garnet captures P-T-X conditions during porphyroblast growth, this post-growth modification via coupled dissolution-reprecipitation results in partial resetting (Dempster et al., 2019). Within GR01 porphyroblasts are typically comprised of both clear and cloudy garnet in varying proportions. Cloudy bands form irregular morphologies, typically surrounding the margins (Figure. 5.7) and

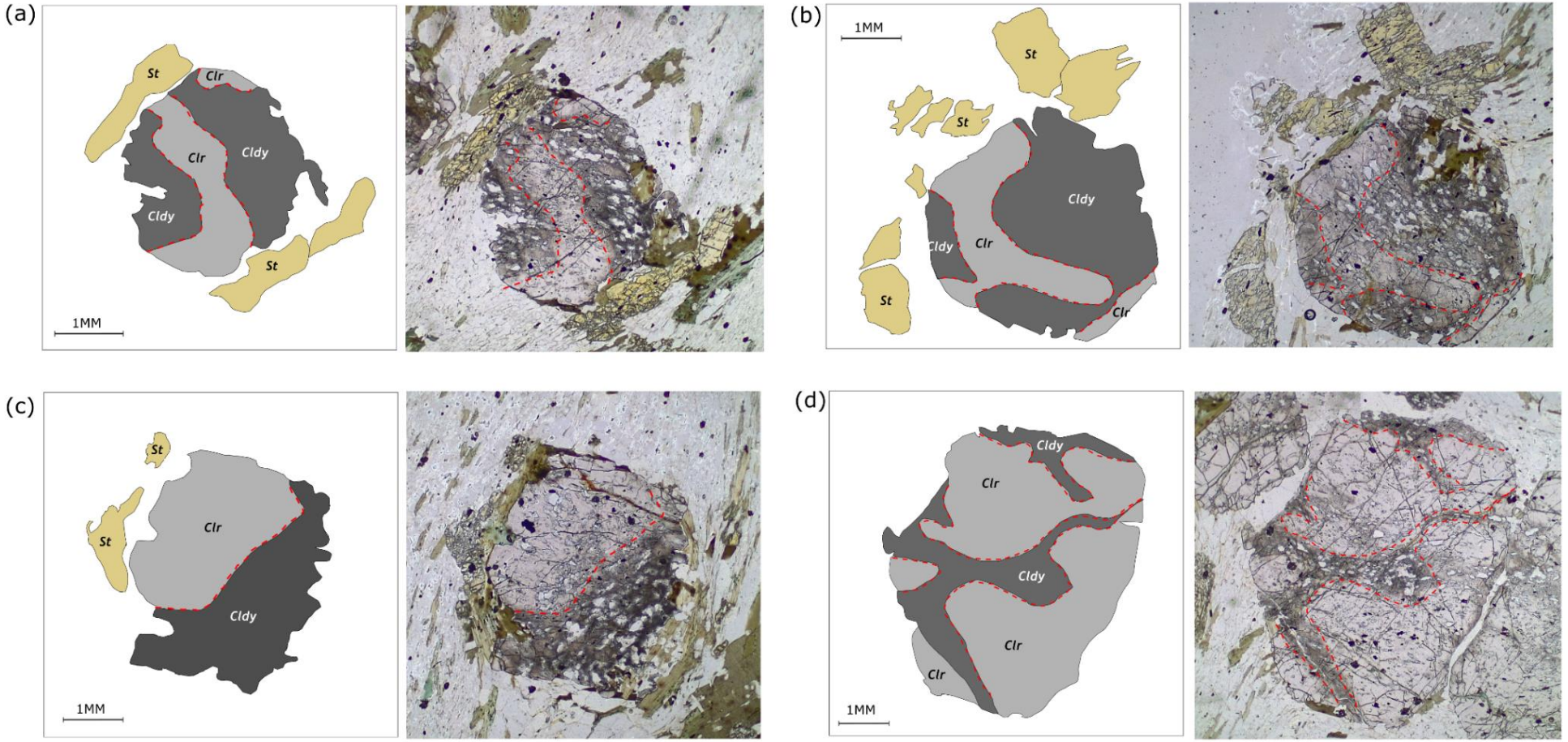

FIGURE 5.7: TLM images and cartoons illustrating the geometry of cloudy garnet and the location of staurolite within GR01 (a) cloudy garnet with geometry consistent with original matrix lithostatic layering, (b) marginally focussed cloudy garnet with clear band focussed around the core (c) cloudiness along one margin of garnet where dissolution is focussed and away from staurolite growth, (d) garnet with no adjacent staurolite that has undergone limited dissolution-reprecipitation, primarily along fractures and margins

fractures (Figure. 5.7d), although occasionally cutting though grains in apparently random orientations (Figure. 5.7b) (Figure. 5.8). Where more than one band of cloudy garnet is present within a porphyroblast they tend to be parallel (Figure. 5.7a-b).

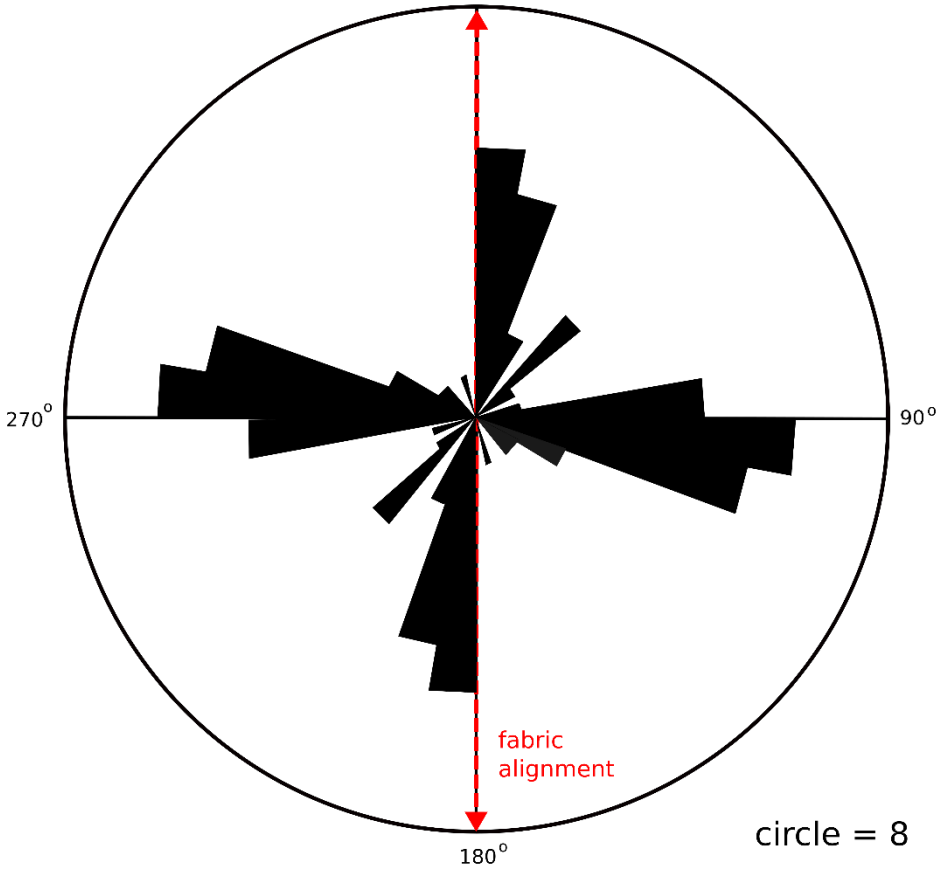

Figure 5.8: Alignment of cloudy bands in staurolite-zone schist GR01 across all partially cloudy garnet measure against matrix fabric alignment which is at 180°

5.2.3.1 Results: texture of cloudy garnet

Cloudy garnet is texturally distinct from clear garnet, containing a high concentration of 10s-100s μm quartz inclusions and a large population of rounded <3 μm fluid inclusions (Figure. 5.9). Fluid inclusions typically comprise 2-10 vol.% of garnet. Quartz inclusions are irregularly shaped and display no alignment (Figure. 5.9c) and typically have a thin, <10 μm fluid inclusion-poor rim surrounding them. Fluid inclusions are rounded to sub-rounded (Figure. 5.10d) and show evidence of alignment (Figure. 5.10a-b). However, not all fluid inclusions are aligned, some appear randomly distributed in BSE imaging (Figure. 5.9d).

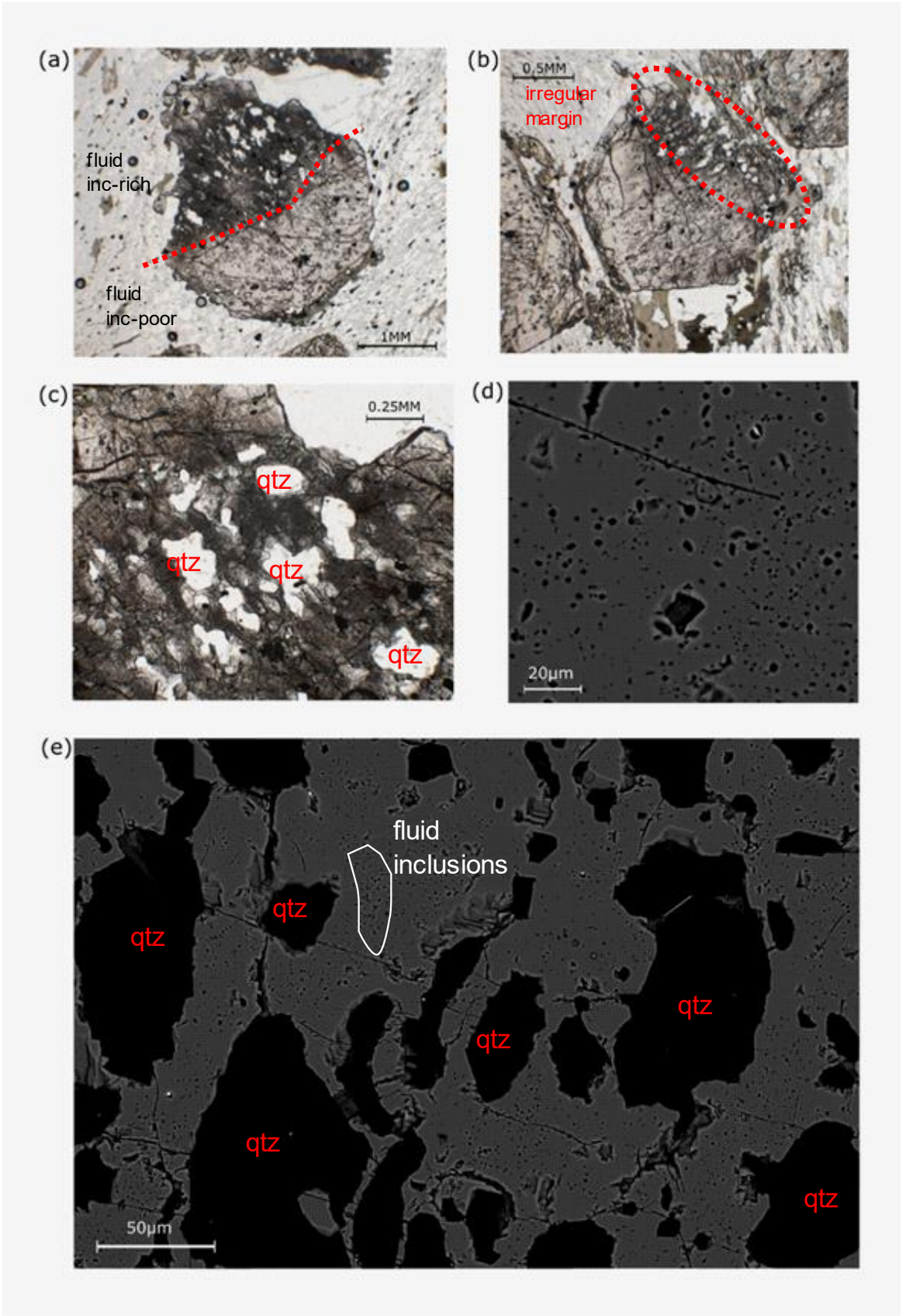

FIGURE 5.9: Textural characteristics of cloudy garnet using transmitted light microscopy (TLM) and BSE imaging, (a) cloudy garnet (top half of porphyroblast) appears darker than clear garnet in PPL due to the abundance of fluid inclusions (b) PPL image of cloudy garnet illustrating irregular margins due to extensive dissolution, (c) irregular quartz inclusions in PPL, (d) BSE image of sub-rounded unaligned fluid inclusions within cloudy garnet, and (e) BSE image of cloudy garnet, large black inclusions are irregular quartz formed during dissolution-reprecipitation while <3µm inclusions may represent fluid inclusions

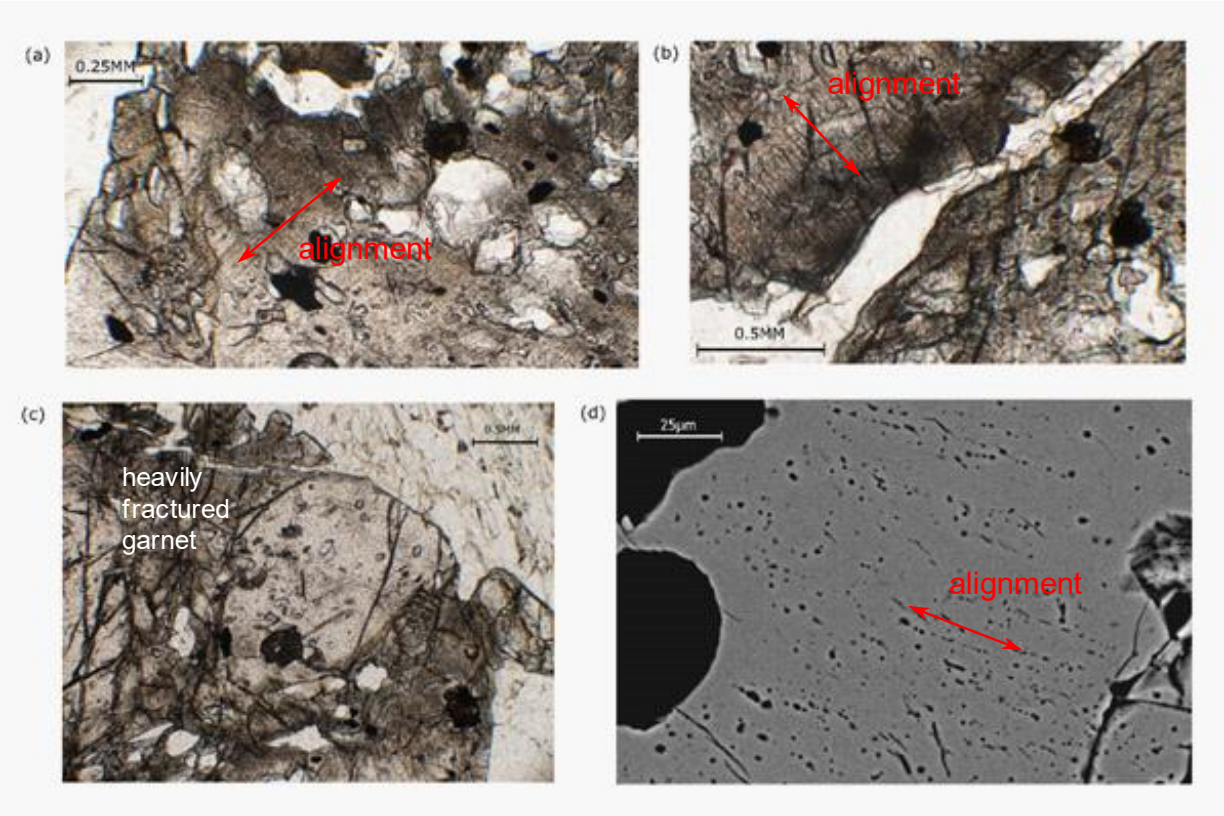

FIGURE 5.10: Fluid inclusion alignment in cloudy garnet in GR01, (a-b) PPL images of alignment of fluid inclusions in GR01-4, (c) PPL image of garnet GR01-9 where cloudy garnet formation is focussed along fractures, this altered garnet shows limited evidence of alignment, and (d) fluid inclusion alignment as it appears in BSE imaging

The extent of cloudiness of individual garnet porphyroblasts varies, some porphyroblasts are entirely clear while others are comprised of up to 75% cloudy garnet. Within predominantly clear porphyroblasts the fluid inclusions in the locally cloudy zones are typically unaligned (Figure. 5.10c). Fluid inclusion alignment is visible using transmitted light microscopy (Figure. 5.10a-b) however, using backscattered electron (BSE) imaging at higher magnification allows the identification of individual fluid inclusions and planes of alignment (Figure. 10d). Fluid inclusion alignment is relatively consistent within a single porphyroblast (Figure. 5.11), with a dominant primary plane of alignment and a second less frequent alignment which is roughly perpendicular (Figure. 5.12). A large number of fluid inclusions pictured within cloudy garnet using BSE imaging show no evidence of alignment (Figure. 5.9d).

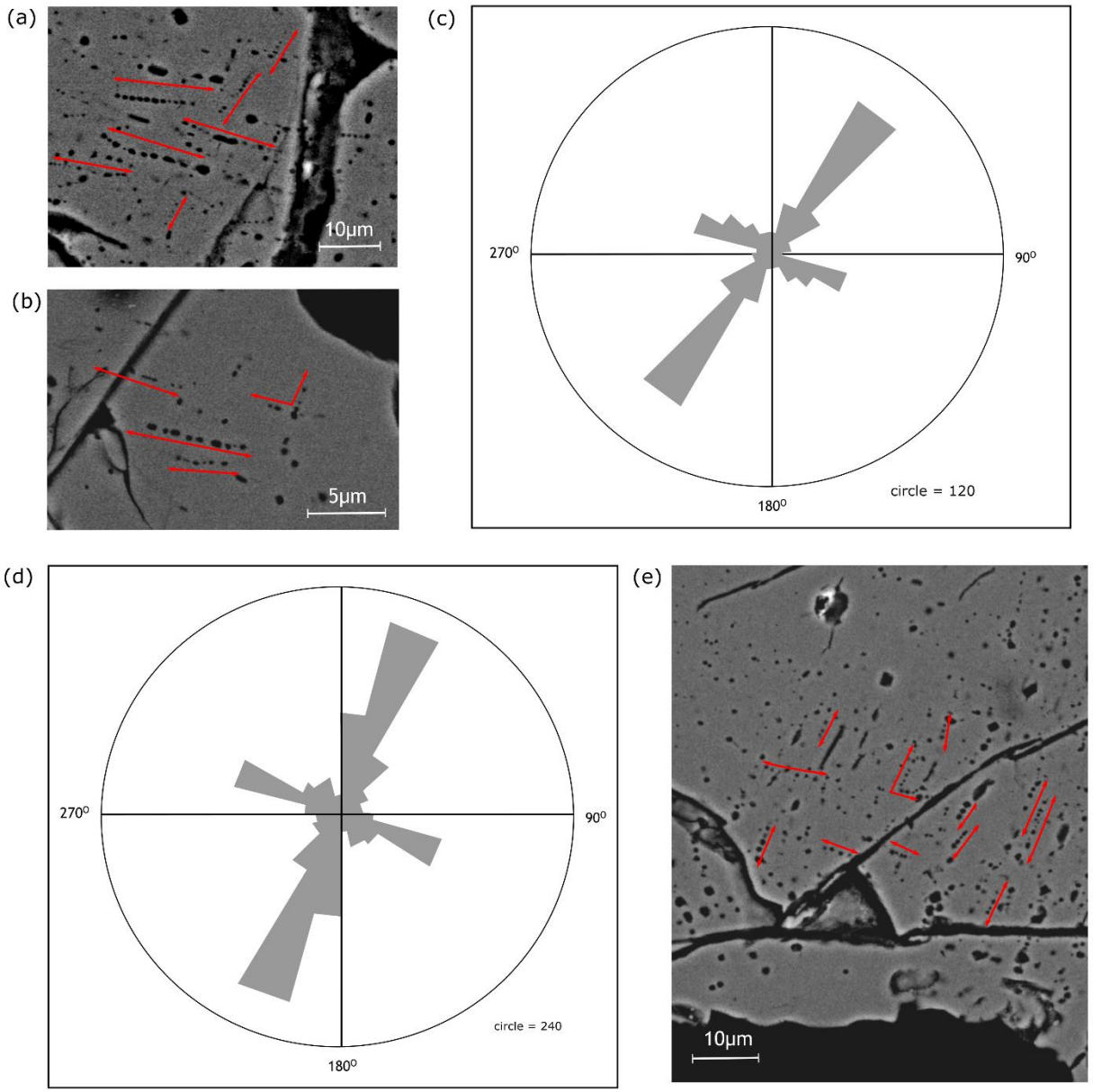

FIGURE 5.11: Fluid inclusion alignment in GR01, (a-b) BSE image of fluid inclusions within cloudy garnet with red arrows indicating alignment of inclusions in GR01-2, (c) rose diagram showing the orientation of the two planes of alignment in GR01-2, secondary alignment generally forms 70-90° from primary, (d) fluid inclusion alignment in GR01-9, (e) BSE image of fluid inclusion alignment illustrating the two ca. perpendicular planes

Within cloudy garnet mineral inclusions are more abundant and display a wider range of compositions than within clear garnet, most notably quartz inclusions increase in abundance. Quartz inclusions form much larger (>200 µm), irregularly shaped morphologies (Figure. 5.9e) than within clear garnet. Rutile and xenotime are present alongside zircon and ilmenite in cloudy garnet. Within clear garnet, allanite is present (Figure. 5.5) but there is no monazite, while cloudy garnet contains monazite (Figure. 5.13) and no allanite. Monazite inclusions do occur occasionally within larger quartz inclusions in clear garnet however, this is rare.

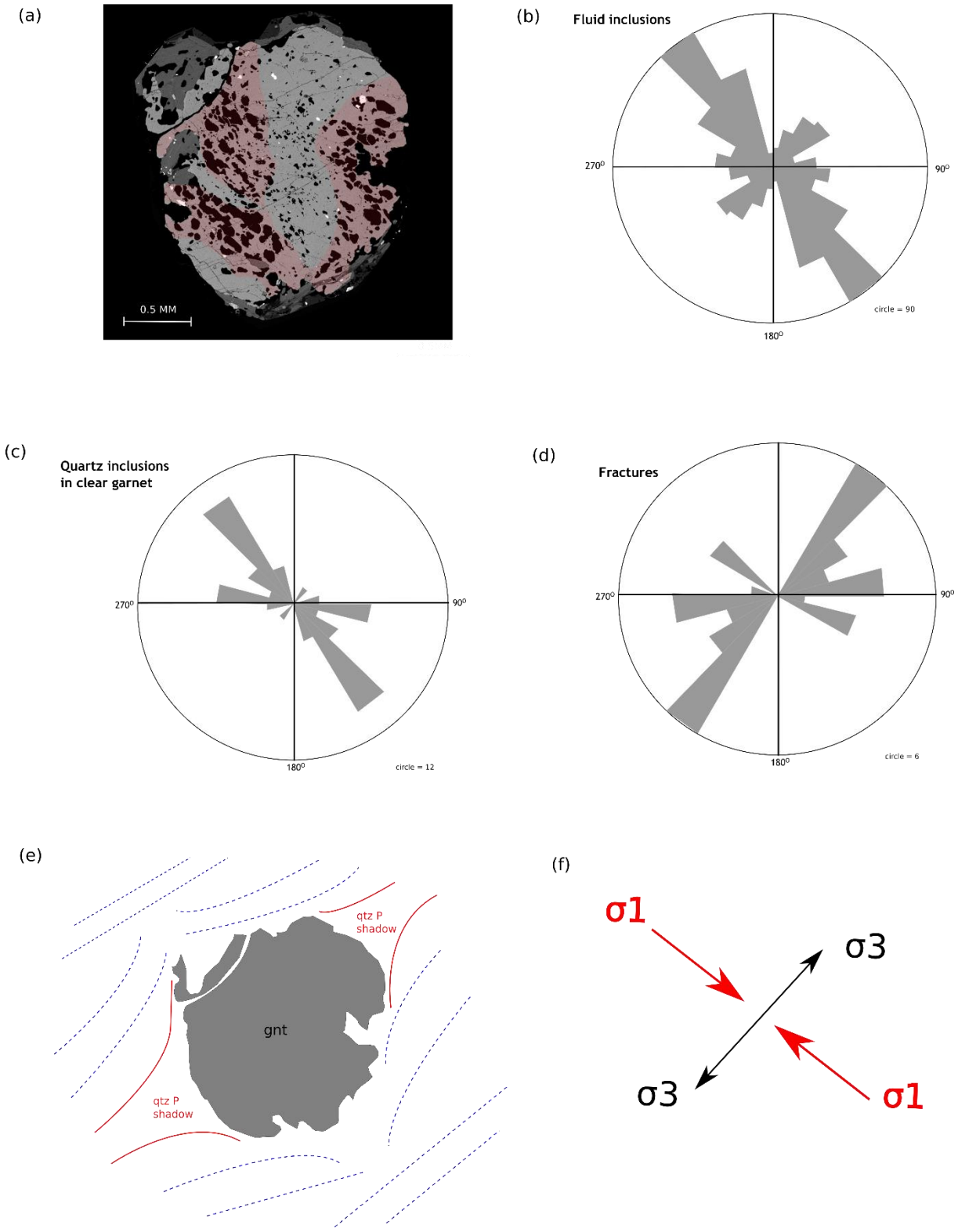

FIGURE 5.12: Alignment of fluid inclusions in GR01-9, (a) BSE image of garnet GR01-9 with cloudy domains highlighted in red, the remaining garnet is clear, (b) alignment of fluid inclusions within cloudy garnet, alignment occurs along one primary plane with minor alignment approximately perpendicular, (c) alignment of long axis of quartz inclusions within clear garnet, a facet of matrix fabric during garnet formation, and (d) the alignment of main fractures (>1 mm) in the porphyroblast, (e) cartoon illustrating matrix fabrics and the location of quartz pressure shadows surrounding GR01-9, and (f) stress field of garnet GR01-9

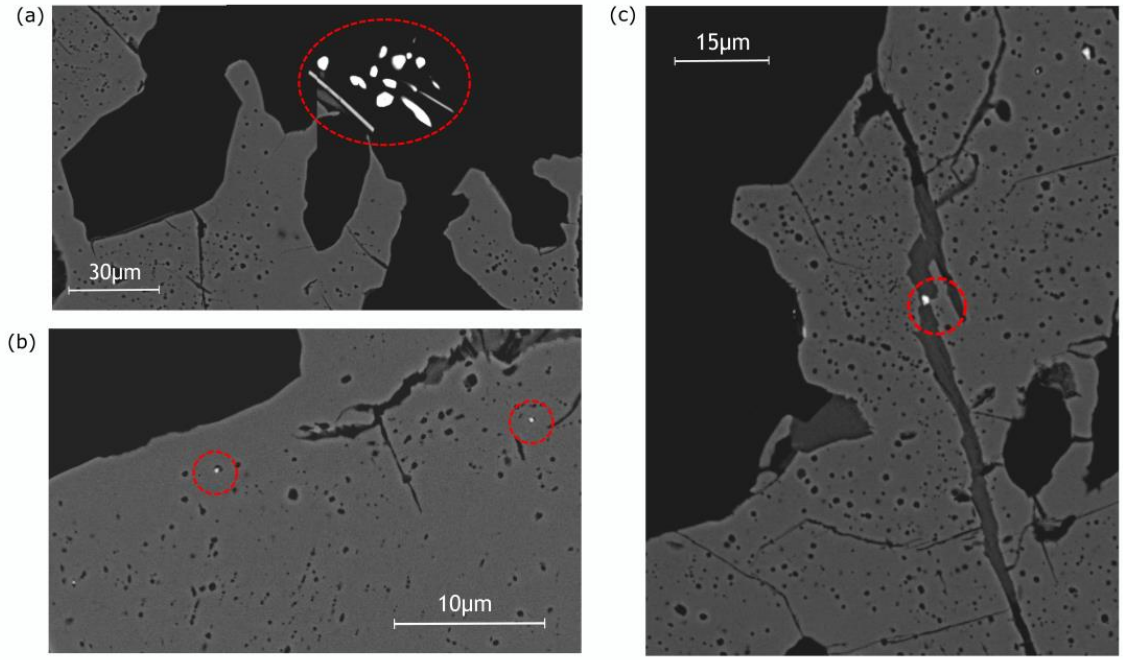

FIGURE 5.13: BSE images of monazite within cloudy garnet; (a) monazite within a large, irregularly shaped quartz inclusion formed during coupled dissolution-reprecipitation, (b) monazite within quartz-filled fracture, and (c) small monazite includions hosted in small inclusion, likely a fluid inclusion, (left) and garnet (right)

Monazite within cloudy garnet, particularly larger monazite, is commonly associated with infilled fractures (Figure. 5.13b) and quartz inclusions (Figure. 5.11c). Some smaller monazite inclusions occur within fluid inclusions and occasionally encapsulated within garnet (Figure. 5.13d). Clear garnet contains around 1.2 μm^2 allanite per mm^2 of garnet while cloudy garnet contains 0.11 μm^2 monazite per mm^2. EDX analysis reveals monazite contains a higher proportion og LREE such as Ce and Nd while allanite contains more HREE, such as Gd (Figure. 5.14). Rutile rarely appears as small needles, <5 µm white it more commonly rutile forms irregular patches within large, detrital ilmenite inclusions (Figure. 5.15).

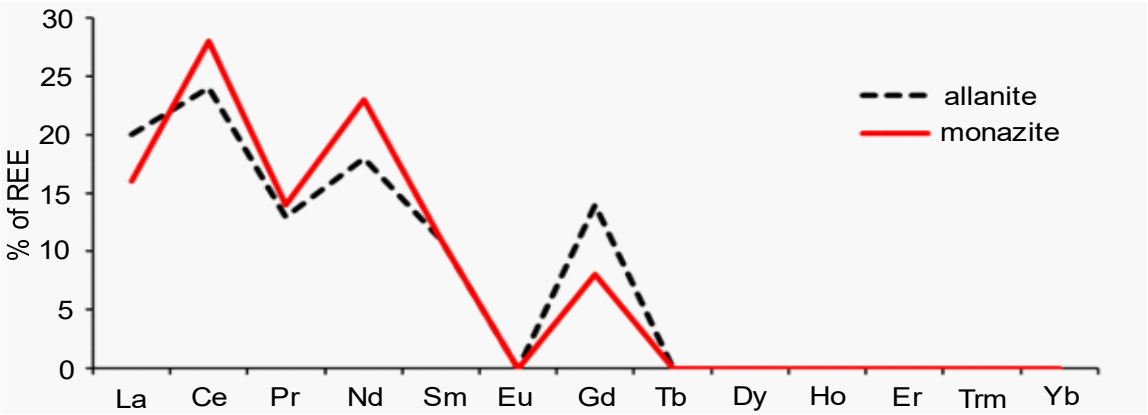

FIGURE 5.14: REE profiles of parent allanite, from clear garnet and product monazite, from cloudy garnet illustrating the proportion of REE across the phases. Values are averaged from 5 EDX (energy dispersive x-ray) spot analyses of each mineral phase

Surrounding all mineral inclusions there is a thin rim of garnet that is typically fluid inclusion-free, typically <20 μm wide (Figure. 5.9e). This rim appears to be present irrespective of the inclusion type but varies depending on the size of inclusions appearing thickest surrounding large inclusions or clusters of inclusions (Figure. 5.9e).

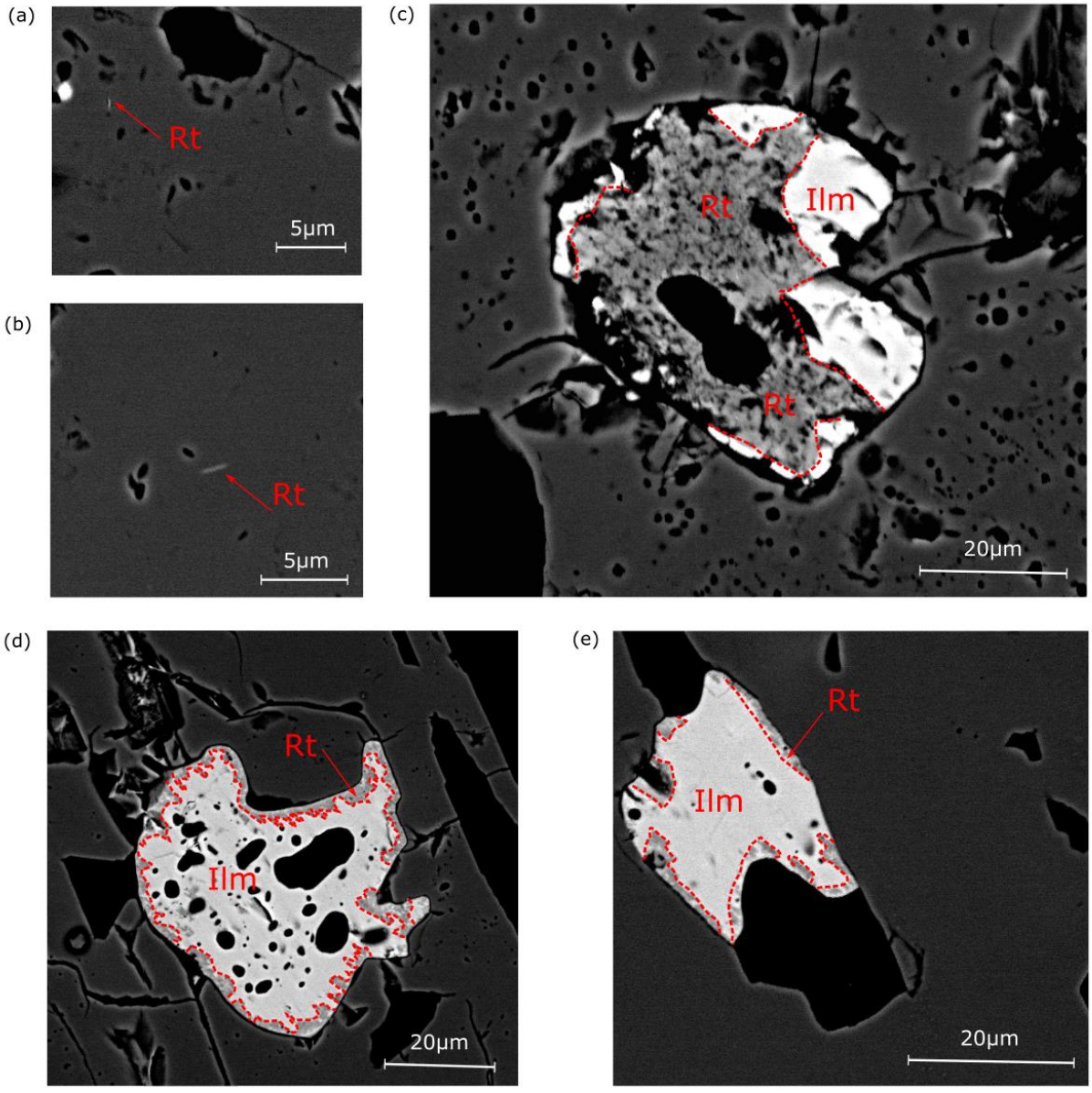

FIGURE 5.15: BSE images of morphology of rutile needles in cloudy garnet (a-c) and clear garnet (d-e); (a-b) authigenic rutile needles, (c) patchy rutile replacement with only ilmenite rims remaining, (d-e) less extensive rutile replacement with exsolution lamellae focussed at the margins of detrital ilmenite in clear garnet

Cloudy garnet has a high fracture density. There are major fractures consistent with those in clear garnet however they show more evidence of branching within cloudy garnet. The branching fractures are consistently >45º and commonly perpendicular (Figure. 5.16). These major fractures can contain a silica-rich fracture fill in both clear and cloudy garnet. Additionally, radial fractures surrounding inclusions are present, they commonly have a curved morphology and are only rarely infilled (Figure. 5.16). They are typically <100 µm long, however they occasionally appear longer surrounding larger quartz inclusions, particularly where they connect adjacent inclusions. Both radial microcracks and major fractures are more abundant in cloudy garnet than clear garnet.

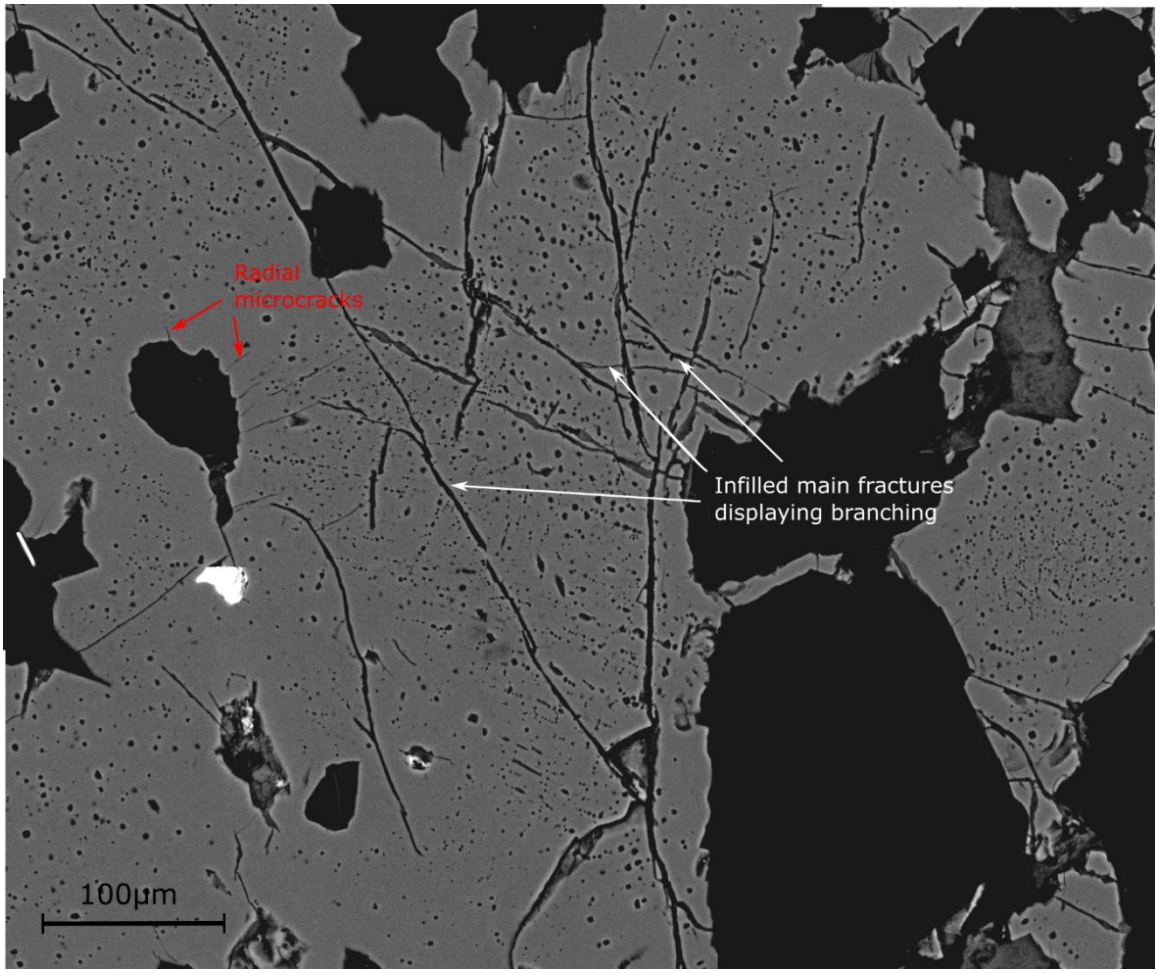

FIGURE 5.16: BSE image of fracture density and morphology within cloudy garnet in GR01-4 comprising radial microcracks surrounding quartz inclusions and infilled factures with branching, typically branches are 45-90º from the main fracture

5.2.3.2 Results: chemistry of cloudy garnet

Cloudy garnet has an altered chemistry compared to clear garnet (Figure. 5.17). Within cloudy garnet almandine and pyrope are higher than adjacent clear, ca. +7-10 mol.% in Fe and ca. +2-4 mol.% in Mg. While grossular and spessartine typically are typically lower in cloudy garnet, ca. -6-10 mol.% in Ca and ca. -5 mol.% in Mn. Mn behaves less consistently than the other cations, occasionally at the rims of garnet there is a high spessartine content (Figure. 5.18c). The change in chemistry at the cloudy-clear margins is gradual and the distance over which the composition changes varies for each cation (Figure. 5.17). Mn^{2+} shows a gradual change over ca. 50 µm while Ca^{2+} shows the sharpest change, with chemistry adjusting over 15 µm (Figure 5.17c).

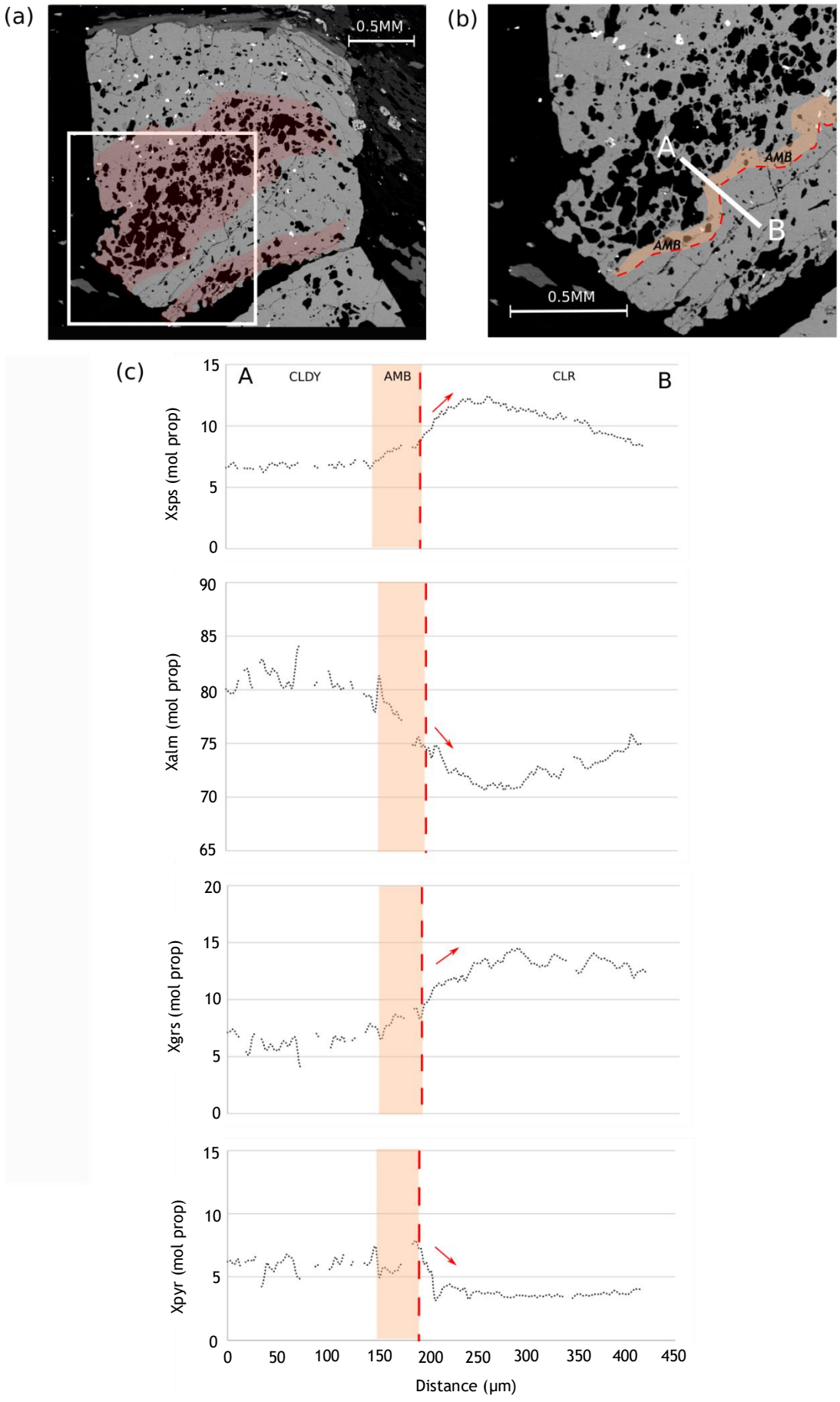

FIGURE 5.17: Chemistry associated with cloudy-clear boundary, (a-b) BSE images showing the location of the transect within GR01-2, (c) profiles for Mn, Fe, Mg and Ca across transect A-B, in orange is garnet with 'ambiguous' texture and the red line delineates the boundary

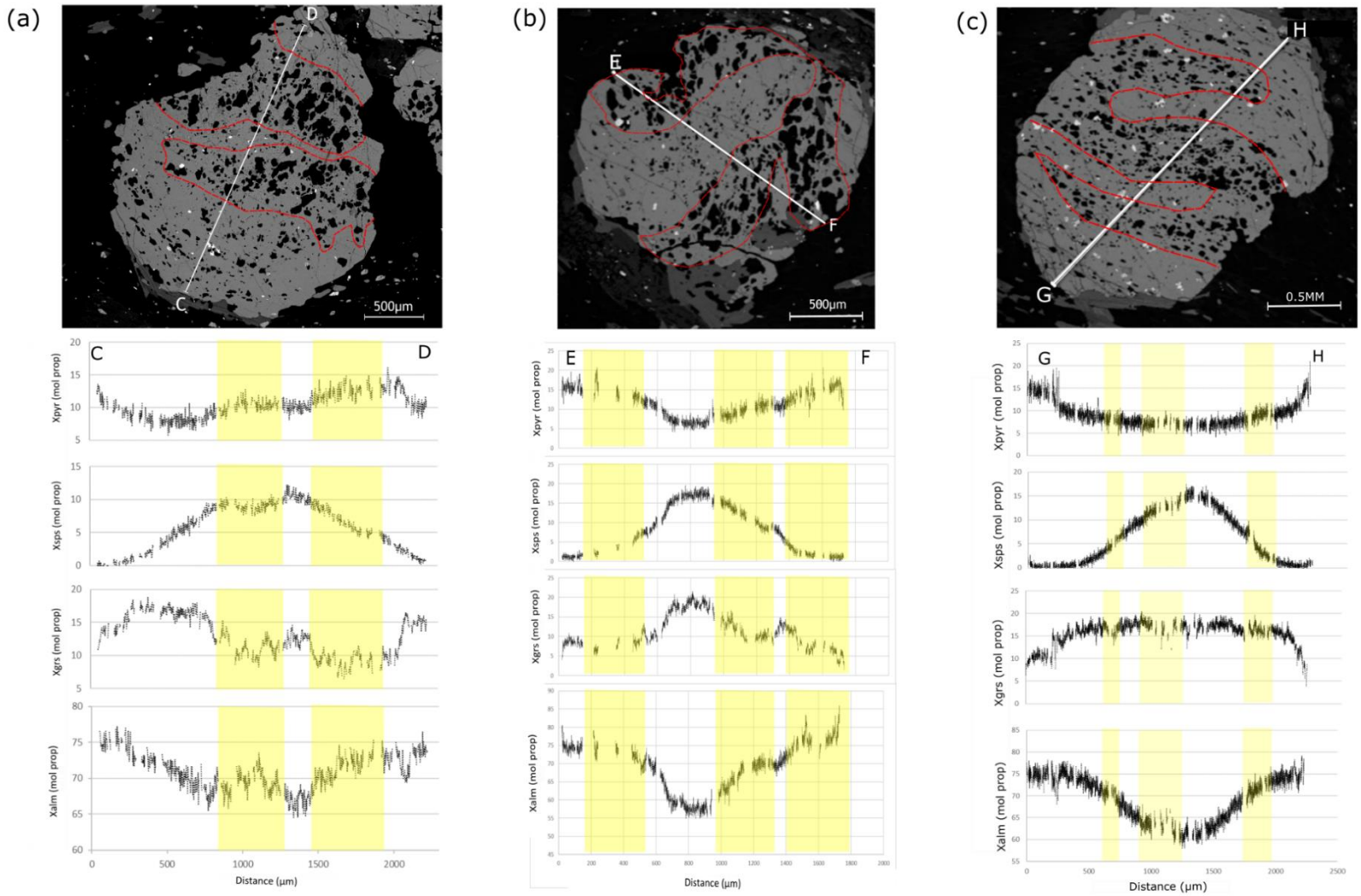

FIGURE 5.18: Transects of the molecular proportions of Mg, Mn, Ca and Fe across porphyroblasts within GR01, BSE images show the location of transects with red lines delineating cloudy areas and accompanying yellow in the plots highlighting cloudy garnet, (a) transect A-B across porphyroblast 9, (b) transect C-D across porphyroblast 4, (c) transect E-F across porphyroblast 1

5.2.3.3 Interpretation of cloudy garnet

Coupled dissolution-reprecipitation of garnet involves the breakdown of garnet in the presence of fluids resulting in the production of staurolite expressed through the reaction, garnet + muscovite + quartz → staurolite + biotite + H_2O (Dempster et al., 2017). The volume loss of garnet associated with the formation of fluid and quartz inclusions enables the transportation of some material in the fluid phase (Ruiz-Agudo et al., 2014), e.g. Al is transported away from the porphyroblast to the site of staurolite formation. Garnet volume decreases by ca. 39% on average through the formation of fractures, mineral inclusions and fluid inclusions during dissolution-reprecipitation (Figure. 5.19). This volume deficit in cloudy garnet is the result of garnet consumption to form staurolite. The creation of interconnected porosity is critical for the propagation of coupled dissolution-reprecipitation as it enables fluid infiltration to unmodified garnet at the reaction

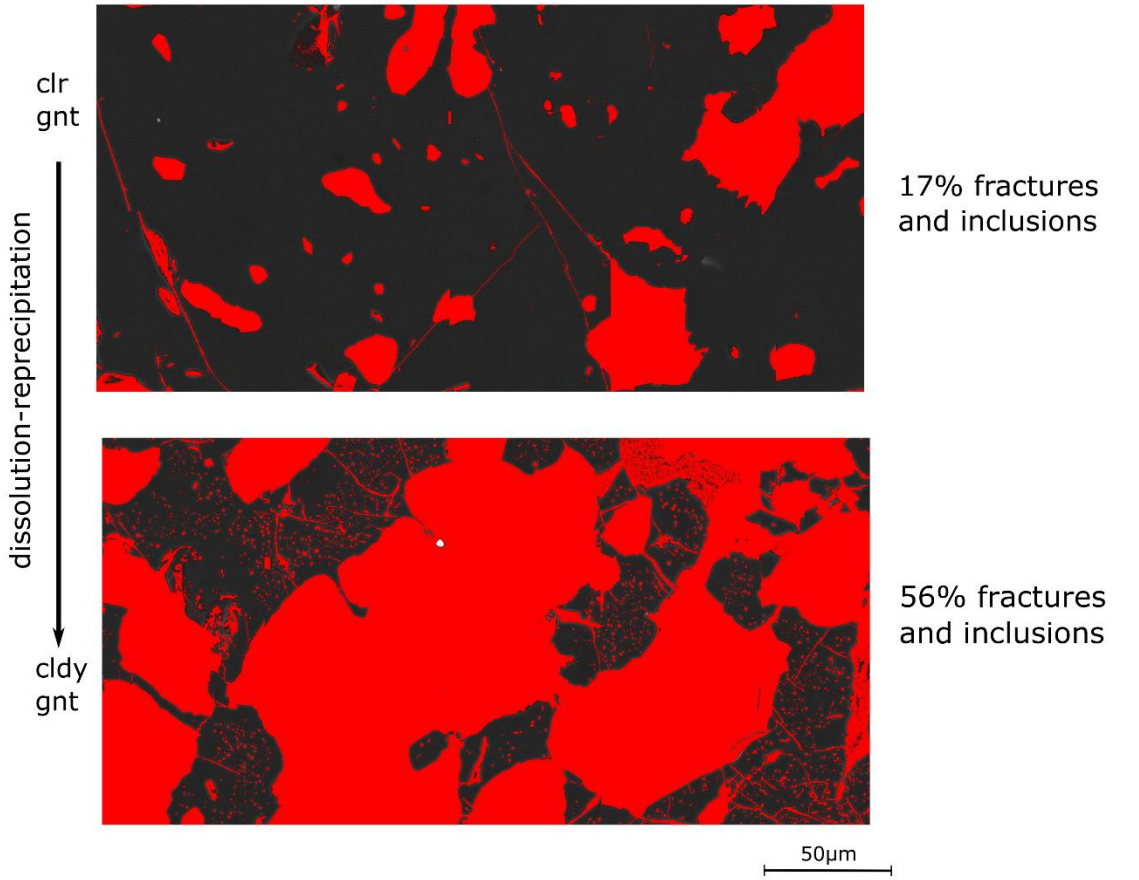

FIGURE 5.19: Altered BSE images of garnet replacement in cloudy garnet following dissolution reprecipitation, image produced in imagej using dark colour thresholds to highlight low mean atomic number features thus capturing fractures, quartz and fluid inclusions, highlighted in red

front (Putnis & Putnis, 2007; Putnis & Austrheim, 2010; Ruiz-Agudo et al., 2014; Luquot et al., 2015; Putnis, 2015).

During experiments on pyroxene and amphibole, couple dissolution-reprecipitation commonly involves the formation of a silica-rich amorphous phase (Keller et al., 2006; Bukovská et al., 2015; Konrad-Schmolke et al., 2018). This amorphous phase allows the direct repolymerization of product phase(s) from fluids, as well as promoting fluid flow through the creation of inclusion or grain boundaries (Konrad-Schmolke, et al., 2018). While quartz inclusions within cloudy garnet are crystalline rather than amorphous, this may be a feature of the longer timescales involved in natural samples versus the experimental amorphous studies. The inclusions may represent an intermediate phase during dissolution-reprecipitation of garnet, or what is preserved following the repolymerisation of the 'amorphous' phase. The apparently random replacement of garnet by quartz during dissolution-reprecipitation may instead be controlled by crystal defects, along which the amorphous material may preferentially form (Konrad-Schmolke, 2018). All reported amorphous phases are more chemically complex silicate minerals than quartz, however garnet has not been analysed in the context of amorphous phases. Quartz is a product phase formed during both staurolite formation (garnet + muscovite + water → staurolite + biotite + quartz) and sillimanite formation (garnet + muscovite → sillimanite + biotite + quartz). During coupled dissolution-reprecipitation quartz may form following garnet dissolution and assist with the transport of alkalis (e.g. Al, Fe, Mg and Mn) between reactant and product phases (Konrad-Schmolke et al., 2018).

Monazite is the second most abundant mineral inclusion by volume within cloudy garnet. Monazite may be detrital however it typically disappears early in the regional metamorphic history, well before mid-amphibolite facies (Overstreet, 1967; Williams, 2001). The monazite within garnet is likely metamorphic forming at the expense of allanite at the garnet-staurolite isograd at ca. 500^{o}C (Wing et al., 2003; Corrie & Kohn, 2008; Gregory et al., 2007; Spear, 2010). When garnet undergoes dissolution-reprecipitation, fluids may promote the allanite to monazite transformation. The result is clear garnet containing allanite and no monazite, and cloudy garnet contains monazite and no allanite. Clear garnet contains more allanite than cloudy garnet contains monazite. Clear garnet more

rarely contains fine monazite confined to quartz inclusions however these were likely captured from the matrix during garnet growth. Allanite generally contains less Ce per mol than monazite owing to its more variable composition (Ercit, 2002), as a result the volume of monazite produced from allanite following coupled dissolution-reprecipitation decreases. Garnet is more compatible with heavy rare earth elements (HREE) (Rubatto, 2002; Sinh, V.B.T et al., 2019) so during the allanite to monazite transformation garnet may incorporate some of the HREE from allanite dissolution, accounting for the difference and producing monazite with a higher light rare earth element (LREE) profile (Figure 5.14). Rutile needles also form exclusively within cloudy garnet, indicative that they too form during dissolution-reprecipitation (Hwang et al., 2019).

The increased abundance and variety of mineral inclusions in cloudy garnet is further evidence of the ability of fluids involved in coupled dissolution-reprecipitation to transport high field strength elements (HFSE), such as Ce, P and Th for monazite, or potentially Zr for zircon. Mineral inclusions produce fluid pathways through the creation of (a) microcracks and fractures (Whitney et al., 1996; Whitney et al., 2000), and (b) boundaries between the inclusion and host (Hames & Menard, 1993). These boundaries may enable the escape of fluids from host garnet immediately adjacent to inclusions producing fluid inclusion-free rims.

Fluid inclusions within garnet are the result of rapid growth in a fluid-rich environment (Crawford & Hollister, 1986). Coupled dissolution-reprecipitation has the ability to produce fluid inclusions within the precipitating product phase (Martin et al., 2011; Ruiz-Agudo et al., 2014; Putnis, 2015; Dempster et al., 2017). Fluid inclusions are relics of porosity resulting from the partial healing of fluid pathways and channels that assisted in the transportation of fluid and material to and from the reaction interface during coupled dissolution-reprecipitation (Martin et al., 2011). Dissolution is assumed to be the most kinetically difficult process, and therefore the limiting factor, while precipitation is relatively fast (Ruiz-Agudo et al., 2014). Fluid inclusions can be primary, formed during growth, or secondary, formed after growth (Shepherd, 1990). The prevalence of fluid inclusions in cloudy garnet indicates that they also form during the coupled dissolution-reprecipitation process. Fluid inclusions may be aligned as a result of (a) active deformation (Hollister, 1986), (b) the crystallographic structure of garnet (Dempster et al.,

2017), or (c) healing of microcracks and fractures (Shepherd, 1990). Active deformation would produce one consistent plane of alignment parallel to the main extensional stress, σ3, in continuity with the matrix fabric. The crystallographic structure of garnet is the crystal-preferred orientation of the lattice during growth or deformation (Powell, 1966; Kleinschodt & McGrew, 2000; Mainprice et al., 2004).

It is primarily a facet of (a) matrix fabric (Powell, 1966), (b) nucleation of multiple proto-porphyroblasts, and (c) epitaxy (Eitel, 1964; Powell, 1966). The large number of influencing factors means crystallographic orientation of garnet is variable, fluid inclusions produced in this way should form localised regions with different orientations. Fluid-filled fractures and microcracks have a high surface energy and as such heal rapidly in mid-crustal conditions resulting in a series of aligned fluid inclusions (Shepherd, 1990). Fractures within these garnets are predominantly extensional forming parallel to the dominant compressive stress, σ1 (Figure. 5.20). The orientation of microcracks is less predictable, forming radially surrounding inclusions, preferentially at corners (Whitney et al., 2000). Mineral inclusions in cloudy garnet are unaligned and irregularly shaped (Dempster et al., 2017) producing a wide array of potential fracture orientations. Alignment from the healing of the dominant extensional fractures would be parallel to σ1, but highly variable due to the potential influence of microcracks.

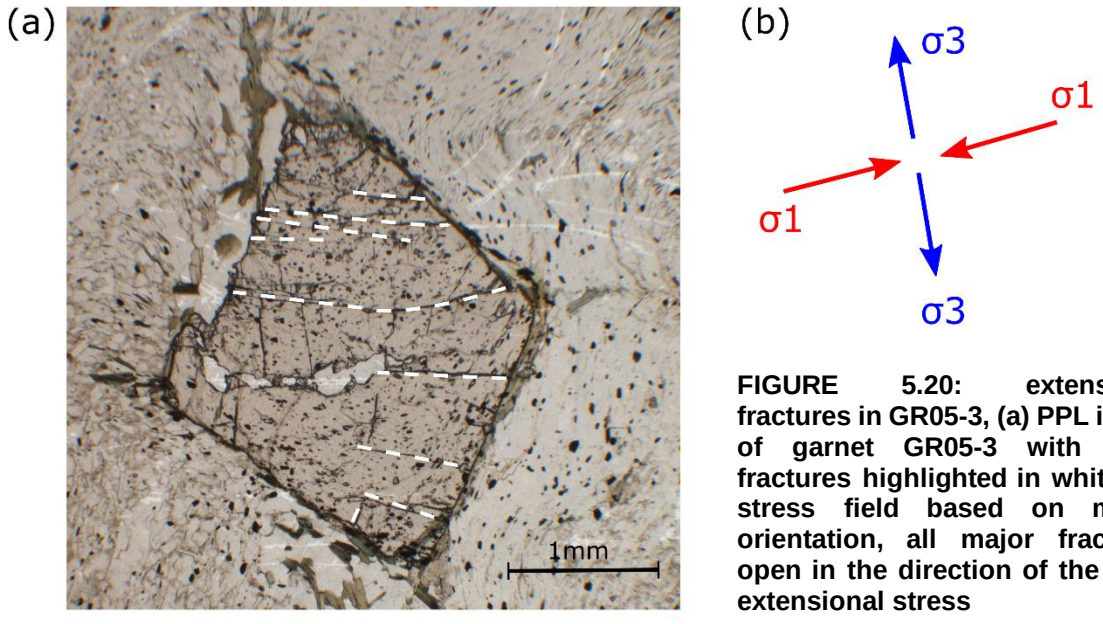

FIGURE 5.20: extensional fractures in GR05-3, (a) PPL image of garnet GR05-3 with main fractures highlighted in white, (b) stress field based on matrix orientation, all major fractures open in the direction of the main extensional stress

Fluid inclusions in cloudy garnet typically display a dominant alignment with another less well-defined plane perpendicular to it (Figure. 5.12b), different areas within the garnet contain fluid inclusions aligned to these different orientations. The primary alignment matches the orientation of quartz inclusions within adjacent clear garnet (Figure. 5.12c), a facet of the matrix fabric which is aligned parallel to σ3. The second alignment, approximately perpendicular to primary, forms along the same plane as extensional fractures (Figure. 5.12d). Fluid inclusion alignment appears to be predominantly a facet of healing of extensional fractures within these schists. The secondary alignment of fluid inclusions is parallel to matrix foliation, displaying the same alignment as inclusions trapped within garnet during growth. Both planes of fluid inclusion alignment are therefore controlled primarily by deformation.

Unaligned fluid inclusions may form asynchronously, either before or after the production of aligned inclusions during coupled dissolution-reprecipitation. However, if this were the case fluid inclusions are unlikely to be exclusively found in cloudy garnet. Sample preparation may remove evidence of fluid inclusion alignment, where the sample cut is >45° from the plane of alignment identification becomes difficult using scanning electron microscopy. This bias is unlikely to be the cause for all unaligned fluid inclusions as they comprise a majority of the population. There are likely three different populations of fluid inclusions within cloudy garnet; (a) primary inclusions formed during garnet growth, (b) those formed during coupled dissolution-reprecipitation, and (c) those formed later, associated with the eradication of transient porosity and fractures (Goldstein, 2003).

During coupled dissolution-reprecipitation, garnet chemistry is modified owing to partial re-equilibration with the fluid phase (Martin et al., 2011; Ague & Axler, 2016; Dempster et al, 2017; Dempster et al., 2019). Dissolution-reprecipitation forms sharp boundaries (Putnis, 2009) as such the change in chemistry at the cloudy-clear boundary should be abrupt. However, this is not the case and the boundary produces a gradual change in chemistry, particularly the Mn profile (Figure. 5.17c). The distance over which the major element chemistry changes appears to be a facet of diffusion speeds of the divalent cations within garnet. Mn^{2+} has the most rapid diffusion in garnet producing a gradual change while Ca^{2+}

has the slowest diffusion (Carlson, 2006). This creates a sharper profile in Ca-content at the cloudy-clear boundary. The link to diffusion rates is indicative that the boundaries between cloudy and clear garnet are subject to later diffusive modification producing a more gently sloping profile. Initially the chemical boundaries produced during dissolution-reprecipitation are likely abrupt (Altree-Williams et al., 2015).

Coupled dissolution-reprecipitation has the ability to produce cloudy garnet with a modified chemistry (Martin et al., 2011; Dempster et al., 2017; Dempster et al., 2019). During dissolution-reprecipitation, reequilibration occurs with the fluid phase creating garnet with increased pyrope and almandine, and decreased grossular and spessartine than clear parent garnet.

Garnet is a multicomponent mineral and during dissolution-reprecipitation the constituent elements dissolve non-stoichiometrically (Ruiz-Agudo et al., 2014). This differential dissolution, combined with the fact dissolution-reprecipitation is a disequilibrium process (Dempster et al., 2019), produces some variability in the chemistry of the product phase. The chemistry of the product is primarily dependant on the fluid composition and the parent phase composition. Cloudy garnet forms bands which often cut across compositional zones indicating dissolution-reprecipitation is independent of the original garnet composition (Dempster et al, 2017). Garnet changes composition from core to rim, e.g. at the core only trace amounts of Mn is present therefore the fluid can become saturated in Mn more easily precipitating a more Mn-rich product phase. The reverse applies to the Mn-rich rims where reequilibration involves the removal of Mn from garnet.

5.2.4 Ambiguous garnet

Ambiguous garnet commonly occurs between clear and cloudy garnet (Figure. 5.21). The boundary between texturally modified garnet and clear garnet is transitional producing a partially altered intermediate zone ca. 100 μm wide, termed ambiguous garnet.

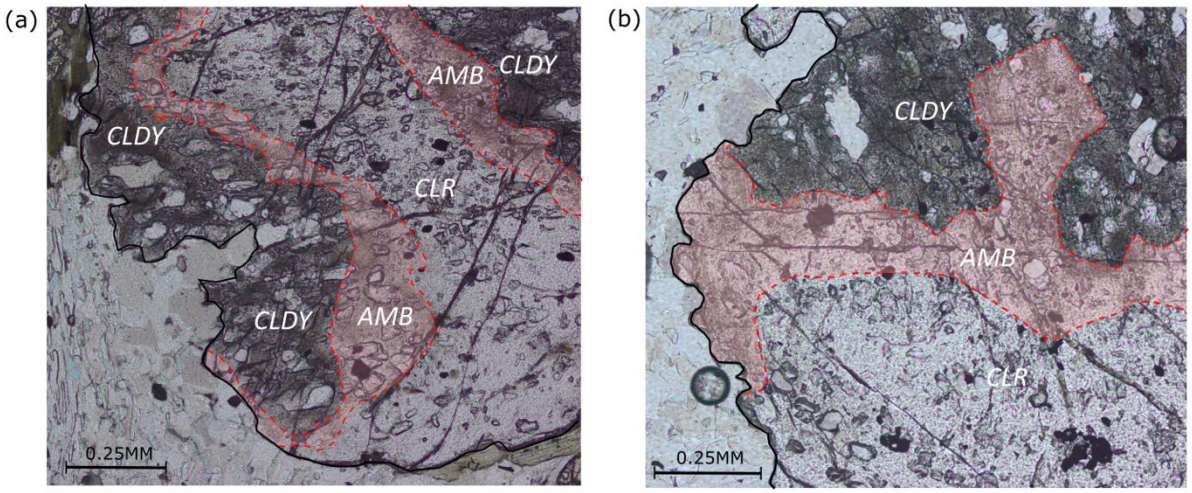

FIGURE 5.21: PPL image displaying the geometry of ambiguous zones occurring between clear and cloudy garnet in (a) GR01-9 and (b) GR01-5

5.2.4.1 Results: texture of ambiguous garnet

Ambiguous garnet contains some fluid inclusions, similar to cloudy garnet however it contains significantly fewer quartz inclusions (Figure. 5.22). Fluid inclusions are less abundant in ambiguous garnet, generally <1%. To maintain consistency in the classification of textures garnet containing >1% fluid inclusions is cloudy, <1% is ambiguous, and <0.1% is clear (Figure 5.2).

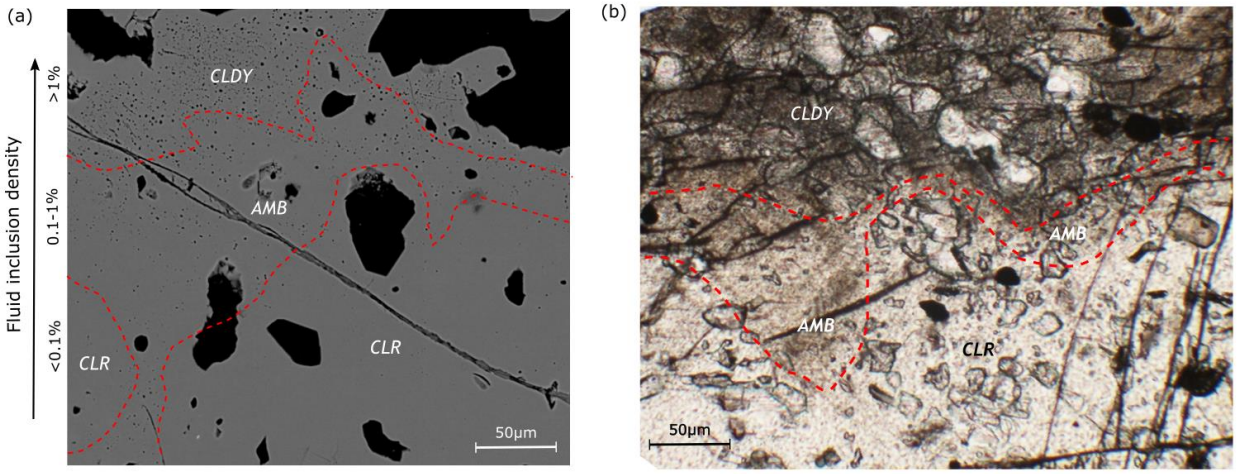

FIGURE 5.22: textural characteristics of ambiguous garnet (a) BSE image of GR01-2 showing the change in fluid inclusion abundance across clear, ambiguous and cloudy garnet, (b) PPL image of cloudy-clear margin within GR01-9, fluid inclusion-rich areas appear darker

There is no significant change to the size or morphology of fluid inclusions between cloudy and ambiguous garnet (Figure. 5.23). Ambiguous garnet contains few mineral inclusions, there are a few instances of monazite, quartz and ilmenite inclusions. Where quartz inclusions are present, they are small, aligned and regularly shaped, more consistent with the geometry of quartz within clear garnet than cloudy (Figure. 5.21-22). Fracturing within the transitional zones is also more similar to that in clear garnet than cloudy, with an absence of small-scale interconnected fractures.

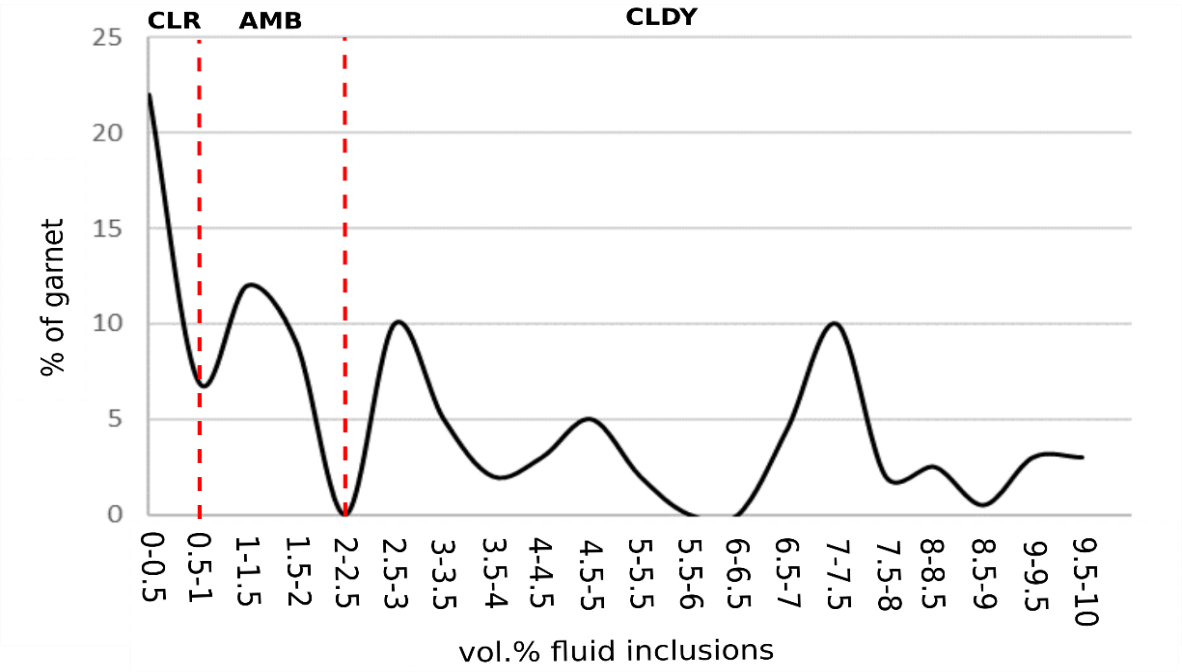

FIGURE 5.23: fluid inclusion abundance in garnet GR01-2 subdivided by classifications clear, ambiguous and cloudy

Results: chemistry of cloudy ambiguous garnet

Within ambiguous zones the chemistry is consistent with cloudy garnet (Figure. 5.17c). The boundary between ambiguous and clear garnet coincides with the beginning of a gradual change in chemistry, particularly a rise in Mn, producing a gently sloping profile into clear, unmodified garnet.

5.2.4.3 Interpretation of ambiguous garnet

The size distribution of fluid inclusions in ambiguous garnet is consistent with that in cloudy garnet (Figure. 5.24). Small fluid inclusions have a high surface energy and can be easily eradicated during textural reequilibration. If ambiguous zones

were a feature of partial textural reequilibration following dissolution-reprecipitation then a coarsening in the size of fluid inclusions would be expected in the transitional zones. It is likely that these zones are formed during coupled dissolution-reprecipitation as a gradual boundary between cloudy and clear garnet. This partial alteration of the texture in ambiguous zones, where the chemistry has been entirely altered is indicative that at staurolite grade textural modification is less effective than chemical modification within garnet.

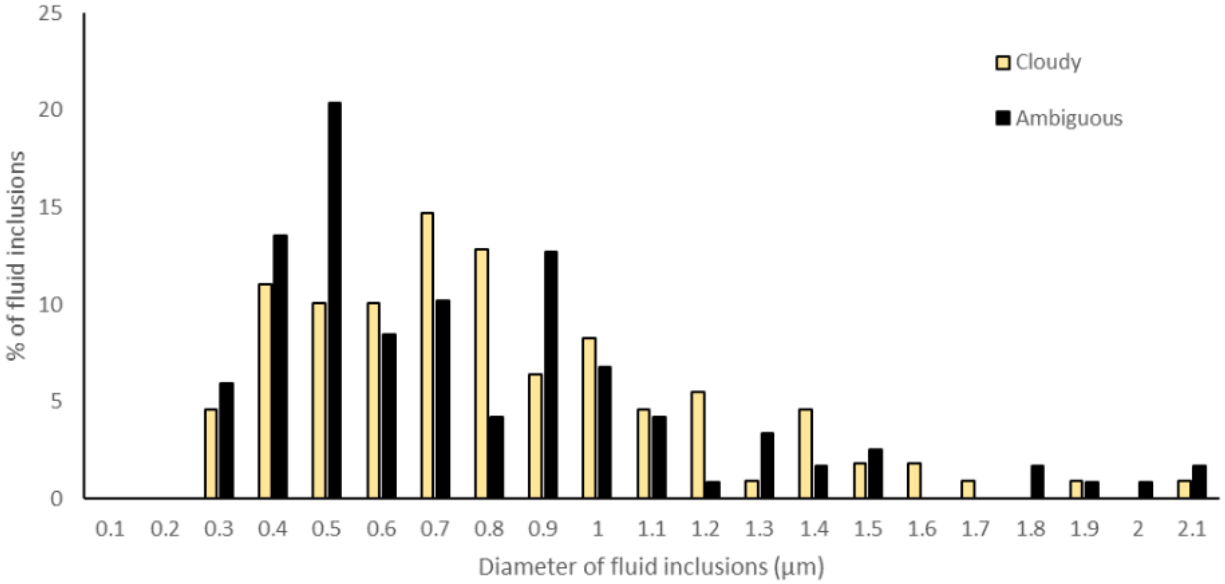

FIGURE 5.24: plot of the size distribution of fluid inclusions within cloudy (yellow) and ambiguous (black) garnet

The abundance of fluid inclusions can vary as a function of; (a) fluid availability, (b) mineral precipitation rates, and (c) active deformation (which may either provide pathways for fluid escape or produce shear zones promoting the infiltration of fluid thus increasing the potential for fluid inclusion formation. Fluid access and availability are the most common limiting factors in dissolution-reprecipitation (Putnis, 2009; Putnis & John, 2010; Ruiz-Agudo et al., 2014). As coupled dissolution-reprecipitation propagates into the garnet, fluid becomes less abundant due to the consumption of H_2O in the staurolite-forming reaction, Fe-rich garnet + muscovite + water → staurolite + biotite + quartz, and entrapment as inclusions. As a result, fewer inclusions are formed in cloudy garnet with increasing distance from the reaction interface. This continues until fluid availability falls below a threshold and coupled dissolution-reprecipitation eventually halts.

5.2.5 Conclusion

The degree of cloudiness of a garnet is linked to the amount of staurolite produced, therefore coupled dissolution-reprecipitation assists in the formation of staurolite through garnet consumption. The process can be fingerprinted using cloudy garnet which contains a high density of fluid and quartz inclusions and shows an altered chemistry with generally lower Mn & Ca, and higher Mg & Fe than clear garnet, although variable depending on the location within the grain. Identifying coupled dissolution-reprecipitation of garnet is made complex through the production of ambiguous zones where chemical transects reflect complete resetting, but textural modification is limited. Based on the morphology of mineral and fluid inclusions these ambiguous zones are likely formed during the initial alteration and do not represent a separate stage of reequilibration following dissolution-reprecipitation. Within staurolite-bearing schists there are two distinct stages in the temporal evolution that can be identified, (1) clear garnet interpreted to form during garnet growth, and (2) cloudy garnet, formed by coupled dissolution-reprecipitation during staurolite growth.

5.3 Sillimanite-zone garnet

5.3.1 Previous work

Garnet within sillimanite-bearing schists can be characterised based on textural and chemical characteristics as primary clear, cloudy and clear inclusion-free rims (Dempster et al., 2019). Typically garnet contains a combination of all three textures within a porphyroblast with generally sharp contacts and more rarely ambiguous zones (Dempster et al., 2019). The absence of ambiguous garnet may be attributable to the absence of primary clear garnet in the higher grade sillimanite schists, and thus the absence of cloudy-clear margins along which ambiguous garnet forms. Clear rims form at the edge of porphyroblasts and surrounding inclusions within garnet, they are particularly well developed adjacent to sillimanite and have a consistent composition indicating they are a feature of reequilibration during sillimanite formation (Dempster et al., 2019). The reequilibration occurs following dissolution-reprecipitation (Dempster et al., 2019), as such clear rims are interpreted as representing an additional stage in

the temporal evolution of garnet. The reequilibrated clear rims will be referred to as secondary clear garnet henceforth, while unmodified garnet that has not undergone coupled dissolution-reprecipitation will be defined as primary clear garnet.

5.3.2 Primary clear garnet

The amount of clear unmodified garnet within the sillimanite-zone schists is very low. Within the sillimanite-rich schist UGR0 unmodified garnet represents on average just 14% of garnet while within the sillimanite-poor schist UGR1, this is slightly higher at 36%. It shares similar characteristics to the clear domains in the staurolite-zone samples. In addition to unmodified 'primary' clear garnet, texturally reequilibrated 'secondary' clear garnet will be discussed separately as it represent an additional stage in modification.

5.3.2.1 Results: texture of primary clear garnet

Primary clear garnet is texturally near identical to that described in the staurolite schists (see section 5.2.2.1), except it is present in significantly lower abundances.

5.3.2.2 Chemistry

Primary clear garnet can be distinguished from cloudy or secondary clear garnet based on its higher Ca contents (Dempster et al, 2019). Primary clear zones typically also display chemistry consistent with growth zoning, with decreasing grossular and spessartine towards the core and complimentary almandine and pyrope profiles (Figure. 5.25).

5.3.2.3 Interpretation of clear garnet

Primary clear garnet is consistent in morphology and chemistry to that within the staurolite-zone schists. The presence of growth zoning and absence of mineral and fluid inclusions consistent with dissolution-reprecipitation is indicative this garnet has undergone limited post-growth modification.

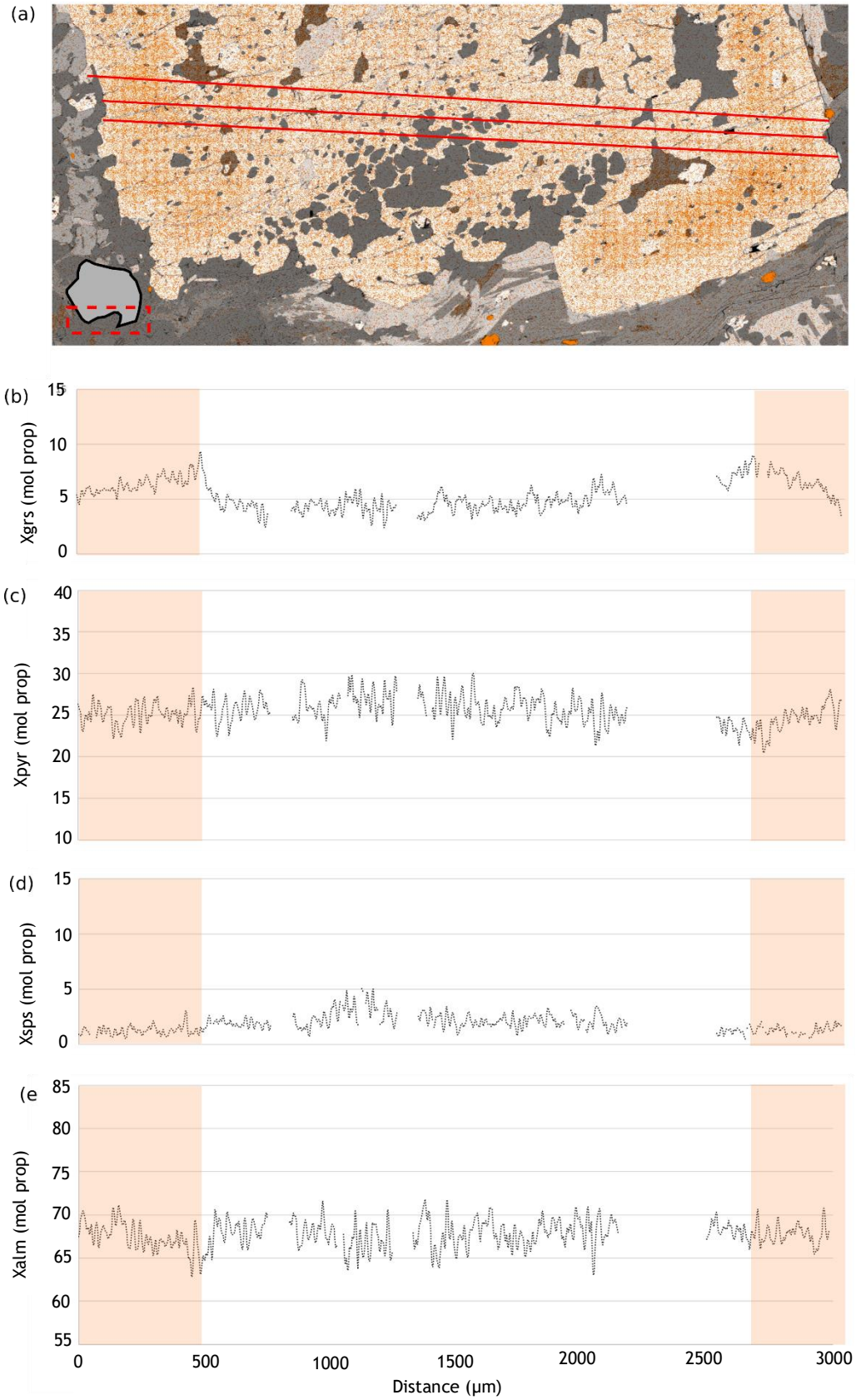

FIGURE 5.25: Transects across UGR0-4 illustrating the chemistry of high Ca, unaltered garnet, (a) X-ray map overlaying a BSE image of UGR0-4 showing the location of the transects, 3 transects were taken and the values combined in excel to produce one plot. High Ca areas of the garnet are highlighted in orange and the accompanying areas are highlighted red in the plots in b-e, (b) profile of the molecular proportion of grossular, (c) molecular proportion of pyrope, (d) molecular proportion of spessartine, (e) molecular proportion of almandine

5.3.3 Cloudy garnet

Sillimanite-bearing schists contain a much larger proportion of cloudy garnet than staurolite-zone. Cloudy garnet typically represents a majority of porphyroblasts with no completely clear grains visible in either the sillimanite-rich or sillimanite-poor samples. The geometry of cloudy zones is generally more regular (Figure. 5.26) than at staurolite-grade (Figure. 5.7), forming preferentially in the core and occasionally developing into atoll garnet where the core is entirely replaced (Figure. 5.26a).

5.3.3.1 Results: texture of cloudy garnet

Within sillimanite-zone garnet, cloudy garnet is texturally less consistent than within staurolite-zone schists. The abundance of both fluid and quartz inclusions is highly variable, with the abundance of these features generally showing a negative correlation with one another. In quartz-rich areas of garnet the abundance of fluid inclusions is much lower, typically <2 vol.% compared to a more consistent value of ca. 4-10 vol.% in staurolite-zone cloudy garnet. Fracture abundance and morphology also varies as a function of mineral inclusion abundance and morphology. Where inclusion abundance is higher, fracture abundance is also higher.

Within ca. 50% of garnet porphyroblasts there are quartz inclusion-rich areas within cloudy zones (Figure. 5.27). These contain up to 70% quartz, with only ca. 30% of the host garnet. These domains typically contain no other mineral inclusion types with an absence of detrital zircon; ilmenite; monazite; and rutile, all of which are typically present in cloudy garnet. The quartz-rich bands are typically located marginally and are present in garnet that hasn't developed atoll structures (Figure. 5.27a). They have a high fracture density, most are <200 μm long and terminate at adjacent quartz inclusions or fractures. The quartz inclusion-rich areas contain limited fluid inclusions owing to the abundance of secondary clear margins around quartz inclusions. Secondary clear rims surrounding inclusions and fractures are generally >100 μm and have a sharp contact with adjacent cloudy garnet. Only in rare pockets containing limited quartz and fracturing do fluid

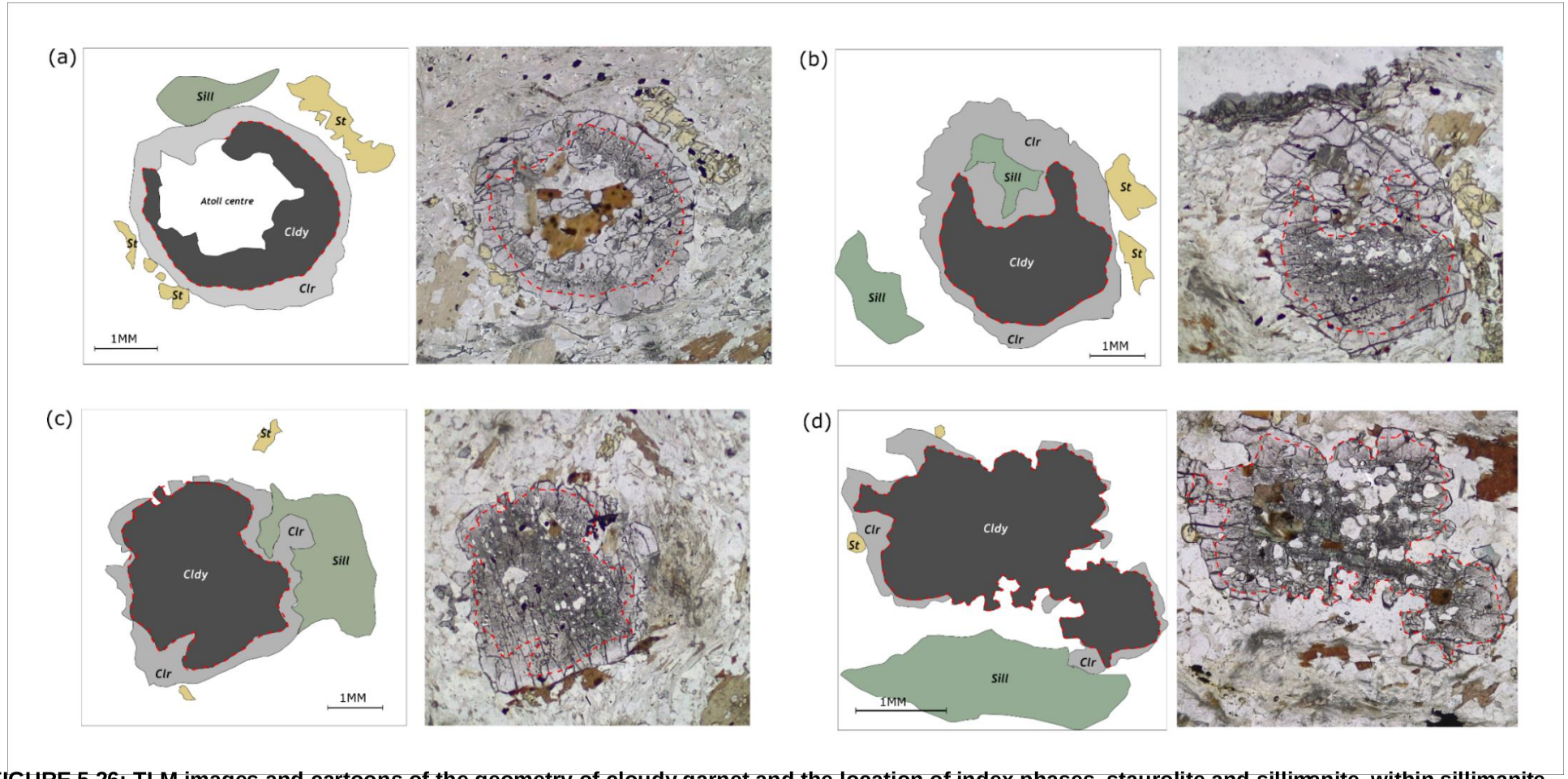

FIGURE 5.26: TLM images and cartoons of the geometry of cloudy garnet and the location of index phases, staurolite and sillimanite, within sillimanite schist UGR0, (a) atoll garnet with replaced core (b) garnet with large sillimanite inclusion with an extensive clear rim, dissolution appears to have been focussed along clear areas where margins are irregularly indicating they were initially cloudy but have been reequilibrated,(c) proto-atoll garnet, (d) heavily dissolved garnet which is predominantly cloudy, only clear, planar garnet is located adjacent to small staurolite porphyroblasts

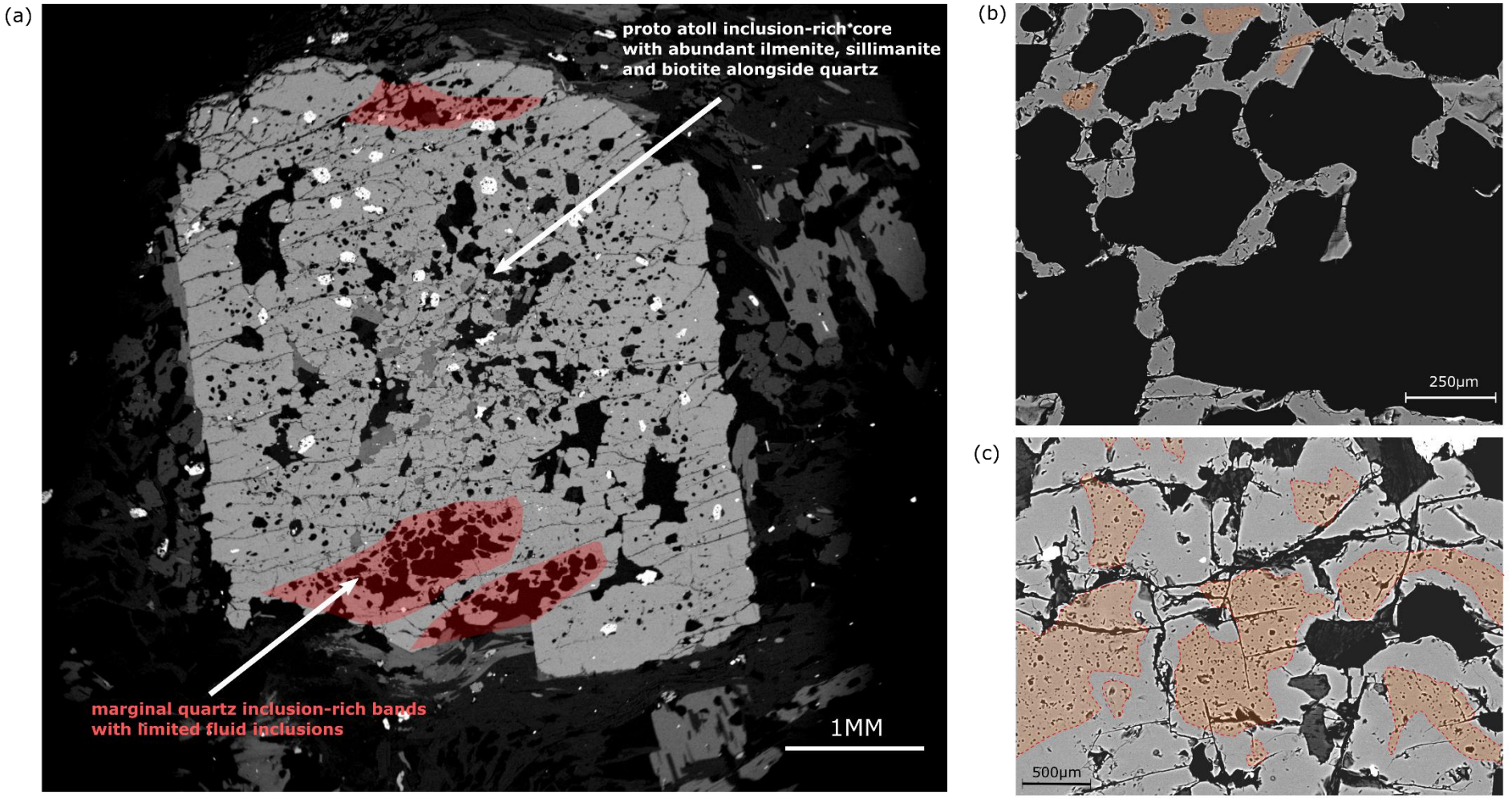

FIGURE 5.27: quartz inclusion abundance and the influence on fluid inclusions, (a) BSE image of UGR0-4 illustrating the location of marginal quartz-rich bands, (b) BSE image of the texture of these quartz-rich domains with limited fluid inclusions and predominantly secondary clear garnet, (c) typical texture of cloudy garnet in sillimanite-zone schists where secondary rims are present but comprise a small proportion of garnet while fluid inclusions comprise >1%

inclusion abundances reach >1%, comparable to abundance within staurolite-zone samples (Figure. 5.27).

Cloudy garnet contains fewer quartz inclusions than within cloudy garnet in the staurolite-zone schists, comprised of <20% quartz typically (Figure. 5.27a). The lower frequency of mineral inclusions results in large fluid inclusion-rich areas of garnet (Figure. 5.27c). The garnet is heavily fractured, most fractures are infilled with quartz and typically vary in length from 10s to 100s μm, terminating at the nearest adjacent quartz inclusion or fracture (Figure. 5.27c). Quartz inclusions are irregularly shaped but atypically small for those produced during dissolution-reprecipitation, generally <100 μm (Figure. 5.27c). Larger quartz inclusions, up to 500 μm, are rare and where present consistently host sillimanite. Alongside quartz inclusions are ilmenite, rutile, zircon and monazite. The proportions of most other inclusions are consistent with staurolite zone cloudy garnet except that of ilmenite and rutile. The modal abundance of rutile is higher at sillimanite-zone, ca. 1.2%, while the proportion of ilmenite is lower, ca. 1%, compared to staurolite=zone where ilmenite comprises ca. 1.5% of the rock and rutile contents are <0.5%.

5.3.3.2 Results: chemistry of cloudy garnet

Cloudy garnet has low Ca chemistry (Figure. 5.25), similar to that at staurolite grade (Figure. 5.17). Chemical analyses of quartz-rich bands of garnet are complicated by the absence of fracture- and inclusion-free garnet, producing a lot of variability and noise in the profile not linked to garnet composition. However, spot analyses of garnet within these areas reveals an extremely low Ca, high Mg chemistry consistent with garnet that has undergone coupled dissolution-reprecipitation.

5.3.3.3 Interpretation of cloudy garnet

The change in chemistry following dissolution-reprecipitation in sillimanite zone schists mimics the cloudy garnet in staurolite-zone schists suggesting all cloudy garnet formed synchronously during staurolite formation (Dempster et al., 2019). The products of fluid-mediated reactions tend to exhibit higher defect densities in their crystal lattice (Spruzeniece et al., 2017), as a result cloudy garnet is more

reactive than clear garnet (Dempster et al., 2019). The sillimanite-zone schists have undergone more dissolution-reprecipitation during staurolite formation producing more reactive, cloudy garnet and in turn potentially promoting the formation of sillimanite (Dempster et al., 2019).

The quartz inclusion-rich areas (Figure. 27) may represent those formed from the initial propagation of fluids during coupled dissolution-reprecipitation at staurolite-grade. These quartz-rich areas are parallel to the extensional fracture network in the rock and so the morphology is likely linked to exploitation of fractures by fluids during staurolite formation. During the initial stages of coupled dissolution-reprecipitation, fluid availability is higher increasing the potential for quartz formation while as the process progresses fluid availability decreases, and the result is the formation of less mineral inclusion-rich cloudy garnet. The formation of vast large volumes of quartz as inclusions during dissolution-reprecipitation is commonly reported (Martin et al., 2011; Steele-MacInnis et al., 2012; Ruiz-Agudo et al., 2014; Putnis, 2015; Dempster et al., 2017) but remains enigmatic. Quartz may represent an 'amorphous' phase formed during dissolution-reprecipitation (Konrad-Schmolke et al., 2018). These amorphous phases preferentially form surrounding defects (Konrad-Schmolke et al., 2018). Within these schists the highest defect densities are typically in originally quartz inclusion-rich bands, owing to the high fracture density due to the abundance of microcracks surrounding quartz inclusions (see section 5.2.2.3). This may encourage further growth of quartz and thus propagate dissolution-reprecipitation within these quartz-rich bands. The eradication of most inclusion types in the quartz-rich cloudy bands indicates that dissolution is particularly effective in these domains. This dissolution results in the removal of chemically durable inclusions and the mobilisation and transportation of HFSE (high field strength elements).

5.3.4 Secondary Clear garnet

Secondary clear garnet appears to be exclusive to the sillimanite-zone schists. It shares similar characteristic to primary clear garnet but is found locally surrounding mineral inclusions and porphyroblast rims and has a low Ca content consistent with modification via dissolution-reprecipitation.

5.3.4.1 Results: texture of secondary clear garnet

Secondary clear garnet is focussed around mineral inclusions and adjacent silicate infilled fracture networks (Figure. 5.28b), and at porphyroblast rims (Figure. 5.28a). Secondary clear domains contain very few fluid inclusions (Figure. 5.28), (typically <0.1%) forming zones texturally identical to unaltered, clear garnet. The secondary clear mineral inclusions rims contain high fracture densities and additional irregularly shaped quartz inclusions (Figure. 2.28b) typical of cloudy garnet, while secondary clear porphyroblast margins are generally inclusion-free and contain limited fractures (Figure. 5.28d). Fluid inclusion-free rims are also present at staurolite grade surrounding mineral inclusions, but they are 10s μm wide compared to 100s μm within the sillimanite-bearing schists. Clear rims are widest adjacent to sillimanite inclusions reaching >500 μm wide in places (Figure. 5.28d). Similarly, clear margins are widest proximal to mats of matrix sillimanite, clear margins are typically 100-200 μm wide reaching >1 mm adjacent to abundant sillimanite (Figure. 5.28c).

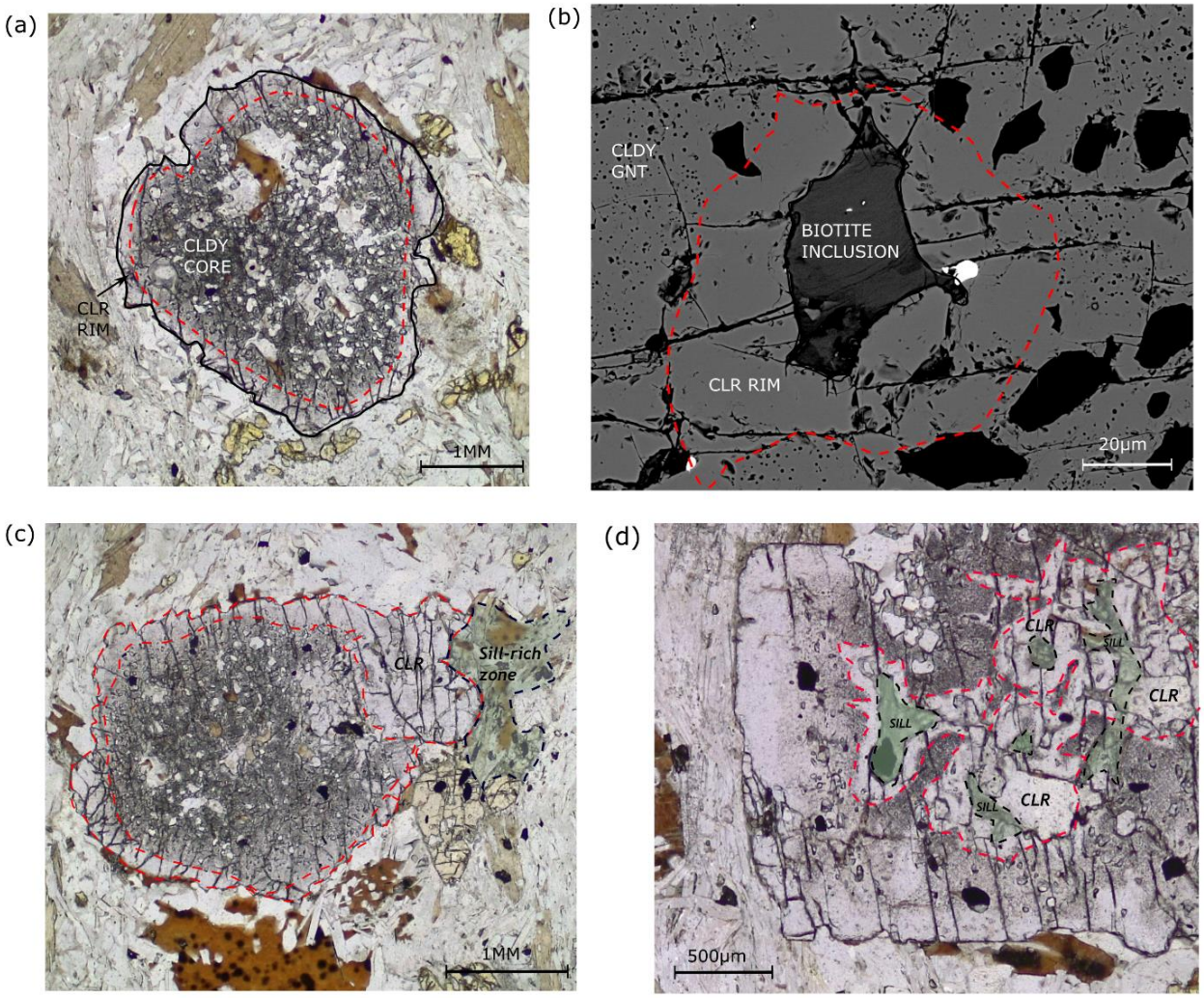

FIGURE 5.28: Location and morphology of secondary clear garnet within sillimanite-zone garnet in UGR0 with red line denoting secondary clear-cloudy boundaries, (a) PPL image of UGR0-1 with a clear outer margin and cloudy core that appears darker due to this high fluid inclusion abundance, (b) BSE image of clear inclusion rim in UGR0-4 surrounding biotite inclusion with <1% fluid inclusions, (c) well-developed clear rim adjacent to sillimanite at garnet margins in UGR0-6, (d) thick clear inclusion rims surrounding sillimanite inclusions within UGR0-4

5.3.4.2 Results: chemistry of secondary clear garnet

In contrast to the high Ca profiles typical of unaltered garnet, secondary clear rims have especially low grossular contents (Figure 5.29 & 5.30). Clear margins have low and constant Mn and Ca values (Figure. 5.29) while Fe and Mg transects are more variable (Figure. 5.29). Pyrope and almandine increase in the secondary clear rims compared to adjacent garnet, Mg increases from ca. 20 mol.% in cloudy garnet to 23 mol.% at the clear margins while Fe is just 71 mol.% in cloudy garnet increasing to 73-74 mol.% in secondary clear margins.

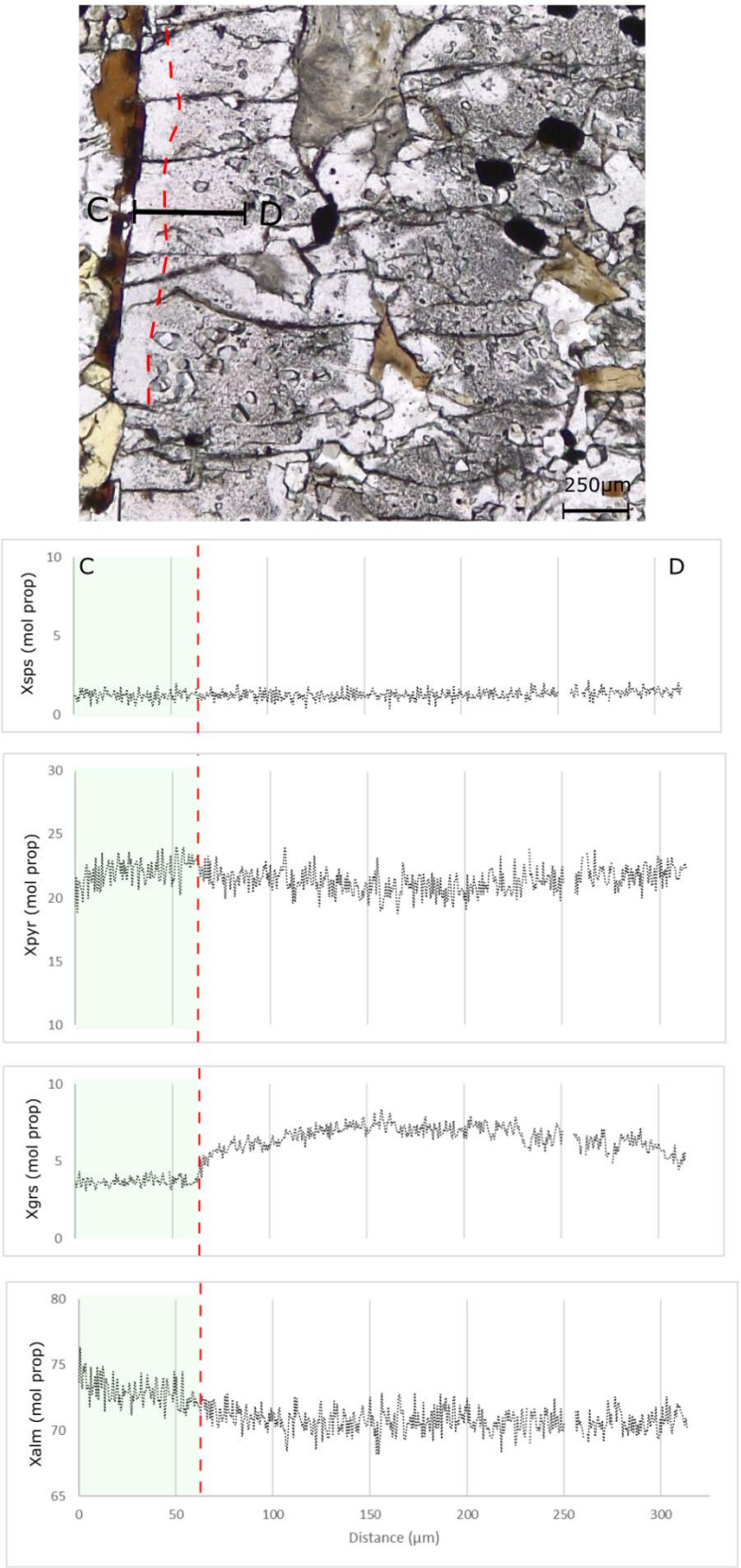

FIGURE 5.29: Transect from clear rim C into cloudy garnet D within UGR0-4, (a) location of transect in PPL image (b) spessartine profile, (c) pyrope profile, (d) grossular profile, (e) almandine profile, (b-e) highlighted in green is the clear rim

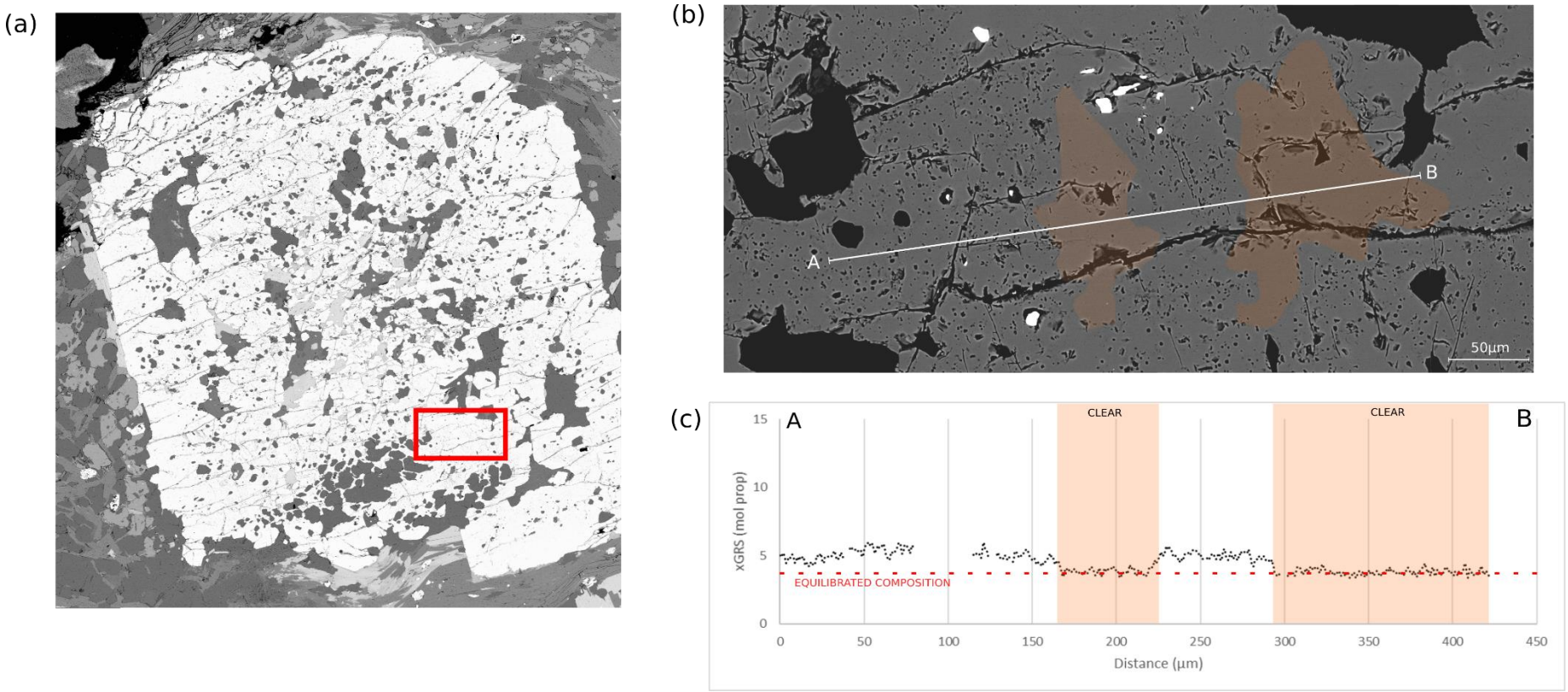

FIGURE 5.30: Transect A-B across UGR0-4 illustrating the contrasting chemistry between fluid inclusion-rich cloudy and reequilibrated regions (a) BSE image of the location of the transect within UGR0-4, (b) BSE image of the area from (a) showing the change in texture across transect A-B. in orange is reequilibrated garnet with <1% fluid inclusions, predominantly surrounding filled fractures and small quartz inclusions in this area, (c) changing molecular proportion of grossular across A-B, the red line denotes the equilibrated composition which coincides with the equilibrated garnet in (b).

5.3.4.3 Interpretation of secondary clear garnet

Secondary clear garnet has a low Ca chemistry, suggesting it has been modified and thus represents an additional stage in garnet's evolution which can be used to understand the temporal evolution of the rocks as a whole. Grossular contents in primary clear garnet are high at ca. 10 mol.% decreasing to just ca. 5 mol.% in cloudy garnet, while re-equilibrated secondary clear garnet is Ca-poor at 4 mol.%. As a result, Ca is a useful tool in deciphering the reaction history of a garnet where textural analyses may produce ambiguous results. Ca has the ability to monitor the history of garnet at higher grade where reequilibration occurs making textural classification more complex. Generally, the more stages of modification garnet undergoes, the lower the Ca content becomes in the schists.

The appearance of secondary clear garnet margins in sillimanite-bearing samples, paired with the increased abundance of secondary clear fluid inclusion-free rims in sillimanite-rich UGR0 compared to sillimanite-poor UGR1 (Dempster et al., 2019) suggests the textural reequilibration is associated with the sillimanite-forming process. Wide, clear porphyroblast margins are exclusive to the sillimanite-zone schists. In the staurolite-zone schists these margins regions are often consistently cloudy, typically pivotal in allowing the infiltration of fluids and commencing coupled dissolution-reprecipitation. The decrease in Ca and increase in Mg in secondary clear rims surrounding mineral inclusions produces a composition consistent with the secondary clear reequilibrated garnet margins (Figure. 5.31). This indicates that both reequilibrated porphyroblast margins and inclusion rims form concomitantly producing low Ca, high Mg zones.

Metamorphic rocks typically have low porosity, <1 vol.%, and permeability limiting diffusive behaviour between fluid inclusions and the host mineral, thus promoting preservation (Bakker, 2009). However, both recrystallization and grain boundary migration may result in complete annealing of grains and eradication of fluid inclusions (Bakker, 2017). Porphyroblast margins appear to have undergone complete recrystallization with the elimination of mineral inclusions and fractures alongside fluid inclusions, producing a relatively homogeneous garnet. Reequilibrated inclusion rims are less homogeneous, fluid inclusions are

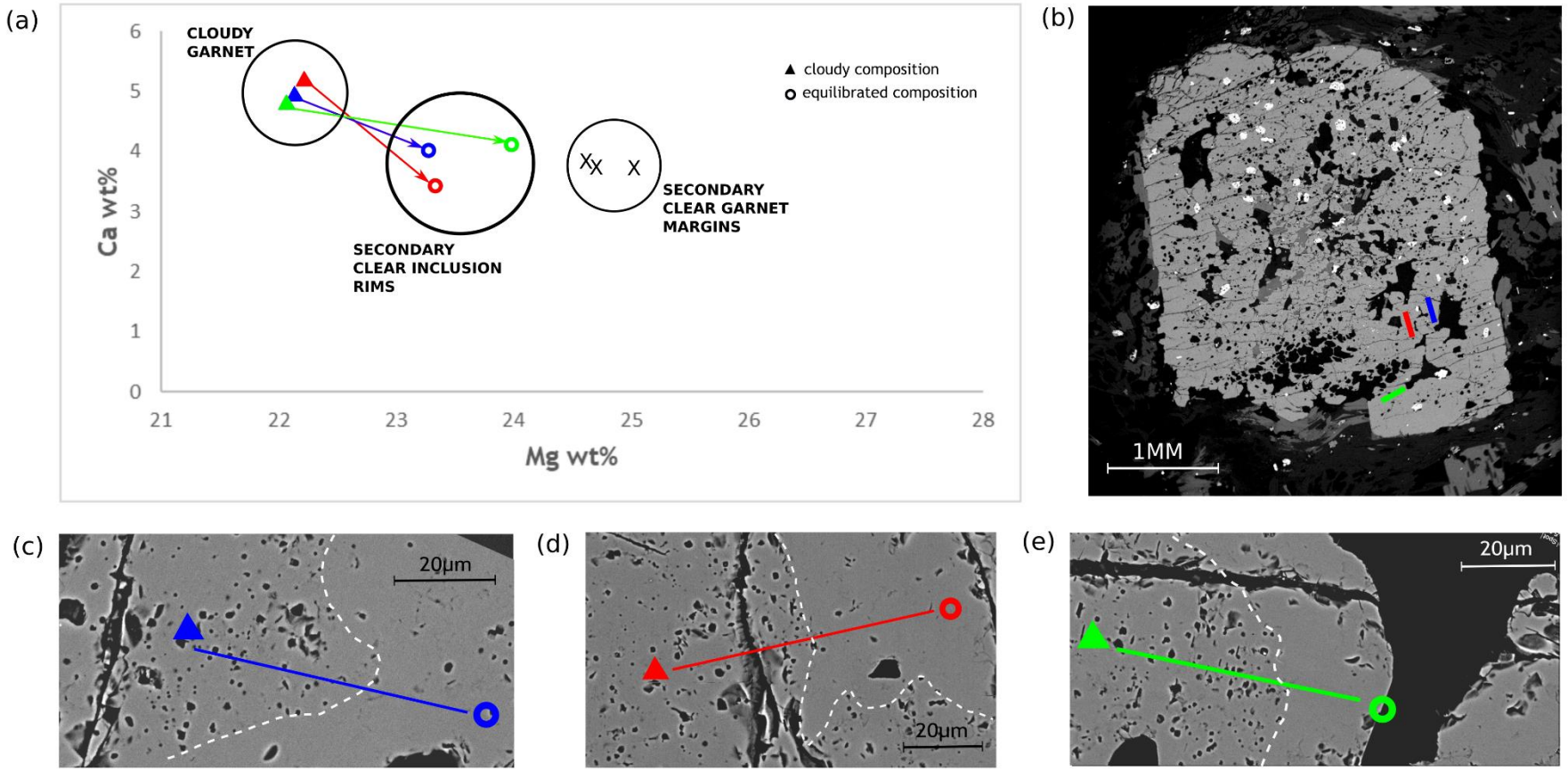

FIGURE 5.31: The chemistry of clear inclusion rims compared to clear margins of garnet, (a) plot of the changing chemistry of 3 transects across cloudy, fluid inclusion-rich domains into clear, reequilibrated rims. The change in chemistry during reequilibration is similar to that at clear margins, (b) BSE image of the location of transects within UGR0-4, (c) location of transect 1 with boundary marked in white, (d) location of transect 2, (e) location of transect 3

eradicated while fractures and mineral inclusions are, at least partially, preserved. Fluid availability appears to be the most important factor in the equilibration of fluid inclusions (Bodnar, 2003). Garnet porphyroblast margins and inclusion rims within garnet are likely fluid rich areas. Garnet margins are in contact with the matrix where porosity and permeability is high, while inclusions in cloudy garnet form interconnected pathways of fractures and microcracks enabling fluid access. During sillimanite formation, alongside extensive dissolution in the core of garnet, a dissolution-reprecipitation process may be occurring in fluid-rich areas; surrounding mineral inclusions and at porphyroblast rims.

Where dissolution-reprecipitation is closely coupled the product phase may be a pseudomorph of the dissolved parent phase, preserving original features and morphology through epitaxial nucleation (Putnis & Putnis, 2007; Putnis & Austrheim, 2010; Ruiz-Agudo et al., 2014). Dissolution and precipitation may be more closely coupled surrounding mineral inclusions than at garnet margins, thus preserving fractures and smaller mineral inclusions of monazite or ilmenite in secondary clear inclusion rims. Due to increase fluid availability dissolution is more effective at porphyroblast margins potentially resulting in a temporal decoupling between dissolution and reprecipitation eradicating fractures and inclusions and precipitating a more homogeneous product.

5.3.5 Conclusion

The textural modification associated with coupled dissolution-reprecipitation, increased fluid and mineral inclusion and fracture density, begins to be eradicated at higher temperatures producing secondary clear, reequilibrated garnet. During sillimanite formation the textures that are produced from coupled dissolution-reprecipitation during staurolite formation become replaced by a more homogeneous product phase in fluid-rich areas. Cloudy garnet is replaced by secondary clear garnet and the chemistry is altered effectively to produce a low Ca, high Mg product. This reequilibration produces another identifiable stage in garnet modification. While secondary clear garnet appears texturally similar to unmodified garnet, the low Ca chemistry combined with the specific locality (surrounding inclusions and at porphyroblast margins) of the secondary clear domains allow this stage to be fingerprinted.

5.4 Controls on cloudiness

Despite regular patterns of coupled dissolution-reprecipitation reported elsewhere in garnet (Martin et al., 2011), the geometry of cloudy garnet within these schists is highly variable. Within staurolite-zone rocks cloudy garnet is focussed along the margins (Figure. 5.7c) and fractures (Figure. 5.7d) in grains, occasionally cross-cutting grains and forming altered bands (Figure. 5.7a-b). Within sillimanite-zone garnet, cloudy zones are larger (Figure. 5.26) forming atoll (Figure. 5.26a) or proto-atoll structures (Figure. 5.26b-d). Fluid pathways for dissolution-reprecipitation cannot be traced in cloudy garnet due to the transient nature of porosity (Putnis, 2009). The high interfacial energy associated with the formation of porosity promotes pore coarsening and hinders the preservation of small fracture networks (Ruiz-Agudo et al., 2014). These preservational problems combined with the heterogeneous nature of garnet makes understanding reaction front propagation complex. In porphyroblasts where cloudy garnet is less developed, i.e. in staurolite-bearing schists, the morphology of the inclusion-rich zones can assist in understanding how coupled dissolution-reprecipitation propagates within garnet.

5.4.1 Stress field

The patchy and irregular replacement of a parent phase during fluid-mediated alteration has previously been attributed to fracturing (Jamtveit et al., 2009). Active deformation produces tensile fractures parallel to the main compressive stress and perpendicular to the orientation of tensile stress (Figure. 5.32). Where garnet forms cloudy bands they appear to be influenced by active deformation, most bands form along these tensile planes (Figure. 5.33).

Fractures enable fluid access to new reactive parent surfaces within garnet (Jamtveit & Austrheim, 2010; Dempster et al., 2017). From these planes the reaction front can then propagate parallel to the fracture into unaltered garnet producing thick bands of cloudy garnet surrounding major fractures. While this model fits a majority cloudy garnet within staurolite-zone schists there must be additional controlling factors with the ability to form a variety of cloudy geometries.

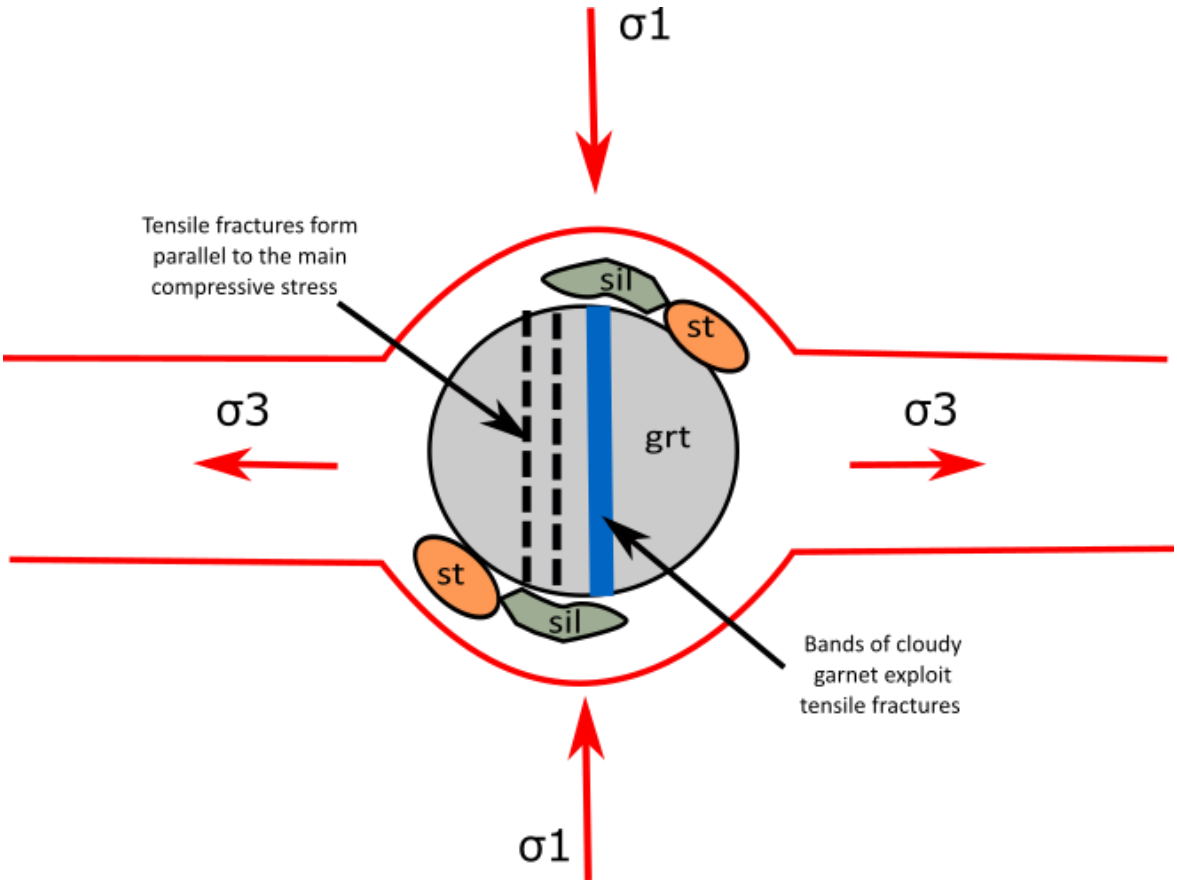

FIGURE 5.32: Model for the propagation of dissolution-reprecipitation and the formation of cloudy garnet along tensile fractures parallel to the main compressive stress

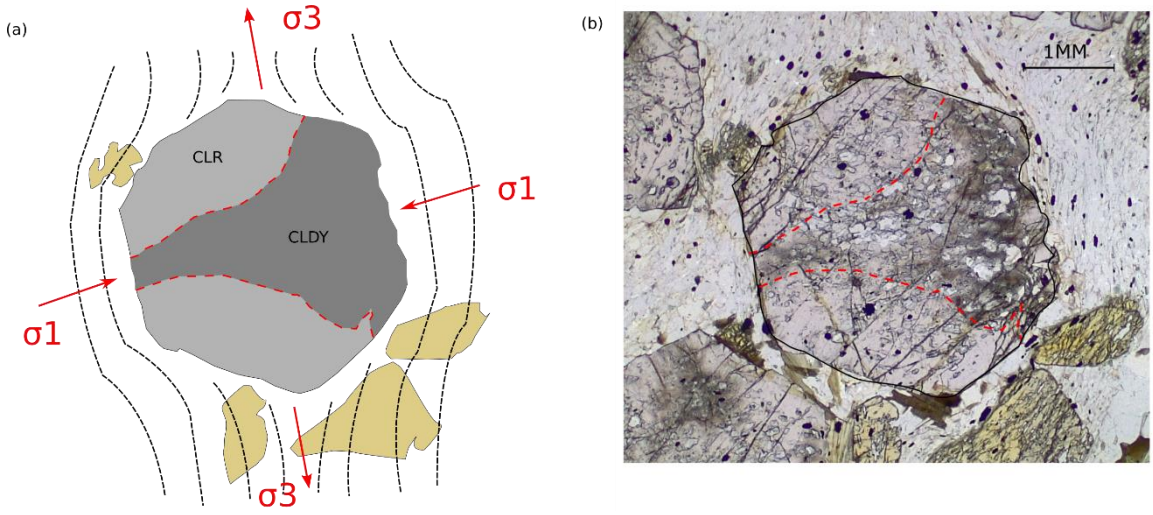

FIGURE 5.33: Geometry of cloudy garnet in staurolite-zone GR01-8, (a) cartoon of the location of main stress fields with the cloudy band forming along extensional fractures, (b) PPL image of garnet illustrating matrix fabrics and the location of cloudiness

5.4.2 Original sedimentary mineralogy and lithology

During regional metamorphism large fluid fluxes control reaction progress, due to heterogeneous permeability within mid-crustal rocks these fluids are commonly channelized (Ague, 2011). Channelization may be controlled by a number of features in metasedimentary rocks such as layering, fractures and folds (Ferry & Gerdes, 1998). Lithostatic layering is of significant importance, estimates of fluid fluxes across layers are an order of magnitude slower than flow parallel to layering (Ferry & Gerdes, 1998). The conduits can transport large volumes of fluid and heat, promoting reactivity in layered rocks (Ferry, 1992; Ferry & Gerdes, 1998; Ague, 2011). Within sillimanite-zone schists the original sediments are more finely interbedded (refer to petrology in chapter 4), this produces more permeable domains between mica-rich and quartz-rich layers which can act as conduits. Staurolite zone schists contain thicker layers generally (refer to petrology in chapter 4). The less layered staurolite-zone sediments may not have the ability to transport as much fluid as the sillimanite-zone schists due to the lower potential for lithological channel structures and thus decreased fluid availability. As a result, fluid availability may be lower in the staurolite-zone schists inhibiting garnet dissolution and the resulting sillimanite formation (garnet + muscovite → sillimanite + biotite + quartz).

During amphibolite facies metamorphism, Al ions have low mobility (Carmichael, 1969). As a result, Al-silicates, such as staurolite, preferentially form in Al-rich zones (Passchier & Trouw, 2005). Therefore, within these schists staurolite and sillimanite preferentially form in pelitic layers. Staurolite appears skeletal where it impinges into quartz-rich fabrics as growth is limited to grain boundaries where Al is more available (Passchier & Trouw, 2005). As a result, garnet contained within a more quartz-rich matrix has less potential for Al silicate index mineral growth, and thus less potential coupled dissolution-reprecipitation.

5.4.3 Inclusion banding within garnet

Grain boundaries play an important role in enabling fluid access to reaction fronts during dissolution-reprecipitation. The boundaries promote fluid transport one order of magnitude higher than transient porosity formed during dissolution-reprecipitation (Jonas et al., 2014). On a smaller scale, inclusion boundaries within a single porphyroblast may behave the same way, enabling fluid infiltration and promoting reactivity. In fact, the fluid flux that can be accommodated by grain boundaries in the average pelite is several orders of magnitude lower than that produced through devolitization therefore intragranular transport must also be invoked to accommodate fluids (Walther & Wood, 1986).

Where cloudy bands form that don't fit the model based on the exploitation of tensile fractures (as in Figure. 5.33), they instead form parallel to the matrix fabric (Figure. 5.34). Coupled dissolution-reprecipitation is focussed in garnet adjacent to quartzofeldspathic matrix layers, thus garnet that contains a high proportion of original quartz inclusions (Figure. 5.33). Quartz has a low bulk modulus of 36GPa (Wang et al., 2015) compared to garnet which ranges from 168-176GPa depending on its composition (Leitner et al., 1980; Yagi et al., 1987; O'Neill et al., 1991). During decompression the difference between the inclusion and confining pressure reaches a critical value resulting in fracturing as quartz inclusions change volume more rapidly than the surrounding garnet (Whitney et al., 2000). The result is a series of radial cracks <100 – 1000s μm long surrounding

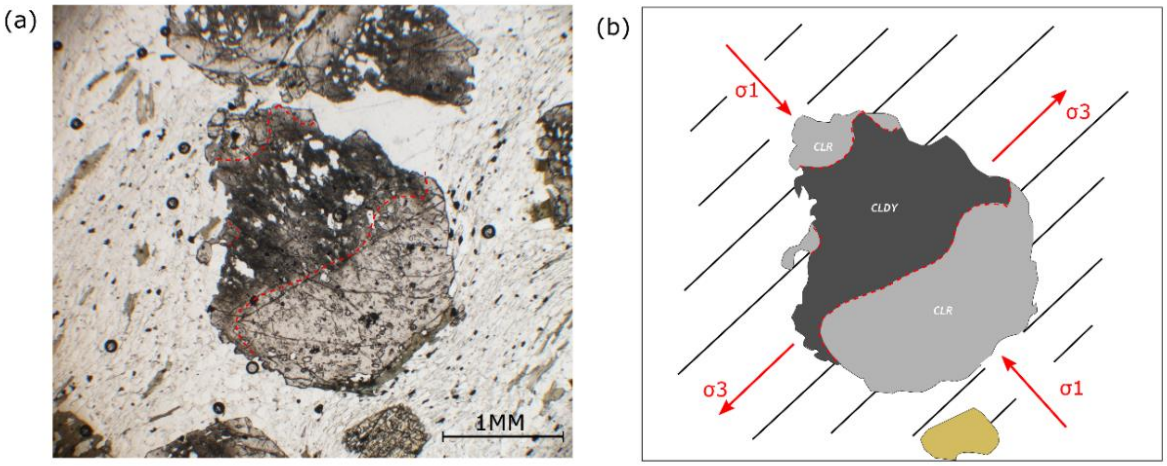

FIGURE 5.34: Geometry of cloudy garnet in staurolite-zone GR01-4, (a) PPL image of garnet illustrating matrix fabrics and the location of cloudiness, (b) cartoon of the location of main stress fields with the cloudy band forming parallel to matrix fabrics

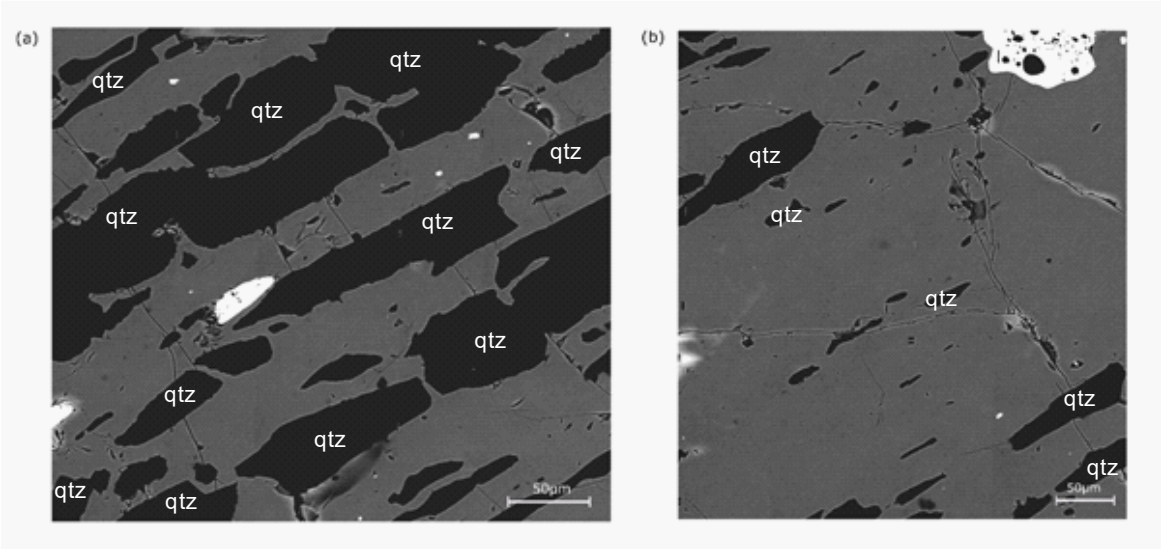

FIGURE 5.35: BSE image illustrating textural differences between compositional bands in clear, staurolite-absent schist GR02-5, (a) quartz inclusion-rich layer of garnet with multiple microcracks connecting inclusions, (b) quartz-poor garnet with few microcracks instead dominated by large fractures

and intersecting quartz inclusions (Figure. 5.35) (Gillet et al., 1984; Engleder, 1987; Whitney et al., 2000; Whitney et al., 2008). Ilmenite has a higher bulk modulus of 176GPa (Wilson et al., 2005; Cunha et al., 2019), similar to that of garnet meaning the difference in confining pressure is not great enough to produce fractures surrounding ilmenite inclusions. Ilmenite-rich layers of garnet remain structurally intact during pressure changes (Figure. 5.36b) producing fewer

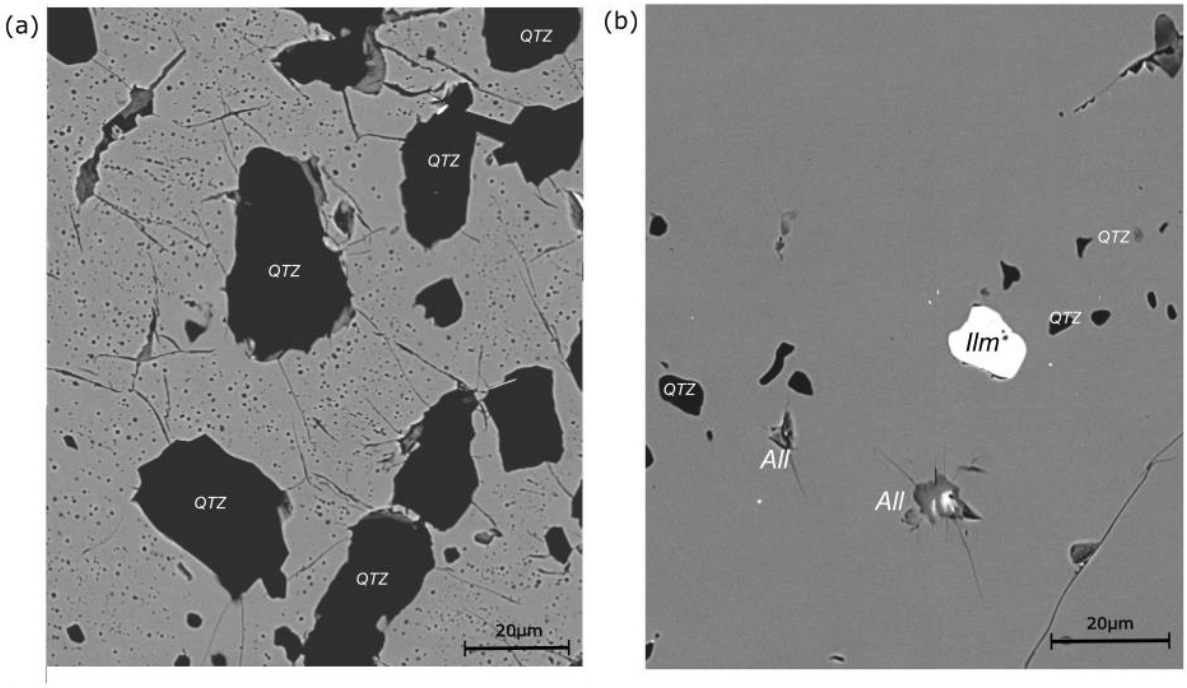

FIGURE 5.36: BSE images of the textural contrasts between clear and cloudy garnet in GR01-4, (a) heavily fractured, quartz inclusion-rich cloudy garnet showing high interconnectivity (b) quartz inclusion-poor clear garnet with limiting fracturing

potential pathways and inhibiting dissolution-reprecipitation. Microcracks are often interconnected (Figure. 5.36a), and as such can be exploited by fluids. Garnet that overgrows quartzofeldspathic matrix layers is thus more prone to dissolution-reprecipitation owing to the abundance of quartz inclusions and the increased potential for fracturing.

5.4.4 The propagation of dissolution-reprecipitation in garnet

Channelized flow can explain an outcrop-scale contrast in fluid infiltration in apparently similar rocks (Ague, 2011). Given the importance of fluids in coupled dissolution-reprecipitation, it is impossible to say whether the staurolite-bearing and sillimanite-bearing schists have experienced different P-T-t conditions purely from the index mineralogy (Dempster et al., 2019). Sillimanite schists contain more of the reactive altered garnet and higher Ca promoting sillimanite formation (Dempster et al., 2019). Contrastingly, the staurolite-bearing samples contain a much lower proportion of cloudy garnet creating a less reactive rock and inhibiting sillimanite formation in the reaction history (Figure. 5.37). There is likely a structural and/or mineralogical difference between the lower and upper Glen Roy samples which in turn affects fluid availability promoting infiltration in the sillimanite-bearing schists and promoting coupled dissolution-reprecipitation. The result is outcrops that appear to be different grade based on their index mineralogy, but textural and chemical analyses reveal this mineralogical contrast could just reflect disparate fluid histories.

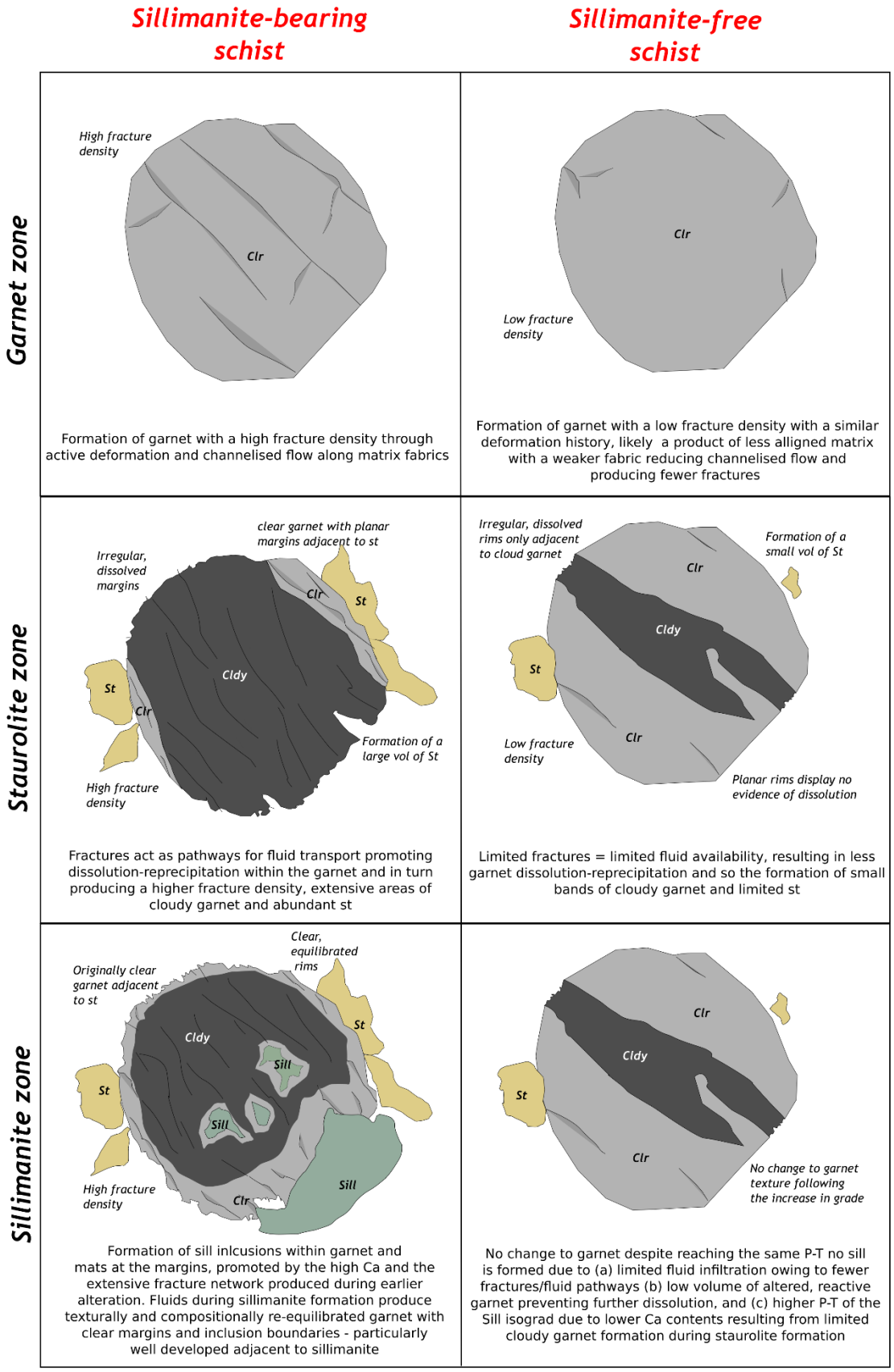

FIGURE 5.37: Model for the progression of the sillimanite and staurolite schists with increasing grade and the potential controls on the degree and morphology of dissolution-reprecipitation

A model for the progressive sequence of dissolution-reprecipitation within these rocks is detailed below.

(1) Coupled dissolution-reprecipitation begins at staurolite grade, typically at the margins of garnet porphyroblasts, when a fluid comes into contact with the garnet (Altree-Williams et al., 2015).

(2) Modification of garnet chemistry associated with coupled dissolution-reprecipitation during staurolite formation releases Ca; garnet + muscovite + water → staurolite + biotite + quartz (Dempster et al., 2019). Modification of texture produces quartz and fluid inclusion-rich garnet with abundant fractures (Dempster et al., 2017).

(3) The degree of spatial coupling at the reaction interface between dissolution and reprecipitation influences the preservation of original garnet morphology and nanoscale features (Putnis & Putnis, 2007; Lanari & Engi, 2017).

(4) The reaction front propagates away from the margins into unmodified garnet, initially exploiting areas of high permeability (Ferry & Gerdes, 1998).

(5) Fluid then utilises planes of weakness produced by (a) active deformation, and/or (b) channelized fluid flow (Ague, 2011). The structurally controlled dissolution-reprecipitation produces irregular cloudy morphologies (Figure. 7).

(6) Once cloudiness reaches a threshold and fluid access to the spessartine-rich core is secured, the control on cloudiness switches from fracture-controlled to chemistry-controlled. Spessartine-rich cloudy zones of the core are more reactive and preferentially undergo dissolution-reprecipitation producing atoll garnets (Figure. 26). This is a feature solely present in the sillimanite-zone schists owing to increased fluid pathway creation and availability within the originally finely interbedded sediments, promoting

dissolution-reprecipitation in these schists over the originally more thickly bedded staurolite-zone schists.

(7) Coupled dissolution-reprecipitation continues until fluid pathways are sealed. At the margins between cloudy and clear garnet ambiguous garnet forms which potentially represents partial textural modification owing to decreased fluid availability as dissolution-reprecipitation dissipates. The more interconnected pathways and initial permeability present, the more potential staurolite formation,

(8) Sillimanite formation occurs, garnet + muscovite → sillimanite + biotite + quartz, promoted within staurolite-rich rocks which have undergone more modification due to; (a) the release of Ca during coupled dissolution-reprecipitation moving the sillimanite isograd to lower P-T space (Dempster et al., 2019), (b) the high quartz inclusion abundance, and thus microcrack abundance, in cloudy garnet promoting fluid infiltration (Whitney et al., 2000), and/or (c) the increased reactivity of cloudy garnet due to the increased density of lattice defects in the product phase (Spruzeniece et al., 2017; Dempster et al., 2019).

(9) Sillimanite formation results in the textural and chemical reequilibration of cloudy garnet forming secondary clear garnet. The process occurs preferentially in fluid-rich areas surrounding inclusions and at garnet porphyroblast margins.

Chapter 6 Zircon populations

6.1 Classification of zircon

Within the Leven and Appin schists two distinct populations of zircon exist; microzircon and detrital zircon (Figure. 6.1). Microzircon are metamorphic in origin while detrital zircon are inherited during sedimentation, evidenced by internal zoning and modification within detrital grains (Figure. 6.1d-e). Dissolution of detrital zircon produces altered grains with irregular margins (Rubatto, 2002) while dissolution of microzircon involves the elimination of the entire grain due to its small size (Hay & Dempster, 2009). Detrital zircon may provide a host for

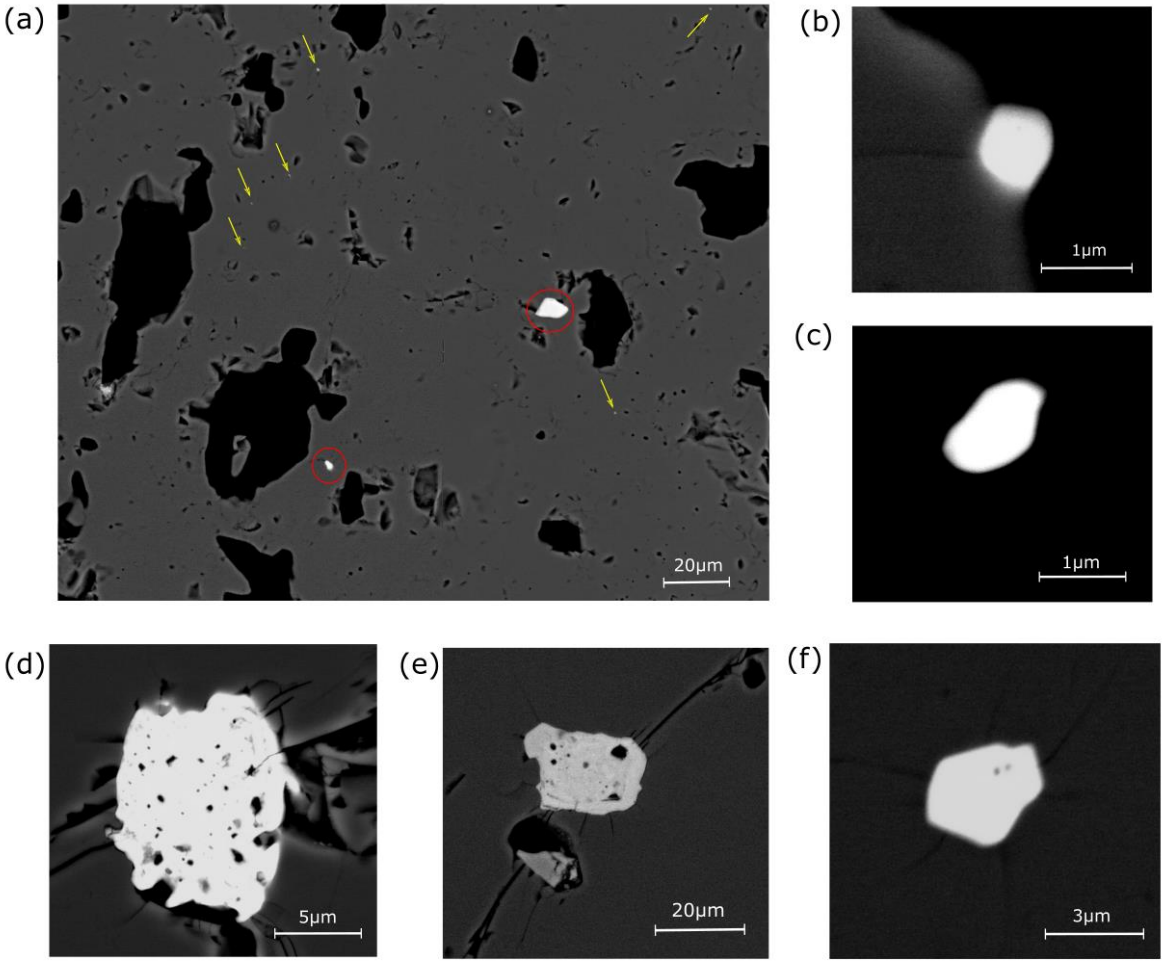

FIGURE 6.1: backscattered electron (BSE) images of zircon within garnet GR01-9 (a) location of microzircon (yellow arrows) and detrital zircon (red circles) within garnet (b) typical detrital zircon morphology, irregular dissolved margins and evidence if internal alteration and zoning (c) high contrast image of microzircon, planar margins with no internal structure (d) Detrital zircon typically show microcracks, especially around larger grains, (e) <1 µm^2 microzircon on inclusion boundary between garnet and quartz, (f) fine detrital zircon with evidence of internal homogeneity

the nucleation of new metamorphic zircon as outgrowths (Dempster et al., 2008; Kirkland et al., 2018) while microzircon form new distinct crystals (Dempster et al., 2004; Peterman et al., 2016). Owing to their different origins and metamorphic responses the populations must be distinguished.

6.1.1 Size constraints

Microzircon and detrital zircon can be separated based on their internal structure and size (Figure. 6.1). if zircon displays internal structure in BSE (backscattered electron) imaging this is indicative of a major change in composition within the grain. Zircon is unlikely to develop such large changes within a prograde metamorphic event, and if it did then the internal changes would be consistent across the entire population. Microzircon are finer and display no structure (Figure. 6.1b-c), while detrital zircon are coarse and display growth zoning (Figure. 6.1d-f). High resolution imaging using an SEM (scanning electron microscope) can distinguish internal structure in zircon larger than ca. 2μm^2. It follows that zircon below this threshold could be detrital or microzircon as the internal structure is too fine to discern, therefore size constraints are required to characterise the zircon. In order to accurately set size limits, all the size data collected from the staurolite- and sillimanite- zone schists was plotted producing a trimodal size distribution chart (Figure. 6.2). Biotite-zone schists were plotted separately as the detrital origins of the phyllite schists are likely disparate from the Leven Schists, paired with the contrast in microzircon size distribution across grade between the Leven Schists and the Appin Phyllites.

Within the Leven Schists, microzircon produce a distinct peak easily distinguished at 0.8 μm^2 (Figure. 6.2a). As such, the upper size threshold for microzircon was placed at 1 μm^2, therefore any zircon <1 μm^2 can be classified as metamorphic microzircon. Detrital zircon do not product one distinct peak; the dataset is limited, and detrital grains have a wide size distribution resulting in ambiguity surrounding the lower size constraint. Inclusions >3 μm^2 all show evidence of internal structures or zonation (Figure. 6.1f) and can therefore be classified as detrital zircon. Zircon between 1-3 μm^2 cannot be easily classified. This uncertain zircon was removed from the interpretation to avoid ambiguity. However, attention was paid to the proportion of uncertain zircon to ensure no substantial changes in the ambiguous population size, indicative of a change in the size

distribution of detrital or microzircon. The biotite-zone Appin Phyllites also produce a trimodal distribution chart however microzircon are slightly coarser within these schists instead peaking at ca. 2 μm^2 with most microzircon between 1-2 μm^2 (Figure. 6.2b). The cut off for microzircon within biotite-zone schists are therefore higher, zircon <3 μm^2 are classified as microzircon and those >5 μm^2 are detrital zircon producing a small area of uncertainty between 3-5 μm^2.

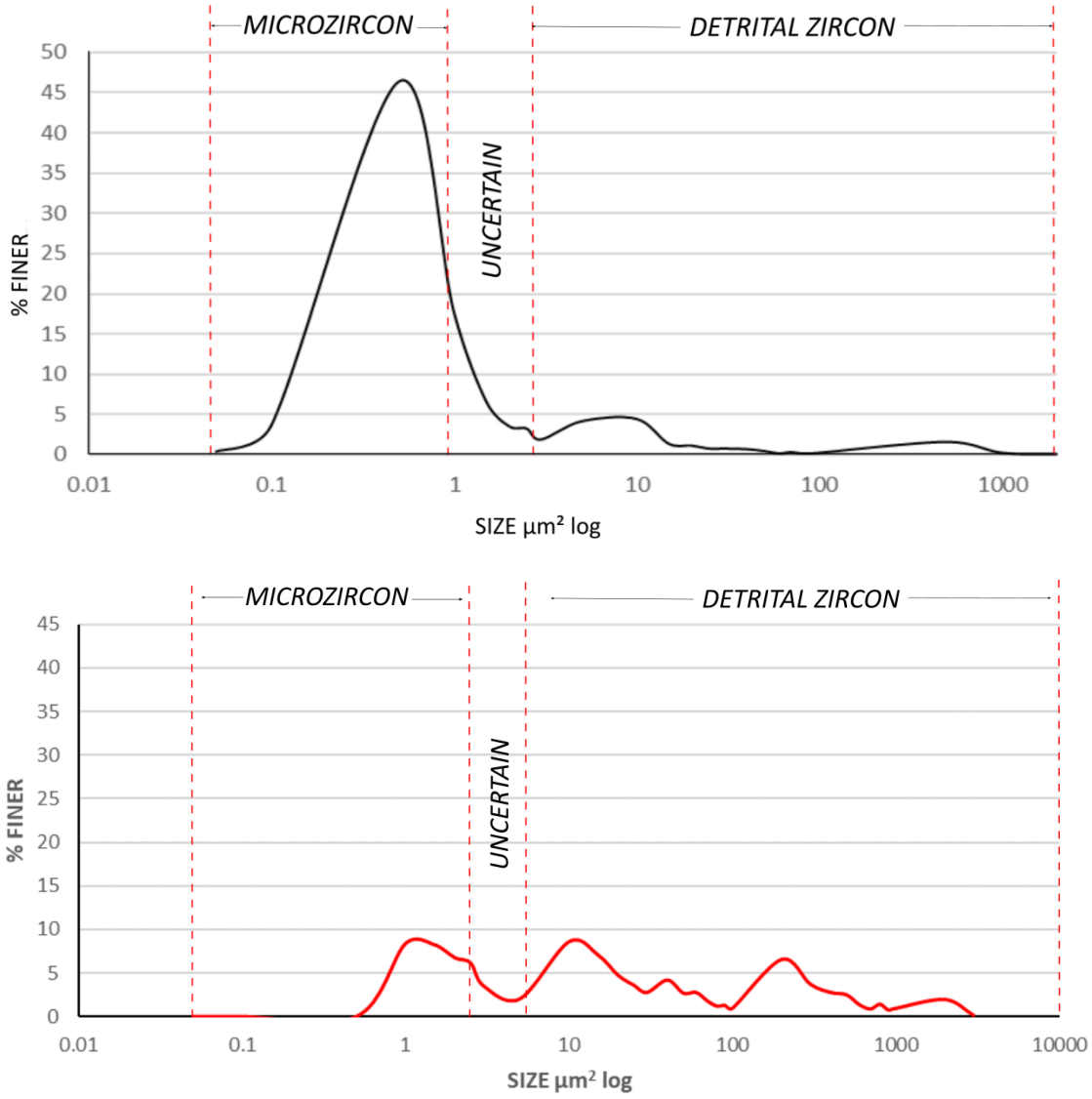

FIGURE 6.2: trimodal size distribution charts for zircon size data showing the location of zircon size thresholds collected from (a) staurolite- and sillimanite-zone Leven Schists, and (b) biotite-zone Appin Phyllites

6.1.2 Significance of microzircon

The difference in size is the most obvious morphological change between micro and detrital zircon. Sample preparation as polished sections could produce different cuts of detrital zircon some of which appear morphologically similar to microzircon and are <1 μm^2, falling within the size threshold. However, the abundance of microzircon makes it unlikely that this is the case for a significant number of grains. A model was produced to determine the size distribution of 150 parallel cuts through the smallest detrital grain (3 μm). Of the 150 cuts only 8 would produce zircon small enough to fit within the microzircon size margins (<1 μm), i.e. only 5%. Microzircon comprise 82% of the zircon populations analysed while detrital zircon make up just 18%, therefore this sampling bias would only account for a small proportion of the analysed microzircon.

There is a contrast in the proportion of minerals that host microzircon and detrital zircon suggesting they are not just a small population of detrital grains (Figure. 6.3). The proportion of microzircon is not proportional to the modal mineralogy of the rock instead showing a preference for one or more phases which varies depending on grade and mineralogy. The distribution of microzircon is not random within the schists suggesting there is a mineralogical control on their growth and that they are metamorphic, a separate population from inherited detrital zircon. Within the biotite-zone pelitic schists biotite hosts 30% of the microzircon despite comprising just 6% of the rock, similarly within quartz-rich layers the biotite represents just 8% of the rock but contains 65% of microzircon (Figure. 6.3). Garnet contains a large proportion of microzircon despite representing a small proportion of the budget within the staurolite-zone schists and particularly within the sillimanite-zone (Figure. 6.3).

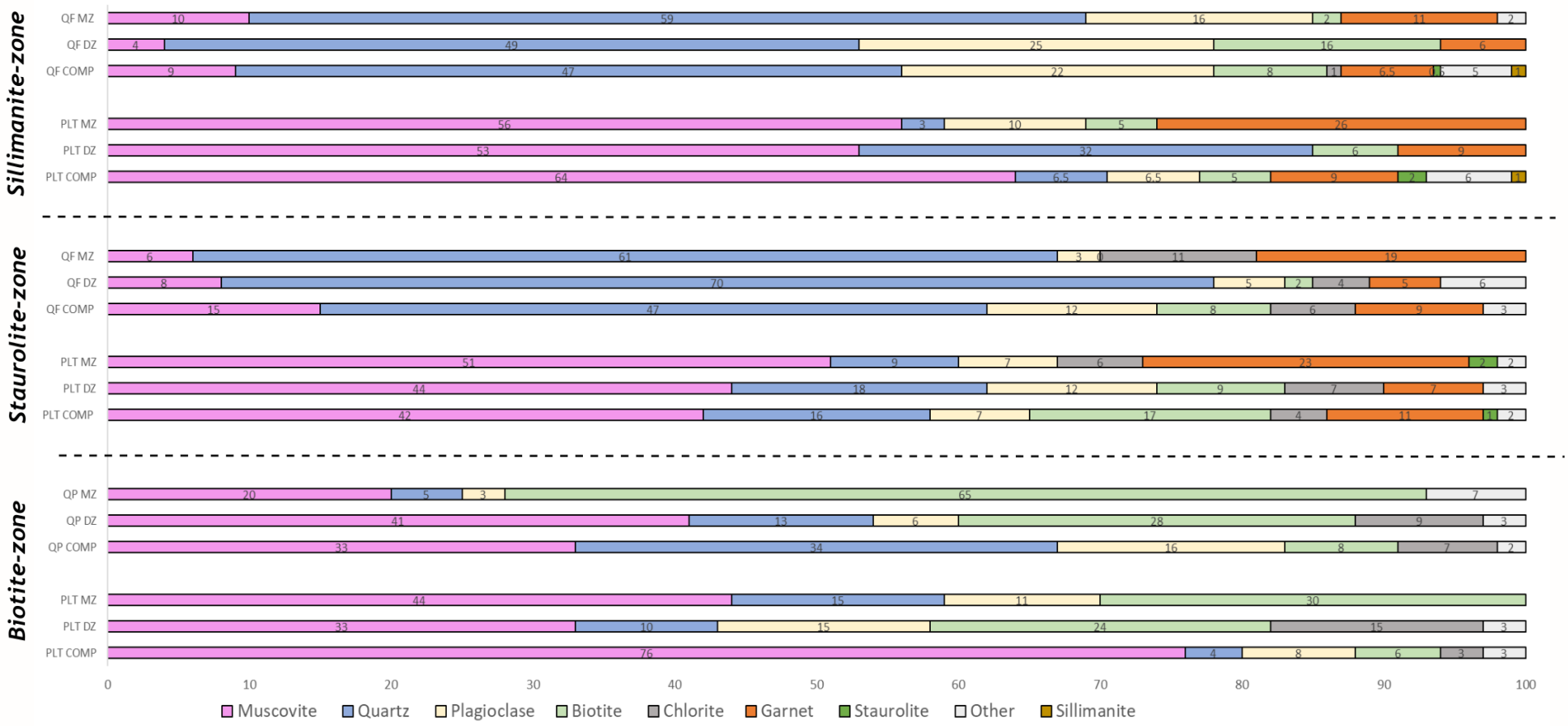

FIGURE 6.3: modal mineralogy and changing microzircon (MZ) and detrital zircon (DZ) distribution within host minerals across biotite, staurolite and sillimanite grade. Measured across all compositions, quartz-rich pelite (QP) and pelite (PLT) at biotite-zone and within quartzofeldspathic (QF) and pelite (PLT) in the staurolite and sillimanite-zone schists. Data from biotite schists was collected from Ball 2-8, for staurolite-zone schists was collected from GR01 and UGR0 for sillimanite-zone

6.2 Zircon abundance and morphology within garnet

Porphyroblast phases capture details about the metamorphic history not preserved in matrix phases. Garnet is particularly useful in the context of understanding zircon behaviour due to its ability to record changing P-T-X conditions during growth and post-growth modification, such as coupled dissolution-reprecipitation (Jiang & Lasaga, 1990; Chakraborty & Ganguly, 1991; Spear et al., 1991; Raimondo et al., 2017; Dempster et al., 2017). Analysis of zircon distribution and morphology within garnet should assist in understanding the factors that promote or inhibit zircon growth and dissolution. As garnet grows matrix minerals adjacent to the growing face are either dissolved or incorporated as inclusions (Passchier & Trouw, 2005). Detrital zircon is typically encapsulated by growing garnet as it is not a reactant in garnet formation and is difficult to eradicate during low-medium grade metamorphism owing to its supposed high chemical durability. Microzircon can be passive inclusions, those captured during growth, or growth inclusions which form at the growing edge of garnet due to the presence of Zr-rich fluids (Figure. 6.4).

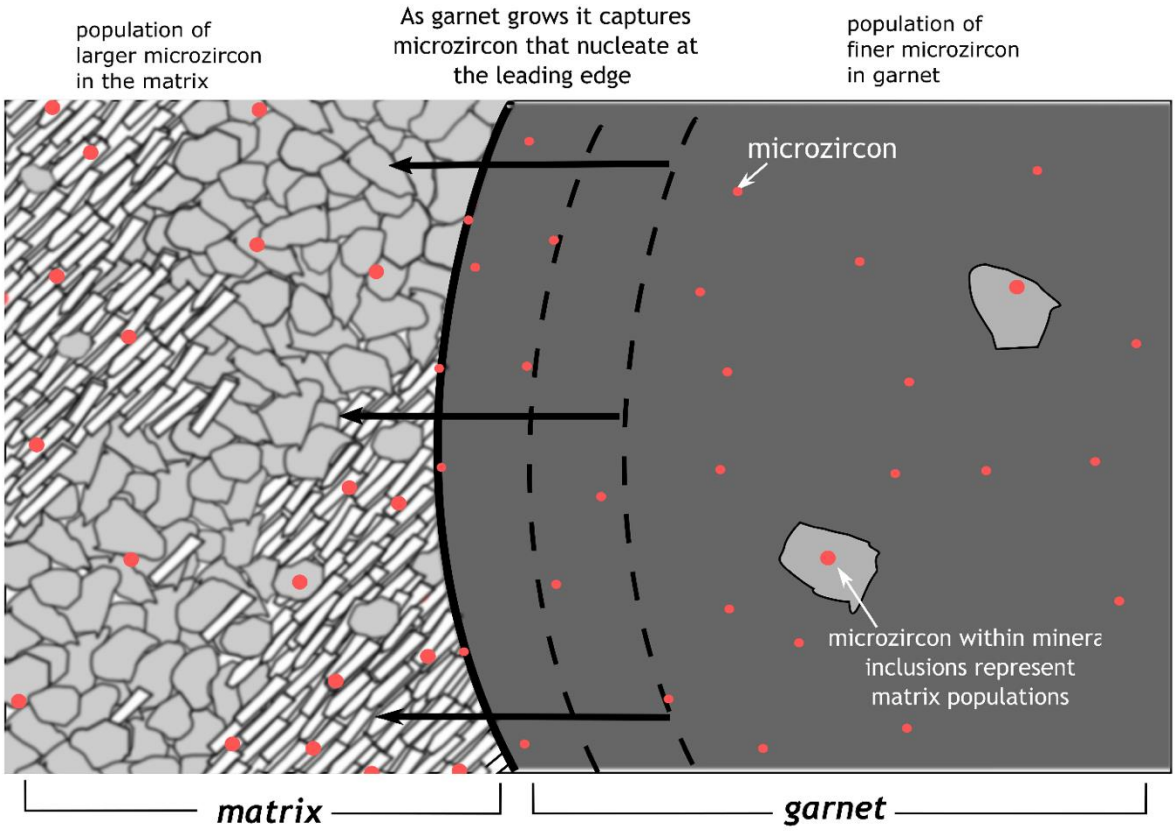

FIGURE 6.4: 2 populations of microzircon are preserved in garnet (a) coarser microzircon originally formed in the matrix and preserved in garnet within inclusions – predominantly quartz, and (b) a finer population of newly formed microzircon nucleating at the garnets growing edge following the dissolution of matrix microzircon

Distinguishing between the passive microzircon inclusions and growth inclusions is difficult. Aside from the change in size, the morphology is likely to be similar, microzircon are consistently euhedral with regular margins and display no evidence of dissolution.

This study analysed in total 3434 zircon. Within the Glen Roy staurolite- and sillimanite-zone schists, 2206 zircon were identified phases; 1556 microzircon, 365 detrital zircon and 285 unclassified ambiguous zircon. The remaining 1228 zircon are sampled from biotite-zone Appin Phyllites. The Appin Phyllite data was solely collected by me as part of an undergraduate BSc research project, on understanding zircon dissolution and growth, and is unpublished. The report produced at the end of this project is attached in Appendix 1. The Appin Phyllites do not contain garnet, however they assist in further understanding controls on zircon dissolution and growth across grade and so the results will be presented in this chapter. Zircon populations were mapped in both the matrix and porphyroblast phases, biotite within the Appin Phyllites, and garnet and staurolite within the Leven Schists. Mapping zircon populations assists in understanding the distribution, abundance and morphology of zircon across grade, as well as the influence coupled dissolution-reprecipitation has on zircon preservation and/or growth within garnet.

6.2.1 Biotite-zone schists

Biotite-zone schists are comprised of interbedded pelites and quartz-rich pelites with large biotite porphyroblasts, up to 4 mm, which show partial retrogression to chlorite. The Appin Phyllites at Onich have undergone at least three events (Roberts & Treagus, 1977; Pattison & Harte, 2001); an early regional event, a contact event and finally a period of retrogression. The schists contain vestiges from all three stages, an early formed aligned matrix, large contact biotite porphyroblasts, and finally retrograde chlorite. Analyses of zircon within each of these phases can assist in understanding how zircon populations change temporally.

6.2.1.1 Results: zircon morphology in biotite-zone schists

The quartz-rich pelite contains a population of larger detrital zircon while the pelite contains a population of smaller detrital grains (Figure. 6.5). the coarsest detrital zircon are located within heavy mineral bands and they are slightly aligned in this layer. Microzircon is also more abundant in the pelite matrix than the quartz-rich pelite matrix.

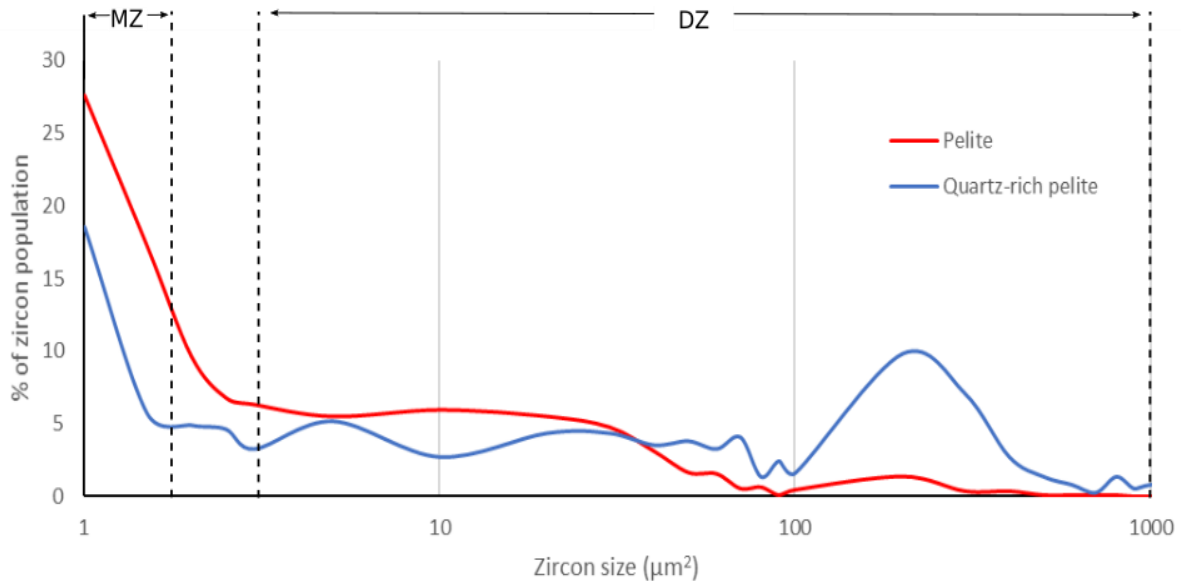

FIGURE 6.5: zircon size distribution within pelite and quartz-rich pelite

Large detrital zircon are typically more euhedral with smaller, subhedral grains more commonly possessing irregular, embayed margins and evidence of internal dissolution (Figure. 6.6).

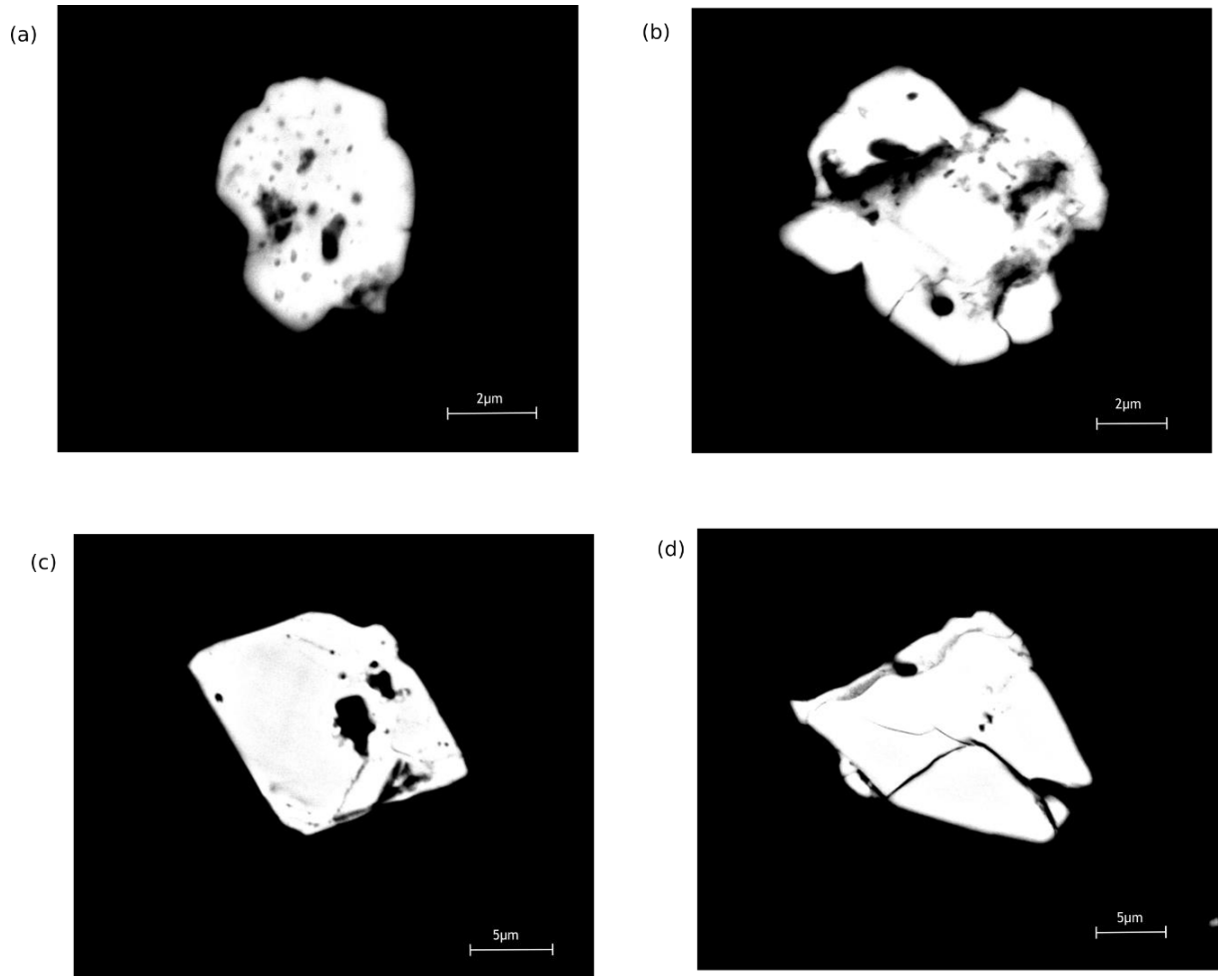

FIGURE 6.6: BSE image of detrital zircon morphology in Ball 2.8 (a-b) small, irregularly-shaped detrital zircon with evidence of marginal dissolution, (c-d) larger euhedral-subhedral detrital zircon with planar margins and limited internal alteration

68% of detrital grains imaged within these schists contain outgrowths. Outgrowths vary in thickness from >1 µm to >10 µm thick in places. They typically have an irregular morphology, exploiting grain boundaries (Figure 6.7a & c) and more rarely entirely encase detrital grains (Figure 6.7b). Detrital grains occur predominantly within the matrix.

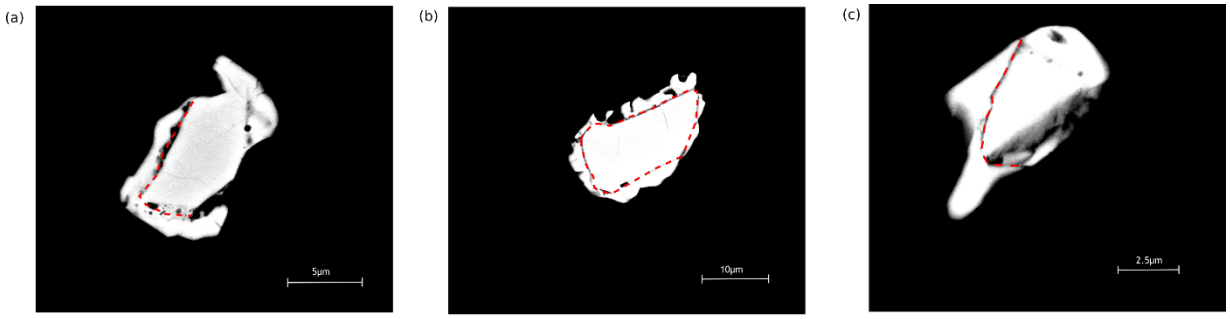

FIGURE 6.7: BSE image of outgrowth morphology on detrital zircon in Ball 2.8, (a) outgrowth focussed along one margin of detrital zircon, (b) thin, fringe of outgrowth surrounding large detrital grains, and (c) outgrowth morphology along grain margins

Biotite porphyroblasts contain a larger proportion of coarser microzircon than the matrix (Figure. 6.8). Most microzircon in the matrix and within biotite porphyroblasts are <1 μm^2, a majority of <1 μm^2 microzircon are found in the matrix, while 2-3 μm^2 are predominantly located in biotite porphyroblasts (Figure 6.8). The pelite is dominated by microzircon with a much lower proportion of detrital zircon while the quartz-rich pelite contains predominantly detrital zircon and much fewer microzircon (Figure. 6.9).

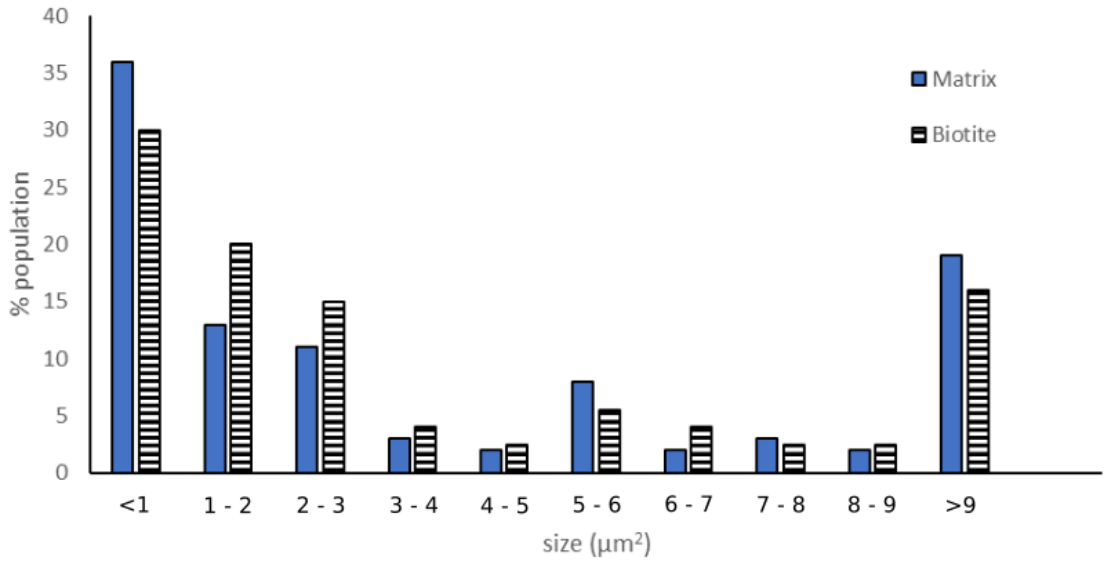

FIGURE 6.8: size distribution of zircon within the matrix and biotite porphyroblast phase

6.2.1.2 Results: zircon distribution in biotite-zone schists

Within the quartz-rich pelite, biotite porphyroblasts host just 24% of the detrital zircon with the remaining 76% in the matrix. Similarly, in the pelite biotite porphyroblasts contain only 26% of the detrital zircon and the remaining 74% are hosted within the matrix. The heavy mineral band contains a much larger proportion of porphyroblast-hosted detrital zircon with biotite porphyroblasts containing 41% of detrital zircon, and the remaining 59% in matrix phases.

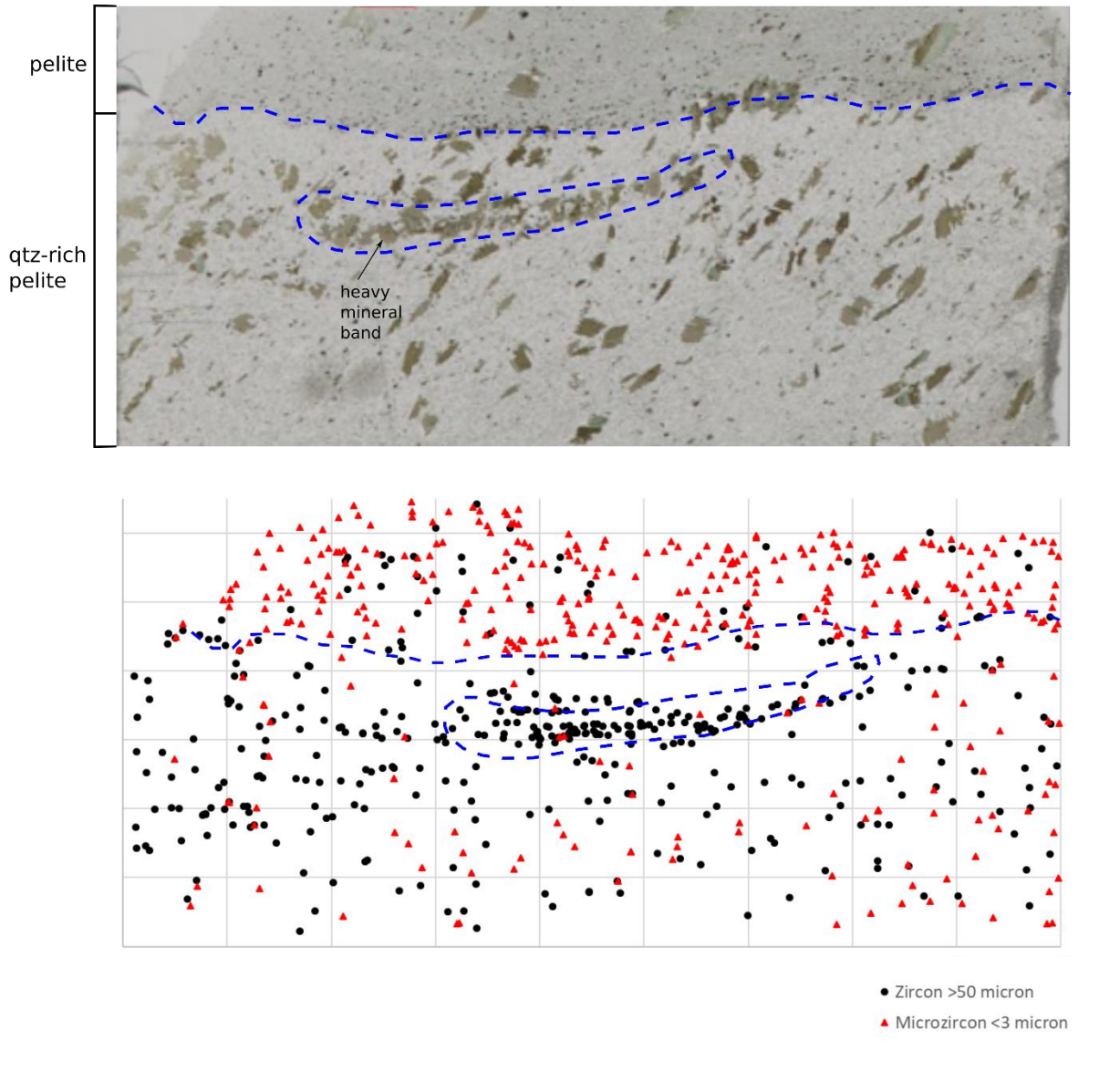

FIGURE 6.9: zircon distribution across the pelite, quartz (qtz)-rich pelite and heavy mineral band in sample Ball 2.9, (a) PPL image of analysed area illustrating compositional banding, (b) detrital zircon (black) and microzircon (red) in the mapped area, produced using EDX mapping

Within both the pelite and quartz-rich pelite, detrital zircon are predominantly hosted within muscovite (Figure. 6.3). Despite a low modal abundance of 6-8% biotite in both the pelite and quartz-rich pelite, biotite grains contain a large proportion of zircon, particularly microzircon (Figure. 6.3). 65% of the microzircon in the quartz-rich pelite are within biotite however it only comprises 8% of the modal mineralogy. Microzircon are most abundant in muscovite in the pelite, containing 44% of the population, however it also represents a large volume of the rock at 76%. Biotite contains 30% of the microzircon and comprises just 6% of the pelite (Figure. 6.3).

Within the matrix, 81% of detrital zircon are located on grain boundaries and only 19% occur as inclusions within a single host grain. While 82% of microzircon in the matrix are located within a single host and just 18% of microzircon impinge on grain boundaries.

The pelite contains 32 microzircon per mm^2 while the quartz-rich pelite contain 11 microzircon per mm^2. The pelite contains 6 microzircon per mm^2 while the quartz-rich pelite contains 4 microzircon per mm^2. The large grain size of the detrital zircon in the quartz-rich pelite means despite containing less detrital zircon it has a larger volume of detrital zircon than the adjacent pelite that contains finer detrital zircon.

In the quartz-rich pelite 65% of the microzircon population are within biotite porphyroblasts while within the pelite just 30% of microzircon are within porphyroblasts and the remaining 70% are within the matrix. Across both compositions the matrix microzircon populations are predominantly hosted within muscovite; in quartz-rich pelite 56% of microzircon are within muscovite, followed by plagioclase which contains 34% of microzircon and finally quartz which contains just 10% of microzircon. Similarly in the pelite, muscovite contains 67%, 22% are within plagioclase and finally quartz contains the least microzircon at 11%.

Chlorite retrogression in biotite porphyroblasts from 2-16%, chlorite contains no microzircon (Figure. 6.3). A 2% altered biotite grain contains 85% microzircon and 15% detrital zircon, while a more retrogressed grain, ca. 16% chlorite, contains a larger proportion of detrital zircon, 62%, and a smaller proportion of microzircon, just 38%.

6.2.1.3 Interpretation of biotite-zone schists

Zircon abundance varies between the pelite and quartz-rich pelite (Figure. 6.9). Microzircon growth appears to be focussed in the pelite which contains abundant microzircon, the quartz-rich pelite contains much less microzircon. The pelite contains more, finer detrital zircon while the quartz-rich pelite contains fewer coarse detrital zircon. The smaller population of detrital zircon in the pelite may be a population of more metamict, broken detrital grains (Dempster & Chung, 2013). Radiation damage increases the reactivity of zircon by promoting leaching

and dissolution, thus potentially yielding larger volumes of Zr^{4+} in the fluid and increasing the potential for new zircon formation (Hay & Dempster, 2009a). Alternatively, the quartz-rich pelite contains a population of coarser, more structurally intact, less metamict zircon while are potentially less reactive to hydrothermal fluids. As a result, the available Zr^{4+} produce through detrital zircon dissolution in the quartz-rich pelite is potentially lower, accounting for the production of less metamorphic zircon as microzircon.

Outgrowths form around most grains and display morphological evidence of growth in situ, they are typically extremely delicate and unlikely to survive transportation (Rasmussen, 2005), and occasionally form along grain boundaries. The larger abundance of detrital zircon within the quartz-rich pelite may promote zircon crystallization primarily as outgrowths, limiting the amount of microzircon formed. Alternatively, microzircon growth is promote in the pelite where there is an absence of detrital zircon, and thus a structure for outgrowths to nucleate on.

At high temperature zircon dissolution is more effective owing to the higher kinetic energy of the cations, where temperatures are lower, as within these rocks, a more corrosive fluid is required to mobilise Zr^{4+} (Weber et al., 1994; Nasdala et al., 2001). The formation of microzircon and outgrowths on non-metamict grains required the transportation of Zr^{4+} beyond the grain scale. Fluid composition is therefore an essential component to allow the mobilization and transportation of Zr^{4+} for new zircon growth. The dehydration reactions involved in the formation of mica at each stage of the metamorphic history would produce reactive halogen-rich fluids capable of transporting Zr^{4+}.

The schists show a temporal change in zircon distribution and morphology through the three identified stages in the evolution of the Appin Phyllites (Roberts & Treagus, 1977; Pattison & Harte, 2001). The early regional event formed the aligned muscovite-rich matrix and within it a population of large microzircon. The contact event formed biotite porphyroblasts and a population of finer microzircon within it, and potentially some microzircon growth in the matrix. The retrograde event sees unique, during this period of low temperature alteration chlorite is formed containing no microzircon. During the chlorite-biotite reaction microzircon is formed within the product biotite, however during the biotite-chlorite transformation microzircon is dissolved and no new zircon crystallization

occurs in the product chlorite. Microzircon are most abundant within biotite in the schists indicating that the most growth occurs during this stage. Additionally, there is an indication that there is a metamorphic control on zircon formation based on the increase in the size of microzircon throughout the reaction history (Dempster et al., 2008).

The absence of microzircon in chlorite may be a facet of lower fluid availability during retrograde reactions. During peak metamorphism fluid is more readily available and while the presence of a fluid is essential for chloritization to occur, fluid availability is commonly the limiting factor during retrograde reactions (Barker, 1998). The absence of abundant fluids may explain the lack of new microzircon growth within chlorite during retrogression. The preservation potential of microzircon requires consideration, their nanocrystalline structure means they can be fully dissolved by hydrothermal fluids (Dempster et al., 2008; Hay & Dempster, 2009a). Retrogression creates corrosive fluids capable of stripping out microzircon. As a result, layers with large proportions of biotite have greater dissolution potential, particularly the heavy mineral band which contains <30% biotite. The absence of microzircon within the more biotite-rich heavy mineral band and quartz-rich pelite may be in part a facet of preservation following chloritization.

6.2.1.4 Conclusion

There appears to be a strong lithological control on the distribution and morphology of zircon. The quartz-rich pelite contains fewer microzircon and few, coarse detrital zircon while the micaceous pelite contains more microzircon and abundant, fine detrital zircon. Microzircon are more abundant and slightly larger in biotite porphyroblasts than adjacent matrix phases, indicating there is also a temporal change in zircon dissolution and crystallization. Most notably, the absence of microzircon within chlorite is indicative that retrograde reactions are unique, resulting in zircon dissolution and no new crystallization.

6.2.2 Staurolite-zone garnet

Staurolite-zone garnet can be subdivided into unmodified clear garnet and garnet that has undergone coupled dissolution-reprecipitation producing ambiguous and/or cloudy garnet with a modified texture and chemistry (Dempster et al., 2017). Clear garnet contains zircon populations formed during and prior to garnet growth while ambiguous and cloudy garnet assist in understanding the influence of coupled dissolution-reprecipitation on the preservation and growth of zircon. The abundance and morphology of zircon will be analysed across these classifications to understand how the well constrained temporal evolution of Glen Roy garnet influences zircon populations.

6.2.2.1 Results: zircon in clear garnet

Staurolite-zone garnet contains microzircon and detrital zircon which display a variety of textures (Figure. 6.10). Clear garnet has undergone no chemical or textural modification following growth. Most of the zircon trapped within this garnet formed during garnet growth. Some zircon may be a vestige of earlier formed matrix populations. Instead of being dissolved and reprecipitated during garnet growth, these microzircon were sheltered by their host mineral which was encapsulated as an inclusion within garnet during growth instead of being dissolved (Figure. 6.4).

Clear garnet contains mineral inclusions which typically vary in abundance and composition relative to the composition of the matrix layer the garnet overgrew (Passchier & Trouw, 2005). Micaceous layers of the matrix produce garnet with abundant ilmenite inclusions and limited quartz inclusions, while growth over quartzofeldspathic matrix produces more inclusion-rich garnet, generally dominated by quartz. The composition of the matrix influences the abundance and distribution of zircon (Figure. 6.11) (Dempster et al., 2004; Rasmussen, 2005; Dempster et al., 2008). Quartzofeldspathic matrix layers contain less microzircon and fewer, large detrital zircon while micaceous matrix layers generally have significantly more microzircon, and a large population of finer detrital zircon (Figure. 6.5). microzircon within the garnet that overgrows pelitic matrix is on average 0.39 +/- 0.23 μm^2, while within garnet that overgrew quartzofeldspathic matrix the average for microzircon is 0.38 +/- 0.23 μm^2.

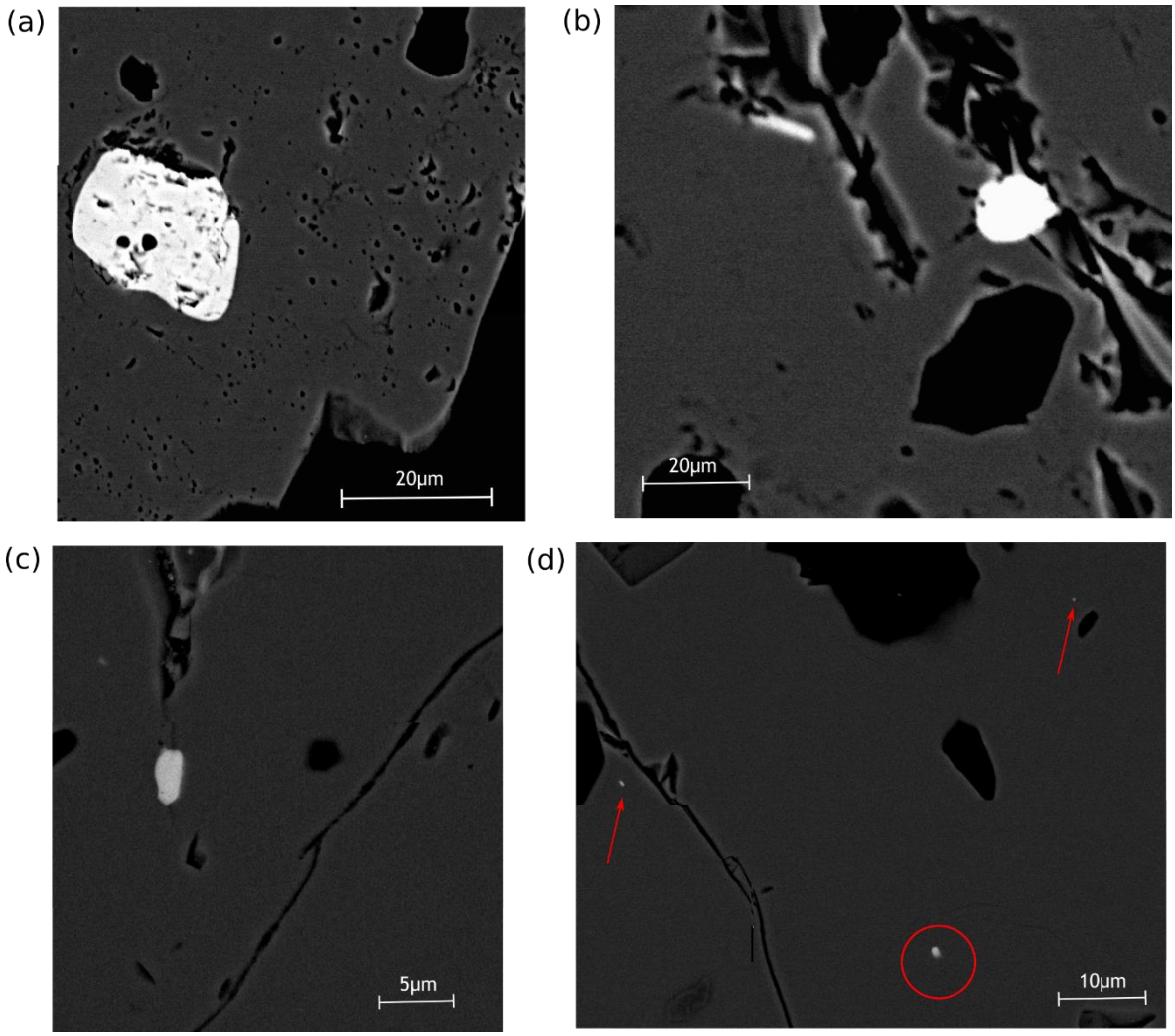

FIGURE 6.10: BSE images of zircon morphology in clear garnet in staurolite-zone schists, (a) heavily altered detrital zircon, (b) large structurally intact detrital zircon, (c) smaller detrital zircon, (d) uncertain zircon ca. 2 µm and two <1 µm microzircon

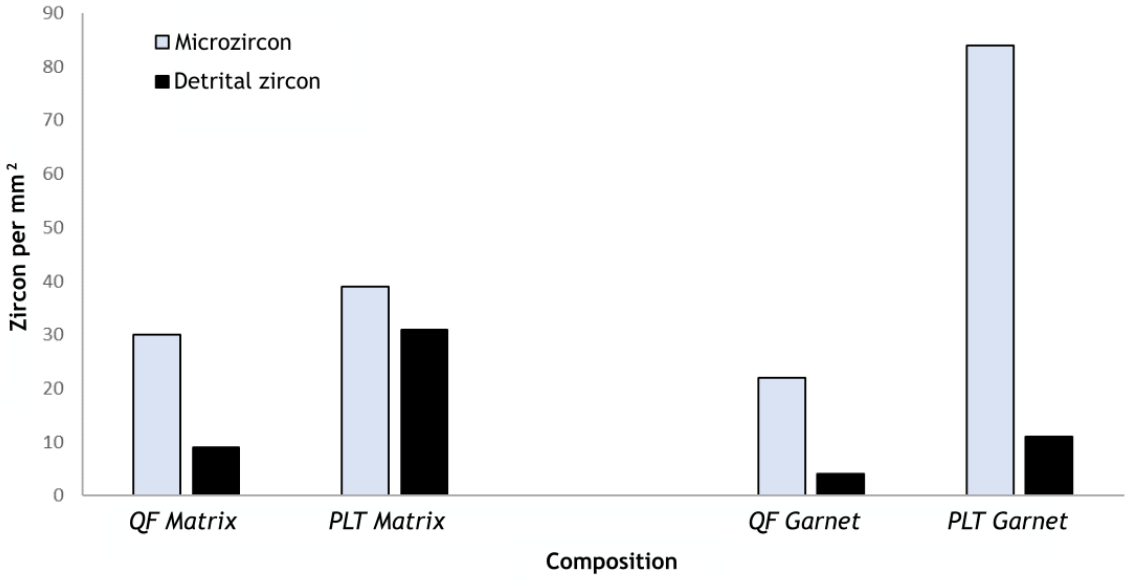

FIGURE 6.11: Detrital and microzircon abundances within GR05-7 and adjacent matrix as a function of original compositional layering of quartzofeldspathic (QF) and micaceous pelite (PLT) sediments

The matrix contains fewer microzircon than garnet porphyroblasts. The matrix in GR02 contains on average 35 microzircon per mm^2 while garnet GR02-5 contains 72 microzircon per mm^2. Detrital zircon behaves antithetically, the matrix contains 25 detrital zircon per mm^2 and garnet contains just 8 detrital zircon per mm^2. The contrast between the microzircon-poor quartzofeldspathic matrix and microzircon-rich pelitic matrix is exaggerated when garnet overgrows such lithological bands. In the matrix there is ca. 15-20% less microzircon in quartz-rich layers and adjacent mica-rich while within garnet this difference is >50%. In GR02-1 there is 74% more microzircon within garnet that overgrew micaceous matrix than adjacent garnet that overgrew quartzofeldspathic matrix. The matrix in the same sample contains just 14% more microzircon within micaceous matrix than adjacent quartz-rich layers. Microzircon within garnet are on average slightly finer than microzircon within the matrix (Figure. 6.12).

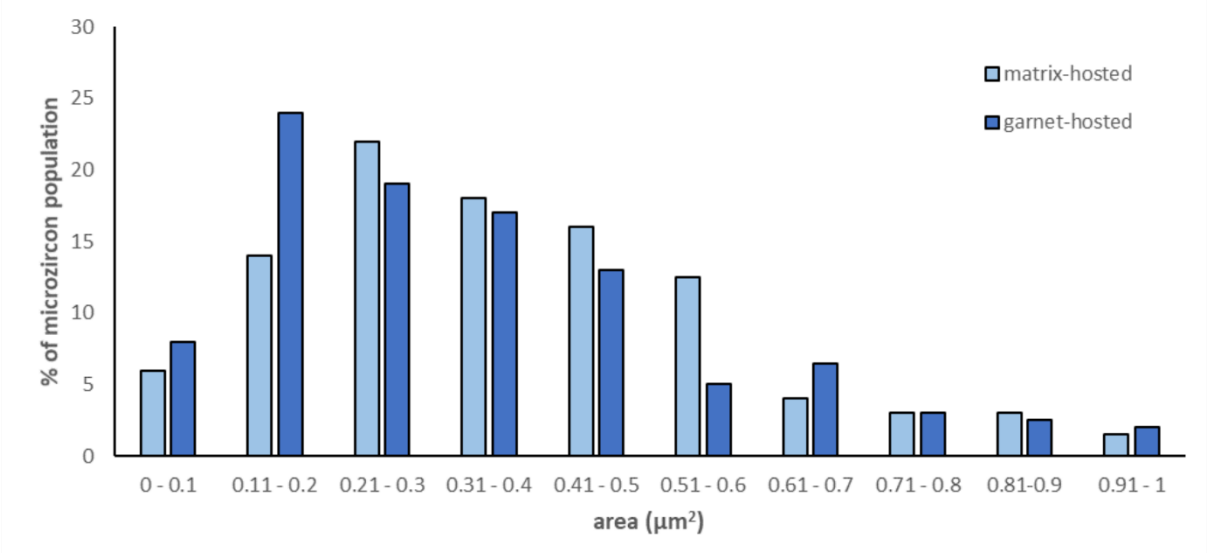

FIGURE 6.12: Size distribution plot for microzircon within all analysed staurolite-zone schists within the matrix (green) and within garnet (orange)

Microzircon and detrital zircon appear to show random patterns of distribution from core to rim in clear garnet (Figure. 6.13). While some porphyroblasts show a higher abundance of microzircon in the core, elsewhere a majority of microzircon are hosted closer to the rims. Frequently at the rim of porphyroblasts, within the outer 100-200 µm, the abundance of microzircon is lower than the adjacent margin (Figure. 6.13). Microzircon additionally show no change in morphology from core to rim, maintaining a random size distribution and displaying no obvious change to the shape or structure of grains.

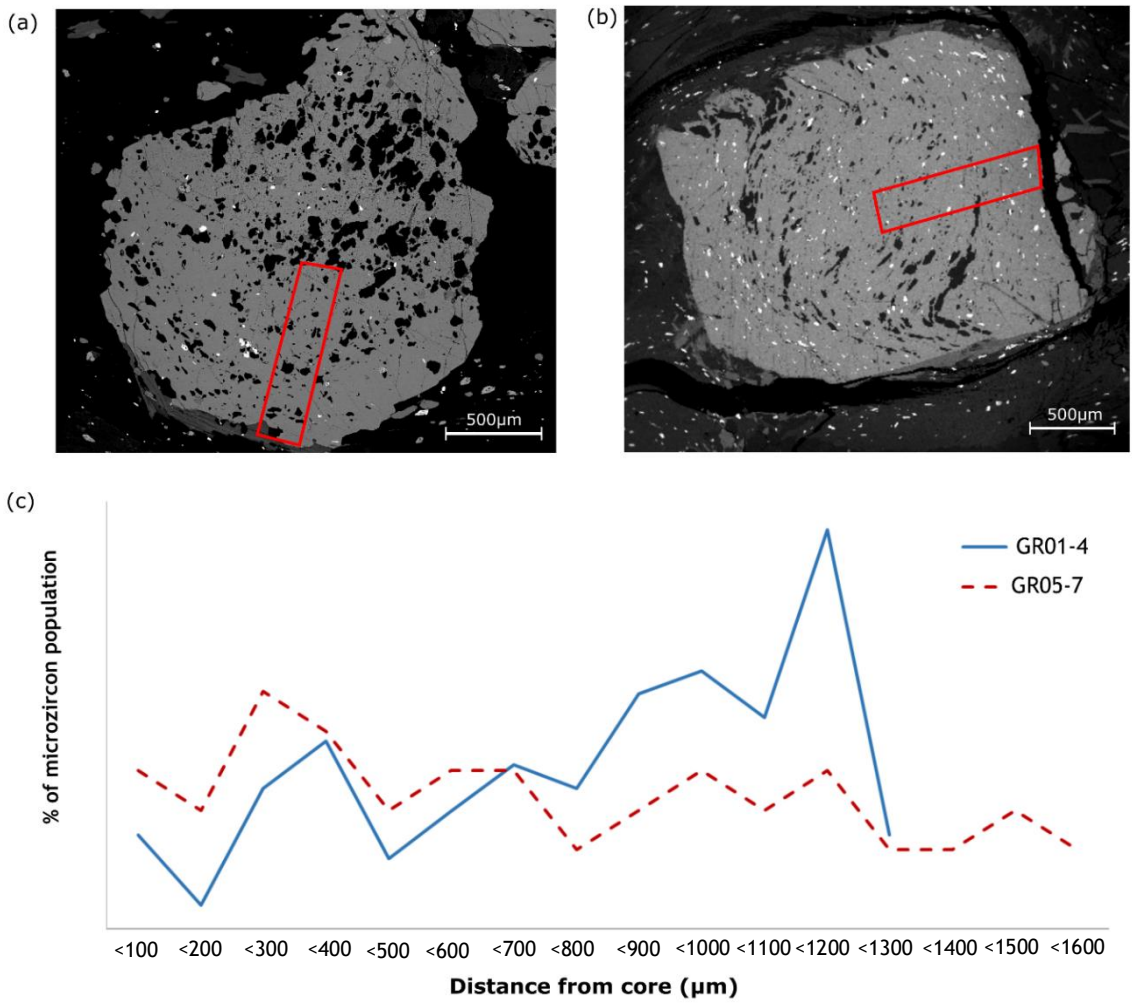

FIGURE 6.13: Microzircon distribution within transects of clear garnet in GR01-4 and GR05-7 from core to rim (a) location of transect on GR01-4 on BSE image, (b) location of transect GR05-7 on BSE image, (c) plots showing the % of the population hosted at 100µm intervals from the core

The abundance of both microzircon and detrital zircon is variable between garnet porphyroblasts within a single polished section. Within GR02 porphyroblast 8 contains 68 microzircon per mm^2 while GR02-7 contains almost double, 103 microzircon per mm^2. Detrital zircon shows a similar trend with a lot of variability

between porphyroblasts, many of which correlate to the increased or decreased microzircon abundances (Figure. 6.14).

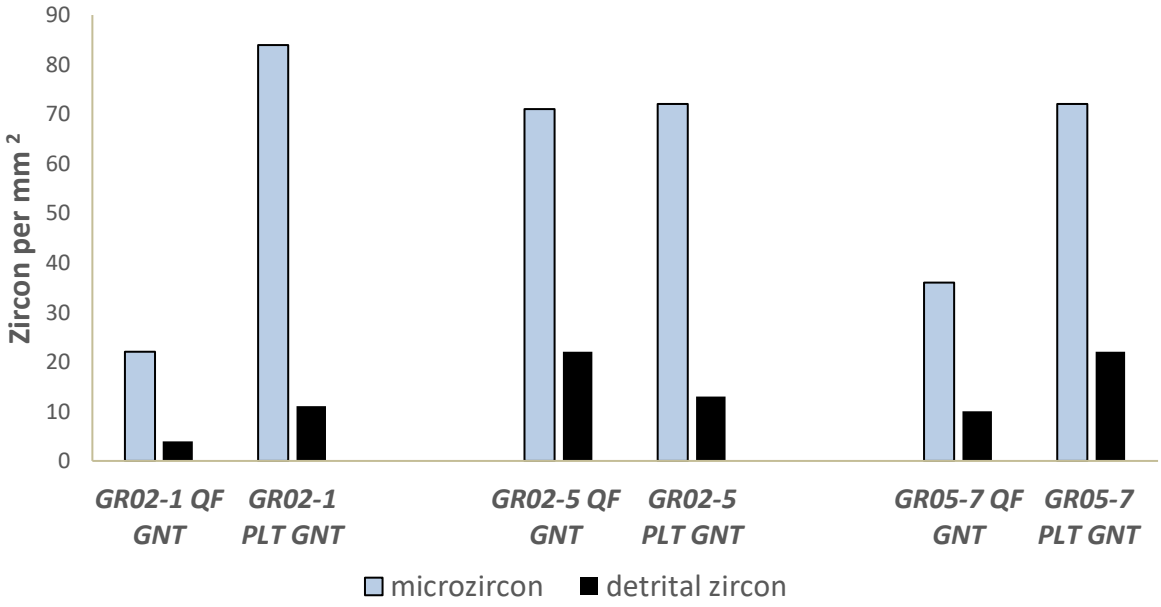

FIGURE 6.14: microzircon and detrital zircon abundance per mm^2 across QF GNT – garnet that has overgrown quartzofeldspathic matrix – and PLT GNT – garnet that has overgrown pelitic matrix layers within 3 clear garnet porphyroblasts across GR02 and GR05

Microzircon show a spatial association with detrital zircon and ilmenite. Ilmenite and detrital zircon are both most abundant within heavy mineral bands. Detrital zircon is the largest source of Zr in these schists and commonly shows evidence of dissolution (Figure.6.10a). Where detrital zircon is abundant in garnet, microzircon is more abundant (Figure. 6.14). Microzircon also display a spatial link to detrital zircon, typically occurring in clusters in close proximity to detrital grains (Figure. 6.15). Microzircon commonly appear clustered around and included within large detrital ilmenite inclusions (Figure. 6.16). Mica-rich layers of the matrix contain more ilmenite while quartz-rich layers contain less, consistent with garnet that has overgrown micaceous and quartzofeldspathic matrix. The lower abundance of ilmenite in originally quartzofeldspathic layers of garnet and higher abundance in originally pelitic layers is complimentary to the patterns of microzircon (Figure. 6.17). There is a lot of variability in the abundance of ilmenite locally within the schists, however micaceous layers have consistently higher ilmenite contents than the immediately adjacent quartzofeldspathic layer (Figure. 6.17). Mn concentrations within ilmenite in biotite-zone Ball 2.8 average 1.24 +/- 0.7 wt.%, while following garnet growth in GR02 Mn contents are much lower, 0.07 +/- 0.19 wt%.

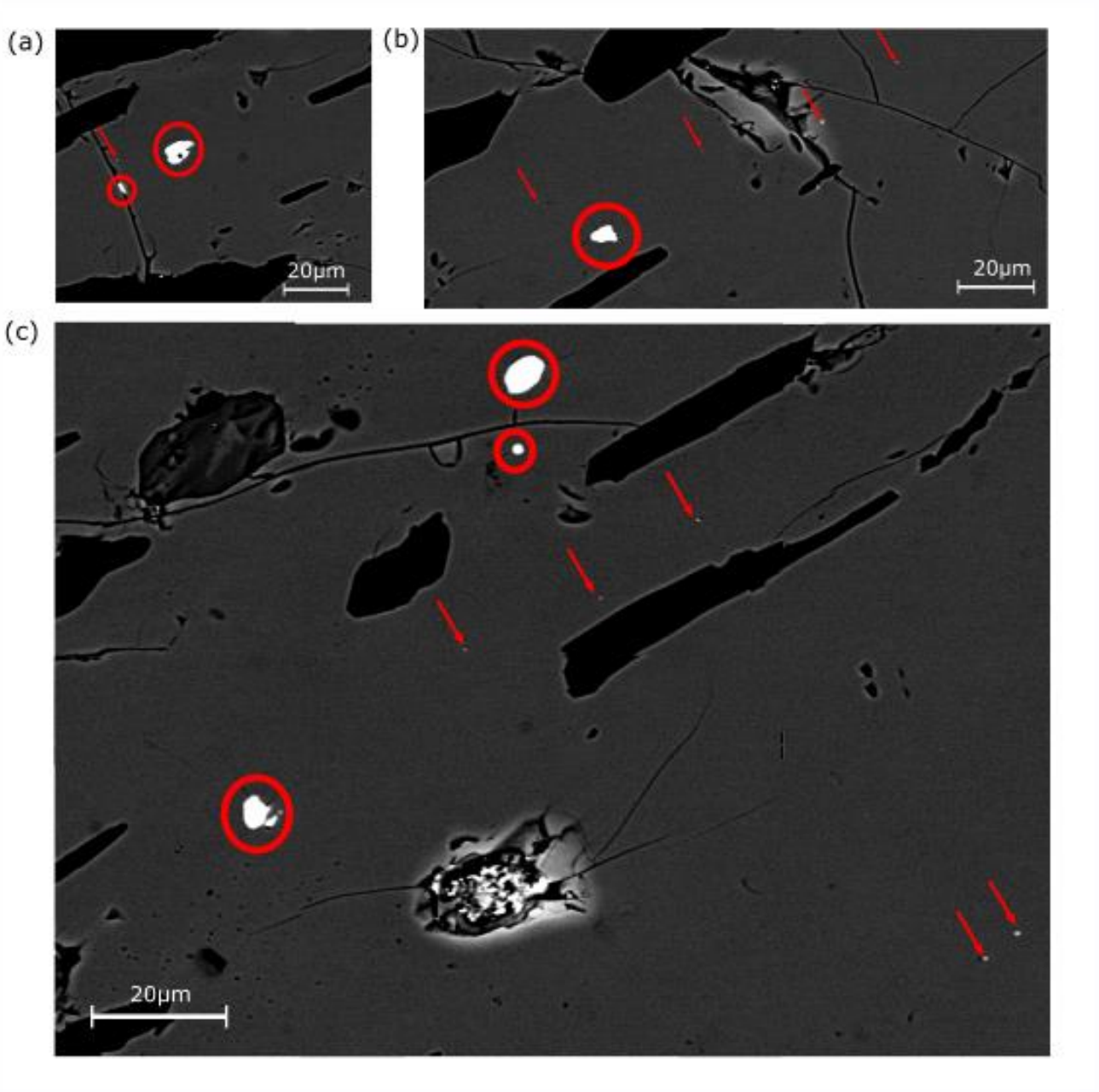

FIGURE 6.15: BSE images of detrital zircon (circled) with microzircon in close proximity (arrows) included within garnet GR02-5, (a) 2 detrital zircon and a microzircon within microzircon-poor originally quartzofeldspathic garnet, (b) detrital zircon with 4 nearby microzircon surrounding nearby fractures, and (c) cluster of detrital zircon and microzircon

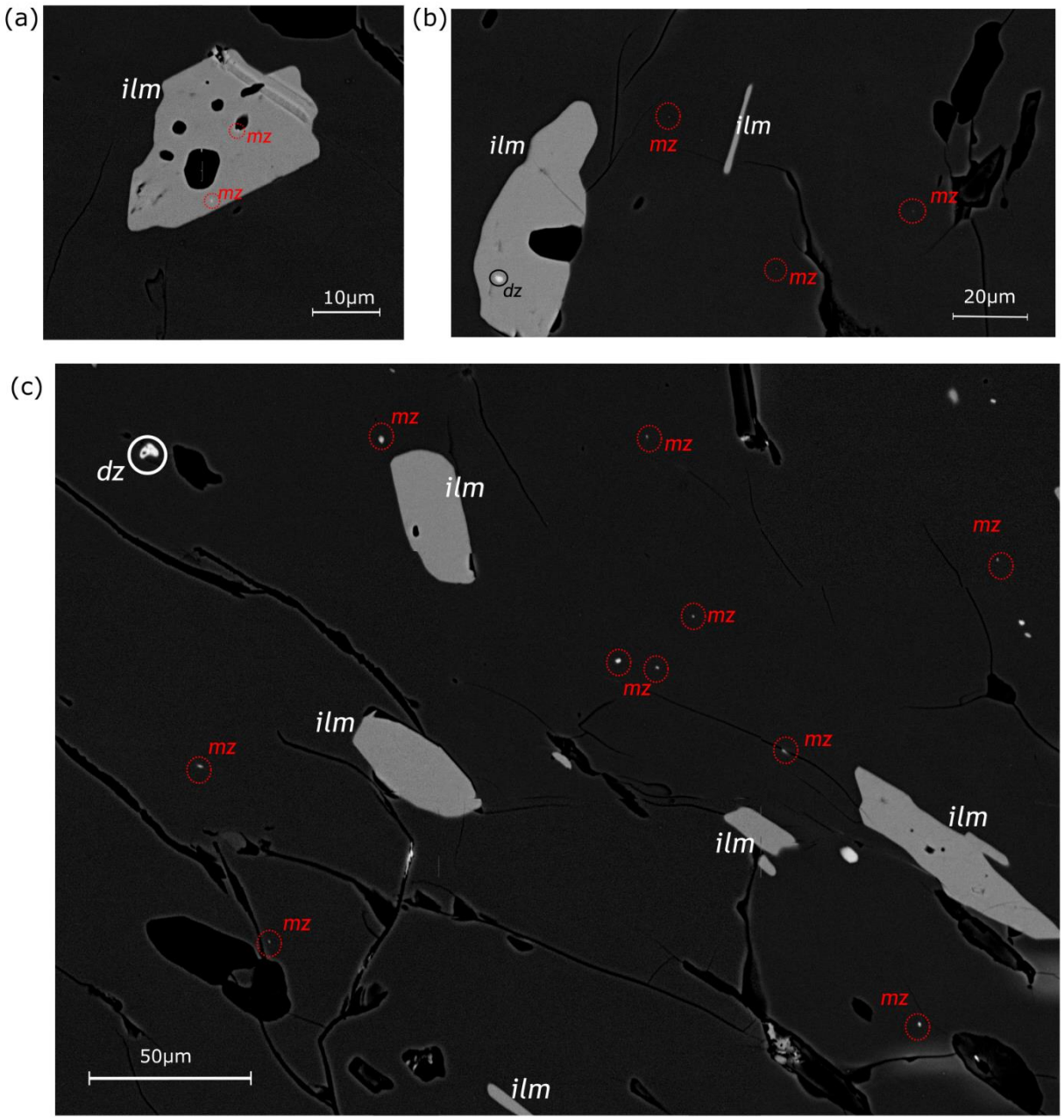

FIGURE 6.16: BSE images of ilmenite (ilm) and microzircon (mz) inclusions within clear garnet, (a) ilmenite hosting 2 microzircon, (b) large detrital ilmenite hosting a detrital zircon (dz) with microzircon in close proximity, <100 µm away, (c) cluster of microzircon in detrital zircon-poor area with abundant ilmenite inclusions

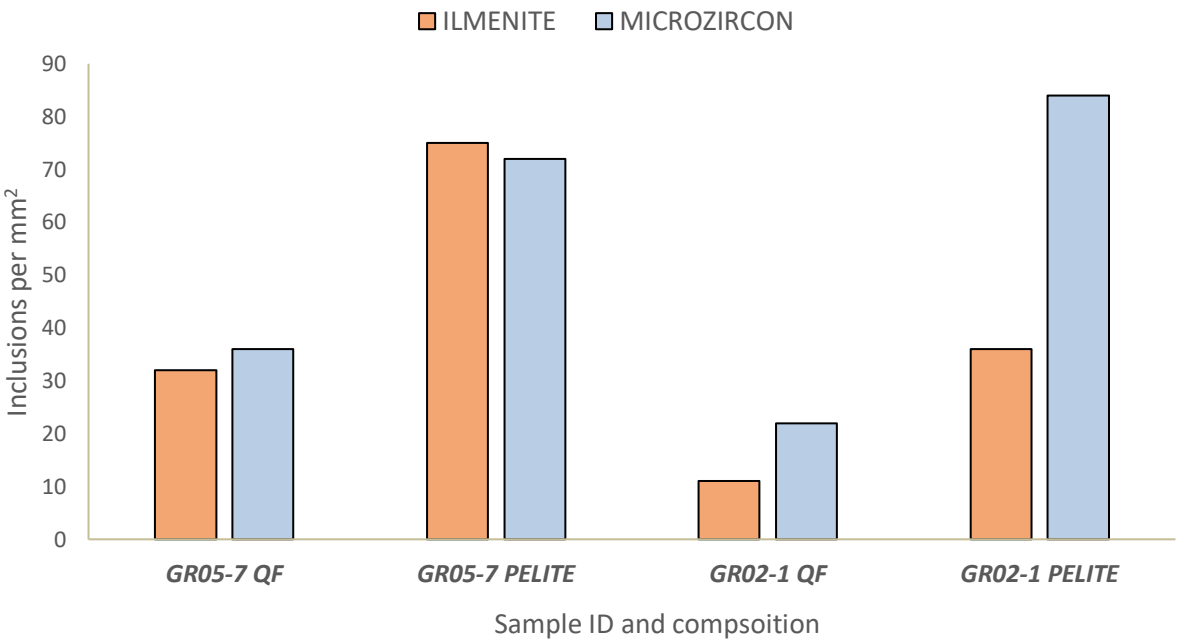

FIGURE 6.17: Ilmenite and microzircon distribution within originally quartzofeldspathic (QF) and pelitic bands of garnet in clear garnet GR05-7 and GR02-1

6.2.2.2 Interpretation of zircon in clear garnet

Examination of zircon distribution in clear garnet provides and understanding of any initial disparity in zircon populations formed during garnet growth, prior to any modification. Garnet has many characteristics which may influence zircon growth or preservation and produce a heterogeneous distribution of zircon inclusions within garnet, prior to coupled dissolution-reprecipitation.

Garnet contains concentric growth zoning where Mg and Fe increase from core to rim and Ca and Mn display complimentary profiles, decreasing from core to rim (Atherton, 1968; Dempster, 1985; Chakraborty, 1991; Carlson, 2006; Gatewood et al., 2015). Microzircon do not display a consistent pattern from core to rim showing no preference for the divalent chemistry of garnet. If zircon preferentially formed in Mn-rich garnet, then grains would be clustered within the core of the concentrically zoned garnet. Microzircon distribution shows no correlation with garnet chemistry. There is also no change to the morphology of microzircon concentrically suggesting that microzircon form irrespective of the stage of porphyroblast growth. However, neither microzircon or detrital zircon are

homogeneously distributed throughout clear garnet suggesting there are other factors within garnet or the matrix that promote or inhibit growth.

The matrix mineralogy controls the amount of potential zircon growth by influencing the amount of Zr available. Quartzofeldspathic matrix layers contain fewer, coarse detrital zircon and few microzircon while the micaceous matrix contains more abundant, finer detrital zircon and significantly more microzircon. The higher microzircon abundances in pelitic metasediments have previously been attributed to high halogen contents producing corrosive fluids (Rasmussen, 2005) and the structural state of the zircon population, where pelite yields a larger population of fine, potentially radiation-damaged detrital grains (Dempster & Chung, 2013). Garnet that overgrows micaceous layers contains more microzircon than quartzofeldspathic layers, producing ilmenite inclusion-rich garnet with abundant microzircon and quartz inclusion-rich garnet with less microzircon. The larger population of fine, more potentially metamict detrital zircon (Hay & Dempster, 2009a) and the large microzircon population in micaceous layers work together to produce more potential zircon growth within these layers, and in the garnet that overgrows it, compared to garnet that overgrows quartzofeldspathic layers.

Microzircon are finer in garnet than the matrix, paired with the increasing abundance this is indicative that a majority of microzircon are dissolved and recrystallized during garnet growth, not just captured from the matrix. Although, microzircon are predominantly included within matrix mineral phases, generally they have more opportunity to grow in the matrix compared to within porphyroblast phases. Microzircon nucleate at the growing edge of garnet and quickly become encapsulated resulting in the formation of fine microzircon within garnet. Most of the microzircon are inclusions within matrix phases meaning that matrix microzircon has not become coarser following garnet growth as the zircon were already encapsulated.

The contrast between microzircon populations between quartzofeldspathic and pelitic layers is exaggerated within garnet. The abundance of microzircon within the quartzofeldspathic matrix is similar to that within adjacent quartz inclusion-rich garnet, however microzircon increase in abundance in garnet that overgrew micaceous garnet compared to the adjacent micaceous matrix layers (Figure.

6.11). Within the mica-rich matrix either; (a) there is an additional Zr source that dissolves or recrystallizes as garnet grows increasing the potential for new zircon growth, (b) the mica-rich matrix may produce more fluid through devolatilization, or potentially more pathways within the more reactive layer, promoting the dissolution of zircon and enabling the transportation of Zr, and/or (c) the finer, more metamict detrital zircon population is more reactive and undergoes preferential dissolution during garnet growth thus promoting Zr release and microzircon growth.

Detrital zircon is the primary repository of Zr within most rocks (Bea & Montero, 1999; Degeling, 2002; Bea et al., 2006; Kohn & Kelly, 2018). As such, it is likely the source of much of the Zr for microzircon growth. Garnet contains more microzircon than the matrix, suggesting dissolution of detrital zircon must be ocurring. Detrital zircon has a higher bulk modulus and as such undergoes volume changes as a result of changing pressure more slowly than the surrounding garnet. The result is the formation of microcracks surrounding detrital zircon within the host garnet as it changes volume (Figure. 6.18) (Whitney et al., 1996; Whitney et al., 2000). These small-scale fractures often become interconnected and act as fluid pathways (Figure. 6.18b), promoting zircon dissolution and Zr transportation to a proximal site more favourable for microzircon nucleation and growth. Ilmenite contains Zr contents up to 1000s ppm (Bingen et al., 2001; Charlier et al., 2007; Bea et al., 2006) however, the Zr content of ilmenite in these schists are likely highly variable due to the inherited nature of the detrital grains. Ilmenite may either act as a source of Zr (Bingen et al., 2001; Bea et al., 2006; Morisset & Scoates, 2008) and/or structurally promotes the formation of new metamorphic zircon (Beckman & Möller, 2018). Microzircon form typically >20μm from ilmenite, if ilmenite were acting as a nucleation site and promoting zircon formation structurally microzircon would likely form in contact or within closer proximity to ilmenite. Ilmenite could act as a source for Zr however, ilmenite has been linked to the cores of garnet, recrystallizing at the almandine isograd and releasing Mn (Woodsworth, 1977; Jiang et al., 1996), and potentially Zr. Ilmenite reactivity is also influenced by Ca fluxes (Liou et al., 1998; Angiboust & Halov, 2017). At the peristerite solvus, which coincides with the almandine isograd (Brown, 1962; Crawford, 1966), ilmenite may become unstable and recrystallize.

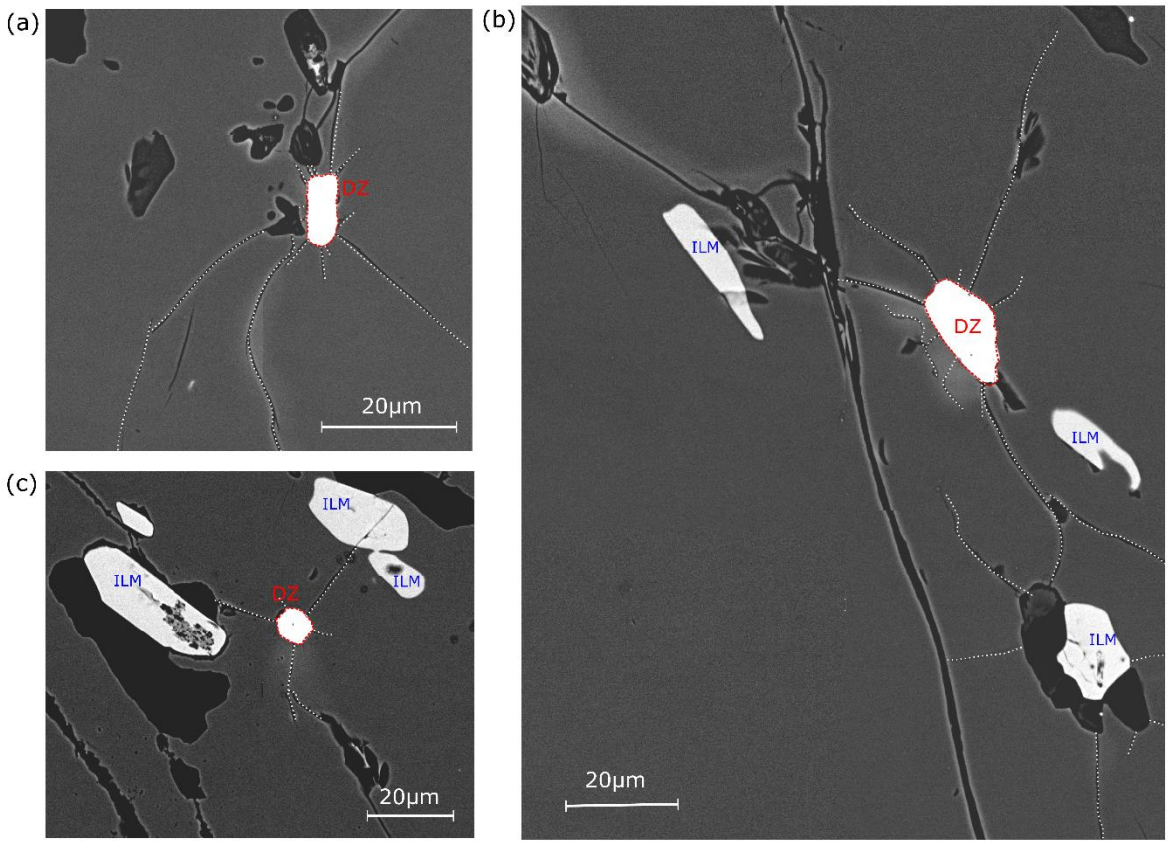

FIGURE 6.18: BSE images of microcrack networks surrounding microzircon in clear garnet GR05-7, (a) microcracks surrounding detrital zircon (b) microcracks from detrital zircon connect with infilled large fractures providing an interconnected pathway for fluids to surrounding ilmenite grains, (c) cracks penetrate surrounding detrital ilmenite grains enabling fluid access to interior

However, owing to the detrital nature of ilmenite, the Mn contents are inherited and thus variable. The contrasting Mn concentrations between the biotite-zone schists at Onich and the garnet-zone schists at Glen Roy may be a facet of the original sedimentology and not grade.

Microzircon within ilmenite may form as a result of exsolution, in the presence of Si-rich fluids, a process reported to form zircon rims surrounding ilmenite inclusions within mafic plutonic rocks (Morisset & Scoates, 2008). Within the plutonic rocks, Zr diffuses to the margins as the rock cools slowly and reacts with silicates at the rim (Morisset & Scoates, 2008). However, in the absence of protracted periods at high temperature, Zr may react with Si-rich fluids that penetrate ilmenite and form zircon inclusions in the interior of grains. Ilmenite and detrital zircon are both more abundant in micaceous layers than adjacent quartzofeldspathic. The higher microzircon population within garnet that overgrows initially pelitic sediments is likely primarily a facet of increased input

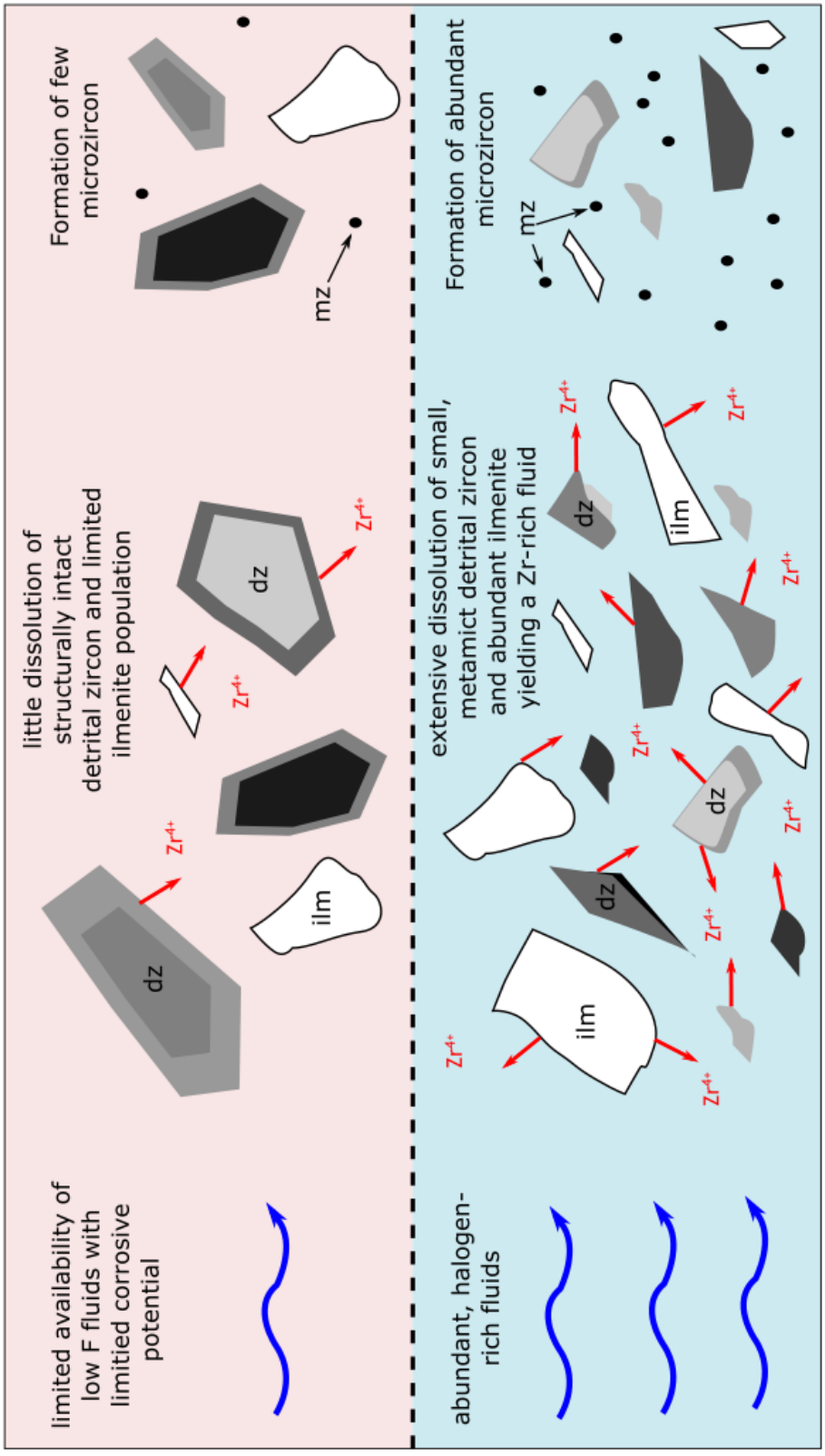

FIGURE 6.19: Schematic diagram illustrating the formation of disparate microzircon populations within the quartzofeldspathic (QF) matrix and pelite (PLT) matrix. The composition of the layer influences the abundance and distribution of the final zircon population by controlling the degree of dissolution and thus the amount of Zr for potential microzircon growth in the matrix and thus in the overgrowing garnet

of Zr to the system through (a) the more reactive, metamict fine detrital zircon population, and (b) the abundant detrital ilmenite population (Figure. 6.19).

The primary control on zircon distribution within garnet appears to be the abundance of Zr-bearing mineral inclusions, namely ilmenite and detrital zircon, which in turn is a feature of the original sedimentary lithology. Pelitic matrix layers contain a greater abundance of Zr sources, paired with the higher halogen content which promotes Zr transportation and the increased reactivity of the fine, metamict population of detrital zircon this encourages new zircon growth.

6.2.2.3 Results: zircon in cloudy garnet

When garnet undergoes coupled dissolution-reprecipitation, during staurolite formation, the result is a mineral and fluid inclusion-rich garnet with partial resetting of the chemistry, disrupting growth zoning (Dempster et al., 2017). Analysis of cloudy garnet enables an understanding of the influence dissolution-reprecipitation has on the zircon populations previously defined in clear garnet (6.2.1.1).

Cloudy garnet contains less microzircon than clear garnet (Figure. 6.20). On average cloudy garnet contains 53% less microzircon than clear garnet within the same porphyroblast (Table. 6.1). Ambiguous garnet, a textually intermediate state that displays the same modified chemistry as cloudy garnet, contains similar zircon abundances as cloudy domains (Table 6.1). Based on this similarity, ambiguous garnet will be paired with cloudy in this chapter as both have undergone the same modification. The contrast in microzircon abundance between cloudy and clear garnet is most obvious within GR01-9 (Table. 6.1). Clear garnet contains 94 microzircon per mm^2 while in cloudy domains in the same garnet abundance is lower with just 30 microzircon per mm^2. Microzircon represents 32 μm^2 per mm^2 of clear garnet while within cloudy microzircon comprises 8 μm^2 per mm^3.

TABLE 6.1: staurolite-zone garnet data across 3 mapped porphyroblasts in GR01 illustrating changes to zircon population sizes between clear and cloudy garnet

		Total area analysed (mm^2)	Microzircon per mm^2	Detrital zircon per mm^2	Uncertain zircon per mm^2
GR01-2	**Clear**	1.28	80	21	4
	Cloudy	1.21	19	10	13
	Ambiguous	0.16	22	4	7
GR01-4	**Clear**	1.53	106	17	9
	Cloudy	0.75	40	11	7
	Ambiguous	0.22	21	14	11
GR01-9	**Clear**	0.72	94	14	14
	Cloudy	0.97	30	5	6
	Ambiguous	0.11	17	3	3
Average	**Clear**	3.53	93	17	9
	Cloudy	2.93	30	9	9
	Ambiguous	0.49	20	7	7

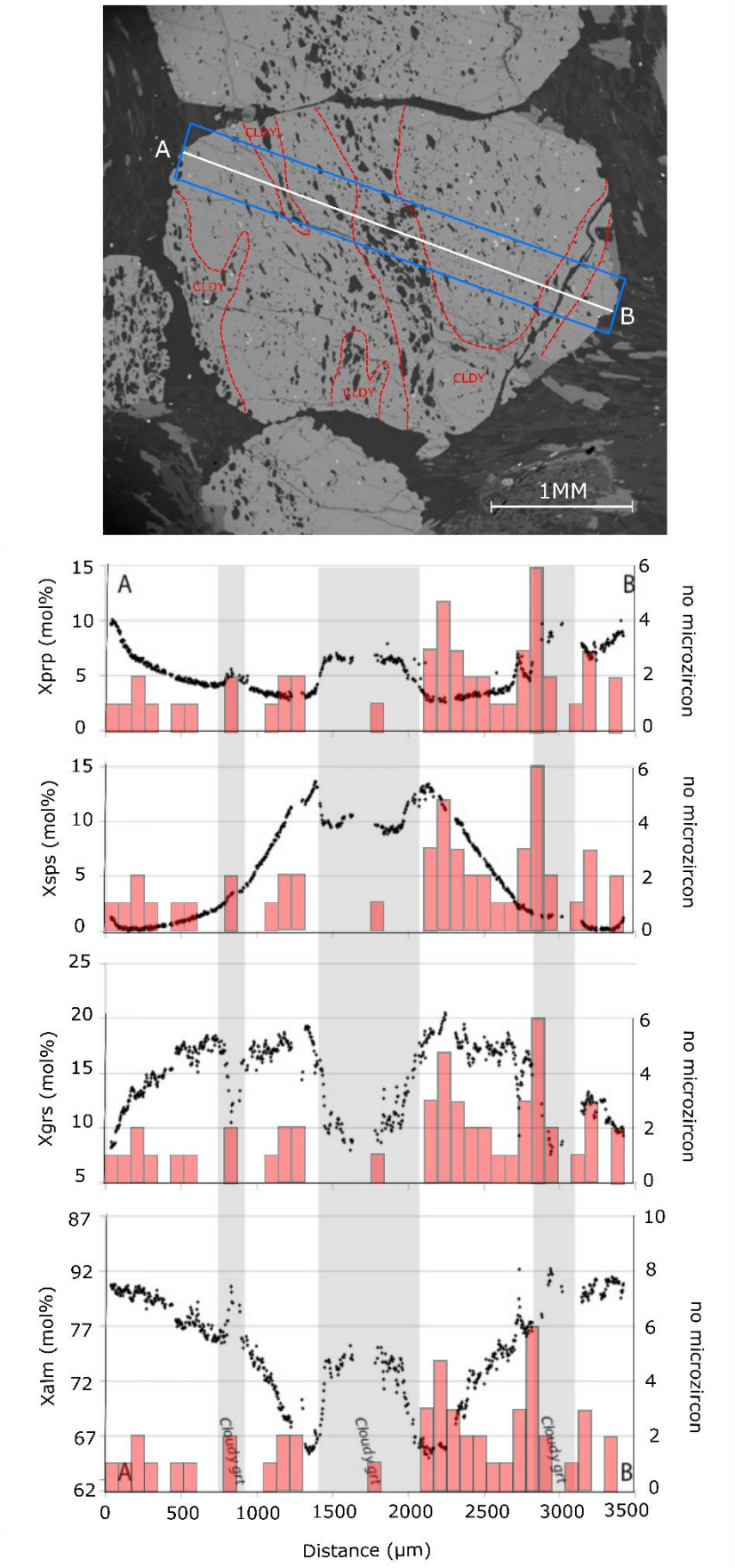

FIGURE 6.20: Transect A-B and accompanying BSE image illustrating the location of the chemical transect (white) and the imaged microzircon transect (blue) within garnet GR01-6. Chemical transects plotted as a scatter are adapted from Dempster et al (2017) against a bar plot of microzircon abundance

Cloudy garnet contains a larger population of finer microzircon, <0.4 μm^2 than clear garnet (Figure. 6.21a). Average size values between clear and cloudy garnet reveal the same pattern with microzircon finer on average in cloudy garnet, however the large errors on the values produce some overlap. Microzircon within clear garnet are on average 0.35 +/- 0.23 μm^2 and within cloudy garnet microzircon average 0.28 +/- 0.17 μm^2. Cloudy garnet contains a smaller population of finer detrital zircon (Figure. 6.21b). Detrital zircon and microzircon also display a close spatial link within cloudy garnet (Figure. 6.22), microzircon

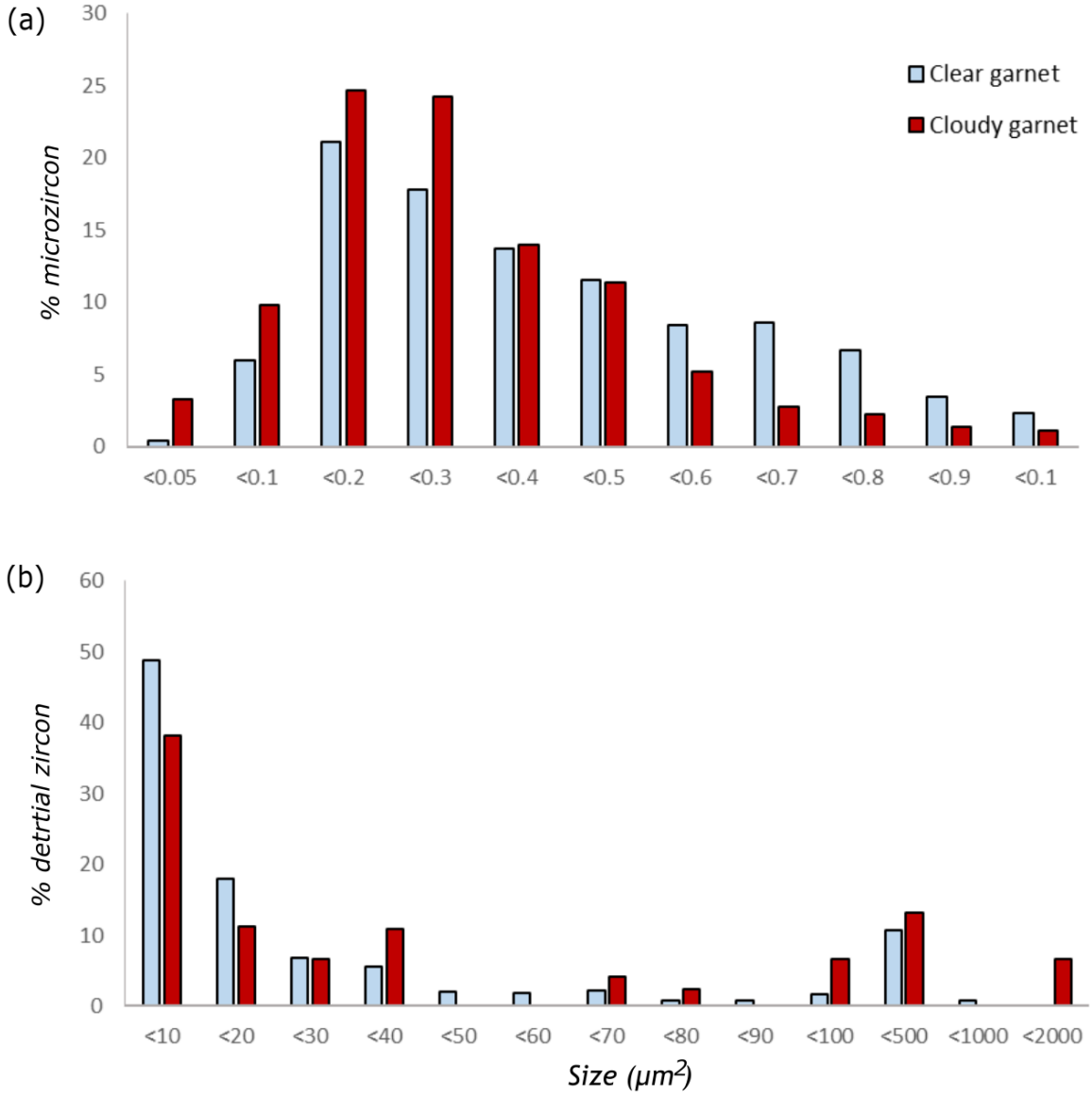

FIGURE 6.21: size distribution of microzircon (a) and detrital zircon (b) across cloudy and clear garnet within GR01

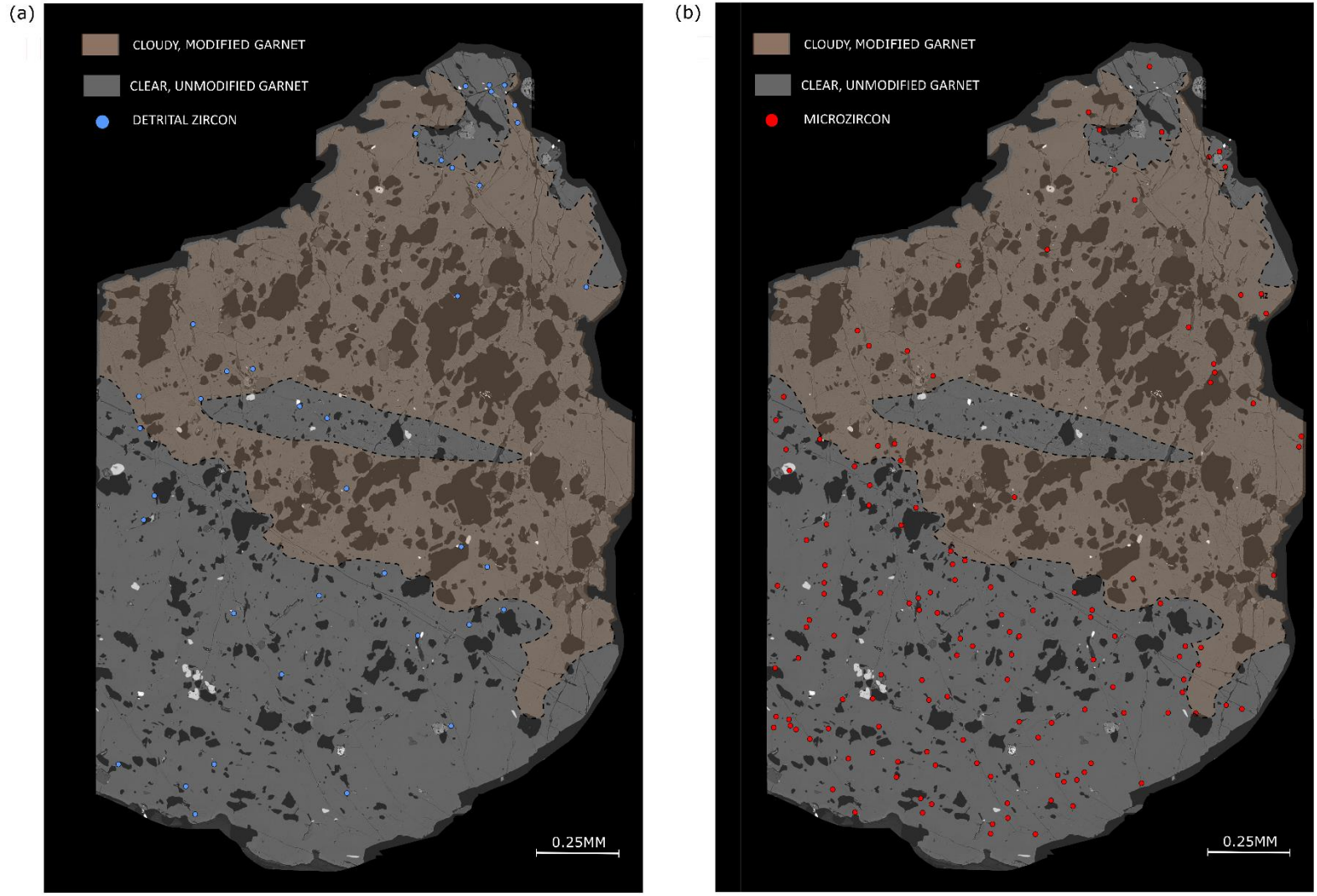

FIGURE 6.22: BSE maps of GR01-4, pink bands represent cloudy garnet while remaining garnet is clear. Maps illustrate the location of (a) detrital zircon, and (b) microzircon

typically occur <100 µm from the nearest detrital grain. Within GR01-4 over 76% of microzircon are within 100 µm of the nearest detrital grain and within GR01-2 over 85% of microzircon occur <100 µm from detrital zircon. There is typically a microzircon-free rim >10 µm wide surrounding detrital zircon, only rarely containing any microzircon.

Microzircon within cloudy garnet commonly occur within inclusions (Figure. 6.23). Microzircon may be hosted within garnet itself (Figure. 6.24a), within quartz inclusions (Figure. 6.24b), fluid inclusions (Figure. 6.24c-d), and more rarely within ilmenite (Figure. 6.16a). Within cloudy garnet 35% of microzircon are within inclusions, while <5% of microzircon are hosted within inclusions in clear garnet (Figure. 6.23). Most commonly microzircon are hosted within fluid inclusions in cloudy garnet (Figure. 6.45c-d), followed closely by quartz inclusions (Figure. 6.24b).

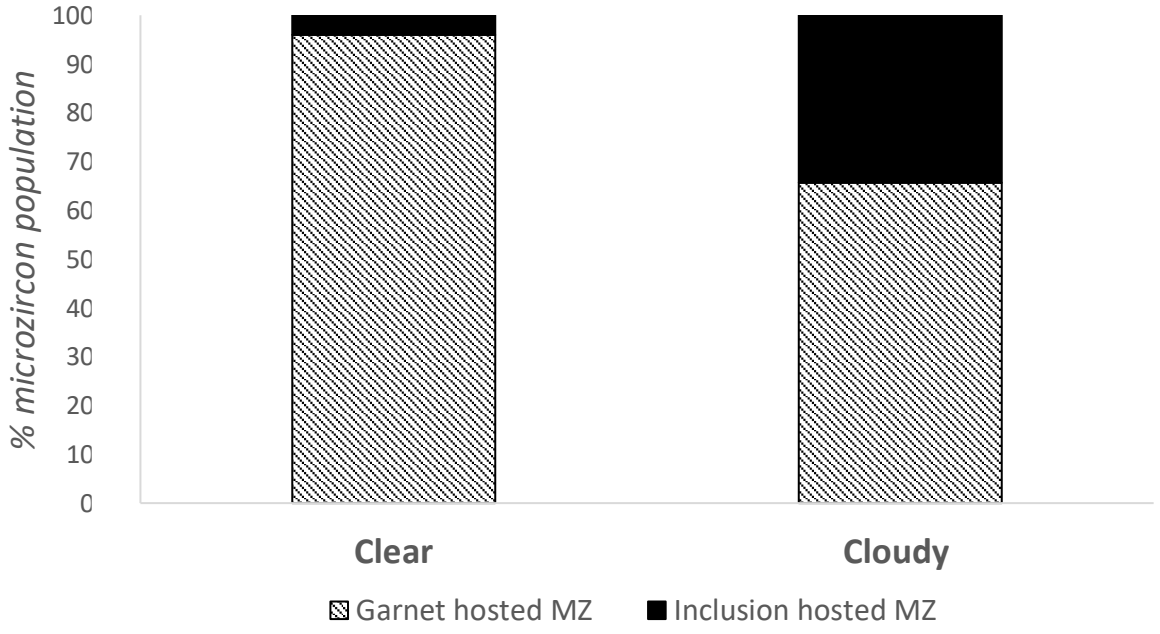

FIGURE 6.23: the proportion of microzircon (MZ) hosted within garnet and inclusions (mineral or fluid) within clear and cloudy garnet within GR01-9

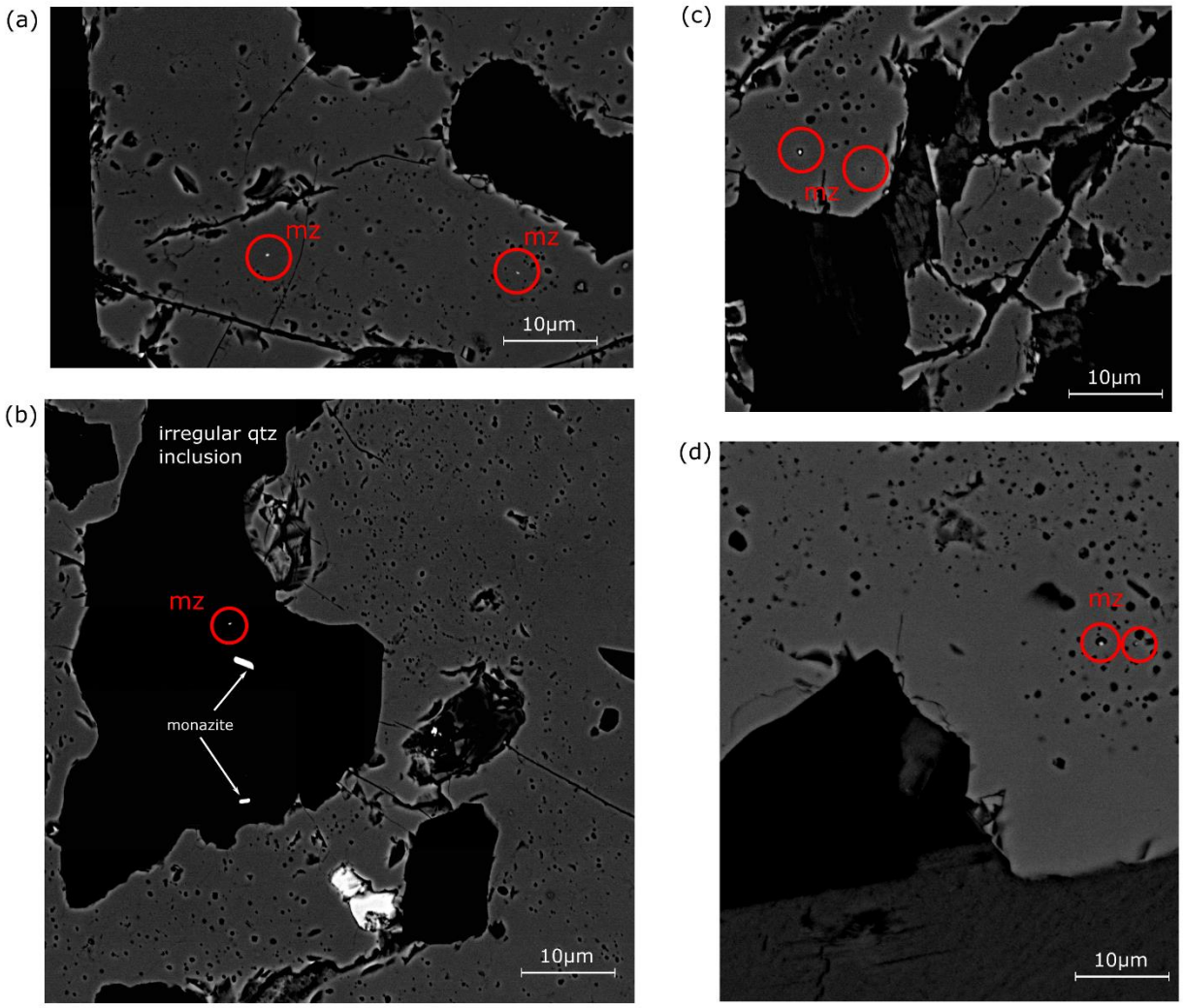

FIGURE 6.24: microzircon hosts within cloudy garnet GR01-2, (a) microzircon directly encapsulated by garnet porphyroblast, (b) microzircon within large, irregularly shaped quartz inclusion, (c-d) microzircon within small, fluid inclusions

6.2.2.4 Interpretation of zircon in cloudy garnet

Garnet decreases in volume by just ca. 15% due to replacement by quartz and fluid inclusions through coupled dissolution-reprecipitation. Microzircon are either initially low in the more reactive garnet or populations are partially removed during coupled dissolution-reprecipitation. One of the controls over cloudy garnet formation is the original composition of the matrix the garnet overgrew (see section 5.2.3.3). Dissolution-reprecipitation occurs preferentially in silicate inclusion-rich areas of garnet that overgrew quartzofeldspathic matrix layers. The abundance of quartz inclusions within originally quartzofeldspathic layers produces microcracks within the host garnet (Whitney et al., 2000). Microcracks

in turn result in more potential fluid availability for dissolution-reprecipitation. Within GR01-9 cloudy garnet contains >75% less microzircon than adjacent clear garnet, a much larger reduction in microzircon than between garnet that overgrew quartzofeldspathic matrix and garnet that overgrew pelitic matrix. Garnet that overgrew quartzofeldspathic matrix generally contains ca. 38% less microzircon than garnet that overgrew pelitic. Originally lithological layering may in part account for the lower volume of microzircon within cloudy garnet however it is not solely responsible indicative that coupled dissolution-reprecipitation has an impact on zircon populations.

There is an increase in fine microzircon within cloudy garnet compared to clear garnet (Figure. 6.21). Therefore, following modification there is a change in the size distribution of microzircon, the size of the population decreases. Zircon size is influenced primarily by the duration of growth and availability of Zr. There is no initial disparity in microzircon size between garnet that overgrew quartzofeldspathic matrix versus garnet that overgrew pelitic matrix. The finer population of microzircon in cloudy garnet is therefore not a facet of original microzircon populations formed during and prior to garnet growth. If the microzircon populations within cloudy garnet were preserved populations formed prior to coupled dissolution-reprecipitation then they should be relatively uniform with the microzircon population in clear garnet. Alternatively, if the microzircon within cloudy garnet were preserved during coupled dissolution-reprecipitation then an increase in size would be typical. Finer microzircon have a larger surface energy and as such are preferentially dissolved during coupled dissolution-reprecipitation leaving a population of larger microzircon in modified garnet. The change in size indicates that during coupled dissolution-reprecipitation a new population of finer microzircon form to the detriment of original coarser populations. Coupled dissolution-reprecipitation is interpreted to be a relatively fast process (Putnis & Putnis, 2007; Ruiz-Agudo et al., 2014). The reaction front propagates quickly potentially producing a population of fine microzircon which become encapsulated within the rapidly reprecipitating product phase. The larger size of detrital zircon within cloudy garnet (Figure. 6.21b) may be the result of preferential dissolution of finer, possibly metamict zircon (Hay & Dempster, 2009a). Alternatively, the population of coarser detrital zircon may be preserved from garnet that overgrew quartzofeldspathic matrix, which is preferentially

exploited by fluids during coupled dissolution-reprecipitation and thus represents a majority of cloudy garnet.

Microzircon hosted within inclusions are more abundant in cloudy garnet than clear (Figure. 6.23). A majority of these inclusion-hosted microzircon occur within fluid inclusions. Dissolution-reprecipitation is a volume reduction process (Putnis, 2015), as a result the product phase is more porous, and this porosity is preserved as fluid inclusions. Fluid inclusions may either form surrounding microzircon or microzircon form within the inclusions. Fluid inclusions are typically absent surrounding inclusions in these schists, particularly in cloudy garnet (see section 5.2.3.1). Microzircon may occasionally precipitate from fluids more slowly than the surrounding garnet resulting in the formation of a fluid film surrounding the authigenic zircon.

Coupled dissolution-reprecipitation involves the partial replacement of garnet with large, irregularly shaped quartz inclusions and small rounded fluid inclusions (Martin et al., 2011; Dempster et al., 2017; Dempster et al., 2019). This reduction in volume doesn't account for the significantly larger reduction in microzircon populations suggesting that dissolution-reprecipitation results in the removal of microzircon from modified domains. The remaining microzircon in cloudy garnet may be a preserved population from clear garnet or a newly formed population resulting from coupled dissolution-reprecipitation. The change in size distribution of microzircon paired with the increased proportion of microzircon within fluid and quartz inclusions in cloudy garnet is indicative that microzircon are forming during coupled dissolution-reprecipitation. There is a disparity between the amount of microzircon removed and that formed, considerably more Zr is dissolved than is precipitated as new microzircon or outgrowths.

There may also be an additional source of Zr following coupled dissolution-reprecipitation. Within the matrix and cloudy garnet that has been subject to coupled dissolution-reprecipitation, monazite replaces allanite. Detrital monazite is rare, it can survive sedimentary processes but is extremely reactive at low metamorphic grades (Foster & Parrish, 2003) suggesting any monazite present is metamorphic. The monazite isograd is difficult to locate, likely forming between the garnet isograd (Harrison et al., 1995) and the staurolite isograd (Smith & Barreiro, 1990; Spear, 2010). Typically, within regionally metamorphosed pelitic

schists it appears closer to the staurolite isograd between 525-600°C (Corrie & Kohn, 2008; Janots et al., 2009; Spear, 2010). However, within garnet there are a number of heterogeneities that influence this temperature e.g. the Y concentration (Spear & Pyle, 2010) or the Ca concentration (Janots et al., 2007). Allanite has the ability to incorporate significant quantities of Zr (Bea et al., 2006) across a range of sites (Ercit, 2002) while monazite contains no Zr (Kelsey & Powell, 2011). During the allanite to monazite transformation during coupled dissolution-reprecipitation, Zr could be released from allanite thus increasing the disparity in the amount of Zr released and that incorporated into new zircon growth.

6.2.2.5 Results: zircon in the matrix

The pelite matrix contains on average 59 microzircon per mm^2 while the quartzofeldspathic matrix contains 41 microzircon per mm^2. 5.2 vol.% of the matrix is zircon within the staurolite-zone schists. Most microzircon occur within grains, while detrital zircon are predominantly located on grain boundaries (Figure. 6.25). Outgrowths are present on most detrital zircon grains but are very thin, typically <1 µm.

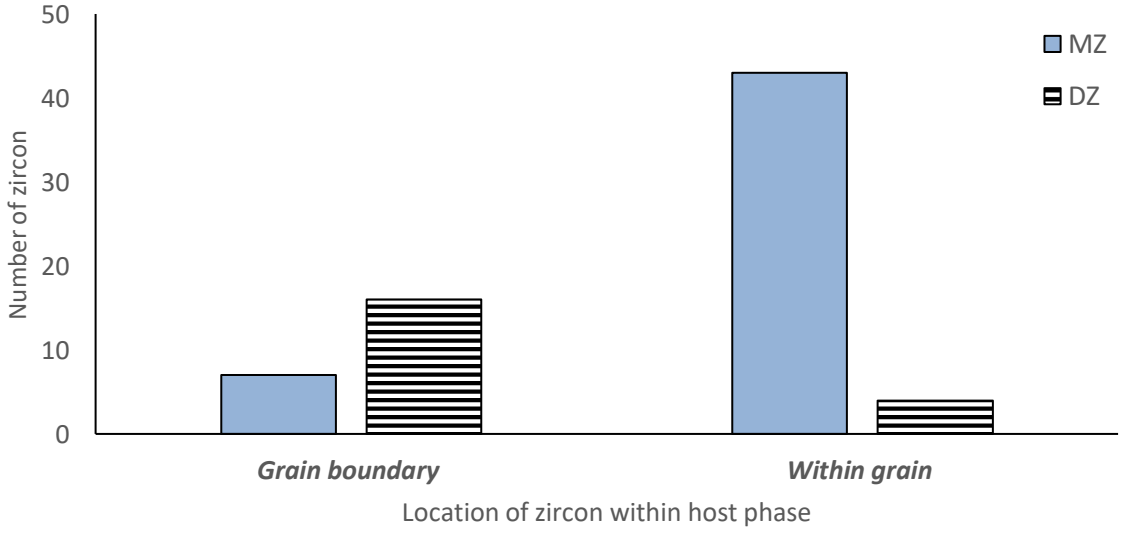

FIGURE 6.25: abundance of microzircon (MZ) and detrital zircon (DZ) on grain boundaries or included within host phases within the matrix in GR01 per mm^{2c}

Microzircon are most abundant within muscovite in the pelite matrix, hosting >50%, while quartz hosts >60% of microzircon in the quartzofeldspathic matrix (Figure. 6.26). Detrital zircon and microzircon are proportional within the quartzofeldspathic and pelitic matrix i.e. phases which host a large proportion of detrital zircon also host a lot of microzircon (Figure. 6.26). Chlorite is the exception, despite containing detrital zircon, typically more than plagioclase, it contains no microzircon (Figure. 6.26). there is no change in microzircon abundance in the matrix surrounding cloudy garnet.

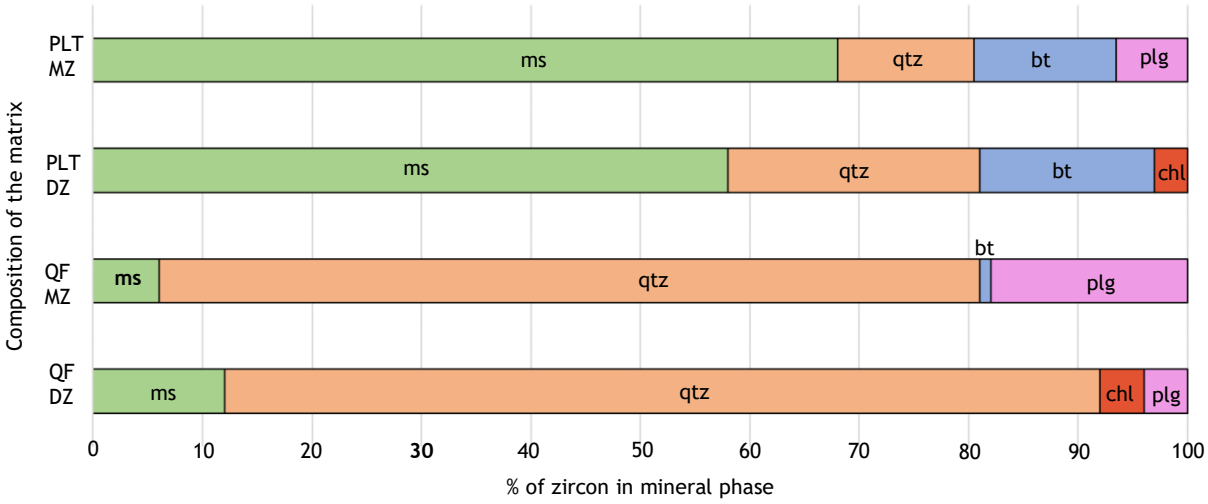

FIGURE 6.26: distribution of microzircon (MZ) and detrital zircon (DZ) across quartzofeldspathic (QF) and pelite (PLT) matrix phases within staurolite-zone schist GR02

6.2.2.6 Interpretation of zircon in the matrix

The absence of microzircon on grain boundaries is likely a facet of preservation. Grain boundaries act as fluid pathways during fluxes promoting dissolution of nanocrystalline microzircon, while populations within grains are sheltered from dissolution. The absence of thick outgrowths suggests that new zircon growth at this grade predominantly occurs as microzircon. This is likely owing to temperature, at higher temperatures, Zr transport is more efficient and therefore Zr can be transported longer distances to form outgrowths on non-metamict grains instead of nucleating into separate microzircon neoblasts.

Microzircon and detrital zircon abundance within phases are generally proportional to the modal mineralogy. Within the pelite both microzircon and

detrital zircon are most abundant within mica, and within the quartzofeldspathic matrix, microzircon and detrital zircon are predominantly quartz-hosted (Figure. 6.3). This is generally the case for most minerals except biotite porphyroblasts and chlorite. Similar to the biotite-zone schists (see section 6.2.1.2), chlorite contains no microzircon despite containing a large proportion of detrital zircon. This is further indication that during retrogression microzircon are dissolved and no new microzircon growth occurs.

The staurolite-zone matrix contains more microzircon than the biotite-zone matrix. The Appin Phyllites and Leven Schists may have completely disparate origins, and both display complex tectonothermal histories which makes comparing the schists difficult. However, notably within both the Leven Schists and Appin Phyllites microzircon abundance is much higher in porphyroblast phases than adjacent matrix, the mineralogy of the matrix also has an influence on the potential metamorphic zircon growth.

6.2.2.7 Conclusion

Clear garnet has undergone limited post-growth modification. Zircon populations are representative of those formed prior to and during garnet growth. Garnet contains more microzircon than the matrix it overgrows and it is heterogeneously distributed. Zircon distribution seems to be primarily influenced by the original sedimentary lithology of the matrix, micaceous matrix produces garnet with abundant ilmenite and fine detrital zircon, both of which potentially act as a source of Zr for microzircon growth. The result is garnet that has overgrown pelitic metasediments with abundant microzircon, and garnet that has overgrown quartzofeldspathic matrix layers with up to 50% less microzircon. During staurolite formation, coupled dissolution-reprecipitation of garnet influences zircon populations, particularly microzircon. Detrital zircon appears lower in these bands but how much of this disparity is a facet of the original sedimentation and lithology is unclear. Microzircon are significantly lower in cloudy garnet than adjacent clear, up to 75%. Cloudy garnet also contains a larger population of fine microzircon which are occasionally contained in irregular quartz and fluid inclusions that form during coupled dissolution-reprecipitation – all indicative that the population at least partially forms during the modification process.

6.2.3 Sillimanite-zone garnet

Sillimanite-zone schists display the same textural complexities present within the staurolite schists with cloudy modified garnet and clear unmodified garnet. Dissolution-reprecipitation is more extensive within the sillimanite-zone schists with just 14% of garnet unmodified. Sillimanite-zone garnet also includes a wider array of textures with the addition of secondary clear garnet. Secondary clear garnet is reequilibrated during sillimanite formation, eradicating fluid and mineral inclusions from cloudy domains and resetting the chemistry to produce a low Ca, high Mg product (Dempster et al., 2019). Secondary clear garnet preferentially forms surrounding mineral inclusions and at garnet margins where fluid availability is higher. The sillimanite-zone garnet can assist in understanding the impact of more extensive dissolution-reprecipitation and this additional stage of reequilibration on zircon populations.

6.2.3.1 Results: zircon in clear garnet

Clear, unmodified garnet within the sillimanite-zone schists is limited (See petrology in section 4.3). Within sillimanite-poor UGR1 there are some Ca-rich texturally clear domains interpreted as unmodified (Figure. 6.27). Sillimanite-zone schists contain less obvious compositional banding in the matrix, composed of originally more finely interbedded sediments (See petrology in section 4.3). The quartzofeldspathic and pelite layering in the staurolite-zone schists produces obvious layering in inclusion trails within garnet. Within the sillimanite-zone schists the originally more finely interbedded layers produce a more homogeneous inclusion pattern, making any original matrix layering the garnet overgrew difficult to infer. Garnet UGR1-1 contains similar amounts of zircon per mm^2 as quartzofeldspathic layers within staurolite-zone garnet (Table. 6.2) however less microzircon than the micaceous layers within the staurolite schists (Figure. 6.28).

Micrzircon and detrital zircon show a spatial link to fractures in UGR1-1 with microzircon commonly occurring <10 μm from the nearest fracture (Figure. 6.29). microzircon rarely form within or in contact with fractures while detrital zircon

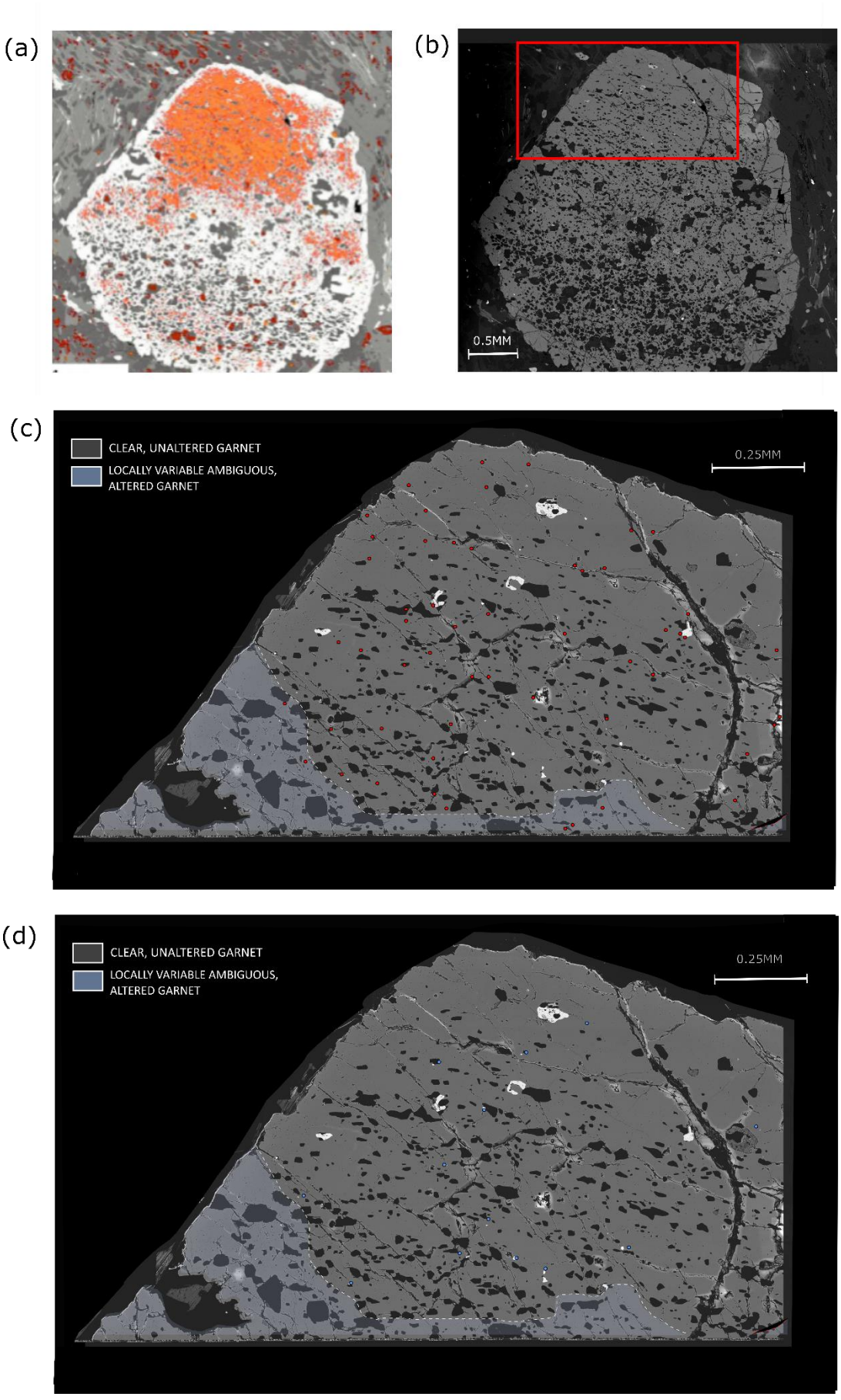

FIGURE 6.27: zircon within unmodified garnet UGR1-1 (a) combined BSE and X-ray map showing high Ca unmodified garnet in orange (from Dempster et al., 2017), (b) location of mpa within UGR1-1, (c) BSE map illustrating microzircon abundance, (d) BSE map of detrital zircon abundance

TABLE 6.2: sillimanite-zone zircon abundance data averaged across 6 analysed garnet within each textural classification and thus at different stages of modification

	Total area analysted (mm^2)	*Microzircon per mm^2*	*Detrital zircon per mm^2*
Unmodified, clear garnet	3.28	53	17
Cloudy garnet	3.25	41	8
Secondary clear inclusion rims	1.05	37	11
Secondary clear garnet margins	0.51	2	12

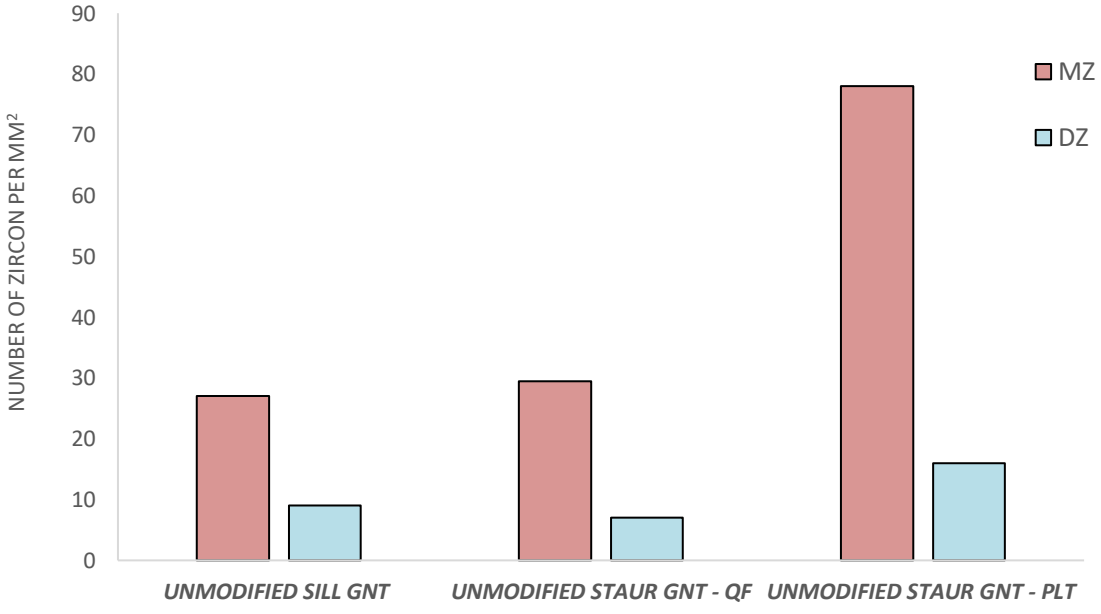

FIGURE 6.28: microzircon (MZ) and detrital zircon (DZ) abundance per mm^2 within clear, unmodified sillimanite-zone garnet (GNT) and clear, unmodified staurolite-zone garnet that overgrew quartzofeldspathic (QF) matrix and pelitic (PLT) matrix

are typically located within fractures. The distance from fractures were compared with randomly generated spatial points in order to quantify the pattern (see chapter 3 methods). The result is a significantly larger peak in the analysed microzircon <10 µm from fractures compared to the random values (Figure. 6.30) Transects across these fractures reveal high Ca chemistry consistent with clear, unmodified garnet.

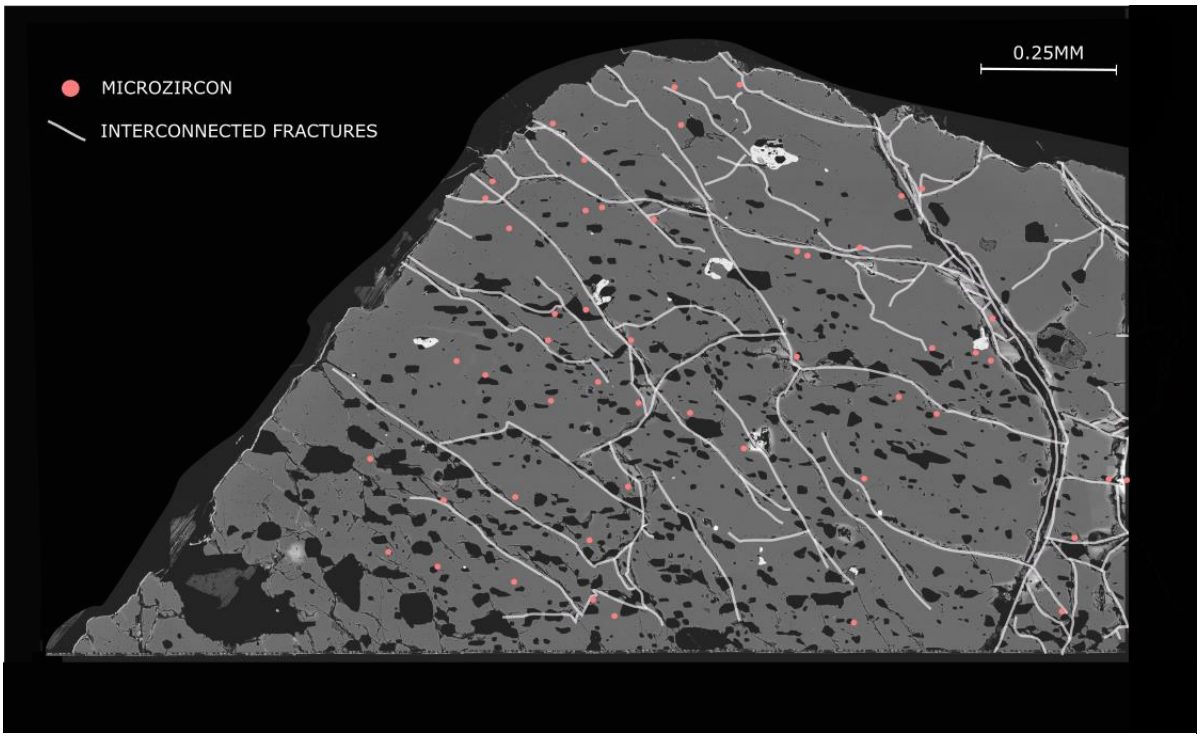

FIGURE 6.29: BSE map of UGR1-1 of the spatial relationship between interconnected fractures (white) and microzircon (pink)

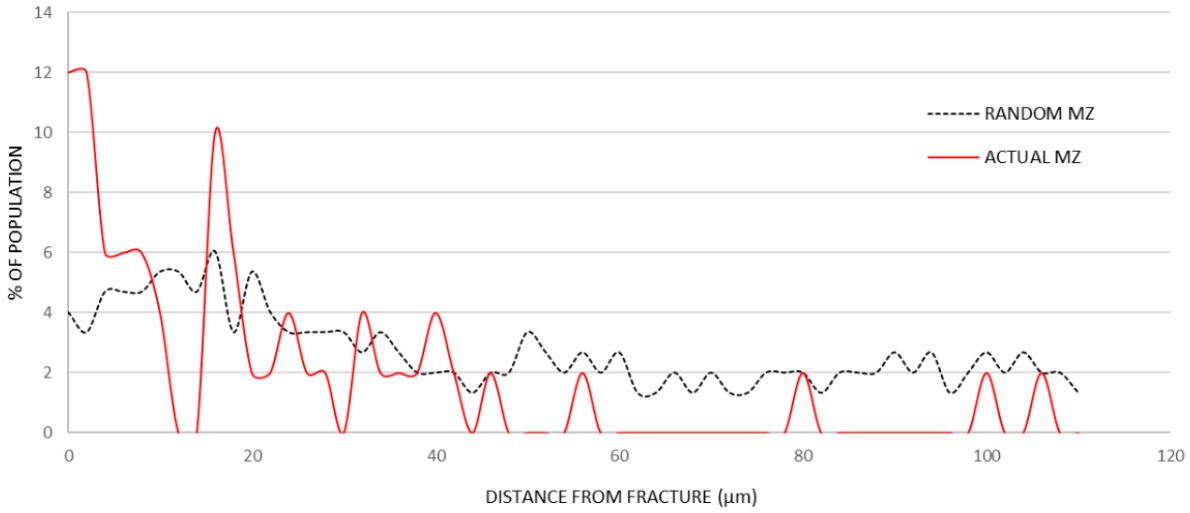

FIGURE 6.30: the distance of microzircon from fractures in UGR1-1 vs the distance from fractures of randomly generated spatial points

6.2.3.2 Interpretation of zircon in clear garnet

Microzircon and detrital zircon show a close spatial link to fractures within UGR1-1. The absence of low Ca, high Mg chemistry adjacent to fractures in UGR1-1 is indicative that there has been no modification adjacent to fractures. Microzircon therefore formed synchronously or prior to garnet growth. Rather than microzircon forming adjacent to fractures, fractures may form adjacent to microzircon. Microzircon may form proximally to detrital zircon, potentially metamict detrital grains act as a source of Zr for microzircon growth. The bulk modulus of detrital zircon varies from 223-250 GPa (Özkan & Jamieson, 1978; Hazen & finger, 1979; Marqués et al., 2006), significantly higher than garnet at ca. 170 GPa (Leitner et al., 1980). Garnet therefore decreases in volume more rapidly under increasing pressure than the included zircon, the result is fracturing around zircon as its volume decreases more slowly (Whitney et al., 1996; Whitney et al., 2000). The structural state of zircon will influence its ability to withstand pressure, more metamict zircon within garnet will reach the pressure threshold less readily, thus resulting in less microcracking. These fractures therefore likely form following microzircon growth within detrital and microzircon-rich domains.

The association between microzircon and fractures may not be visible in staurolite-zone schists based on the lower fracture density (Figure. 6.31). The fractures within the sillimanite-zone schists are commonly parallel-sub-parallel

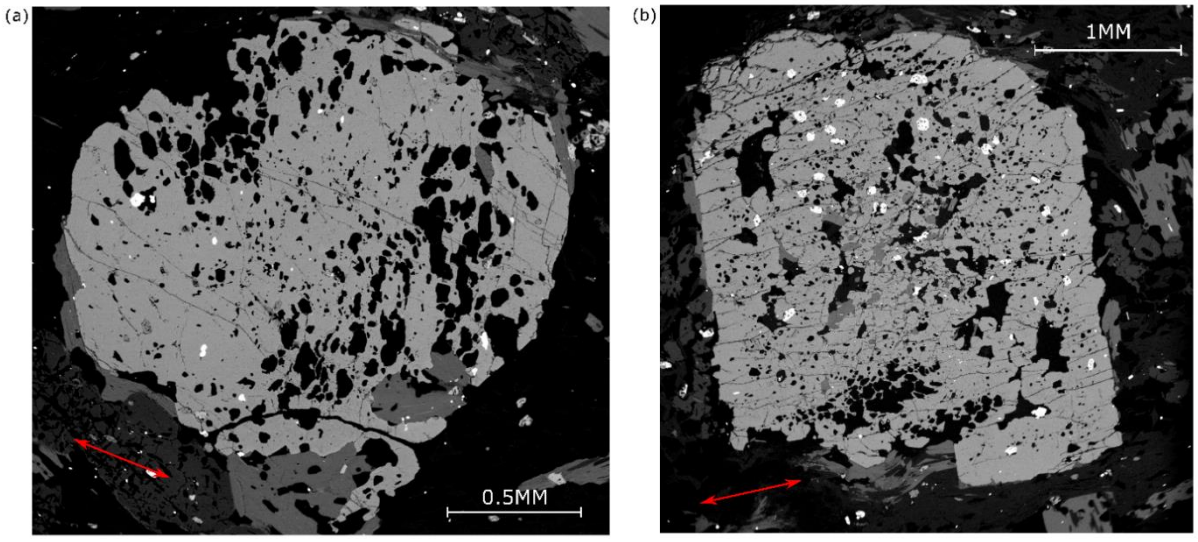

FIGURE 6.31: BSE images of fracture abundance and morphology within the Leven schists, (a) staurolite-zone garnet GR01-4 has few parallel transgranular fractures, (b) sillimanite-zone garnet UGR0-4 has a higher fracture abundance, particularly parallel transgranular fractures

(Figure. 6.31) indicative they are a feature of deformation. The disparity in fracture patterns is likely attributable to subtleties in the deformational histories of the staurolite-zone and sillimanite-zone Leven Schists.

6.2.3.3 Results: zircon in cloudy garnet

Cloudy garnet has undergone coupled dissolution-reprecipitation during staurolite formation. Cloudy garnet in sillimanite-zone schists displays all the textural and chemical characteristics of cloudy garnet in the staurolite-zone schists (Dempster et al., 2019). Cloudy garnet is much more abundant at sillimanite-zone, comprising >70% of garnet. As a result, the morphology of cloudy zones within porphyroblasts varies slightly. Staurolite-zone cloudy garnet typically forms bands and is often confined to marginal regions and surrounding fractures (see section 5.2.3.1, Figure. 5.7). Within the sillimanite-zone schists, cloudy garnet comprises a majority of porphyroblasts and commonly forms atoll structures where the core of the garnet is entirely replaced by inclusions (see section 5.3.3.1, Figure. 5.26). Sillimanite-zone garnet contains local quartz inclusion-rich bands occasionally, these bands display a slightly different inclusion pattern than surrounding more quartz-poor modified garnet (see section 5.3.3.1, Figure. 5.27).

Modified cloudy garnet contains less microzircon than clear garnet (Table. 6.2). Additionally, these microzircon are predominantly hosted within fluids inclusions. Within UGR0-4, 82% of the microzircon in cloudy garnet is located within fluid inclusions. Outgrowths are more common in sillimanite-zone schists than staurolite-zone schists Detrital zircon typically contain outgrowths <10 µm thick (Figure. 6.32).

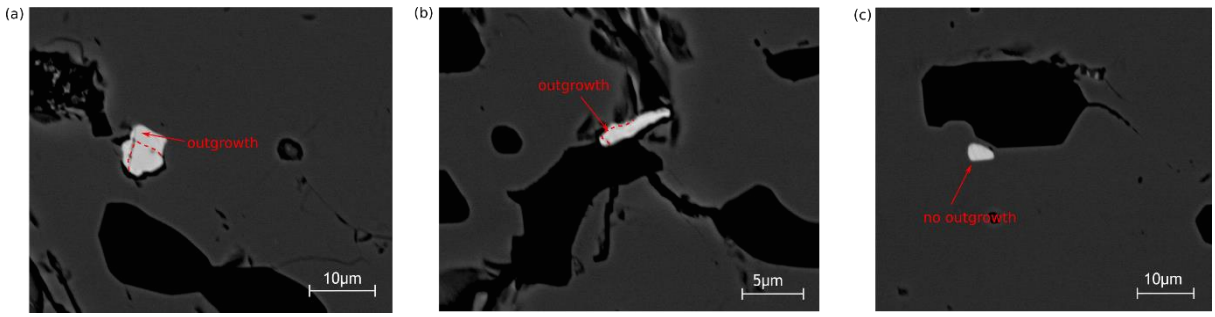

FIGURE 6.32: BSE images of outgrowth morphology in sillimanite-zone schists, (a) large detrital zircon with thick outgrowth, (b) detrital zircon with thinner outgrowth, and (c) more rarely detrital zircon appear to show no evidence of outgrowths in the sillimanite-zone schists

Quartz inclusion-rich bands within cloudy garnet contain the fewest microzircon, averaging 4 microzircon per mm^2 and 2 detrital zircon per mm^2. These bands additionally contain no monazite, ilmenite or additional inclusions, primarily containing large, irregularly shaped quartz inclusions that comprise >50% of the volume, with very limited zircon. In the quartz-poor cloudy garnet immediately surrounding quartz-rich bands microzircon is more abundant than cloudy garnet located further from quartz-rich bands (Figure. 6.33). There is texturally no difference between these proximal (<100 µm to quartz-rich bands) and distal (>100 µm to quartz-rich bands) cloudy domains (Figure. 6.33a).

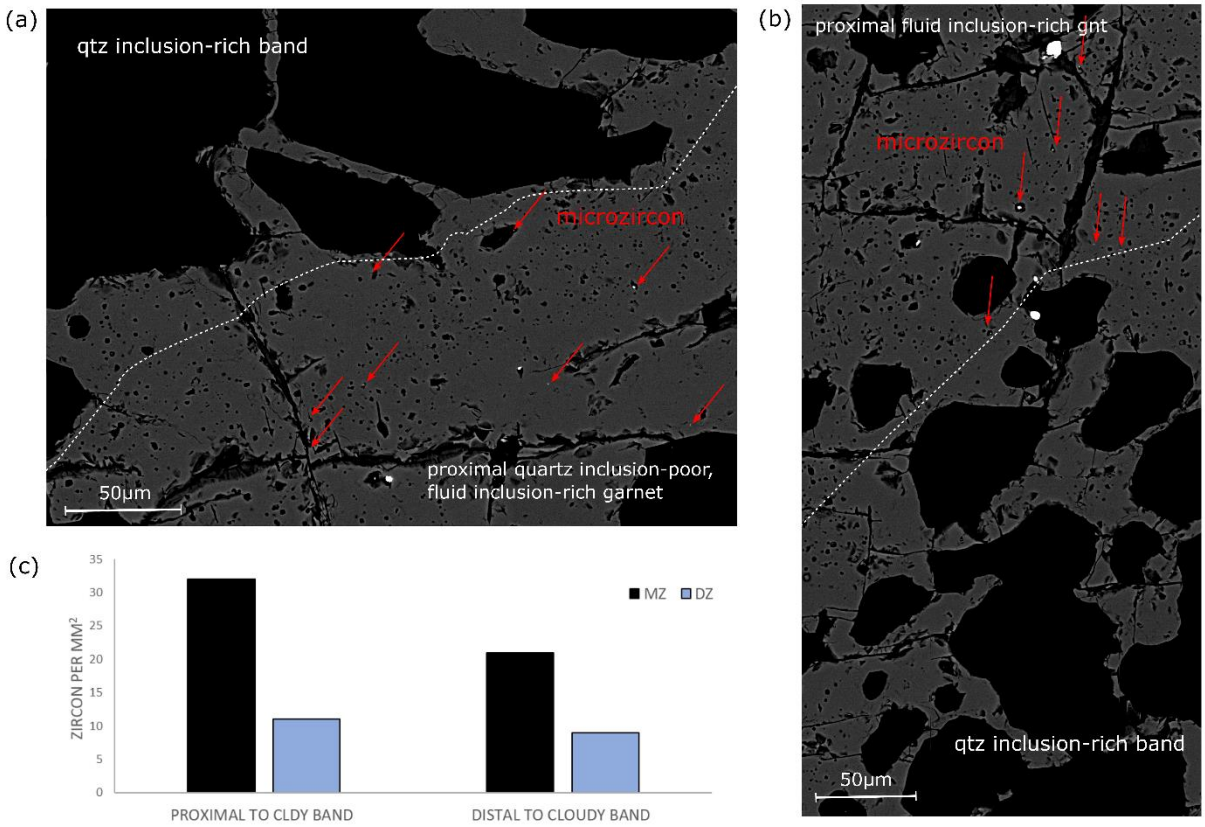

FIGURE 6.33: (a-b) BSE image of qtz-rich bands in UGR0-4 and the location of proximal cloudy garnet (<100µm) containing abundant microzircon, and (c) plot of the abundance of zircon in proximal (<100µm) and distal (>100µm) areas from qtz-rich bands

6.2.3.4 Interpretation of zircon in cloudy garnet

Quartz inclusion-rich bands within sillimanite-zone garnet have undergone more extensive dissolution, and thus garnet replacement, during coupled dissolution-reprecipitation. The higher microzircon abundance immediately surrounding these quartz-rich bands within adjacent quartz-poor cloudy garnet is indicative that

some of the zircon dissolved from the quartz-rich band forms microzircon in the adjacent less modified garnet. Quartz inclusion-rich areas may represent areas of garnet that were initially exploited during staurolite growth. Quartz-rich bands tend to be parallel, similar to the morphology of cloudy bands in less modified porphyroblasts within the staurolite-zone schists (see section 5.2.3.1, Figure 5.7).

The sillimanite-zone garnet has undergone more extensive modification where either coupled dissolution-reprecipitation was more rapid or lasted longer with sillimanite-zone schists than within the staurolite-zone schists. Microzircon are predominantly hosted within fluid inclusions, if coupled dissolution-reprecipitation occurred more rapidly then microzircon may precipitate from fluid inclusions following entrapment in rapidly reprecipitated host garnet. Alternatively, if coupled dissolution-reprecipitation proceeded for a longer time then further dissolution by fluids reaching the reaction front may have hindered the preservation of microzircon, where those trapped within fluid or mineral inclusions were sheltered and thus predominantly preserved.

6.2.3.5 Results: zircon in secondary clear garnet

Secondary clear garnet has undergone an additional stage of modification during sillimanite growth (Dempster et al., 2019). This modification eradicates the cloudy texture associated with staurolite formation, removing mineral and fluid inclusions, and resets the chemistry to an equilibrated low Ca, high Mg composition (Dempster et al., 2019). Secondary clear garnet forms exclusively in fluid-rich areas surrounding mineral inclusions and at the rim of garnet porphyroblasts.

Secondary clear garnet contains less microzircon than cloudy and unmodified clear garnet and cloudy garnet (Table. 6.2). Secondary clear garnet forms at porphyroblast margins and inclusion rims, secondary clear garnet at inclusion rims consistently contains more microzircon than secondary clear garnet at porphyroblast margins. Secondary clear porphyroblast margins are more texturally homogeneous, there are very limited fractures and mineral inclusions. Secondary clear garnet that forms rims surrounding mineral inclusions typically contains fractures and small mineral inclusions such as ilmenite and microzircon. The amount of microzircon within garnet porphyroblast margins is almost 95% lower

than at inclusion rims in the interior of porphyroblasts. Detrital zircon in secondary clear garnet is consistent in abundance with cloudy garnet, and only slightly lower than primary clear garnet (Figure. 6.2). The size of microzircon and detrital zircon is consistent with those in sillimanite-zone cloudy garnet.

6.2.3.6 Interpretation of zircon in secondary clear garnet

The additional stage of modification during sillimanite-zone formation produces secondary clear garnet with limited microzircon. During the re-equilibration that accompanies sillimanite formation microzircon dissolution is effective, particularly at porphyroblast margins. Cloudy garnet contains 10% more microzircon than secondary clear inclusion rims and over 95% more microzircon than within secondary clear garnet at porphyroblast margins. Grain boundaries are the primary fluid pathways in a rock, garnet margins are more proximal to boundaries promoting more extensive modification and perhaps more microzircon dissolution. While inclusion rims still undergo microzircon dissolution this is likely limited by the fluid availability owing to their location within the interior of porphyroblasts. While microzircon are readily removed from secondary clear domains, dissolution of detrital zircon appears ineffective with detrital zircon abundance consistent with cloudy garnet (Table. 6.2). The consistency in the size distribution of microzircon between sillimanite-zone cloudy garnet and secondary clear is perhaps indicative that no new microzircon are formed at this stage and instead dissolution dominates. Instead microzircon within the secondary clear domains are preserved populations from either; (a) growth of garnet, and/or (b) coupled dissolution-reprecipitation during staurolite growth.

Secondary clear inclusion rims are primarily surrounding irregular quartz inclusions, typical of those that form as a result of coupled dissolution-reprecipitation during staurolite formation. The products of dissolution-reprecipitation are more reactive owing to higher defect densities within the mineral lattice (Dempster et al., 2017; Spruzeniece et al., 2017). Secondary clear garnet likely forms in cloudy domains owing to this increased reactivity.

6.2.3.7 Results: zircon in the matrix

The sillimanite-zone matrix is comprised of interbedded micaceous pelites and quartzofeldspathic layers. The pelitic matrix contain on average 31 microzircon per mm^2 and 5 detrital zircon per mm^2. The quartzofeldspathic matrix contains less zircon, average 21 microzircon per mm^2 and 4 detrital zircon per mm^2. Zircon comprises <3 vol.% of the matrix within these schists. More than 98% of microzircon within the matrix of the sillimanite-zone schists are hosted within a single grain with <2% occurring on grain boundaries (Figure. 6.34). Similarly, detrital zircon are predominantly hosted within grains but a much larger proportion occur on grain boundaries (Figure. 6.34).

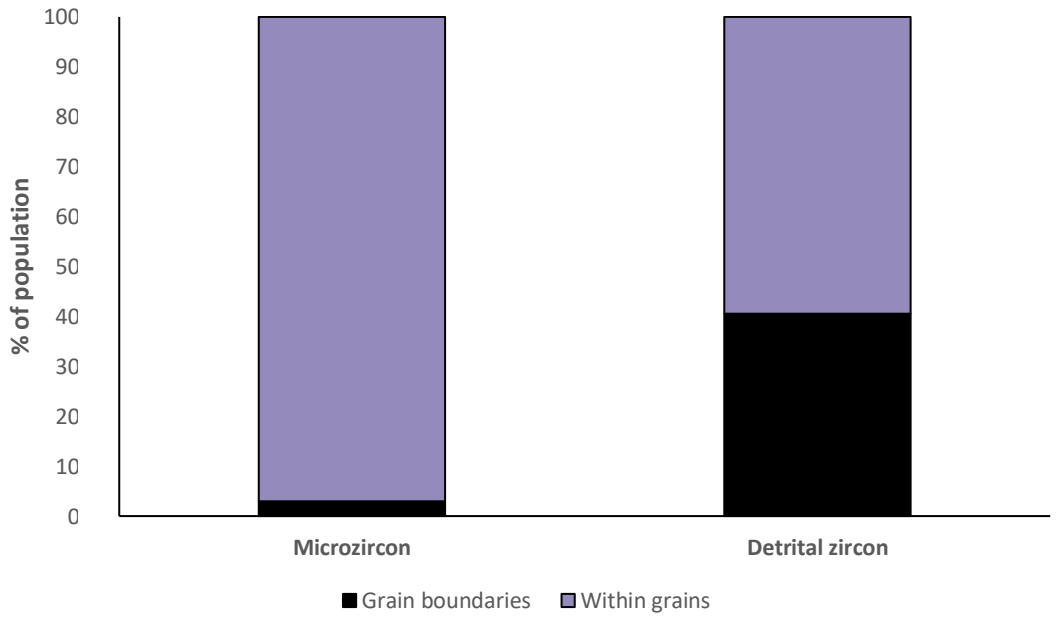

FIGURE 6.34: proportion of microzircon and detrital zircon hosted within grains and at grain boundaries within sillimanite-zone matrix UGR0-3

Microzircon are predominantly hosted within quartz in the quartzofeldspathic matrix and muscovite in the mica=rich pelite (Figure. 6.35). Detrital zircon display the same pattern, most abundant in quartz in quartzofeldspathic matrix nd muscovite in the pelitic matrix (Figure. 6.35). Similar to the staurolite-zone schists, phases which host a large proportion of detrital zircon appear to host more microzircon within the sillimanite schists (Figure. 6.35). Chlorite again contains no microzircon however it is present in low modal abundances in the staurolite-zone schists (Figure. 6.3).

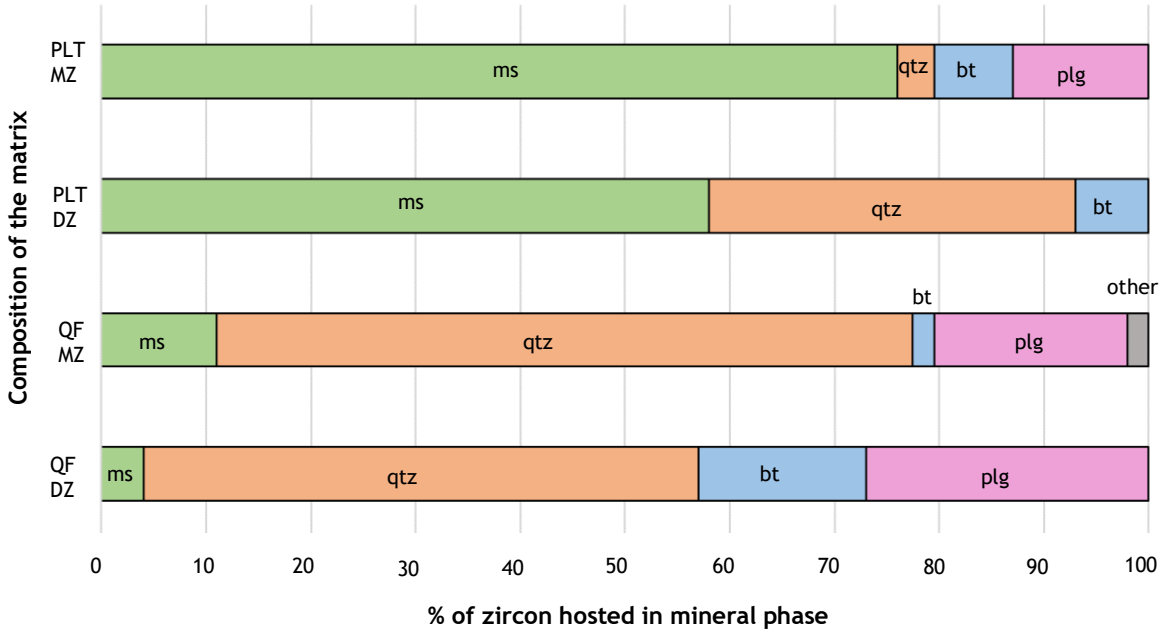

FIGURE 6.35: distribution of microzircon (MZ) and detrital zircon (DZ) across quartzofeldspathic (QF) and pelitic (PLT) matrix phases within sillimanite-zone schist UGR0

6.2.3.8 Interpretation of zircon in the matrix

Microzircon are the least abundant in the matrix of sillimanite-zone schists compared to the lower grade samples analysed in this study. However, the sillimanite schists contain significantly more outgrowths surrounding detrital grains. Higher temperatures promote nucleation of zircon around existing detrital zircon as Zr can be transported longer distances to existing detrital grains and nucleate around those instead of forming separate microzircon.

The decrease in microzircon and detrital zircon present on grain boundaries may be in part a facet of coarsening o the matrix with increasing grade but is likely also influenced by the increased dissolution of zircon at higher temperatures. Grain boundaries are fluid pathways and hydrothermal fluids produced during metamorphism are detrimental to zircon, particularly microzircon, populations. Those within grains are generally more sheltered from fluids during fluxes and less prone to dissolution. The mode of zircon appears to decrease in these schists when compared with staurolite-zone schists which are comprised of >5 vol.% zircon, decreasing to <3 vol.% zircon in sillimanite-zone schists. This is indicative the processes that are occurring in the porphyroblasts are likely also occurring in the

matrix. Hydrothermal fluids eliminate grains preferentially from grain boundaries via dissolution however there is no evidence off reprecipitation of zircon in the matrix or porphyroblast phases.

6.2.3.9 Conclusion

Sillimanite-zone schists have undergone more extensive dissolution-reprecipitation during staurolite formation and an additional partial reequilibration during sillimanite formation. Where the degree of modification increases within garnet, the abundance of microzircon decreases and more rarely detrital zircon populations also decrease. Where mineral inclusion abundance increases in the sillimanite-zone schists, the abundance of secondary clear garnet surrounding them increases, and thus the size of the microzircon population also decreases. The quartz inclusion-rich bands in garnet contain the lowest proportion of microzircon likely due to the presence of these reequilibrated, secondary clear rims.

6.3 Controls on zircon dissolution and growth

6.3.1 Mineralogy of host rock

The Appin and Leven schists are both comprised of interbedded quartz-rich and mica-rich layers. Pelites contain more microzircon than adjacent quartzofeldspathic layers, a well-established pattern (Dempster et al., 2004; Rasmussen, 2005; Dempster et al., 2008). Similarly, detrital zircon vary in size and abundance depending on the matrix lithology. Pelites contain a large number of finer detrital zircon while quartzofeldspathic beds contain fewer, coarse detrital zircon (Figure. 6.14).

Microzircon is absent in chlorite. During prograde metamorphism fluids are generated within the rocks while during retrograde metamorphism fluids enter the rock from an external source. During retrogression, fluids enter the rocks along conduits such as fractures. During prograde metamorphism these rocks retain fluid until the Zr is redistributed as microzircon and/or outgrowths, finally their tensile strength is exceeded and fluids escape, likely carrying little or no Zr. During retrogression, the fluids enter the rock, dissolve Zr and escape through the same conduits, carrying Zr before it can be reprecipitated as new zircon.

The importance of detrital zircon population size and distribution is evidenced through the analysis of garnet GR02-5. Within this garnet the compositional inclusion layering in garnet, i.e. the composition of the matrix the garnet overgrew, does not reflect the change in microzircon size and distribution. Quartz inclusion-rich garnet that overgrew originally quartzofeldspathic matrix typically contains fewer large detrital zircon and around 50% less microzircon than adjacent ilmenite-rich garnet that overgrew pelitic matrix layers. Originally quartzofeldspathic garnet in GR02-5 contains 71 microzircon per mm^2, consistent with originally pelitic garnet that contains 72 microzircon per mm^2 (Figure. 6.36). The anomalously high microzircon counts within the quartz-rich garnet can be attributed to a disproportionally large population of finer, potentially more reactive detrital zircon. Typically, detrital zircon are larger in quartz-rich bands 105 +/- 66μm^2 than adjacent ilmenite-rich bands 11 +/- 8μm^2. The mean size of detrital zircon in the originally quartzofeldspathic garnet in GR02-5 is 16 +/- 19μm^2 compared with 13 +/- 13μm^2 within the adjacent originally pelitic garnet in GR02-5. Finer detrital zircon may represent fragments of metamict larger grains, making them more prone to dissolution as their lattice would be weakened (Ellsworth et al., 1994; Dempster & Chung, 2013). The finer detrital zircon population within the pelite matrix and thus the garnet the garnet that overgrows it in GR02-5 may increase the dissolution potential, thus releasing more Zr and enabling more zircon growth within these layers.

6.3.2 Host phase

Porphyroblast phases contain larger numbers of microzircon per mm^2 than the matrix (Figure. 6.37). The disparity between the matrix and porphyroblast abundance may be, at least in part, a facet of preservation. Zircon in the matrix are more prone to dissolution as grain boundaries act as fluid pathways promoting dissolution. Evidenced by the absence of microzircon on grain boundaries within the staurolite-zone schists where 86% of microzircon in the matrix are located within grains and just 14% on grain boundaries (Figure. 6.25). Microzircon on grain

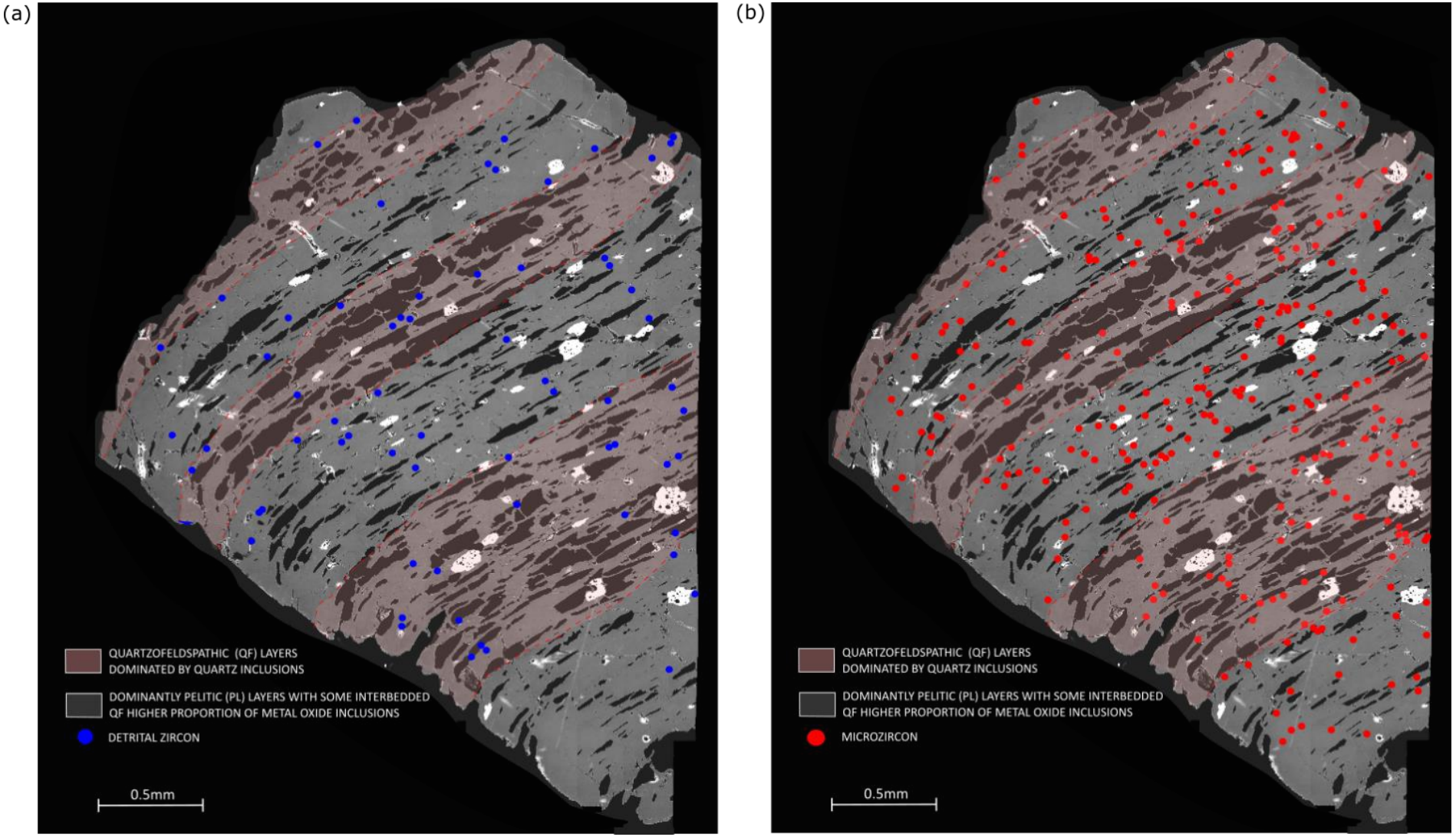

FIGURE 6.36: (a) detrital zircon and (b) microzircon abundance across GR02-5 compositionally banded clear garnet

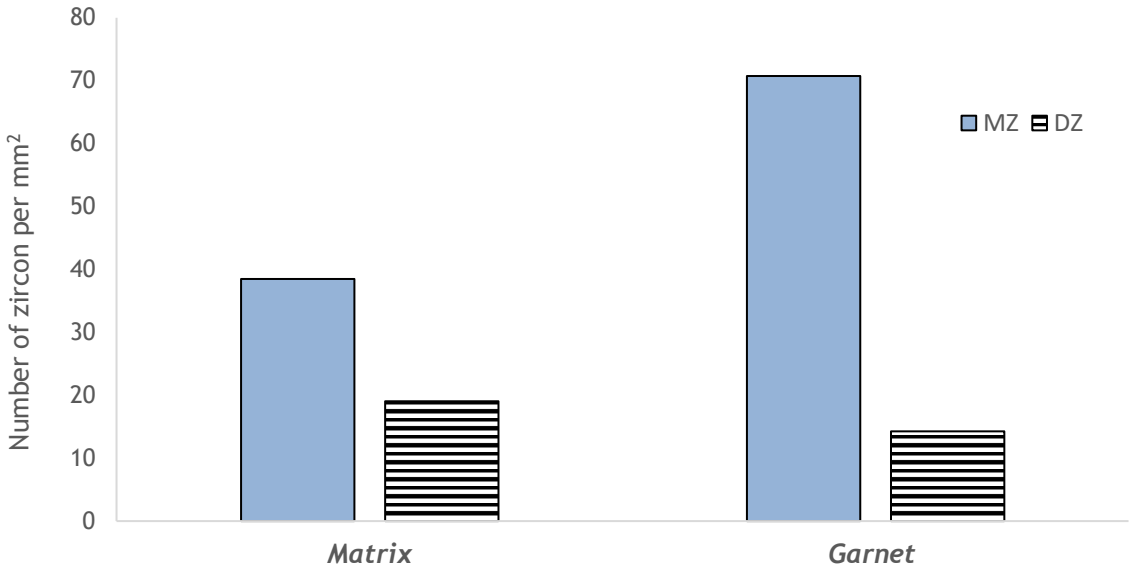

FIGURE 6.37: plot of detrital zircon and microzircon abundances per mm^2 in GR01 within the matrix vs within unmodified garnet

boundaries are also coarser than those within the matrix. This increase in the population size at grain boundaries is consistent with dissolution occurring and potentially eliminating finer grains with a higher surface energy preferentially.

Porphyroblast phases are coarser and thus have a smaller surface area in contact with other phases sheltering microzircon from pervasive fluids enabling the survival of a larger number of the population. Microzircon in porphyroblasts are finer than within the matrix (Table. 6.3), visible within garnet and biotite across the Leven and Appin schists. The decrease in microzircon size in garnet porphyroblasts has been interpreted as a facet of the temporal change in zircon size throughout the reaction history (Dempster et al., 2008). However, microzircon show no change in their size distribution across a concentrically zoned garnet i.e. from core to rim. If zircon became finer throughout the reaction history then earlier formed garnet in the core should contain a population of coarser microzircon, gradually fining to the later-formed rims. The later formed microzircon in the matrix may instead have had more opportunity to grow producing a population of coarser grains. Int eh same way increased fluid availability can inhibit preservation, it can promote growth. In porphyroblasts microzircon become trapped quickly after growth (Figure. 6.4). Unless zircon is located at the grain boundary or adjacent to a fluid-bearing fracture there is no subsequent opportunity for growth.

TABLE 6.3: Changing microzircon size between the matrix and the main porphyroblast phases across biotite-zone and staurolite-zone schists, errors are to σ1

		Number of microzircon (n)	*Microzircon average size (μm²)*
Biotite-zone	Matrix	525	1.12 +/- 0.3
	Biotite	63	0.85 +/- 0.32
Staurolite-zone	Matrix	214	0.43 +/- 0.12
	Garnet	1142	0.38 +/- 0.11
	Staurolite	14	0.23 +/- 0.06

Even within porphyroblast phases there is some variation in the amount of zircon present with mineralogy. Garnet contains the most microzircon followed by staurolite and finally biotite (Figure. 6.38). The abundance of microzircon is likely linked to the stage of growth and durability of the host mineral. Garnet forms relatively early in the metamorphic history of the Leven schists, it is also difficult to recrystallize while staurolite forms much later. Similarly, biotite in the Appin

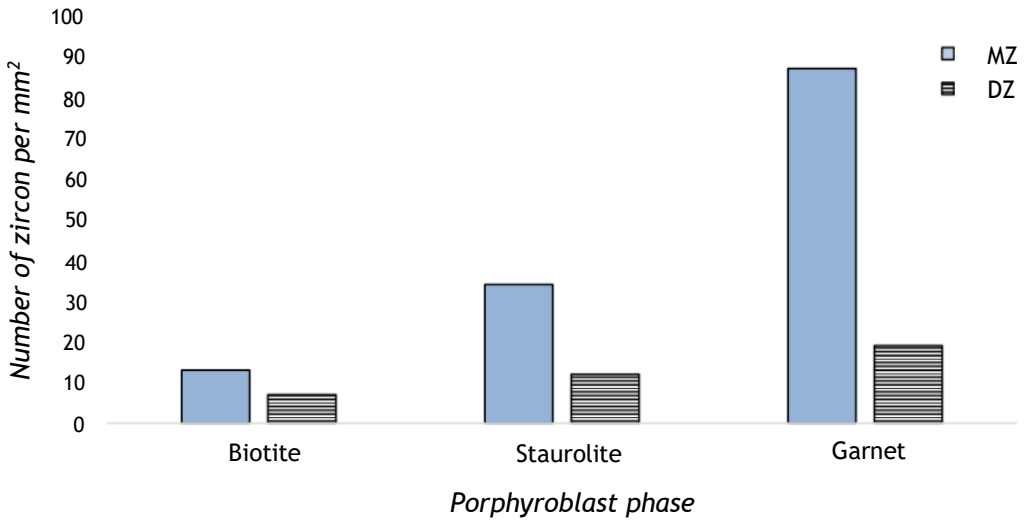

FIGURE 6.38: change in microzircon and detrital zircon abundance within different porphyroblast phases, all measured within staurolite-zone schist GR01

schists forms late in the metamorphic history and is significantly easier to recrystallize than garnet or staurolite, producing relatively few microzircon. Microzircon have been identified in all phases within the schists except sillimanite and chlorite. The absence of microzircon in sillimanite could be related to higher temperatures inhibiting zircon formation paired with the structure of fibrolite limiting the preservation potential. Microzircon is absent within chlorite across all grade, this is particularly obvious in biotite-zone schists where chlorite retrogression is more extensive. The biotite schists are comprised of ca. 14% chlorite, mostly hosted within biotite, while the staurolite-zone schists contain just ca. 1.2% chlorite and the sillimanite schists contain trace amounts <1%. The absence of microzircon within chlorite is indicative that during retrogression fluids have the ability to dissolve microzircon during the replacement process. Within biotite-zone schists chlorite contains 20% of the detrital zircon but no microzircon (Figure. 6.3). The formation of microcracks surrounding detrital zircon may enable fluid access and promote chloritization of host biotite, therefore initially the amount of detrital zircon hosted in biotite was likely higher but chloritization is focussed in these zones. Retrograde reactions may be less effective at forming zircon due to changes to Zr solubility in the fluid with decreasing temperature, or sluggish kinetics (Turner, 1968). Fluid availability is typically the limiting factor during retrogression while zircon recrystallization has been proven to be largely fluid driven (Smit et al., 2018), paired with the lower temperatures decreasing diffusion and thus transport rates (Putnis, 2009).

6.3.3 Grade

Temperature is typically ascribed as the primary control on outgrowth abundance (Rubatto, 2002), where increasing temperature increases the amount of metamorphic zircon growth as outgrowths. However, detrital zircon within the biotite-zone schists have extensive outgrowths while within the Leven Schists most detrital grains show no evidence of outgrowths (Figure. 6.39). With increasing grade, the amount of zircon formed as outgrowths appears to decrease. It is possible that pressure is an influencing factor, increasing pressure has been attributed to decreasing zircon outgrowth abundance (Kohn & Kelly, 2018). The biotite-zone rocks are polymetamorphosed undergoing a regional event and mosr recently being contact metamorphosed while the staurolite- and sillimanite-zone rocks have most recently undergone regional metamorphism. However,

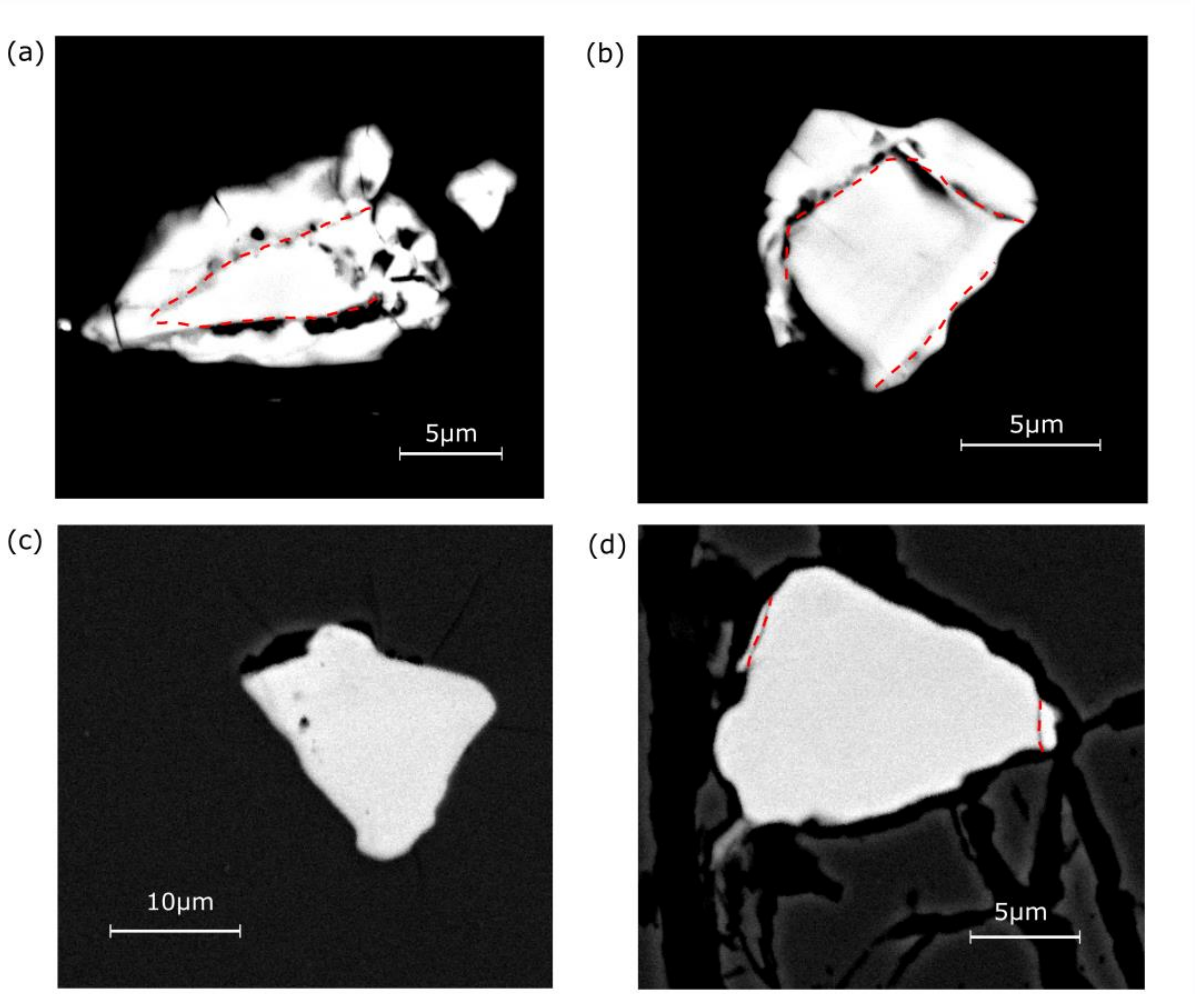

FIGURE 6.39: changing outgrowth morphology across the biotite- and staurolite-zone schists, (a-b) biotite-zone detrital zircon with extensive outgrowths (c) sillimanite-zone detrital zircon with no outgrowths, and (d) staurolite-zone detrital zircon within heavily fractured garnet with evidence of minor outgrowths

outgrowths are reported in other regionally metamorphosed pelites (Rubatto et al., 2001; Rasmussen, 2005; Hay et al., 201; Chen et al., 2019), indicative that more subtle pressure changes may not have an impact on outgrowth abundance.

Microzircon also decrease in size with increasing grade generally, at biotite-zone microzircon are predominantly 1-2 μm^2 while within the higher grade Leven schists they are finer, averaging 0.41 μm^2 within the staurolite-zone schists and 0.38 μm^2 within the sillimanite-zone (Table 6.4). There is overlap between the errors on the average size values and a much larger sample size would be required to reduce these however the size distribution reveals a similar pattern (Figure 6.40). There is little change between the size distribution of microzircon between the

TABLE 6.4: changes to abundance and size distribution of microzircon (MZ) and detrital zircon (DZ) within porphyroblast phases with grade, within biotite-zone rocks the analysed porphyroblast phase was biotite and within staurolite and sillimanite-zone it was garnet

	Abundance per mm²		*Average size (μm²)*	
	MZ	*DZ*	*MZ*	*DZ*
Biotite-zone	13	7	1.05 +/- 0.63	54 +/- 123
Staurolite-zone	124	22	0.4 +/-0.22	33 +/- 56
Sillimanite-zone	49	16	0.39 +/- 0.2	27 +/- 21

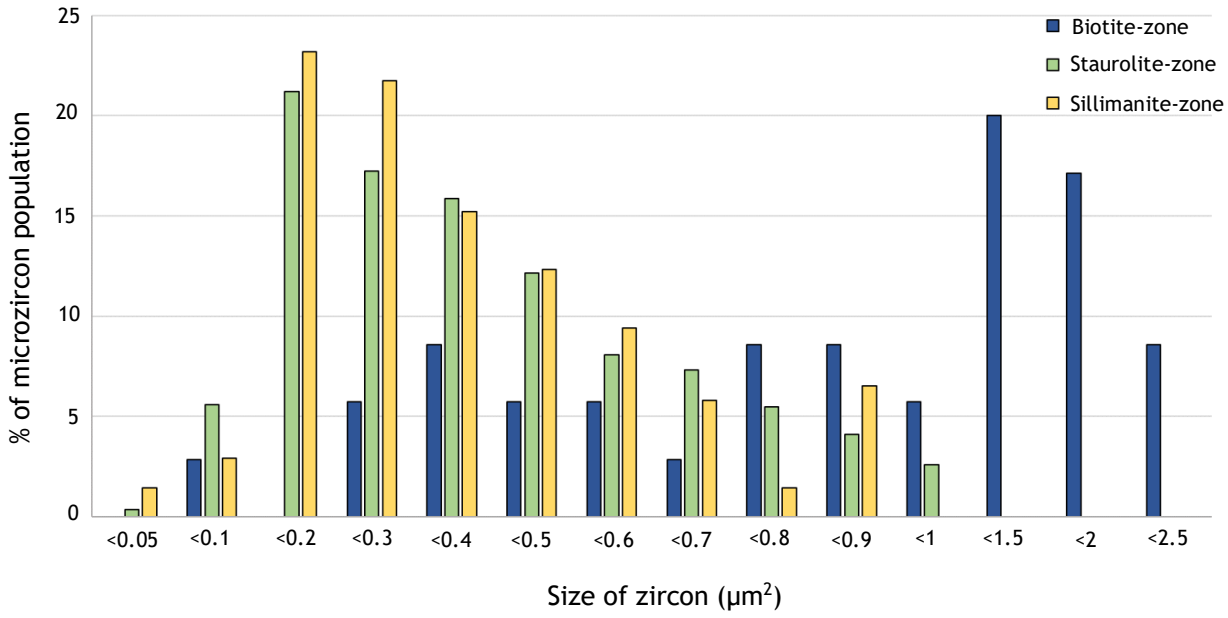

FIGURE 6.40: size distribution of microzircon within porphyroblasts with increasing grade from biotite-zone to sillimanite-zone, where biotite-zone data was collected from biotite porphyroblasts and staurolite- and sillimanite-zone from garnet porphyroblasts

sillimanite- and staurolite-zone schists but the biotite-zone schists show a higher proportion of coarser microzircon (Figure. 6.40). The decrease in microzircon size with grade is unexpected, where temperature increases so too does intercrystalline transport (Putnis, 2009) resulting in an increase in the average grain size. Increased diffusion rates assist in the growth of many major phases, such as quartz, muscovite, plagioclase, etc. However, with accessory minerals such as zircon, the transport distance for materials between neighbouring grains is considerably larger. It is possible that the growth of major phases inhibits the growth of these accessory phases by removing grain boundaries that act as fluid pathways (Jones et al., 1972), therefore inhibiting the transport of Zr towards the surface of existing grains and instead resulting in the formation of smaller zircon. The degree of deformation also influences the amount of zircon growth and dissolution through reaction kinetics. Low strain areas of a rock are likely to be less affected by fluids (Beckman & Möller, 2018) thus inhibiting zircon dissolution and reprecipitation.

6.3.4 Dissolution-reprecipitation

Once garnet undergoes coupled dissolution-reprecipitation, the characteristics of the zircon population changes (Figure. 6.41). There is a reduction in the amount and size of microzircon and also a coarsening of the original detrital grains. Dissolution is more effective on finer grains as they have a higher surface energy and therefore are easier to equilibrate. As a result, microzircon and finer detrital zircon are preferentially removed during coupled dissolution-reprecipitation producing the contrast in the size distribution. In general, garnet reveals that increased modification of the host phase results in a decrease in the number of microzircon. Clear garnet contains the most microzircon, cloudy garnet contains fewer and the secondary clear garnet contains considerably less microzircon (Figure. 6.42).

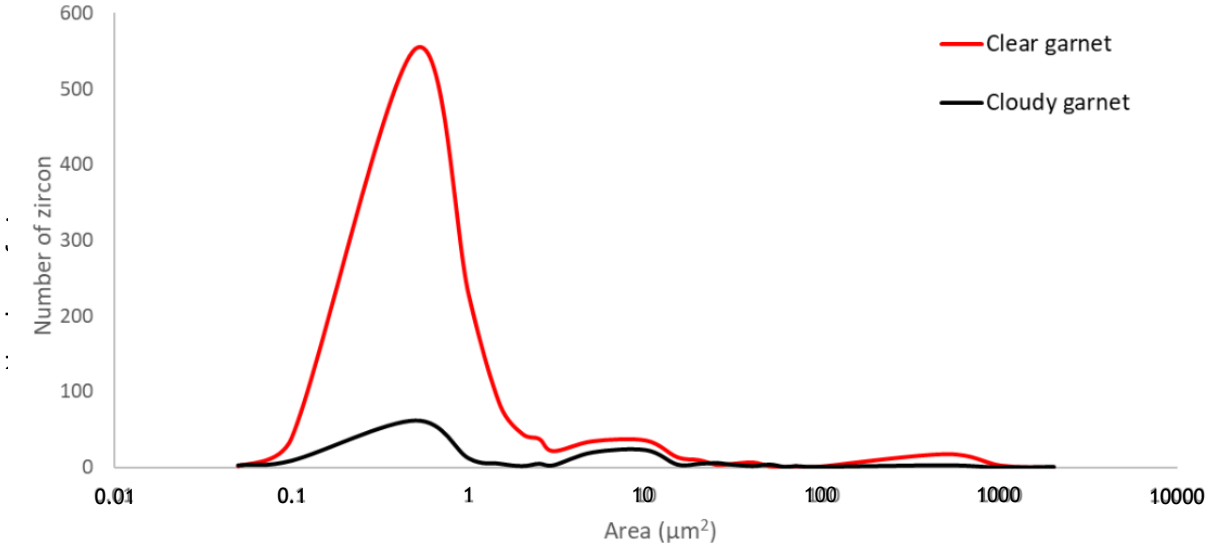

FIGURE 6.41: abundance and size distribution of zircon populations within clear and cloudy garnet across equal areas, zircon <1µm² is classified as microzircon while >3µm² is detrital zircon

6.3.5 Conclusion

There are a number of factors that influence zircon populations but coupled dissolution-reprecipitation and fluid-mediated garnet modification appears to be the most detrimental to microzircon populations. The mode of zircon decreases within these schists following coupled dissolution-reprecipitation. Following dissolution-reprecipitation of garnet, mineral and fluid inclusion-rich cloudy garnet forms, within which both microzircon and detrital zircon are less abundant than unmodified garnet. Microzircon become smaller in modified garnet, while detrital zircon become coarser. Additional modification results in reequilibration of the inclusion-rich cloudy texture in garnet and eradicates more microzircon but has little effect on detrital zircon.

Metamorphic zircon forms outgrowths on detrital grains and microzircon. The Zr removed during dissolution of zircon during dissolution-reprecipitation is higher than the amount of Zr that reforms as zircon following dissolution-reprecipitation, where does the Zr go? Zr may escape the garnet in fluids, however in the adjacent matrix there is no evidence of new zircon growth. Therefore, the Zr likely enters another phase. Within clear garnet, microzircon on average makes up 38µm² per mm² of garnet, whereas in cloudy garnet this decreases to 8µm² per mm² of

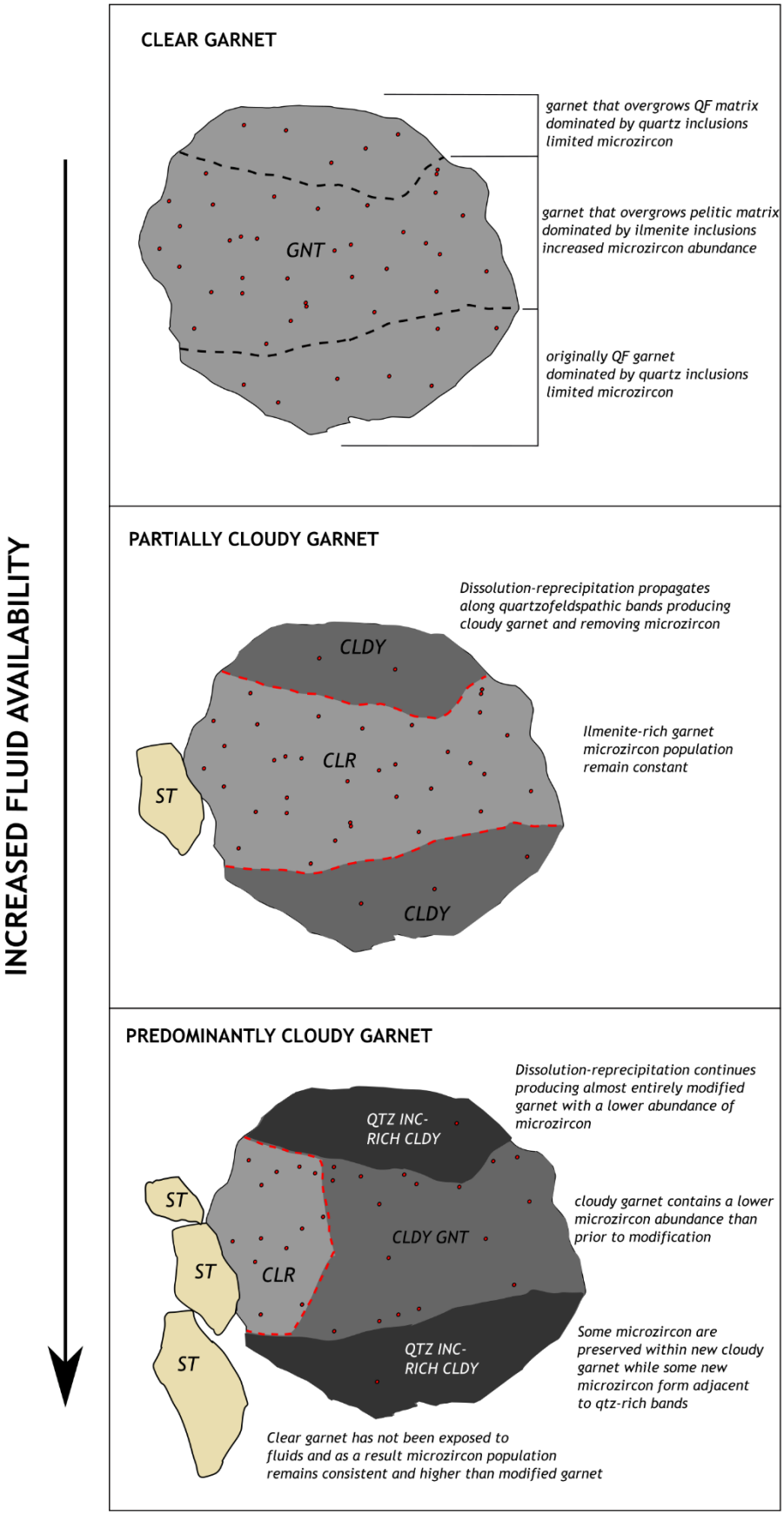

FIGURE 6.42: The development of cloudy garnet through dissolution-reprecipitation and its influence on microzircon populations. As garnet is consumed to form staurolite the remaining modified cloudy garnet contains fewer microzircon. The more modified a domain is, the fewer microzircon are present

garnet. There is a 79% loss in the area of zircon following dissolution-reprecipitation. Within the average 3mm^2 garnet, alteration of a whole porphyroblast would result in the disappearance of 93.51μm^2 of zircon. At higher temperatures, the trivalent iron site within garnet undergoes expansion which may promote the accommodation of larger Zr^{4+} ions (0.72 A) in the smaller Fe^{3+} site (0.65 A) (Degeling, 2002). If this zircon was to be incorporated into garnet it would represent 185 ppm Zr while within ilmenite it could replace Ti and would represent >1 wt%. This is a detectable quantity and analysis of the trace element chemistry of the major phases may reveal where the Zr is incorporated. There is a significant and consistent change in the microzircon and detrital zircon population size and morphology with increasing grade, and thus increasing degree of modification.

Chapter 7 Conclusion

7.1 A model for the evolution of zircon

7.1.1 Biotite-zone Appin Phyllites

Detrital zircon are inherited populations and vary depending on the original sedimentary lithology of the host rock. The Appin Phyllites are interbedded pelites and quartz-rich pelites, the pelitic layers contain a larger population of fine detrital zircon while the quartz-rich pelite contains fewer large detrital zircon. The mode of detrital zircon decreases early in the metamorphic history and new metamorphic zircon forms as microzircon and outgrowths on detrital grains. There is more metamorphic zircon growth within the pelite than the quartz-rich pelite. This may be a facet of (a) the population of fine, and thus more potentially metamict, detrital zircon are more reactive than coarser detrital zircon in the quartz-rich pelite (Hay & Dempster, 2009a, or (b) the higher halogen contents of the pelite layer producing a potentially more corrosive fluid and enhancing dissolution (Rasmussen, 2005).

The Appin Phyllites have been polymetamorphosed, recording an early regional event and a later contact event. During the initial regional event, coarser microzircon form within the aligned matrix while during the contact event, a population of finer microzircon are formed within the biotite porphyroblasts. Biotite porphyroblasts also contain a larger number of microzircon than the adjacent matrix. There may be a temporal change in the morphology of microzircon, where they decrease in size and increase in abundance through time (Dempster et al., 2008). While microzircon form during prograde metamorphism, retrogression appears to be unique with no new zircon growth occurring. Chlorite contains no microzircon despite containing a large proportion of detrital zircon. During chloritization microzircon are dissolved from the biotite but there is no evidence of new zircon crystallization occurs within the chlorite or adjacent minerals. Fluids may escape more rapidly during retrogression resulting in the removal of dissolved Zr before new metamorphic zircon forms.

7.1.2 Staurolite-zone Leven Schists

The Leven Schists display the same original disparity in detrital and microzircon populations across the changing mineralogy, more microzircon growth occurs in pelitic layers of the matrix than quartzofeldspathic layers. New metamorphic zircon growth within the staurolite-zone schists occurs predominantly as microzircon with very limited outgrowth formation around existing detrital grains compared to the biotite-zone schists.

The higher temperatures associated with the staurolite-zone schists enhance detrital zircon dissolution, yielding more Zr and resulting in the formation of more metamorphic zircon in the higher-grade rocks. Similar to the biotite-zone schists, the porphyroblast phase contains more microzircon than the matrix. Detrital ilmenite may act as an additional source of Zr within these schists, releasing Zr as it recrystallizes at the almandine isograd. The result is more microzircon growth within garnet where ilmenite has recrystallized. Microzircon in the garnet are finer, likely because they become encapsulated by the growing porphyroblast quickly with little subsequent opportunity for growth. In the less stable matrix microzircon may have more opportunity to grow thus forming coarser microzircon.

Garnet undergoes coupled dissolution-reprecipitation when it meets a fluid with which it is not in equilibrium, the result is dissolution of the parent garnet and reprecipitation of a low Ca cloudy garnet. Cloudy garnet contains much less microzircon than adjacent clear. There is no change in zircon abundance between entirely clear garnet porphyroblasts and clear garnet within partially cloudy porphyroblasts, suggesting Zr does not form new microzircon elsewhere in the porphyroblast. There is therefore a decrease in the mode of zircon, zircon is likely accommodated within a mineral phase. At higher temperatures, thermal relaxation of the lattice off mineral occurs, this allows potentially larger ions to substitute in smaller sites in the lattice. This may be occurring in garnet, as temperatures increase and Zr dissolution occurs, Zr may be incorporated as a non-essential constituent into the Fe site in the garnet lattice instead of reforming new zircon.

7.1.3 Sillimanite-zone Leven Schists

The sillimanite-zone schists contain cloudy garnet, formed during staurolite formation as described in 7.1.2, and an additional stage of modification that occurs during sillimanite formation, forming secondary clear garnet. During sillimanite formation reequilibration occurs to produce a homogeneous product phase locally surrounding mineral inclusions at garnet porphyroblast margins.

Sillimanite-zone schists contain the least microzircon and detrital zircon across the matrix and porphyroblast phases consistent with increased zircon dissolution and Zr transportation at higher temperatures. There is an increase in the formation of outgrowths in place of microzircon as the increased temperature enhances Zr transportation and nucleation surrounding detrital grains.

The sillimanite-zone schists may not have experienced higher P-T conditions than the staurolite-zone. The sillimanite-bearing schists appear to be comprised of more finely interbedded metasediments than the staurolite-zone schists, an increase in bedding planes may result in increased fluid infiltration and thus fluid availability for sillimanite formation. In the staurolite-zone, sillimanite absent schists, the thicker bedding planes produces fewer conduits and thus lower potential permeability inhibiting sillimanite formation and thus producing schists which appear lower grade.

As alteration increase, the amount of microzircon decreases. Dissolution becomes more effective at the higher temperatures associated with the sillimanite forming reaction and thus dissolution and reprecipitation are less closely coupled, producing homogeneous, inclusion-poor secondary clear garnet.

7.2 Significance of the results

Fluid-mediated dissolution-reprecipitation is the most common mineral reaction mechanism within the solid Earth (Konrad-Schmolke et al., 2018). Despite their importance, little is known about dissolution-reprecipitation processes. Zircon has the ability to trace fluid flow and associated metamorphic process, including dissolution-reprecipitation, through changes in the morphology and distribution of zircon populations.

U/Th-Pb dating in zircon is a widely utilised absolute dating tool, however, linking the ages produced to a stage in a complex tectonothermal history proves difficult. Within polymetamorphosed terranes the history of dissolution and crystallization of zircon is complex, as evidenced in this study. Zircon growth is seemingly not confined to individual stages in the P-T path and is heavily influenced by modification of the host phase, as in garnet, and the ability of other mineral phases to incorporate Zr. This is contrary to the simple model of zircon behaviour produced from thermodynamic modelling, where dissolution dominates during prograde metamorphism and zircon growth occurs during retrogression (Fraser et al., 1997; Kohn et al., 20115; Beckman & Möller, 2018). Zircon growth described in this study instead appears periodic while dissolution is likely more continuous, dependant primarily on the availability of fluids.

7.3 Future work

Further analysis should focus on understanding the timing of zircon growth by looking at the composition. The Th content of crystallising zircon has the ability to track changes to the bulk rock Th/U (Yakymchuk et al., 2018). Monazite and allanite are the dominant Th hosts within metamorphic rocks (Bea, 1996; Bea & Montero, 1999). Following the formation of monazite during coupled dissolution-reprecipitation the bulk rock Th concentration would be lower producing lower Th/U in microzircon that forms following coupled dissolution-reprecipitation than original populations that formed during or prior to garnet growth. Th analysis of microzircon would therefore assist in understanding how much of the zircon population in modified garnet is preserved and how much forms as a result of coupled dissolution—reprecipitation.

An understanding of how Zr is distributed in these rocks prior to and following coupled dissolution-reprecipitation which would have assisted in tracking where the Zr goes following dissolution-reprecipitation. Theoretically Zr can be traced using values from other studies which have closely analysed Zr within major and accessory mineral phases in metamorphic rocks (Fraser et al., 1997; Bingen et al., 2001; Degeling et al., 2001; Degeling, 2003; Bea et al., 2006; Kelsey & Powell, 2011; Kohn & Kelly, 2018). However, none of these studies recognise microzircon which have the ability to skew values significantly. Most Zr content studies utilise LA-ICP-MS or ion microprobes with spot sizes bigger than a microzircon. Studies

typically quote a high range of values produced for the Zr contents of host minerals, these values may be so varied owing to the accidental analysis of microzircon within the sample spots. A database of Zr concentrations within major and accessory phases in metamorphic rocks where microzircon have been mapped, and thus can be removed from results, is required to trace where Zr that isn't incorporated into Zr goes.

Errors produced on average sizes of zircon within different domains commonly overlap from this study based on the small sample size. Difficulty imaging and identifying microzircon due to their small size means that with the current imaging capabilities manual analysis is required. This is time consuming and subject to human error and/or bias. Automatic feature mapping techniques using EDX on the SEM tend to miss the finer populations of microzircon, even at high resolution. A much larger sample size is required to better quantify changes in microzircon abundance and morphology between different mineral phases and across different grades. There are also potentially smaller microzircon that cant be captured on the SEM using current imaging capabilities. These smaller zircon could potentially record even finer subtleties in the metamorphic history.

Ague, J.J. (1997) Crustal mass transfer and index mineral growth in Barrow's garnet zone, northeast Scotland. *Geology*, **25**, 73-76.

Ague, J.J. (2011) Extreme channelization of fluid and the problem of element mobility during Barrovian metamorphism. *American Mineralogist,* **96**, 333-352.

Ague, J.J. & Eckert, J.O. (2012) Precipitation of rutile and ilmenite needles in garnet: Implications for extreme metamorphic conditions in the Acadian Orogen, U.S.A. *American Mineralogist*, **97**, 840-855.

Ague, J.J. & Carlson, W.D. (2013) Metamorphism as garnet sees it: The kinetics of nucleation, growth, equilibration, and diffusional relaxation. *Elements,* **9**, 439-445.

Ague, J.J. & Axler, J.A. (2016) Interface coupled dissolution-reprecipitation in garnet from subducted granulites and ultrahigh-pressure rocks revealed by phosphorous, sodium, and titanium zonation. *American Mineralogist,* **101**(7), 1696-1699.

Akoagi, M., Hashimoto, S. & Kojitani, H. (2018) Thermodynamic properties of $ZrSiO_4$ zircon and reidite and of cotunnite-type ZrO_2 with application to high-pressure high-temperature phase relations in $ZrSiO_4$. *Physics of the Earth and Planetary Interiors,* **281**, 1-7.

Altree-Williams, A., Pring, A., Ngothai, Y & Brugger, J. (2015) Textural and compositional complexities resulting from dissolution-reprecipitation reactions in geomaterials. *Earth-Science Reviews,* **150**, 628-651.

Andersen, T. (2004) Detrital zircons as tracers of sedimentary provenance: limiting conditions from statistics and numerical simulation. *Chemical Geology,* **216**(3-4), 249-270.

Anderson, J. (1956) II. – he Moinian and Dalradian rocks between Glen Roy and the Monadhlaith Mountains, Inverness-shire. *Transactions of the Royal Society of Edinburgh,* **63**(1), 15-36.

Anderson, A.J., Wirth, R. & Thomas, R. (2008) The alteration of metamict zircon and its role in the remobilization of high-field-strength elements in the Georgeville Granite, Nova Scotia. *Canadian Mineralogist*, **46**, 1-18.

Angiboust, S. & Harlov, D.E. (2017) Ilmenite breakdown and rutile-titanite stability in metagranitoids: Natural observations and experimental results. *American Mineralogist,* **102**, 1969-1708.

Ashley, K.T., Law, R.D. & Thigpen, J.R. (2016) Garnet morphology distribution in the northern part of the Moine supergroup, Scottish Caledonides. *Journal of Metamorphic Geology,* **35**, 77-94.

Atherton, M.P. (1968) The variation in garnet, biotite and chlorite composition in medium grade pelitic rocks from the Dalradian, Scotland, with particular reference to the zonation in garnet. *Contributions to Mineralogy and Petrology*, **18**, 347-371.

Atherton, M.P. & Edmunds, W.M. (1966) An electron microprobe study of some zoned garnets from metamorphic rocks. *Earth and Planetary Science Letters*, **1**, 185-193.

Ayers, J.C., Zhang, L., Luo, Y., Peters, T.J. (2012) Zircon solubility in alkaline aqueous fluids at upper crustal conditions. *Geochimica et Cosmochimica Acta*, **96**, 18-28.

Bakker, R.J. (2009) Reequilibraion of fluid inclusions: Bulk-diffusion. *Lithos*, **112**, 277-288.

Bakker, R.J. (2017) Re-equilibration processes in fluid inclusion assemblages. *Minerals*, **7**:117, 19 pp.

Balan, E., Maui, F., Pickard, C.J., Farnan, I. & Calas, G. (2003) The aperiodic state of zircon: an ab initio molecular dynamics study. *American Mineralogist*, **88**, 1769-1777.

Banno, S. & Chii, S. (1978) A model to explain the Mn enrichment in the rim of zoned garnet. *Geochemical Journal*, **12**, 153-257.

Barker, A.J. (1998) Introduction to metamorphic textures and microstructures. S. Thornes, Surrey.

Barrow, G. (1893) On an intrusion of muscovite-biotite gneiss in the southeastern Highlands of Scotland and its accompanying metamorphism. *Quarterly Journal of the Geological Society of London*, **49**, 330-358.

Barrow, G. (1912) On the geology of Lower Dee-side and the southern Highland Border: *Geological Association of London, Proceedings*, **23**, 274-290.

Baruah, J., Kotoky, P. & Sarma, J.N. (1995) Zircons in Jhanji River Sediments, Assam. *Bulletin of Pure and Applied Science*, **14F**, 35-40.

Baxter, E.F., Caddick, M.J., Dragovic, B. (2017) Garnet: A rock-forming mineral petrochronometer. *Reviews in Mineralogy & Geochemistry*, **83**, 469-533.

Bea, F. (1996) Controls on the trace element composition of crustal melts. *Transactions of the Royal Society of Edinburgh, Earth Sciences*, **87**, 33-41.

Bea, F. & Montero, P. (1999) Behaviour of accessory phases and redistribution of Zr, REE, Y, Th, and U during metamorphism and partial melting of metapelites in the lower crust: An example from the Kinzigite Formation of Ivrea-Verbano, NW Italy. *Geochimica et Cosmochimica Acta*, **63**(7/8), 1133-1153.

Bea, F., Montero, P. & Ortega, M. (2006) A LA-ICP-MS evaluation of Zr reservoirs in common crustal rocks: Implications for Zr and Hf geochemistry, and zircon-forming processes. *Canadian Mineralogist*, **44**, 693-714.

Beckman, V. & Möller, C. (2018) Prograde metamorphic zircon formation in gabbroic rocks: The tale of microtextures. *Journal of Metamorphic Geology,* **36**, 1221-1236.

Bell, T.H. & Johnson, S.E. (1989) Porphyroblast inclusion trails: the key to orogenesis. *Journal of Metamorphic Geology,* **7**, 279-310.

Bindeman., I.N., Schmitt, A.K., Lundstrom, C.C. & Hervig, R.L. (2018) Stability of zircon and its isotopic ratios in high-temperature fluids: Long-Term (4 months) isotope exchange experiment 850^{o}C and 50 MPa. *Frontiers in Earth Science,* **59**(6), 1-32.

Bingen, B., Austrheim, H. & Whitehouse, M. (2001) Ilmenite as a source for zirconium during high-grade metamorphism? Textural evidence from the Caledonides of Western Norway and implications for zircon geochronology. *Journal of Petrology*, **42**(2), 355-375.

Bodnar, R.J. (2003) Reequilibration of fluid inclusions. *In:* Samson, I., Anderson, A. & Marshall, D. (eds) Fluid inclusions: Analysis and interpretation. Mineralogical Association of Canada, Short Course 32, 213-230.

Boehnke, P., Watson, E.B., Trail, D., Harrison, T.M. & Schmitt, A.K. (2013) Zircon saturation re-visited. *Chemical Geology,* **351**, 324-334.

Bond, G. (1948) Outgrowths on zircon from Southern Rhodesia: Geological Magazine, v. 85, p. 35-40.

Botis, S.M., Pan, Y. & Ewing, R.C. (2013) Hydrogen incorporation in crystalline zircon: Insight from ab initio calculations. *American Mineralogist*, **98**, 745-751.

Breeding, C.M., Ague, J.J., Grove, M. & Rupke, A.L. (2004) Isotopic and chemical alteration of zircon by metamorphic fluids: U-Pb age depth-profiling of zircon crystals from Barrow's garnet zone, northeast Scotland. *American Mineralogist*, **89**, 1067-1077.

Brown, S.J.A. & Fletcher, I.R. (1999) SHRIMP U-Pb dating of the preeruption growth history of zircons from the 340ka Whakamaru Ignimbrite, New Zealand: Evidence for >250 k.y. magma residence times. *Geology,* **27**(11), 1035-1038.

Brown, W.L. (1962) Peristerite unmixing in the plagioclases and metamorphic facies series. *Norsk Geologisk Tidsskrift,* **42**(2), 354-382.

Bucholz, C.E., Eddy, M.P., Jagoutz, O., Bowring, S.A., Schmidt, M.W. & Sambuu, O. (2017) Constraining the time scales of magmatic differentiation with U-Pb zircon geochronology. *Geology,* **45**, 11-14.

Bukovská, Z., Wirth, R. & Morales, L.F. (2015) Pressure solution rocks: focussed ion beam/transmission electron microscopy study on orthogneiss from South Armorican Shear Zone, France. *Contributions to Mineralogy and Petrology,* **170**: 31, 13 pp.

Butterfield, J.A. (1936) Outgrowths on Zircon. *Geological Magazine*, **73**, 511-516.

Caddick, M.J., Konopásek, J. & Thompson, A.B. (2010) Preservation of garnet growth zoning and the duration of prograde metamorphism. *Journal of Petrology*, **3**(11), 2327-2347.

Carlson, W.D. (1991) Competitive diffusion-controlled growth of porphyroblasts. *Mineralogical Magazine,* **55**, 317-330.

Carlson, W.D. (2002) Scales of disequilibrium and rates of equilibration during metamorphism. *American Mineralogist*, **87**, 185-204.

Carlson, W.D. (2006) Rates of Fe, Mg, Mn and Ca diffusion in garnet. *American Mineralogist,* **91**, 1-11.

Carlson, W.D. (2011) Porphyroblast crystallization: Linking mechanisms, kinetics, and microstructures, *International Geology Review,* **53**, 406-455.

Carlson, W.D., Denison, C. & Ketcham, R.A. (1995) Controls on the nucleation and growth of porphyroblasts: kinetics from natural textures and numerical models. *Geological Journal,* **30**, 207-225.

Carmichael, D.M. (1969) On the mechanism of prograde metamorphic reactions in quartz-bearing pelitic rocks. *Contributions to Mineralogy and Petrology,* **20**, 244-267.

Carosi, R., Lombardo, B., Molli, G., Musumeci, G. & Pertusati, P.C. (1998) The south Tibetan detachment system in the Rongbuk valley, Everest region. Deformation features and geological implications. *Journal of Asian Earth Sciences,* **16**(2-3), 299-311.

Casillas, R., Nagy, G., Pantó, G., Brändle, J. & Fórizs, I. (1995) Occurrence of Th, U, Y, Zr, and REE-bearing accessory minerals in late-Variscan granitic rocks from the Sierra de Guadarrama (Spain). *European Journal of Mineralogy*, **7**, 989-1006.

Cave, B.J., Stepanov, A.S., Craw, D., Large, R.R., Halpin, J.A. & Thompson, J. (2015) Release of trace elements through the sub-greenschist facies breakdown of detrital rutile to metamorphic titanite in the Otago Schist, New Zealand. *The Canadian Mineralogist*, **53**, 379-400.

Cawood, P.A., Nemchin, A.A., Leverenz, A., Saeed, A. & Balance, P.F. (1999) U/Pb dating of detrital zircons: Implications for the provenance record of Gondwana margin terranes. *Bulletin of the Geological Society of America,* **111**(8), 1107-1119.

Cawood, P.A., Nemchin, A.A., Smith, M. & Loewy, S. (2003) Source of the Dalradian Supergroup constrained by U-Pb dating of detrital zircon and implications for the East Laurentian Margin. *Journal of the Geological Society, London, **160***, 231-246.

Chakoumakos, B.C., Murakami, T., Lumpkin, G.R. & Ewing, R.C. (1987) Alpha-decay-induced fracturing in zircon. The transition from crystalline to the metamict state. *Science,* **236**, 1556-1559.

Chakraborty, S. & Ganguly, J. (1991) Compositional zoning and cation diffusion in garnets. *In:* Ganguly, J. (ed) *Diffusion, atomic ordering, and mass transport: selected topics in geochemistry*. Springer-Verlag, New York. 120-175.

Charlier, B., Skär, Ø., Korneliussen, A., Duchesne, J.C. & Auwera, V. (2007) Ilmenite composition in the Tellnes Fe-Ti deposit, SW Norwau: fractional crystallization, postcumulus evolution and ilmenite-zircon relation. *Contributions to Mineralogy and Petrology*, **154**, 119-134.

Chen, B., Ma, Z., Wang, B. & Meng, G. (2019) Zircon growth during subduction and exhumation metamorphism od mafic rocks, Aktyuz terrain, North Tiahshan, Kyrgyzstan. *Acta Geologica Sinica,* **93**(S2), 5-14.

Chernoff, C.B. & Carlson, W.D. (1997) Disequilibrium for Ca during growth of pelitic garnet. *Journal of Metamorphic Geology,* **15**, 421-438.

Chernoff, C.B. & Carlson, W.D. (1999) Trace element zoning as a record of chemical disequilibrium during garnet growth. *Geology,* **27**(6), 555-558.

Claiborne, L.L., Miller, C.F., Walker, B.A., Wooden, J.L., Mazdab, F.K. & Bea, F. (2006) Tracking magmatic proxesses through Zr/Hf ratios in rocks and Hf and Ti zoning in zircons: An example from the Spirit Mountains batholith, Nevada. *Mineralogical Magazine*, **70**(5), 517-543.

Corrie, S.L. & Kohn, M.J. (2008) Trace-element distributions in silicates during prograde metamorphic reactions: implications for monazite formation. *Journal of Metamorphic Geology*, **26**, 451-464.

Cramer, B.D., Schmitz, M.D., Huff, W.D. & Bergström, S.M. (2015) High-Precision U-Pb zircon age constraints on the duration of rapid biogeochemical events during the Ludlow epoch (Silurian Period). *Journal of the Geological Society,* **172**(2), 157-160.

Crawford, M.L. (1966) Composition of plagioclase and associated minerals in some schists from Vermont, U.S.A., and South Westland, New Zealand, with inferences about the peristerite solvus. *Contributions to Mineralogy and Petrology*, **13**, 269-294.

Crawford, M.L. & Hollister, L.S. (1986) Metamorphic fluids: the evidence from fluid inclusions. *Advances in Physical Geochemistry,* **5**, 1-35.

Cui, J., Zhang, Y., Dong, S., Jahn, B., Xu, X. & Ma, L. (2013) Zircon U-Pb geochronology of the Mesozoic metamorphic rocks and granitoids in the coastal tectonic zone of SE China: Constraints on the timing of Late Mesozoic orogeny. *Journal of Asian Earth Sciences,* **62**, 237-252.

Cunha, T.R., Rodrigues, A.D., Rodrigues, J.E., Sampaio, D.V., Moulton, B.J.A., da Costa, R.C. & Pizani, P.S. (2019) Thermal expansion, compressibility and bulk

modulus of ilmenite-type $CoTiO_3$: X-ray diffraction at high pressures and temperatures. *Solid State Sciences,* **88**, 1-5.

Daniel, C.G. & Spear, F.S. (1998) Three-dimensional patterns of garnet nucleation and growth. *Geology,* **26**(6), 503-506.

Davis, G.L., Hart, S.R. & Tilton, G.R. (1968) Some effects of contact metamorphism on zircon ages. *Earth and Planetary Science Letters*, **5**, 27-34.

De Béthune, P., Laudron, D. & Bocquet, J. (1975) Diffusion processes in resorbed garnet. *Contributions to Mineralogy and Petrology,* **50**, 197-204.

Deer, W.A., Howie, R.A. & Zussman, J. (2009) *Rock Forming Minerals: Layered Silicates Excluding Micas and Clay Minerals*, second edition. The Geological Society, London, 81-142.

Deer, W.A., Howie, R.A. & Zussman, J. (2013a) Zircon Zr[SiO4]. *In:* Deer, W.A., Howie, R.A. & Zussman, J. *An Introduction to the rock forming minerals*, third edition. Mineralogical Society of Great Britain and Ireland, London, 12-14.

Deer, W.A., Howie, R.A. & Zussman, J. (2013b) Garnet Group. *In:* Deer, W.A., Howie, R.A. & Zussman, J. *An Introduction to the rock forming minerals*. Mineralogical Society of Great Britain and Ireland, London, 18-27.

Deer, W.A., Howie, R.A. & Zussman, J. (2013c) Staurolite $(Fe^{2+},Mg,Zn)_{3-4}(Al,Fe^{3+}Ti)_{17-18}O_{16}$ $[(Si,Al)O_4]_8H_{3-4}$. *In:* Deer, W.A., Howie, R.A. & Zussman, J. *An Introduction to the rock forming minerals*. Mineralogical Society of Great Britain and Ireland, London, 39-43.

Degeling, H. (2002) Zircon equilibria in metamorphic rocks: The Australian National University, Australia, pp. 230.

Degeling, H., Eggins, S. & Ellis, D.J. (2001) Zr budgets for metamorphic reactions, and the formation of zircon from garnet breakdown. *Mineralogical Magazine*, **65**(6), 749-758.

Dempster, T.J. (1985) Garnet zoning and metamorphism of the Barrovian Type Area, Scotland. *Contributions to Mineralogy & Petrology*, **89**, 30-38.

Dempster, T.J. & Bluck, B.J. (1995) Regional metamorphism in transform zones during supercontinent breakup: Late Proterozoic events of the Scottish Highlands. *Geology*, **23**, 991-994.

Dempster, T.J., Rogers, G., Tanner, P.W.G., Bluck, B.J., Muis, R.J., Redwood, S.D., Ireland, T.R. & Paterson, B.A. (2002) Timing of deposition, oroegenesis and glaciation within the Dalradian rocks of Scotland: constraints on U-Pb zircon ages. *Journal of the Geological Society*, **159**(1), 83-94.

Dempster, T.J. Hay, D.C. & Bluck, B.J. (2004) Zircon growth in slate. *Geology*, **32**(2), 221-224.

Dempster, T.J., Hay, D.C., Gordon, S.H. & Kelly, N.M. (2008a) Micro-zircon: origin and evolution during metamorphism. *Journal of Metamorphic Geology*, **26**, 499-507.

Dempster, T.J., Martin, J.C. & Shipton, Z.K. (2008b) Zircon dissolution in a ductile shear zone Monte Rosa granite gneiss, northern Italy. *Mineralogical Magazine*, **72**(4), 971-986.

Dempster, T.J. & Chung, P. (2013) Metamorphic zircon: tracking fluid pathways and the implications for the preservation of detrital zircon: *Journal of the Geological Society, London*, **170**, 631-639.

Dempster, T.J. & Jess, S.A. (2015) Ikaite pseudomorphs in Neoproterozoic Dalradian slates record Earth's coldest metamorphism. *Journal of the Geological Society,* **172**, 459-464.

Dempster, T.J. La Piazza, J., Taylor, A.G., Beaudoin, N. & Chung, P. (2017a) Chemical and textural equilibration in garnet during amphibolite facies metamorphism: The influence of coupled dissolution-reprecipitation. *Journal of Metamorphic Geology*, **35**, 1111-1130.

Dempster, T.J., Symon, S. & Chung, P. (2017b) Intergranular diffusion rates from the analysis of garnet surfaces: Implications for metamorphic equilibration. *Journal of Metamorphic Geology,* **35**, 585-600.

Dempster, T.J., Gilmour, M.I. & Chung, P. (2018) The partial re-equilibration of garnet porphyroblasts in pelitic schists and its control on prograde metamorphism, Glen Roy, Scotland. *Journal of Metamorphic Geology,* **37**, 383-399.

Eitel, W. (1964) Silicate Science. Academic Press, New York, 204 pp.

Ellsworth, S., Navrotsky, A. & Ewing, R.C. (1994) Energetics of radiation damage in natural zircon ($ZrSiO_4$). *Phys Chem Minerals,* **21**, 140-149.

Engleder, T. (1987) Joints and shear fractures in rocks. *In:* Atkinson, B.K. (ed) Fracture mechanics of rock, Academic, San Diego, California, 27-69.

Ercit, T.S. (2002) The mess that is 'allanite'. *Canadian Mineralogist,* **40**, 1411-1419.

Ewing, R.C. (1999) Nuclear waste forms for actinides. *Proceedings of the National Academy of Sciences of the United States of America,* **96**(7), 3432-3439.

Ewing, R.C., Haaker, R.G. & Lutze, W. (1982) Leachability of zircon as a function of alpha dose. In: Lutze, W. (ed.) *Scientific Basis for Radioactive Waste Management*. V. Elsevier, The Netherlands, 389-397.

Farnan, I., Balan, E., Pickard, C.J. & Mauri, F. (2003) The effect of radiation damage on the local structure in the crystalline fraction of $ZrSiO_4$: investigating the ^{29}Si NMR response to pressure in zircon and reidite *American Mineralogist*, **88**, 1663-1667.

Ferry, J.M. (1992) Regional metamorphism of the Waits River formation, eastern Vermont, delineation of a new type of giant metamorphic hydrothermal system. *Journal of Petrology,* **33**, 45-94.

Ferry, J.M. & Dipple, G.M. (1992) Models for coupled fluid flow, mineral reaction, and isotopic alteration during contact metamorphism, The Notch Peak aureole, Utah. *American Mineralogist,* **77**, 577-591.

Ferry, J.M. & Gerdes, M.L. (1998) Chemically reactive fluid flow during metamorphism. *Annual Review of Earth and Planetary Sciences,* **26**, 255-287.

Finch, R.J. & Hanchar, J.M. (2003) Structure and Chemistry of Zircon and Zircon-Group Minerals. *In:* Hanchar, J.M. & Hoskin, P.W.O. (eds). *Zircon- Reviews in Mineralogy and Geochemistry*, v. 53, Mineralogical Society of America/Geochemical Society, Washington DC, 1-21.

Florence, F.P. & Spear, F.S. (1991) Effects of diffusional modification of garnet growth zoning on P-T path calculations. *Contributions to Mineralogy and Petrology,* **107**(4), 487-500.

Foster, G. & Parrish, R.R. (2003) Metamorphic monazite and the generation of P-T-t paths. *In:* Vance, D., Müller, W. & Villa, I.M. (eds.) Geochronology: Linking the isotopic record with petrology and textures. Geological Society, London, Special Publications 220, 25-47.

Franceschelli, M., Memmi, I. & Ricci, C.A. (1982) Ca distribution between almandine-rich garnet and plagioclase in pelitic and psammitic schists from the metamorphic basement of North-Eastern Sardinia. *Contributions to Mineralogy and Petrology*, **80**(3), 285-295.

Fraser, G., Ellis, D. & Eggins, S. (1997) Zirconium abundance in granulite-facies minerals, with implication or zircon geochronology in high-grade rocks. *Geology*, **25**, 607-610.

Fraser, G.L., Pattison, D.R.M. & Heaman, L.M. (2004) Age of the Ballachulish and Glencoe igneous complexes (Scottish Highlands) and paragenesis of zircon, monazite and baddeleyite in the Ballachulish Aureole. *Journal of the Geological Society,* **161**(3), 447-462.

Froude, D.O., Ireland, T.R., Kinny, P.D., Williams, I.S., Compston, W., Williams, I.R. & Myers, J.R. (1967) Some effects of progressive metamorphism on zircons. *Bulletin of the Geological Society of America*, **78**, 879-906.

Froude, D.O., Ireland, T.R., Kinny, P.D., Williams, I.S., Compston, W., Williams, I.R. & Myers, J.S. (1983) Ion microprobe identification of 4,100-4,200 myr-old terrestrial zircons. *Nature,* **304**, 616-618.

Gaidies, F., Pattison, R.D.M. & de Capitani, C. (2011) Toward a quantitative model of metamorphic nucleation and growth. *Contributions to Mineralogy and Petrology,* **162**, 975-993.

Gangopadhyaya, P.K. & Sen, R. (1972) Trend of regional metamorphism: an example from "Delhi System" of rocks occurring around Bairawas, North-Eastern Rajasthan, India. *Geologische Rundschau,* **61**, 270-281.

Ganguly, J. (2010) Cation diffusion kinetics in aluminosilicate garnets and geological applications. *Reviews in Mineralogy & Geochemistry,* **72**, 559-601.

Gao, S., Luo, T.C., Zhang, H.F., Han, Y.W., Zhao, Z.D. & Hu, Y.K. (1998) Chemical composition of the continental crust as revealed by studies in East China. *Geochimica et Cosmochimica Acta*, **62**, 1959-1975.

Gastil, R.G., Delisle, M. & Morgan, K.R. (1967) Some effects of progressive metamorphism on zircons. *Bulletin of the Geological Society of America,* **78**, 879-906.

Gatewood, M.P., Dragovic, B., Stowell, H.H., Baxter, E.F., Hirsch, D.M. & Bloom, R. (2015) Evaluating chemical equilibrium in metamorphic rocks using major element Sm-Nd isotopic age zoning in garnet, Townshend Dam, Vermont, USA. *Chemical Geology,* **401**, 151-168.

Geisler, T., Pidegon, R.T., Van Bronswijk, W. & Pleysier, R. (2001) Kinetics of thermal recovery and recrystallization of partially metamict zircon: a Rama spectroscopic study. *European Journal of Mineralogy,* **13**, 1163-1176.

Geisler, T., Schaltegger, U. & Tomaschek, F. (2007) Re-equilibration of zircon in aqueous fluids and melts. *Elements*, **3**, 43-50.

Gieré, R. (1986) Zirconalite, allanite and hoegbomite in a marble skarn from the Bergell contact aureole: Implications for mobility of Ti, Zr, and REE. *Contributions to Mineralogy and Petrology*, **93**, 459-470.

Gieré, R. & Sorensen, S.S. (2004) Allanite and other REE-rich epidote-group minerals. *Reviews in Mineralogy and Geochemistry,* **56**, 431-493.

Gillet, P., Ingrin, J., Chopin, C. (1984) Coesite in subducted continental crust: P-T history deduced from elastic model. *Earth and Planetary Science Letters,* **70**, 426-436.

Goldstein, R.H. (2003) Petrographic analysis of fluid inclusions. *In:* Samson, I., Anderson, A. & Marshall, D. (eds) Fluid inclusions: analysis and interpretation, Mineralogical Association of Canada, 9-53.

Goldstein, J.I., Newbury, D.E., Michael, J.R., Ritch, N.W.M., Scott, J.H.H. & Joy, D.C. (2017) Scanning electron microscopy and x-ray microanalysis. 4th Edition, Springer, New York, pp 549.

Grant, J.A. & Weiblen, P.W. (1971) Retrograde zoning in garnet near the second sillimanite isograd. *American Journal of Science,* **270**, 281-296.

Green, T.H. (1994) Experimental studies of trace-element partitioning applicable to igneous petrogenesis – Sedona 16 years later. *Chemical Geology*, **117**, 1-36.

Gregory, C.J., Rubatto, D., Allen, C.M., Williams, I.S., Hermann, J. & Ireland, T. (2007) Allanite micro-geochronology: A LA-ICP-MS and SHRIMP U-Th-Pb study. *Chemical Geology,* **245**, 162-182.

Grew, E.S., Locock, A.J., Mills, S.J., Galuskina, I.O., Galuskin, E.V. & Hälenius, U. (2013) IMA Report Nomenclature of the garnet supergroup. *American Mineralogist,* **98**, 785-911.

Griffin, W.L., Smith, D., Boyd, F.R., Cousens, D.R., Ryan, C.G., Sie, S.H. & Suter, G.F. (1989) Trace-element zoning in garnets from sheared mantle xenoliths. *Geochimica et Cosmochimica Acta,* **53**(2), 561-567.

Guidotti, C.V. (1974) Transition from staurolite to sillimanite zone, Rangeley Quadrangle, Maine. *Geological Society of American Bulletin,* **85**, 475-490.

Hallett, B.W. & Spear, F.S. (2015) Monazite, zircon, and garnet growth in migmatitic pelites as a record of metamorphism and partial melting in the East Humboldt Range, Nevada. *American Mineralogist*, **100**, 951-972.

Hames, W.E. & Menard, T. (1993) Fluid-assisted modification of garnet composition along rims, cracks, and mineral inclusion boundaries in samples of amphibolite facies schists. *American Mineralogist,* **78**, 338-344.

Hanchar, J.M. & Miller, C.F. (1993) Zircon zonation patterns as revealed by cathodoluminescence and backscattered electron images: Implications for interpretation of complex crustal histories. *Chemical Geology*, **110**, 1-13.

Harrison, T.M. (2009) The Hadean crust: Evidence from >4Ga zircons *Annual Review of Earth and Planetary Science*, **37**, 479-505.

Harrison, T.M., McKeegan, K.D. & Lefort, P. (1995) Detection og inherited monazite in the Manaslu leucogranite by $^{208}Pb/^{232}Th$ ion microprobe dating: Crystallisation age and tectonic implications. *Earth and Planetary Science Letters,* **133**, 271-282.

Harte, B. & Henley, K.J. (1966) Occurrence of compositionally zoned almanditic garnets in regionally metamorphosed rocks. *Nature*, **210**, 689-692.

Harte, B. & Hudson, N.F.C. (1979) Pelite facies series and the temperatures and pressures of Dalradian metamorphism in E Scotland. *In:* Harris, A.L., Holland, C.H. & Leake, B.E. *The Caledonides of the British Isles – reviewed*, The Geological Society of London, 323-337.

Haselock, P.J. & Winchester, J.A. (1981) A note on the stratigraphic relationship of the Leven Schist and Monadhliath Schist in the Central Highlands of Scotland. *Geological Journal*, **16**, 237-241.

Hawthorne, F.C., Ungaretti, L., Oberti, R., Caucia, F. & Callegari, A. (1993) The crystal chemistry of staurolite. I. Crystal structure and site populations. *Canadian Mineralogist*, **31**, 551-582.

Hay, D.C. & Dempster, T.J. (2009a) Zircon behaviour during low-temperature metamorphism. *Journal of Petrology*, **50**(4), 571-589.

Hay, D.C. & Dempster, T.J. (2009b) Zircon alteration, formation and preservation in sandstones. *Sedimentology*, **56**, 2175-2191.

Hay, D.C., Dempster, T.J., Lee, M.R. & Brown, D.J. (2010) Anatomy of a low temperature zircon outgrowth. *Contributions to Mineralogy and Petrology*, **159**, 81-92.

Hazen, R.M. & Finger, L.W. (1979) Crystal structure and compressibility of zircon at high pressure. *American Mineralogist*. **64**, 196-201.

Hermann, J. & Rubatto, D. (2003) Relating zircon and monazite domains to garnet growth zones: age and duration of granulite facies metamorphism in the Val Malenco lower crust. *Journal of Metamorphic Geology*, **21**, 833-852.

Hickmott, D.D., Shimizu, N., Spear, F.S. & Selverstone, J. (1987) Trace-element zoning in a metamorphic garnet. *Geology*, **15**, 573-576.

Hickmott, D.D. & Shimizu, N. (1990) Trace element zoning in garnet from the Kwoiek Area, British Columbia: disequilibrium partitioning during garnet growth? *Contributions to Mineralogy and Petrology*, **104**(6), 619-630.

Higgins, M. (2006) Grain and Crystal Sizes. *In*: Higgins, M. (Ed.) *Quantitative textural measurements in igneous and metamorphic petrology*, Cambridge University Press, Cambridge, 38-106.

Holland, H. & Gottfried, D. (1955) The effect of nuclear radiation on the structure of zircon. *Acta Crystal*, **61**, 291-300.

Hollister, L.S. (1966) Garnet zoning: an interpretation based on the Rayleigh Fractionation model. *Science,* **154**, 1647-1651.

Hollister, L.S. (1969) Contact metamorphism in the Kwoiek area of British Columbia: An end member of the metamorphic process. Bulletin of the *Geological Society of America,* **80**, 2465-2494.

Hoskin, P.W.O. & Black, L.P. (2000) Metamorphic zircon formation by solid-state recrystallization of protolith igneous zircon. *Journal of Metamorphic Geology*, **18**, 423-439.

Hoskin, P.W.O. & Schaltegger, U. (2003) The composition of zircon and igneous and metamorphic petrogenesis. *In:* Hanchar, J.M. & Hoskin, P.W.O. (eds). *Zircon-Reviews in Mineralogy and Geochemistry*, v. 53, Mineralogical Society of America/Geochemical Society, Washington DC, 1-21.

Hutton, D.H.W. & Alsop, G.I. (2004) Evidence for a major Neoproterozoic orogenic unconformity within the Dalradian Supergroup of NEW Ireland. *Journal of the Geological Society, London,* **161**, 629-640.

Hwang, S-L., Shen, P., Chu, H-T., Yu, W-F., Iizuka, Y. & Schertl, H.P. (2019) Rutile inclusions in garnet from a dissolution-reprecipitation mechanism. *Journal of Metamorphic Geology*, **00**, 1-20.

Ikeda, T. (1993) Compositional zoning patterns of garnet during prograde metamorphism from the Yanai district, Ryoke metamorphic belt, southwest Japan. *Lithos*, **20**(2), 109-121.

Jamtveit, B., Dahlgren, S. & Austrheim, H. (1997) High-grade contact metamorphism of calcareous rocks from the Oslo Rift, Southern Norway. *American Mineralogist*, **82**, 1241-1254.

Jamtveit, B., Putnis, C.V. & Malthe-Sørenssen, A. (2009) Reaction induced fracturing during replacement processes. *Contributions to Mineralogy and Petrology,* **157**, 127-133.

Jamtveit, B. & Austrheim, H. (2010) Metamorphism: the role of fluids. *Elements,* **6**, 153-158.

Janots, E., Brunet, F., Goffé, B., Poinssot, C., Burchard, M. & Cemic, L. (2007) Thermochemistry of monazite-(La) and dissakite-(La): implications for monazite and allanite stability in metapelites. *Contributions to Mineralogy and Petrology,* **154**, 1-14.

Janots, E., Engi, M., Rubatto, D., Berger, A., Gregory, C. & Rahn, M. (2009) Metamorphic rates in collisional orogeny from in situ allanite and monazite dating. *The Geological Society of America.* **37**, 11-14.

Jiang, J. & Lasaga, A.C. (1990) The effects of post-growth thermal events on growth-zoned garnet: implications for metamorphic P-T history calculations. *Contributions to Mineralogy & Petrology*, **105**, 454-459.

Jiang, S.Y., Palmer, N.R. & Slack, J.F. (1996) Mn-rich ilmenite from the Sullvian Pb-Zn-Ag deposit, British Columbia. *The Canadian Mineralogist*, **34**, 29-36.

Jiao, S., Guo, K., Mao, Q. & Zhao, R. (2010) Application of Zr-in-rutile thermometry: a case study from ultrahigh-temperature granulites of the Khondalite belt, North China Craton. *Contributions to Mineralogy and Petrology,* **162**(2), 379-393.

Jonas, L., John, T., King, H.E., Geisler, T. & Putnis, A. (2014) The role of grain boundaries and transient porosity in rocks as fluid pathways for reaction front propagation. *Earth and Planetary Science Letters,* **386**, 64-74.

Jones, K.A., Morgan, G.J. & Galwey, A.K. (1972) The significance of the size distribution function of crystals formed in metamorphic reactions. *Chemical Geology,* **9**¸137-143.

Kamo, S.L., Czamanske, G.K., Amelin, Y., Fedorenko, V.A., Davis, S.W. & Trofimov, V.R. (2003) Rapid eruption of Siberian flood-volanic rocks and evidence for coincidence with Permian-Triassic boundary and mass extinction at 251 Ma. *Earth and Planetary Science Letters,* **214**, 75-91.

Keller, L.M., Abart, R., Wirth, R., Schmid, D.W. & Kunze, K. (2006) Enhanced mass transfer through short-circuit diffusion: growth of garnet reaction rims at eclogite facies conditions. *American Mineralogist,* **91**, 1024-1038.

Kelly, N.M. & Harley, S.L. (2005) An integrated microtextural and chemical approach to zircon geochronology: Refining the Archaean history of the Napier Complex, East Antarctica. *Contributions to Mineralogy and Petrology*, **149**, 57-84.

Kelly, E.D., Carlson, W.D. & Ketcham, R.A. (2013) Magnitudes of departures from equilibrium during regional metamorphism of porphyroblastic rocks. *Journal of Metamorphic Geology*, **31**, 981-1002.

Kelsey, D.E., Clark, C. & Hand, M. (2008) Themobarometric modelling of zircon and monazite growth in melt-bearing systems: examples using model metapelite and metapsammitic granulites. *Journal of Metamorphic Geology*, **26**, 199-212.

Kelsey, D.E. & Powell, R. (2011) Progress in linking accessory mineral growth and breakdown to major mineral evolution in metamorphic rocks: a thermodynamic approach in the Na_2O-CaO-K_2O-FeO-MgO-Al_2O_3-SiO_2-H_2O-TiO_2-ZrO_2 system. *Journal of Metamorphic Geology*, **29**, 151-166.

Kirkland, C.L., Slagstad, T. & Johnson, T.E. (2018) Zircon as a metamorphic timekeeper: A case study from the Caledonides of central Norway. *Gondwana Research*, **61**, 63-72.

Kleinschodt, R. & McGrew, A.J. (2000) Garnet plasticity in the lower continental crust: implications for deformation mechanisms based on microstructures and SEM electron channeling pattern analysis. *Journal of Structural Geology,* **22**, 795-809.

Kohn, M.J. (2016) Metamorphic chronology – a tool for all ages: Past achievements and future prospects. *American Mineralogist*, **101**, 25-42.

Kohn, M.J., Corrie, S.L. & Markley, C. (2015) The fall and rise of metamorphic zircon. *American Mineralogist*, **100**, 897-908.

Kohn, M.J & Kelly, N.M. (2018) Petrology and geochronology of metamorphic zircon. *In:* Moser. D.E., Corfu, F., Darling, J.R., Reddy, S.M. & Tait, K. *Microstructural geochronology: planetary records down to atom scale, Geophysical Monograph 232*. American Geophysical Union. 25-61.

Kondratiuk, P., Tredak, H., Ladd, A.J.C. & Szymczak, P. (2015) Synchronization of dissolution and reprecipitation fronts during infiltration-driven replacement in porous rocks. *Geophysical Research Letters,* **42**, 2244-2252.

Konrad-Schmolke, M., Halama, R., Wirth, R., Thomen, A., Klitscher, N., Morales, L., Schreiber, A. & Wilke, F.D.H. (2018) Mineral dissolution and reprecipitation mediated by an amorphous phase. *Nature Communications*, **9**: 1637, 9 pp.

Kooijman, E., Smit, M.A., Mezger, K. & Berndt, J. (2012) Trace element systematics in granulite facies rutile: implications for Zr geothermometry and provenance studies. *Journal of Metamorphic Geology*, **30**, 397-412.

Köppel, V. & Grünenfelder, M. (1971) A study of inherited and newly formed zircons from paragenesis and granitised sediments of the Strona-Ceneri-Zone (Southern Alps). *Tschermaks mineralogische und petrographische Mitteilungen,* **51**, 385-410.

Koreshkova, M.Y., Downes, H., Millar, I., Levsky, L., Larionov, A. & Sergeev, S. (2017) Geochronology of metamorphic events in the lower crust beneath NW Russia: a xenolith Hf isotope study. *Journal of Petrology,* **58**(8), 1567-1590.

Košler, J., Fonneland, H., Sylvester, P., Tubrett, M. & Pederson, R.B. (2002) U-Pb dating of detrital zircons for sediment provenance studies – a comparison of laser ablation ICPMS and SIMS techniques. *Chemical Geology,* **182**(2-4), 605-618.

Koritnig, S. (1969) Flourine. *In:* Wedepohl, K.H. (ed.) *Handbook of Geochemistry*. Springer, Berlin Heidelberg New York. 9B-O pp.

Kretz, R. (1959) Chemical study of garnet, biotite and hornblende from gneisses of southwestern Quebec, with emphasis on distribution of elements in coexisting minerals. *Journal of Geology,* **67**, 371-403.

Kröner, A., Wan, Y., Liu, X. & Liu, D. (2014) Dating of zircon from high-grade rocks: which is the most reliable method? *Geoscience Frontiers*, **5**(4), 515.523.

Lal, R.K. & Singh, J.B. (1978) Prograde polyphase regional metamorphism and metamorphic reactions in pelitic schists at Sini, District Singhbhum, India. *Neues Jahrbuch für Mineralogy Abhandlungen*, **131**, 304-333.

Lambert, R.J., Holland, J.G., Winchester, J.A. (1982) A geochemical comparison of the Dalradian Leven Schists and the Grampian Division Monadhliath Schists of Scotland. *Journal of the Geological Society, London,* **139**, 71-84.

Lanari, P. & Engi, M. (2017) Local bulk composition effects on metamorphic mineral assemblages. *Reviews in Mineralogy and Geochemistry,* **83**, 55-102.

Lasaga, A.C. & Rye, D.M. (1993) Fluid flow and chemical reaction kinetics in metamorphic systems. *American Journal of Science*. **293**, 361-404.

Leitner, B.J., Wiender, D.K., Liebermann, R.C. (1980) Elasticity of single crystal pyrope and implications for garnet solid solution series. *Physics of the Earth and Planetary Interiors,* **22**, 111-121.

Lee, J.K.W., Williams, I.S. & Ellis, D.J. (1997) Pb, U and Th diffusion in natural zircon. *Nature,* **390**, 159-162.

Li, B., Ge, J. & Zhang, B. (2018) Diffusion in garnet: a review. *Acta Ceochimica*, **37**, 19-31.

Liati, A. & Gebauer, D. (1999) Constraining the prograde and retrograde P-T-t path of Eocene HP rocks by SHRIMP dating different zircon domains: inferred rates of heating, burial, cooling and exhumation for central Rhodope, northern Greece. *Contributions to Mineralogy and Petrology*, **135**, 340-354.

Loomis, T.P. (1983) Compositional zoning of crystals: A record of growth and reaction history. *In:* Saxena, S.K. (ed.) *Kinetics and Equilibrium in Mineral Reactions: Advances in Geochemistry,* v. 3, Springer Verlag, New York, 1-60.

Loui, J.G., Zhang, R., Ernst, W.G., Liu, J. & McLimans, R. (1998) Mineral paragenesis in the Pianpaludo eclogitis body, Gruppo di Voltri, western Ligurian Alps. *Schweizerische Mineralogische and Petrographische Mitteilungen,* **78**, 317-335.

Luquot, L., García-Ríos, M., Roettling, T., Rodriguez, O., Gouze, P. & Carrera, J. (2015) Study of the dissolution and precipitation mechanisms at the pore-scale using percolation experiments and x-ray microtomography. *Revista de la Sociedad espanõla de mineralogia,* **20**, 11-15.

Mainprice, D., Bascou, J., Cordier, P. & Tommasi, A. (2004) Crystal preferred orientations of garnet: comparison between numerical simulations and electron back-scattered diffraction (EBSD) measurements in naturally deformed eclogites. *Journal of Structural Geology,* **26**(11), 2089-2102.

Marks, M., Halama, R., Wenzel, T. & Markl, G. (2004) Trace element variations in clinopyroxene and amphibole from alkaline to peralkaline syenites and granites: implications for mineral-melt trace-element partitioning. *Chemical Geology*, **211**, 185-215.

Martin, L.A.J., Ballèvre, M., Boulvais, P., Halfpenny, A., Vanderhaeghe, O., Duchêne, S. & Deloule, E. (2011) Garnet re-equilibration by coupled dissolution-reprecipitation evidence from textural, major element and oxygen isotope zoning of 'cloudy garnet'. *Journal of Metamorphic Geology*, **29**, 213-231.

Marqués, M., Florez, M., Recio, J.M., Gerward, L. & Olsen, J.S. (2006) Structure and stability of $ZrSiO_4$ under hydrostatic pressure. *Physical Review,* **B74**, 014104.

Maruyama, S., Liou, J.G. & Suzuki, K. (1982) The peristerite gap in low-grade metamorphic rocks. *Contributions to Mineralogy and Petrology*, **81**(4), 268-276.

Mason, B. & Allen, R.O. (1973) Minor and trace elements in augite, hornblende, and pyrope megacrysts from Kakanui, New Zealand. *New Zealand Journal of Geology and Geophysics*, **16**(4), 935-947.

McLellan, E. (1985) Metamorphic reactions in the kyanite and sillimanite zones of the Barrovian-type area. *Journal of Petrology*, **26**(4), 789-818.

Meldrum, A., Boatner, L.A., Weber, W.J. & Ewing, R.C. (1998) Radiation damage in zircon and Monazite. *Geochimica et Cosmochimica Acta*, **62**(14), 2509-2520.

Meyer, M., John, T., Brandt, S. & Klemd, R. (2011) Trace element composition of rutile and the application of Zr-in-rutile thermometry to UHT metamorphism (Epupa Complex, NW Namibia). *Lithos,* **126**(3-4), 388-401.

Milton, C., Ingram, B.L. & Blade, L.V. (1961) Kimzeyite, a zirconium garnet from Magnet Cove, Arkansas *American Mineralogist*, **46**, 533-548.

Miyazaki, K. (2015) Diffusion-controlled growth and degree of disequilibrium of garnet porphyroblasts: is diffusion-controlled growth of porphyroblasts common? *Progress in Earth and Planetary Science,* **2**(25), 14 pp.

Mojzsis, S.J., Harrison, T.M. & Pidgeon, R.T. (2001) Oxygen-isotope evidence from ancient zircons for liquid water at the Earth's surface 4,300Myr ago. *Nature*, **409**, 178-181.

Möller, A., O'Brien, P.J., Kennedy, A. & Kröner, A. (2003) Linking growth episodes of zircon and metamorphic textures to zircon chemistry: an example from the ultrahigh-temperature granulites of Rogaland (SW Norway). *In:* Vance, D., Müller, W. & Villa, I.M. (eds) 2003. Geochronology: *Linking the Isotopic Record with Petrology and Textures*: Geological Society, London, Special Publications, v. 220, 65-81.

Morisset, C.E. & Scoates, J. (2008) Origin of zircon rims around ilmenite in mafic plutonic rocks of Proterozoic anorthosite suites. *Canadian Mineralogist*, **46**(2), 289-304.

Nasdala, L., Pidgeon, R.T. & Wolf, D. (1996) Heterogeneous metamictization of zircon on a microscale. *Geochimica et Cosmochimica Acta*, Scientific comment, **60**(6), 1091-1097.

Nasdala, L., Wenzel, M., Varva, G., Irmer, G., Wenzel, T. & Kober, B. (2001) Metamictization of natural zircon: accumulation versus thermal annealing of radioactively-induced damage. *Contributions to Mineralogy and Petrology*, **141**, 125-144.

Nehring, F., Foley, S.F. & Hölltä, P. (2010) Trace element partitioning in the granulite facies. *Contributions to Mineralogy and Petrology,* **159**, 493-519.

Nemchin, A.A., Pidgeon, R.T. & Whitehouse, M.J. (2006) Re-evaluation of the origin and evolution of >4.2Ga zircons from the Jack Hills metasedimentary rocks. *Earth and Planetary Science Letters*, **244**, 218-233.

O'Neill, B., Bass, J.D., Rossman, G.R., Geiger, C.A. & Langer, K. (1991) Elastic properties of pyrope. *Physics and Chemistry of Minerals,* **17**, 617-621.

Overstreet, W.C. (1967) The geological occurrence of monazite. U.S. Geological Society Professional Paper 530, Washington, D.C.

Özkan, H. & Jamieson, J.C. (1978) Pressure dependence of the elastic constants of nonmetamict zircon. *Physics and Chemistry of Minerals.* **2**(3), 215-224.

Passchier, C.W. & Trouw, R.A.J. (2005) Porphyroblasts and reaction rims. *In:* Passchier, C.W. & Trouw, R.A.J. Microtectonics. Springer Berlin Heidelberg, New York, 189-233.

Pattison, D.R.M. & Harte, B. (2001) *The Ballachulish Igneous Complex and Aureole: A Field Guide*. Edinburgh Geological Society, Edinburgh, 148 pp.

Pattison, D.R.M. & Tinkham, D.K. (2009) Interplay between equilibrium kinetics in prograde metamorphism of pelites: an example from the Nelson aureole, British Columbia. *Journal of Metamorphic Geology*, **27**, 249-279.

Pattison, D.R.M. & Spear, F.S. (2017) Kinetic control of staurolite-Al_2SiO_5 mineral assemblages: Implications for Barrovian and Buchan metamorphism. *Journal of Metamorphic Geology*, **36**, 667-690.

Pearce, N.J.G. (1990) Zirconium and niobium-bearing ilmenites from the Igaliko dyke swarm, Southern Greenland. *Mineralogical Magazine*, **54**, 585-588.

Peterman, E.M., Snoeyenbos, D.R., Jercinovic, M.J. & Kylander-Clark, A. (2016) Dissolution-reprecipitation metasomatism and growth of zircon within phosphatic garnet in metapelites from western Massachusetts. *American Mineralogist,* **101**, 1782-1806.

Phillips, E.R. & Key, R. M. 1992. Porphyroblast-fabric relationships: an example from the Appin Group of the Glen Roy area. *Scottish Journal of Geology*, **28**(2), p. 89-101.

Phillips, E.R., Key, R.M., Clark, G.C., May, F., Glover, B.W. & Chacksfield, B.C. (1994) Tectonothermal evolution of the Neoproterozoic Grampian and Appin groups, southwestern Monadhlaith Mountains, Scotland. *Journal of the Geological Society London,* **151**, 971-986.

Poldevaart, A. (1955) Zircons in rocks; part 1, sedimentary rocks; part 2, Igneous rocks. *American Journal of Science*, **253**(8), 433-361.

Powell, D. (1966) On the preferred crystallographic orientation of garnet in some metamorphic rocks. *Mineralogical Magazine,* **36**(276), 1094-1109.

Powell, R. & Evans, J.A. (1983) A new geobarometer for the assemblage biotite-muscovite-chlorite-quartz. *Journal of Metamorphic Geology*, **1**, 331-336.

Prakash, D., Patel, D.K., Tewari, S., Yadav, M.K. & Yadav, R. (2017) Metamorphic zonal sequences of pelitic schists and gneisses from the area around Kandra (Jharkhand): Constraints from field and textural relationships. *Journal of the Geological Society of India*, **89**, 139-144.

Prakash, D., Tewari, S. & Chandra Singh, P. (2018) Prograde Barrovian metamorphism along Darjeeling-Tista transect, Eastern Himalaya, India: constraints from textural relationship, phase equilibria and geothermobarometry. *Geological Journal*, **53**, 243-281.

Putnis, A. (2002) Mineral replacement reactions: from macroscopic observations to microscopic mechanisms. *Mineralogical Magazine,* **66**(5), 689-708.

Putnis, A. (2009) Mineral replacement reactions. *Reviews in Mineralogy and Geochemistry,* **30**, 87-124.

Putnis, A. (2015) Transient porosity resulting from fluid-mineral interaction and its consequences. *Reviews in Mineralogy and Geochemistry,* **80**, 1-23.

Putnis, A. & Putnis, C.V. (2007) The mechanism of reequilibration of solids in the presence of a fluid Phase. *Journal of Solid State Chemistry*, **180,** 1783-1786.

Putnis, A. & Austrheim, H. (2010) Fluid-induced processes: metasomatism and metamorphism. *Geofluids*, **10**, 254-269.

Putnis, A. & Austrheim, H. (2012) Mechanisms of metasomatism and metamorphism on the local mineral scale: the role of dissolution-reprecipitation during mineral reequilibration. *In:* Harlov, D.E. & Austrheim, H. (eds.) Metasomatism and the chemical transformation of a rock. Lecture notes in Earth system sciences. Springer-Verlag, Berlin Heidelberg.

Raimondo, T., Payne, J., Wade, B., Lanai, P., Clark, C. & Hand, M. (2017) Trace element mapping by LA-ICP-MS: assessing geochemical mobility in garnet. *Contributions to Mineralogy and Petrology*, **172**(17), 1-17.

Ramburg, H. (1952) Chemical bonds and distribution of cations in silicates. *Journal of Geology*, **60**, 331-355.

Rasmussen, B. (2005) Zircon growth in very low grade metasedimentary rocks: evidence for zirconium mobility ~250ºC. *Contributions to Mineralogy & Petrology*, **150**, 146-155.

Raymond, L.A. (1995) Metamorphic Rocks. *In:* Raymond, L.A. *Metamorphic Petrology,* Wm. C. Brown Communications Inc, Dubuque, 472-656.

Richardson, S.W. & Powell, R. (1976) Thermal causes of the Dalradian metamorphism in the Central Highlands of Scotland. *Scottish Journal of Geology*, **12**, 237-268.

Roberts, J.L. & Treagus, J.E. (1977) The Dalradian rocks of the South-West Highlands – Introduction. *Scottish Journal of Geology*, **13,** 87-99.

Roberts, M.P. & Finger, F. (1997) Do U-Pb zircon ages from granulites reflect peak metamorphic conditions? *Geology*, **25**(4), 319-322.

Robinson, K., Gibbs, G.V. & Ribbe, P.H. (1971) The structure of zircon: a comparison with garnet. *American Mineralogist*, **56**, 782-790.

Rojas-Agramonte, Y., Kroner, A., Demoux, A., Xia, X., Wang, W., Donskaya, T., Liu, D. & Sun, M. (2011) Detrital and xenocrystic zircon ages from Neoproterozoic and Paleozoic arc terranes of Mongolia: Significance for the origin of crustal

fragments in the Central Asian Orogenic Belt. *Gondwana Research,* **19**(3), 751-763.

Rooney, A.D., Chew, D.M. & Selby, D. (2011) Re-Os geochronology of the Neoproterozoic-Cambrian Dalradian Supergroup of Scotland and Ireland: Implications for Neoproterozoic stratigraphy, glaciations and Re-Os systematics. *Precambrian Reseach,* **185**, 202-214.

Rubatto, D. (2002) Zircon trace element geochemistry: partitioning with garnet and the link between U-Pb ages and metamorphism. *Chemical Geology*, **184**, 123-138.

Rubatto, D. (2017) Zircon: The metamorphic mineral. *Reviews in Mineralogy & Geochemistry*, **83**, 261-295.

Rubatto, D., Williams, I.S. & Buick, I.S. (2001) Zircon and monazite response to prograde metamorphism in the Reynolds Range, central Austalia. *Contributions to Mineralogy and Petrology,* **140**(4), 458-468.

Rubatto, D. & Hermann, J. (2007) Zircon behaviour in deeply subducted rocks. *Elements,* **3**, 31-35.

Rubin, J.N., Henry, C.D. & Price, J.G. (1993) The mobility of zirconium and other 'immobile' elements during hydrothermal alteration. *Chemical Geology,* **110**(1-3), 29-47.

Ruiz-Agudo, E., Putnis, C.V. & Putnis, A. (2014) Coupled dissolution and precipitation at mineral-fluid interfaces. *Chemical Geology,* **383**, 132-146.

Ruiz-Agudo, E., King, H.E., Patiño-López, L.D., Putnis, C.V., Geisler, T., Rodriguez-Navarro, C. & Putnis, A. (2016) Control of silicate wreathing by interface-coupled dissolution-reprecipitation processes at the mineral-solution interface. *Geology*, **44**(7), 567-570.

Santosh, M., Wilde, S.A. & Li, J.H. (2007) Timing of Palaeoproterozoic ultrahigh-temperature metamorphism in the North China Craton: Evidence from SHRIMP U-Pb zircon geochronology. *Precambrian Research,* **159**(3-4), 178-196.

Saxena, S.K. (1966) Evolution of zircons in sedimentary and metamorphic rocks. *Sedimentology,* **6**, 1-33.

Schaltegger, U., Fanning, C.M., Günther, D, Maurin, J.C., Schulmann, K. & Gebauer, D. (1999) Growth, annealing and recrystallization of zircon and preservation of monazite in high-grade metamorphism: conventional and in-situ U-Pb isotope, cathodoluminescence and microchemical evidence: *Contributions to Mineralogy and Petrology*, **134**, 186-201.

Schwandt, C.S., Papike, J.J. & Shearer, C.K. (1996) Trace element zoning in pelitic garnet of the Black Hills, South Dakota. *American Mineralogist*, **81**, 1195-1207.

Schwartz, J.J., John, B.E., Cheadle, M.J. Wooden, J.L., Frank, M., Swapp, S. & Grimes, C.B. (2010) Dissolution-reprecipitation of igneous zircon in mid-ocean ridge gabbro, Atlantis Bank, Southwest Indian Ridge. *Chemical Geology,* **274**, 68-81.

Shepherd, T.J. (1990) Geological link between fluid inclusions, dilatant microcracks and palaeostress field. *Journal of Geophysical Research*, **95**(B7) 11115-11120.

Siégel, C., Bryan, S.E., Allen, C.M. & Gust, D.A. (2018) Use and abuse of zircon-based thermometers: A critical review and a recommended approach to identify antecrystic zircons. *Earth Science Reviews,* **176**, 87-116.

Sinh, V.B.T., Osanai, Y., Nakano, N., Adachi, T. & Kitano, I. (2019) Geochronology and REE geochemistry of zircon and garnet in pelitic gneisses from the Higo metamorphic terrane, Kyushu, Japan: Constraints on the timing of high-temperature metamorphism. *Journal of Mineralogical and Petrological Sciences,* **114**(2), 47-59.

Sláma, J., Košer. J. & Pedersen, R.B. (2007) Behaviour of zircon in high-grade metamorphic rocks: evidence from Hf isotopes, trace elements and textural studies. *Contributions to Mineralogy and Petrology*, **154**, 335-356.

Smit, M., Scherer, E. & Cutts, J. (2018) Precision and novel applications in Lu-Hf garnet chronology. *Geophysical Research Abstracts,* EGU General Assembly 2018, **20**, EGU2018-3755.

Smith, D.G.W., de St Jorre, L., Reed, S.J.B. & Long, J.V.P. (1991) Zonally metamictized and other zircon from Thor Lake, Northwest Territories, *Canadian Mineralogist,* **29**, 301-309.

Smith, H.A. & Barreiro, B. (1990) Monazite U-Pb dating of staurolite grade metamorphism in pelitic schists. *Contributions to Mineralogy and Petrology,* **105**, 602-615.

Smithson, F. (1937) Outgrowths on zircon in the middle Jurassic of Yorkshire. *Geological Magazine,* **74**, 281-283.

Spear, F.S. (1991) On the interpretation of peak metamorphic temperatures in light of garnet diffusion during cooling. *Journal of Metamorphic Geology*, **9**, 379-388.

Spear, F.S. (2010) Monazite-allanite phase relations in metapelites. *Chemical Geology,* **279**, 55-62.

Spear, F.S. (2014) The duration of near-peak metamorphism from diffusion modelling of garnet zoning. *Journal of Metamorphic Geology,* **32**, 903-914.

Spear, F.S., Selverstone, J., Hickmott, D., Crowley, P. & Hodges, K.V. (1984) P-T paths from garnet zoning: A new technique for deciphering tectonic processes in metamorphic terranes. *Geology*, **12**, 87-90.

Spear, F.S. & Pyle, J.M. (2010) Theoretical modelling of monazite growth in a low-Ca metapelite. *Chemical Geology,* **273**, 111-119.

Speer, J.A. (1982) Zircon: *Reviews in Mineralogy*, **5**, 67-112.

Spruzeniece, L., Piazolo, S. & Maynard-Casely, H.E. (2017) Deforamtion-resembling microstructure created by fluid-mediated dissolution-precipitation reactions. *Nature Communications*¸ **8**: 14032, 9 pp.

Steele-MacInnis, M., Han, L., Lowell, R.P. Rimstidt, J.D. & Bodnar, R.J. (2012) Quartz precipitation and fluid inclusion characteristics in sub-seafloor hydrothermal systems associated with volcanogenic massive sulfide deposits. *Central European Journal of Geoscience*. **4**(2), 275-286.

Stephenson, D., Mendum, J.R., Fettes, D.J. & Leslie, A.G. (2013) The Dalradian rocks of Scotland: an introduction. *Proceedings of the Geologists' Association,* **124**, 3-82.

Strachan, R.A., Harris, A.L., Fettes, D.J. & Smith, M. (2002) The Highland and Grampian Terranes. *In:* Trewin, N.H. (ed) *The Geology of Scotland.* The Geological Society, London, 96-99.

Tanner, P.W.G. & Bluck, B.J. (1999) Current controversies in the Caledonides. *Journal of the Geological Society, London,* **156**, 1137-1141.

Tanner, P.W.G., Thomas, C.W., Harris, A.L., Gould, D., Harte, B., Treagus, J.E. & Stephenson, D. (2013) The Dalradian rocks of the Highland Border region of Scotland. *Proceedings of the Geologists' Association.* **124**, 215-262.

Thomas, W.A. (2011) Detrital-zircon geochronology and sedimentary provenance. *Bulletin of the Geological Society of America,* **3**(4), 304-308.

Tomaschek, F., Kennedy, A.M., Villa, I.M., Lagos, M. & Bellhaus, C. (2003) Zircon from Syros, Cyclades, Greece – recrystallization and mobilization of zircon during high-pressure metamorphism. *Journal of Petrology*, **44**(11), 1977-2002.

Tracy, R.J. (1982) Compositional zoning and inclusions in metamorphic minerals. *Reviews in Mineralogy and Geochemistry,* **10**.

Tracy, R.J., Robinson, P. & Thompson, A.B. (1976) Garnet composition and zoning in the determination of temperature and pressure of metamorphism, central Massachusetts. *American Mineralogist*, **61**, 762-775.

Trail, D., Mojzsis, S.J., Harrison, T.M., Schmitt, A.K., Watson, E.B. & Young, E.D. (2007) Constraints on Hadean zircon protoliths from oxygen isotopes Ti thermometry, and rare earth elements. *Geochemistry, Geophysics, Geosystems,* **8**, 1-22.

Treagus, J.E., Tanner, P.W.G., Thomas, P.R., Scott, R.A. & Stephenson, D. (2013) The Dalradian rocks of the central Grampian Highlands of Scotland. *Proceedings of the Geologists' Association,* **124**, 148-214.

Troceller, P. & Delmas, R. (2001) Chemical durability of zircon. *Nuclear Instruments and Methods in Physics Research B,* **181**, 408-412.

Tropper, P. (2014) Highlights and breakthroughs: Small grains and big implications: Accessory Ti- and Zr-minerals as petrogenetic indicators in HP and UHP marbles. *American Mineralogist*, **99**, 1197-1198.

Turkina, O.M. & Sukhorukov, V. (2017) Composition and genesis of garnet in the rocks of Palaeoproterozoic gneiss-migmatite complex (Sharyzhalgai uplift, southwestern Siberian craton). *Russian Geology and Geophysics.* **56**(8), 674-691.

Turner, F.J. (1968) Metamorphic Petrology. McGraw-Hill, New York, pp. 403.

Utsomomya, S., Palenik, C.S., Valley, J.W., Cavoise, A.J., Wilde, S.A. & Ewing, E.C. (2004) Nanoscale occurrence of Pb in an Archean zircon. *Geochimica et Cosmochimica Acta,* **68**(22), 4679-4686.

Väisänen, M. & Kirkland, C.L. (2008) U-Th-Pb zircon geochronology on igneous rocks in the Toija and Salittu Formations, Orijärva area, southwestern Finland: Constraints on the age of volcanism and metamorphism. *Bulletin of the Geological Society of Finland,* **80**, 73-87.

Valley, J.W., Reinhard, D.A., Cavoise, A.J., Ushikubo, T., Lawrence, D.F. & Larson, D.J. (2015) Nano- and micro-geochronology in Hadean and Archean zircons by atom-probe tomography and SIMS: new tools for old minerals. *American Mineralogist,* **100**, 1355-1377.

Vavra, G., Schmid, R. & Gebauer, D. (1999) Internal morphology, habit and U-Th-Pb microanalysis of amphibolite-to-granulite facies zircons: geochronology of the Ivrea zone (Southern Alps). *Contributions to Mineralogy and Petrology*, **134**, 380-404.

Vernon, R. (2018) Microstructures of deformed rocks. *In:* Vernon, R. A practical guide to rock microstructure, 2nd edition. Cambridge University Press, Cambridge, 432 pp.

Viete, D.R., Hermann, J., Lister, G.S. & Stenhouse, I.R. (2011) The nature and origin of Barrovian metamorphism, Scotland: diffusion length scales in garnet and inferred thermal time scales. *Journal of the Geological Society, London,* **168**, 115-132.

Villaseca, C., Orejana, D. & Paterson, B.A. (2007) Zr-LREE rich minerals in residual peraluminous granulite, another factor in the origin of low Zr-LREE granitic melts? *Lithos*, **96**, 375-386.

Volkov, Y.F. (1999) Compoiunds with zircon and monazite structure and possibilities for their application for radionuclide immobilization. *Radiokhimiya,* **41**(2), 161-166.

Vonlanthen, P., Fitzgerald, J., Rubatto, D. & Hermann, J. (2012) Recrystallization rims in zircon (Valle D'Arbedo Switzerland): An integrated cathodoluminescence, LA-ICP-MS, SHRIMP and TEM study. *American Mineralogist,* **97**, 369-377.

Vorhies, S.H. & Ague, J. J. (2011) Pressure-temperature evolution and thermal regimes in the Barrovian zones, Scotland. *Journal of the Geological Society, London,* **168**, 1147-1166.

Vorhies, S.H., Ague, J.J. & Schmitt, A.K. (2013) Zircon growth and recrystallization during progressive metamorphism, Barrovian zones, Scotland. *American Mineralogist*, **98**, 219-230.

Walther, J.V. & Wood, B.J. (1986) Fluid—rock interactions during metamorphism. Springer-Verlag, New York, 218 pp.

Wan, Y., Liu, D., Dong, C., Lu, S., Wang, S. & Yang, E. (2011) U-Th-Pb behaviour of zircons under high-grade metamorphic conditions: A case study of zircon dating of meta-diorite near Qixia, eastern Shandong. *Geoscience Frontiers*, **2**(2), 137-146.

Wang, J., Mao, Z., Jiang, F. & Duffy, T.S. (2015) Elasticity of single-crystal quartz to 10 GPa. *Physics and Chemistry of Minerals,* **42**, 203-212.

Wang, W., Dunkley, E., Clarke, G.L. & Daczko, N.R. (2014) The evolution of zircon during low-P partial melting of metapelitic rocks: theoretical predictions and a case study from Mt Stafford, Central Australia. *Journal of Metamorphic Geology,* **32**, 791-808.

Wang, X-L., Zhou, J-C., Griffin, W.L., Wang, R-C., Qiu, J-S., O'Reilly, S.Y., xu, S., Liu, X-M. & Zhang, G-L. (2007) Detrital zircon geochronology of Precambrian basement sequences in the Jiangnan orogen: Dating the assembly of the Yangtze and Cathaysia Blocks. *Precambrian Research,* **159**. 117-131.

Wayne, D.M. & Sinha, A.K. (1988) Physical and chemical response of zircons to deformation. *Contributions to Mineralogy and Petrology*, **98**, 109-121.

Waters, D.J. & Lovegrove, D.P. (2002) Assessing the extent of disequilibrium and overstepping of prograde metamorphic reactions in metapelites from the Bushveld Complex aureole, South Africa. *Journal of Metamorphic Geology*, **20**, 135-149.

Watson, E.B. & Harrison, T.M. (1983) Zircon saturation revisited: temperature and composition effects in a variety of crustal magma types. *Earth and Planetary Science Letters,* **64**(2), 295-304.

Weber, W.J., Ewing, R.C. & Wang, L.M. (1994) The radiation-induced crystalline-to-amorphous transition in zircon. *Journal of Materials Research,* **9**(3), 688-698.

Wells, P.R.A. (1979) P-T conditions in the Moines of the Central Highlands, Scotland. *Journal of the Geological Society, London*, **136**, 663-671.

Westrenen, W.V., Blundy, J.D. & Wood, B.J. (2001) High field strength element/rare earth element fractionation during partial melting in the presence of garnet: Implications for identification of mantle heterogeneities. *Geochrmistry Geophysics Geosystems,* **2**, 19 pp.

Whitehouse, M.J. & Platt, J.P. (2003) Dating high-grade metamorphism – Constraints from rare-earth elements in zircon and garnet. *Contributions to Mineralogy and Petrology*, **145**, 61-74.

Whitney, D.L., Mechum, T.A., Dilek, Y. & Kuehner, S.M. (1996) Modification of garnet by fluid infiltration during regional metamorphism in garnet through sillimanite-zone rocks, Dutchess County, New York. *American Mineralogist*, **81**, 696-705.

Whitney, D.L., Cooke, M.L. & Du Franc, S.A. (2000) Modelling of radial microcracks at corners of inclusions in garnet using fracture mechanics. *Journal of Geophysical Research,* **105**(B2), 2843-2853.

Whitney, D.L., Goergen, E.T., Ketcham, R.A. & Kunze, K. (2008) Formation of garnet polycrystals during metamorphic crystallization. *Journal of Metamorphic Geology,* **26**(3), 365-383.

Wilbur, D.E. & Ague, J.J. (2006) Chemical disequilibrium during garnet growth: Monte Carlo simulations of natural crystal morphologies. *Geology*, **34**(8), 689-692.

Wilde, S.A., Valley, J.W., Peck, W.H. & Graham, C.M. (2001) Evidence from detrital zircons for the existence of continental crust and oceans on Earth 4.4Gyr ago. *Nature*, **409**, 175-178.

Will, T.M., Okrusch, M. & Gruner, B.B. (2004) Barrovian and Buchan type metamorphism in the Pan-African Kaoko belt, Namibia: implications for its geotectonic position within the framework of Western Gondwana. *South African Journal of Geology,* **107**(3), 431-454.

Williams, I.S. (2001) Response of detrital zircon and monazite, and their U-Pb isotopic systems, to regional metamorphism and host-rock partial melting, Cooma Complex, southeastern Australia. *Australian Journal of Earth Sciences,* **48**, 557-580.

Wilson, N.C., Muscat, J., Mkhonto, D., Ngoepe, P.E. & Harrison, N.M. (2005) Structure and properties of ilmenite from first principles. *The Academic Physical Society,* Physical Review **B71**: 075202, 9 pp.

Wing, B.A., Ferry, J.M. & Harrison, T.M. (2003) Prograde destruction and formation of monazite and allanite during contact and regional metamorphism of pelites: petrology and geochronology. *Contributions to Mineralogy and Petrology,* **145**, 228-250.

Wolfe, O.M. & Spear, F.S. (2017) Determining the amount of overstepping required to nucleate garnet during Barrovian regional metamorphism, Connecticut Valley Synclinorium. *Journal of Metamorphic Geology,* **36**, 79-94.

Woodsworth, G.J. (1977) Homogenisation of zoned garnets from pelitic schists. *Canadian Mineralogist,* **15**, 230-242.

Yagi, T., Akogi, M., Shimomura, O., Tamai, H. & Akimoto, S. (1987) High pressure and high temperature equations of the state of majorite. *In:* Manghnani, M.H. &

Sono, Y. (eds) High pressure research in mineral physics, Terrapub, Tokyo, 141-147.

Yakymchuk, C., Kirkland, C.L. & Clark, C. (2018) Th/U ratios in metamorphic zircon. *Journal of Metamorphic Geology,* **36**(6), 715-737.

Yardley, B.W.D. (1977) An empirical study of diffusion in garnet. *American Mineralogist,* **62**, 793-800.

Zack, T., von Eynatten, H. & Kronz, A. (2004) Rutile geochemistry and its potential use in quantitative provenance studies. *Sedimentary Geology*, **171**, 37-58.

Zhao, W.W., Shou, M.F. & Chen, W.T. (2016) Growth of hydrothermal baddeleyite and zircon in different stages of skarnization. *American Mineralogist*, **101**, 2689-2700.

Zwart, H.J. (1960) The chronological succession of folding and metamorphism in the central Pyrenees. *Geologische Rundschau*, **50**, 203-218.

Appendix 1:

Controls on microzircon growth

T. R. McElhinney
School of Geographical & Earth Sciences, Gregory Building, University of Glasgow, Glasgow, G12 8QQ, UK.

ABSTRACT

Zircon is traditionally viewed as highly unreactive, particularly during low grade metamorphic events. Temperature is well established as a first order control on the reactivity of zircon, as such a range of geochemical investigations involving U/Th-Pb dating have been carried out on low grade 'inert' zircon. There is growing evidence to suggest zircon is reacting at low temperatures and new metamorphic zircon is forming as outgrowths on detrital grains and discrete microzircon crystals. This study analyses the distribution and abundance of zircon within biotite schists from the NW Highlands to constrain the controls on zircon dissolution and microzircon growth. Disparity in microzircon abundance across compositional variations indicates the structural integrity of the detrital population is the dominant control on distribution, while the role of nucleation remains ambiguous. Prograde reactions promote crystallization while retrograde reactions promote dissolution, supported by the absence of microzircon in chlorite-retrogressed areas. The late dissolution hinders preservation making crystallization and dissolution difficult to distinguish. Significant further work is required to fully understand the factors controlling microzircon growth but lithology appears to be the dominant control.

INTRODUCTION

Zircon is a common accessory mineral found in a range of sedimentary, igneous and metamorphic rocks. It is believed to have magmatic origins and can undergo multiple growth phases, being eroded from one suite and deposited in another where growth can occur (Hanchar and Hoskin, 2003). Zircon is traditionally regarded as highly unreactive and resistant to metamorphic events (Poldevaart, 1955; Gastil et al., 1967), despite a wealth of evidence to suggest otherwise. Outgrowths were discovered on detrital grains in sandstone calling into question the source of the Zr and zircon's resistant nature (Butterfield, 1936; Bond, 1948). Zircon analysis initially focused on upper amphibolite-granulite facies rocks and the alteration of zircon at elevated temperatures (Usui et al., 2002; Flowers et al., 2010; Kröner et al., 2014), and more recently low-medium grade reactivity (Dempster et al., 2004; Rasmussen, 2005; Dempster et al., 2008; Wang et al., 2014). It transpired Zr was sourced from the dissolution of existing grains (Usui et al., 2002; Flowers et al., 2010; Kröner et al., 2014). Evidence of this reactivity is preserved as dissolution textures and outgrowths on detrital grains, and as newly formed microzircon. Microzircon are discrete, anhedral crystals of very fine zircon which show no internal structure or zoning (Dempster et al., 2004). They have been found in a range of low-medium grade metasediments (Dempster et al., 2004; Hay and Dempster, 2009; Dempster and Chung, 2013; Wang et al., 2014) and their formation is suggested to be based around the lack of nucleation in low temperature events (Dempster et al., 2008). Higher temperatures promote nucleation and the remnants of detrital zircon provide a structure. Where both are absent the newly formed zircon may exist as separate crystals (Dempster et al., 2004). Similar low grade metasediments analysed elsewhere have yielded no microzircon despite containing other evidence of zircon reactivity (Rasmussen, 2005; Hay et al., 2010). This disparity raises questions regarding the conditions required for microzircon growth.

Fluid composition has also been suggested as a possible factor influencing the reactivity of zircon (Gieré, 1986). Zr^{4+} is a high strength field cation and is difficult to mobilise and transport, requiring high temperatures or an extremely corrosive fluid. The release of halogens from dehydration reactions create a more reactive fluid that can remove the Zr^{4+} and transport the cations as F complexes (Wayne and Sinha, 1988; Rasmussen, 2005). There are now a myriad of studies which show zircon is not the unreactive mineral it was once perceived as. However, the factors that influence reactivity are not fully understood. Zircon contains radioactive elements in its lattice, such as U/Th which substitute for Zr (Hanchar and Hoskin, 2003). When these radiogenic elements decay the recoil of the heavy daughter nuclei damages the lattice and produces metamict areas (Holland and Gotfried, 1955; Nasdala et al., 2001). Metamict grains are more reactive than their crystalline counterpart as the weakened lattice aids dissolution and diffusion (Hay and Dempster, 2009). This damage can only be annealed at ~250°C (Holland and Gottfried, 1955; Weber et al., 1994; Nasdala et al., 2001). Zircon's apparent inert nature coupled with its affinity to incorporate trace elements make it a useful dating tool in a wide range of geochemical investigations (Froude et al., 1983; Mojzsis et al., 2001; Wilde et al., 2001; Cawood et al., 2003; Kröner et al., 2014). Where crystallization and recrystallization is occurring U/Th-Pb ages produced are ambiguous (Davis et al., 1968; Kelly and Harley, 2005) highlighting the importance in understanding zircon behavior.

This study analyses the distribution and abundance of detrital and microzircon in low grade metasediments from the NW Highlands in Scotland to understand the factors that control the dissolution and recrystallization of zircon.

GEOLOGICAL SETTING AND SAMPLING

The rocks analysed are biotite schists from the Appin Phyllite group at Onich in the NW Highlands of Scotland. They were sampled at two locations along the coast, 2-8 [NN 61330 03200] and 2-9 [NN 61325 03300]. The sediments are polymetamorphosed, they first underwent a regional event in the Cambrian-Ordovician, before a second low grade contact event following the emplacement of the Ballachulish granite during the Caledonian Orogeny (Roberts and Treagus, 1977; Pattison and Harte, 2001). The sample from 2-8 contains pelite and 2-9 contains pelite and quartz-rich pelite separated by a heavy mineral band. The pelite is composed of just 3% biotite porphyroblasts ranging in size from 1-3mm. The fine <0.125mm matrix is composed of 76% muscovite, 8% plagioclase, 6% quartz and 4% biotite. The quartz-rich pelite has a larger proportion of biotite porphyroblasts, 10%, ranging in size from 1-4mm. The slightly coarser matrix contains 34% quartz, 33% muscovite, 16% plagioclase and 5% biotite. The heavy mineral band represents bedding between the layers, it is slightly more quartz-rich and composed of >30% biotite porphyroblasts. The biotite porphyroblasts show partial retrogression to chlorite and much of the matrix biotite is completely altered. Allanite is consistently present throughout the samples in small proportions (>3%) and is commonly rimmed by epidote. Vestiges from three metamorphic stages are preserved in the rocks. The first comprising the aligned, fine-grained, matrix muscovite muscovite formed during the regional event, the second is the large contact biotite porphyroblasts and finally the chlorite formed during retrogression.

The Appin Phyllite rocks were specifically chosen due to their low grade. No microzircon have been reported in sedimentary rocks and their growth within garnet-amphibolite facies rock is well documented (Dempster et al., 2004; Dempster et al., 2008; Wang et al., 2014) however biotite-zone rocks remain unexplored. The analysis of these

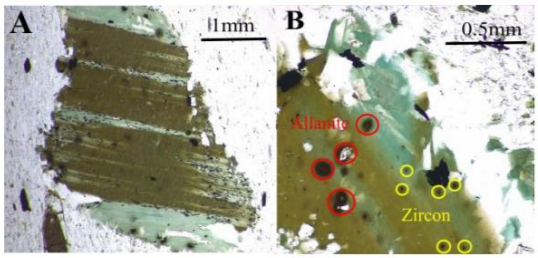

Figure 1. Photomicrograph images of biotite porphyroblasts from polished section 2-8. A: Biotite within quartz-rich pelite showing chlorite retrogression and pleochroic haloes. B. Closer image of biotite showing the distinction between allanite and zircon haloes.

rocks will allow an understanding of whether crossing the chlorite-biotite reaction yields conditions that promote microzircon growth and what the controls are.

METHODOLOGY

The samples were prepared as two polished sections, one from each locality, 2-8 and 2-9. Polished sections were used in place of traditional mineral separates to maintain petrographic context (Hay and Dempster, 2009) and allow distribution analysis. An optical microscope was used to analyse the mineralogy and assess pleochroic halo abundances (Fig. 1A). The samples also contain allanite and care was taken to distinguish between larger allanite and smaller zircon haloes (Fig. 1B). The halo counts allowed preliminary detrital zircon distributions to be surveyed and highlighted areas of interest. The sections were then analysed using an FEI Quanta 200F environmental scanning electron microscope (SEM) operated at 20kV and moderate beam currents to capture backscattered electron (BSE) images of detrital and microzircon. Equal areas of porphyroblast and matrix were selected at random across all compositions and analysed. The BSE images obtained include information on the texture, size, shape and host mineral(s). Section 2-9 was also scanned using energy-dispersive x-ray analysis (EDX) on the Carl Zeiss Sigma SEM to record the location and composition of high mean atomic number features. The features captured an array of other minerals and so the zircon was identified based on Zr-content. This data then allowed the plotting of a location map of all zircon across the pelite and quartz-rich pelite in 2-9. The Sigma SEM only scans >0.8μm^2 area features. Many of the microzircon analysed using BSE imaging are finer than this so the data is missing a portion of the population. Another drawback of this data is the lack of textural information. To distinguish microzircon from detrital zircon, a size threshold of <2.5μm^2 for micro and >10μm^2 for detrital was set and the data was separated accordingly. These values were calculated using a combination of bimodal size distribution charts and the size ranges from BSE imaging. The lack of textural information yielded from the EDX data raised issues on apparently small microzircon representing different cuts of detrital grains, something that can be picked out on BSE imaging based on internal structure. The likelihood of a cut of the smallest detrital grain falling in the <2.5μm^2 microzircon threshold is just 4% meaning the EDX data is statistically significant at the assigned size margins.

RESULTS

Using BSE and EDX 1553 zircon were identified in total, 1008 detrital and 545 microzircon. The BSE imaging identified all three lines of evidence of reactivity within both sections; dissolution (Fig. 2B) and outgrowths (Fig 2A, 2C, 2D) in detrital grains and the crystallization of microzircon (Fig 2E, 2F).

Detrital Zircon

The detrital zircon population range in size from 4μm^2 to 2900μm^2 with the quartz-rich pelites hosting the coarser population. Averages produced between different compositions have large errors because of the limited data collected and the large range of detrital zircon sizes, information on at least 5,000 more grains would be required to produce a robust pattern. The largest grains are located at the heavy mineral band in section 2-9 and are slightly aligned in this layer. Larger grains are generally more euhedral with the smaller, subhedral grains commonly possessing irregular and embayed margins. The detrital zircon are more abundant in the quartz-rich pelite and dominate the zircon population, while they are less common in the pelite (Fig. 3). 68% of the detrital grains imaged contained outgrowths with no significant change in

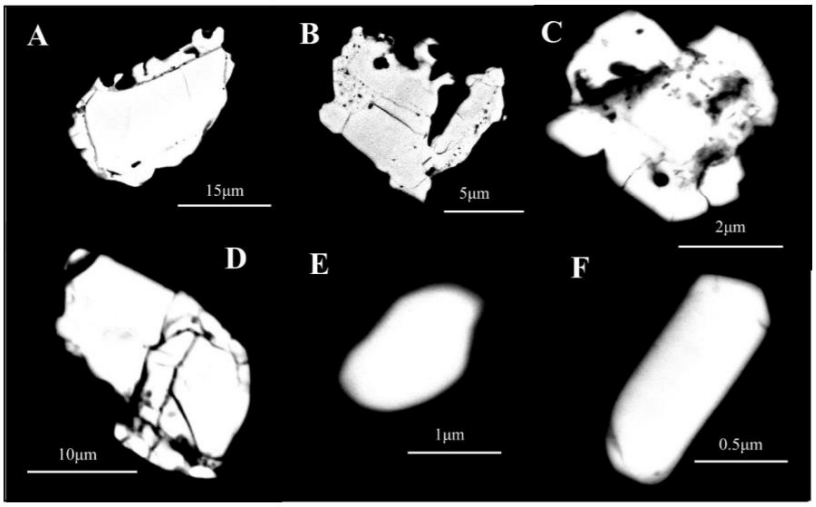

Figure 2: Zircon morphologies captured using BSE imaging from Quartz-rich pelites (Pq) and pelites (Pe) across polished sections 2-8 and 2-9. A. Detrital zircon with delicate fringe indicating growth in situ. The outgrowth also appears to be subject to some later dissolution (Pq 2-8). B. Dissolution texture and alteration within a zircon (Pq 2-8). C. Heavily altered small detrital grain with irregular margins (Pe 2-9). D. Heavily fractured detrital grain damaged during regional deformation (Pq 2-9). E. Irregular shaped microzircon with a lack of internal structure (Pq 2-8). F. Finer, more euhedral microzircon (Pe 2-9).

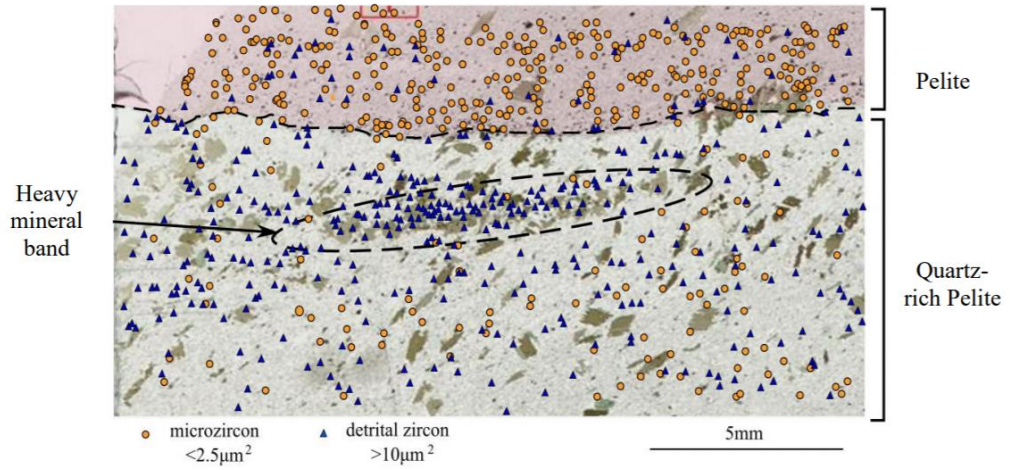

Figure 3: X-Y plot of zircon distribution data from EDX laid over an image of the section to illustrate the location of detrital and microzircon across the 2 main compositional layers and heavy mineral band in 2-9.

abundance or style across the samples. The detrital grains occur predominantly within the matrix, 28% of grains in the quartz-rich layer are within biotite and similarly just 24% of detrital are within biotite in the pelite. The zircon within the porphyroblasts tend to be larger than those in the matrix, so the total area of zircon in the porphyroblasts is greater. In the matrix the largest proportion of detrital zircon occur within muscovite across the pelite and quartz-rich pelite with significantly fewer in plagioclase and quartz (Fig. 4). The heavy mineral band show significantly more zircon within porphyroblasts where 41% of grains occur within biotite. Within the matrix 81% of detrital zircon are located on grain boundaries and only 19% occur as inclusions in a single host.

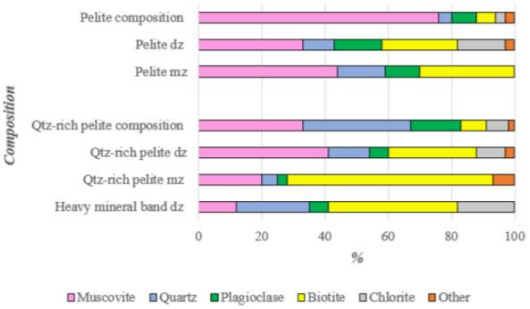

Figure 4: Bar plot representing the modal percentage of constituent minerals and their proportion as hosts of detrital (dz) and microzircon (mz) across the pelite and quartz-rich pelite. Also included are detrital zircon hosts for the heavy mineral band, not for microzircon as there are none in this layer. The other minerals are predominantly allanite and epidote and rutile.

Microzircon

The microzircon range in size from 0.08µm² to 3µm² with most grains between 1-2µm². Microzircon within the matrix are finer than in porphyroblasts across both compositions. In the quartz-rich pelite matrix the mean grain size is 0.66µm² ± 0.12µm² while in porphyroblasts they average 0.87µm² ± 0.58µm². Similarly, in the pelite the matrix contains 1.03 µm² ± 0.7µm² and the biotite contain coarser 1.39 µm² ± 0.62µm² grains. The microzircon are more abundant in the mica-rich layer than the quartz-rich (Fig. 3). The pelite is dominated by microzircon with very few detrital grains and the quartz-rich pelite is dominated by detrital with very few microzircon. The population does not show any obvious variation in shape or texture. 81% of matrix microzircon occur within a single host mineral and only 19% occur on grain boundaries. Within the aligned muscovite grains, the microzircon inclusions are slightly larger than at grain boundaries, 1.41µm² ± 0.84µm² within grains and 0.91µm² ± 0.63µm² between grains. In the quartz-rich pelite 65% of microzircon are found in biotite porphyroblasts while in the pelite just 30% are within biotite and the remaining 70% are in the matrix. Across both compositions the matrix population is dominantly within muscovite, followed by quartz and plagioclase (Fig. 4). In the quartz-rich matrix 56% of microzircon are included in muscovite, 34% in plagioclase and 10% in quartz, a further 7% is contained in other minerals, dominantly rutile. In the pelite 67% are in muscovite, 22% in plagioclase and 11% in quartz. Chlorite retrogression in biotite porphyroblasts varies from 2-6%, microzircon are not present within any of the retrogressed areas of biotite. A 2% altered biotite contains 85% microzircon and 15% detrital while a 16% altered porphyroblast contains predominantly detrital grains and just 38% microzircon.

DISCUSSION

The formation of outgrowths and microzircon indicates dissolution and crystallization of new metamorphic zircon is occurring (Fig. 5). Both the outgrowths and microzircon illustrate a strong metamorphic control on their formation. The outgrowths are commonly irregularly shaped forming along grain boundaries and are extremely delicate

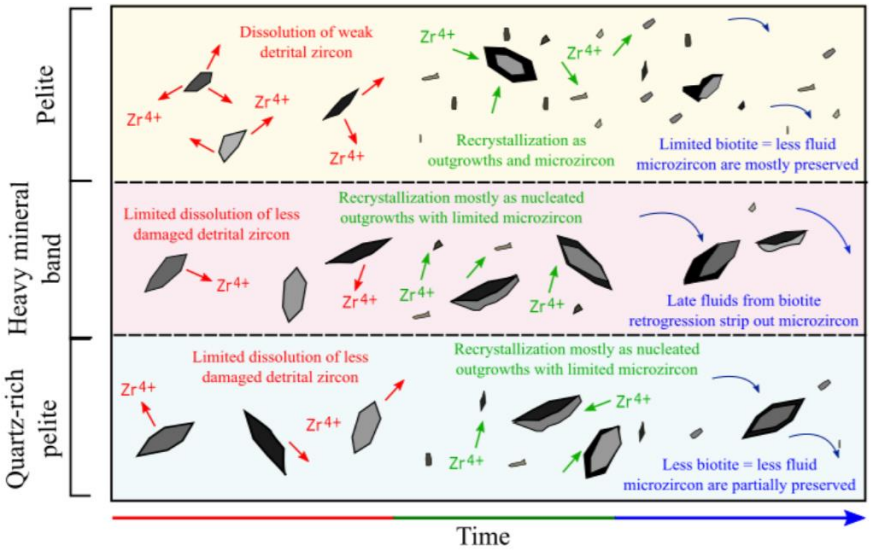

Figure 5: Schematic diagram illustrating the processes within zircon across the three main compositions: quartz-rich pelite, pelite and the heavy mineral band. The composition of the layer influences the abundance and distribution of the final zircon population by controlling the degree of dissolution and crystallization. The result is a pelite composed primarily of microzircon and a quartz-rich pelite and heavy mineral band with very few microzircon and a large number of outgrowths.

indicating growth in situ (Rasmussen, 2005). The metamorphic control on microzircon is evident from the change in grain size across the porphyroblasts and matrix. Dempster et al (2008) reported a reduction in grain size throughout the reaction history, echoed by this study. The coarser microzircon population is confined to porphyroblasts and the later formed, finer population to the matrix. The type of zircon growth can be related to the composition of the layer in which it forms.

Zircon abundances vary across the pelite and quartz-rich pelite, microzircon growth is concentrated in the pelite while the quartz-rich layers contain a larger population of detrital zircon. The results indicate the dissolution of zircon is primarily a consequence of the structural state of existing detrital grains. The pelite contains a population of smaller detrital grains, predominantly comprised of broken fragments of metamict zircon (Dempster and Chung, 2013). Radiation damage promotes partial dissolution and yields larger volumes of Zr^{4+} in the fluid, increasing the potential for new zircon crystallization (Hay and Dempster, 2009). The quartz-rich pelite contains a population of coarser detrital grains which are less reactive to hydrothermal fluids, thus producing less metamorphic zircon. As well as direct weakening of the lattice, Hay and Dempster (2009) propose the swelling of amorphous metamict areas by up to 18%, fracturing grains and creating fluid pathways to aid dissolution. Detrital analysis of an unmetamorphosed analogue of the Appin Phyllite metasediments would provide better constraints on the structural state of zircon prior to dissolution and enhance the understanding of lithological control on microzircon growth. Nucleation could magnify this variation in distribution. The assembly of detrital zircon in the quartz-rich pelite could provide a structure for nucleation of the new zircon, fringing the existing grains instead of remaining as discrete microzircon (Dempster et al., 2004).

Contrary to what structural nucleation dictates large numbers of microzircon occur in close proximity to detrital grains (Fig. 3). The role of nucleation remains ambiguous but BSE analysis of a wider range of samples with varying detrital contents would solidify the link between nucleation and microzircon growth.

The rocks have undergone at least three separate metamorphic phases a regional event, a contact event and a period of retrogression (Roberts and Treagus, 1977; Pattison and Harte, 2001). Textural analysis allows the distinction between these stages in the mineralogy and as such zircon growth can be attributed to specific events. The early regional event formed the aligned muscovite matrix, producing within it a population of large microzircon. The contact event is responsible for forming microzircon within biotite porphyroblasts and elsewhere in the matrix (on grain boundaries and likely within quartz and plagioclase). The late retrogression appears to be unique, removing microzircon without any new crystallization, evident from the lack of microzircon within chlorite. So, during the prograde chlorite-biotite reaction microzircon is formed yet during the retrograde biotite-chlorite there is no apparent new zircon growth.

Fluid composition is essential to allow the mobilization and transportation of Zr^{4+} beyond the grain scale and therefore for the formation of microzircon and outgrowths on non-metamict grains (Rasmussen, 2005). At higher temperatures zircon dissolution is more efficient due to the higher kinetic energy of the cations where temperatures are lower a more corrosive fluid is required to mobilise Zr^{4+} (Weber et al., 1994; Nasdala et al., 2001). The dehydration reactions involved in the formation of mica at each stage of the metamorphic history would produce halogen-rich fluids capable of dissolving and transporting Zr^{4+}. Fluid composition doesn't explain the

disparity between growth in the metamorphic stages but is a background mechanism required for microzircon growth. During peak metamorphism fluid is more readily available and while the presence of an aqueous phase is essential for chloritization (Barker, 1998) fluid availability is commonly the limiting factor during retrograde reactions. The contrast in fluid availability in the prograde and retrograde history could explain the lack of new zircon growth during retrogression. The low preservation potential of microzircon requires consideration. Their nanocrystalline structure means they can be fully dissolved by hydrothermal fluids (Dempster et al., 2008; Hay and Dempster, 2009). Retrogression creates corrosive fluids capable of stripping out microzircon. Layers with larger proportions of biotite would have greater dissolution potential, particularly the heavy mineral band containing 32% biotite. The absence of any microzircon in the heavy mineral band could be attributed to preservation rather than a lack of crystallization. While this process affects abundances, distribution is maintained, with the exception of the >30% biotite layer, as retrograde fluids are limited and sheltered zircon populations are sustained (Hay and Dempster, 2009).

The results indicate that both fluid composition and radiation damage operate simultaneously to promote dissolution. Radiation damage is arguably the more important factor at low grade as the temperature required to dissolve detrital zircon far exceeds that in the Appin Phyllite Group at Onich (Nasdala et al., 2001). Variations in fluid composition provide an explanation for the absence of microzircon in apparently similar low grade metasediments where less halogen-rich fluids may impede the transport of Zr cations.

CONCLUSION

This study adds to a growing body of work that illustrates the importance of regarding zircon as a reactive mineral during low grade metamorphism. The perception of temperature as a first order control on the behavior of zircon is simplistic, temperature is certainly a catalyst but it is one of many factors controlling growth. Lithology, a proxy for radiation damage, appears to be the dominant control on zircon dissolution and crystallization in low temperature metasediments. Radiation damage works concomitantly with fluid composition and possibly nucleation to preferentially produce the discrete microzircon. Future analysis should focus on the separation of crystallization and dissolution by analysing samples with varying degrees of retrogression to better constrain the controls on microzircon growth.

AWKNOWLEDGEMENTS

I thank Tim Dempster for his guidance throughout the research and compilation of this report and Peter Chung for his technical assistance. This work was supported by the University of Glasgow.

REFERENCES

Barker, A.J. 1998, Introduction to Metamorphic Textures and Microstructures, S. Thornes, Surrey.

Butterfield, J.A. 1936, Outgrowths on Zircon: Geological Magazine, v. 73, p. 511-516.

Bond, G. 1948, Outgrowths on Zircon from Southern Rhodesia: Geological Magazine, v. 85, p. 35-40.

Cawood, P.A., Nemchin, A.A., Smith, M. and Loewy, S. 2003, Source of the Dalradian Supergroup constrained by U-Pb dating of detrital zircon and implications for the East Laurentian Margin: Journal of the Geological Society, v. 160, p. 231-246.

Davis, G.L., Hart, S.R. and Tilton, G.R. 1968, Some effects of contact metamorphism on zircon ages: Earth and Planetary Science Letters, v. 5, p. 27-34.

Dempster, T.J., Hay, D.C. and Bluck, B.J. 2004, Zircon growth in slate: Geological Society of America, v. 32 (2), p. 221-224.

Dempster, T.J., Hay, D.C., Gordon, S.H. & Kelly, N.M. 2008, Micro-zircon: origin and evolution during metamorphism: Journal of Metamorphic Geology, v. 26, p. 499-507.

Dempster, T.J. and Chung, P. 2013, Metamorphic zircon: tracking fluid pathways and the implications for the preservation of detrital zircon: Journal of the Geological Society, London, v. 170, p. 631-639.

Dempster, T.J. and MacDonald, F. 2016, Controls on fluid movement in crustal lithologies: evidence from zircon in metaconglomerates from Shetland: Geofluids, v. 16, p. 507-517.

Flowers, R.M., Schmitt, A.K. and Grove, M. 2010, Decoupling of U-Pb dates from chemical and crystallographic domains in granulite facies metamorphism: Chemical Geology, v. 270, p. 20-30.

Froude, D.O., Ireland, T.R., Kinny, P.D., Williams, I.S., Compston, W., Williams, I.R. and Myers, J.S. 1983, Ion microprobe identification 4,100-4,200 Myr-old terrestrial zircons: Nature, v. 304, p. 616-618.

Gastil, R.G., Delisle, M. and Morgan, J.R. 1967, Some effects of progressive metamorphism on zircons: Geological Society of America Bulletin, v. 78, p. 879-906.

Gieré, R. 1986, Zirconolite, allanite and hoegbomite in a marble skarn from the Bergell contact aureole: implications for movbility of Ti, Zr and REE: Contributions to Mineralogy and Petrology, v. 93, p. 459-470.

Hanchar, J.M. and Hoskin, P.W.O. 2003, Zircon-Reviews in Mineralogy and Geochemistry, v. 53. Mineralogical Society of America/Geochemical Society, Washington DC.

Hay, D.C. and Dempster, T.J. 2009, Zircon behavior during low-temperature metamorphism: Journal of Petrology, v. 50 (4), p. 571-589.

Hay, D.C., Dempster, T.J., Lee, M.R. and Brown, D.J. 2010, Anatomy of a low temperature zircon outgrowth: Contributions to Mineralogy and Petrology, v. 159, p. 81-92.

Holland, H. and Gottfried, D. 1955, The effect of nuclear radiation on the structure of zircon: Acta Crystal, v. 61, p. 291-300.

Kelly, N.M. and Harley, S.L. 2005, An integrated microtextural and chemical approach to zircon geomorphology: refining the Archaean history of the Napier Complex, East Antarctica: Contributions to Mineralogy and Petrology, v. 149, p. 57-84.

Kröner, A., Wan, Y., Liu, X. and Liu, D. 2014, Dating of zircon from high-grade rocks: which is the most reliable method?: Geoscience Frontiers, v. 5 (4), p. 515-523.

Mojzsis, S.J., Harrison, T.M. and Pidgeon, R.T. 2001, Oxygen-isotope evidence from ancient zircons for liquid water at the Earth's surface 4,300Myr ago: Nature, v. 409, p. 178-181.

Nasdala, L., Wenzel, M., Vavra, G., Irmer, G., Wenzel, T. and Kober, B. 2001, Metamictization of natural zircon: accumulation versus thermal annealing of radioactivity-induced damage: Contributions to Mineralogy and Petrology, v. 141, p. 125-144.

Nemchin, A.A., Pidgeon, R.T. and Whitehouse, M.J. 2006, Re-evaluation of the origin and evolution of >4.2Ga zircons from the Jack Hills metasedimentary rocks: Earth and Planetary Science Letters, v. 244, p. 218-233.

Pattison, D.R.M. and Harte, B. 2001, The Ballculish Igneous Complex and Aureole: A Field Guide: Edinburgh Geological Society, Edinburgh.

Rasmussen, B. 2005, Zircon growth in very low grade metasedimentary rocks: evidence for zirconium mobility at ~250ºC: Contributions to Mineralogy and Petrology, v. 150, p. 146-155.

Roberts, J.L. and Treagus, J.E. 1977, The Dalradian rocks of the South-west Highlands – Introduction: Scottish Journal of Geology, v. 13, p. 87-99.

Troceller, P. and Delmas, R. 2001, Chemical durability of zircon: Nuclear Instruments and Methods in Physics Research B, v. 181, p. 408-412.

Usui, T., Kobayashi, K. and Nakamura, E. 2002, U-Pb isotope systematics of micro zircon inclusions: Proceedings of the Japan Academy Series B, v. 78 (3), p. 51-56.

Wang, W., Dunkley, E., Clarke, G.L. and Daczko, N.R. 2014, The evolution of zircon during low-P partial melting of metapelitic rocks: theoretical predictions and a case study from Mt Stafford, Central Australia: Journal of Metamorphic Geology, v. 32, p. 791-808.

Wayne, D.M. and Sinha, A.K. 1988, Physical and chemical response of zircons to deformation: Contributions to Mineralogy and Petrology, v. 98, p. 109-121.

Weber, W.J., Ewing, R.C. and Wang, L.M. 1994, The radiation-induced crystalline to amorphous transition in zircon: Journal of Minerals Research, v. 9 (3), p. 688-698.

Wilde, S.A., Valley, J.W., Peck, W.H. and Graham, C.M. 2001, Evidence from detrital zircons for the existence of continental crust and oceans on Earth 4.4 Gyr ago: Nature, v. 409, p. 175-178.